ONLINE DETECTION OF PILOT WORKLOAD BY USING FNIR SENSORS

A THESIS SUBMITTED TO
THE GRADUATE SCHOOL OF INFORMATICS OF
THE MIDDLE EAST TECHNICAL UNIVERSITY
BY

MURAT VURAL

IN PARTIAL FULFILLMENT OF THE REQUIREMENTS FOR THE DEGREE OF
MASTER OF SCIENCE
IN
DEPARTMENT OF INFORMATION SYSTEMS

MARCH 2018

Approval of the thesis:

ONLINE DETECTION OF PILOT WORKLOAD BY USING FNIR SENSORS

Submitted by **MURAT VURAL** in partial fulfillment of the requirements for the degree of **Master of Science in Information Systems, Middle East Technical University** by,

Prof. Dr. Deniz Zeyrek Bozşahin
Dean, **Graduate School of Informatics** _____

Prof. Dr. Yasemin Yardımcı Çetin
Head of Department, **Information Systems** _____

Assist. Prof. Dr. Murat Perit Çakır
Supervisor, **Cognitive Science Dept., METU** _____

Examining Committee Members:

Prof. Dr. Yasemin Yardımcı Çetin _____
Information Systems Dept., METU

Asst. Prof. Dr. Murat Perit Çakır _____
Cognitive Science Dept., METU

Assoc. Prof. Dr. Altan Koçyiğit _____
Information Systems Dept., METU

Assoc. Prof. Dr. Erhan Eren _____
Information Systems Dept., METU

Asst. Prof. Dr. Erol Özçelik _____
Psychology Dept., Çankaya University

Date: *14.03.2018*

I hereby declare that all information in this document has been obtained and presented in accordance with academic rules and ethical conduct. I also declare that, as required by these rules and conduct, I have fully cited and referenced all material and results that are not original to this work.

Name, Last name : Murat VURAL

Signature : _____

ABSTRACT

ONLINE DETECTION OF PILOT WORKLOAD BY USING FNIR SENSORS

Vural, Murat
MSc., Department of Information System
Supervisor: Assist. Prof. Dr. Murat Perit Çakır

March 2018, 190 pages

Measuring mental workload of pilots and evaluating such measurements are important concerns in the aviation domain that requires high safety critical precautions. However, obtaining valid online measures without reducing operational capabilities of pilots remains to be an active area of research in human factors and aviation psychology. The aim of this thesis is to develop online measures for monitoring the changes of pilots' mental workload and establish a basis for follow-up studies that may use these measurements to implement new types of safety precautions in the cockpit. Since Functional Near-Infrared Spectroscopy (fNIRS) technology has been successfully employed in recent human factors studies and fNIRS sensors have an ergonomic design that minimizes the discomfort of pilots as compared to other brain imaging methods, fNIRS optical brain imaging technology is employed in this thesis study. Firstly, changes in the mental workload of pilots are studied as performing offline analyses in well-defined test scenarios in order to devise physiological patterns and algorithms for mental workload assessment. Afterwards, a software that can make online mental workload assessment by using these algorithms is developed and tested. The results indicate that models that are trained over data sampled from all pilots' sessions yielded the highest classification accuracy. SVM with RBF kernel function, LSTM and RNN which are used during the model development yield the highest accuracy scores with the given order, albeit with similar results.

Keywords: fNIR, Mental Workload, Pilot Workload, Online Detection

ÖZ

FNIR SENSÖRLER İLE PİLOT İŞ YÜKÜNÜN ÇEVRİMİÇİ TESBİTİ

Vural, Murat

Yüksek Lisans, Bilişim Sistemleri Bölümü

Tez Yöneticisi: Yrd. Doç. Dr. Murat Perit Çakır

Mart 2018, 190 sayfa

Havacılık gibi emniyet tedbirlerinin kritik olduğu bir alanda, pilotların mental iş yükünün doğru bir şekilde ölçülüp yorumlanması operasyonun güvenli bir şekilde tamamlanmasında kullanılacak önemli bir metottur. Ancak doğru ölçümleri çevrim içi olarak pilotun uçuş kabiliyetlerini sınırlandırmadan yapabilmek insan faktörü ve havacılık psikolojisi açısından üzerinde çalışılan aktif bir çalışma alanı haline gelmiştir. Bu tez çalışmasında pilotların mental iş yükünün simülasyon ortamında ve çevrim içi olarak ölçülmesi ve bu ölçümlerin kullanılarak gerekli tedbirlerin alınmasına vesile olacak çalışmalara zemin hazırlanması hedeflenmiştir. fNIR (Functional Near Infrared Spectroscopy) teknolojisinin insanlı uygulamalardaki başarısı ve sensörlerinin diğer beyin görüntüleme yöntemlerine göre pilotu rahatsız etmeyecek daha ergonomik yapısı nedeniyle ölçümler fNIR sensör ve kontrol üniteleri ile yapılmıştır. İyi tanımlanmış çeşitli test senaryoları ile önce çevrim dışı olarak ölçümler yapılıp algoritmalar üretilmiş, daha sonra da bu algoritmaları kullanarak çevrim içi sonuçlar üretecek bir yazılım geliştirilmiştir. Elde edilen bulgular doğrusal olmayan algoritmalar kullanılarak tüm pilotlardan kısmi verilerle geliştirilen modellerin test sonuçlarının oldukça başarılı olduğuna işaret etmektedir. Yüksek doğruluk skorları veren modeller sırasıyla ancak bir birine çok yakın olarak RBF çekirdek fonksiyonlu SVM, LSTM ve RNN makine öğrenmesi algoritmalarıyla geliştirilmiştir.

Anahtar Sözcükler: fNIR, Mental İş Yükü, Pilot İş Yükü, Çevrimiçi Tespit

To My Family

ACKNOWLEDGEMENTS

I would like to deepest appreciate my supervisor Assist. Prof. Dr. Murat Perit Çakır. Without his support and knowledge this thesis would not be successfully completed.

I am also grateful Turkish Aerospace Industry (TAI) that is generous to utilize its resources and facilities.

I thank to my colleagues and my tactfully managers at TAI.

Lastly, I will always remember emotional support of my mother and sister.

TABLE OF CONTENTS

LIST OF TABLES

LIST OF FIGURES

LIST OF ABBREVIATIONS

ACROSS	Advanced Cockpit for Reduction of Stress and Workload
ANN	Artificial Neural Network
API	Application Brain Interface
ATC	Air Traffic Controller
BCI	Brain Computer Interface
CPDLC	Controller Pilot Data Link Communication
ECG	Electrocardiography
EEG	Electroencephalography
EMG	Electromyogram
EOG	Electro Oculogram
ERP	Event Related Brain Potential
FCU	Flight Control Unit
fMRI	Functional Magnetic Resonance Imaging
fNIR	Functional Near Infrared Spectroscopy
GSR	Galvanic Skin Response
hbo	Hemoglobin with Oxygen
hbr	Hemoglobin without oxygen
hbt	Total Hemoglobin Density
IR	Infrared
LDA	Linear Discriminant Analysis
LED	Light Emitting Diode
LSTM	Long Short Term Memory
MACD	Moving Average Convergence Divergence
MFD	Multi-Functional Displays
MW	Mental Workload

NAN	Not A Number
NIR	Near Infrared Spectroscopy
oxy	Subtraction of Hemoglobin with Oxygen Density and Hemoglobin without Oxygen Density
PET	Positron Emission Tomography
RBF	Radial Bases Function
RNN	Recurrent Neural Network
ROC	Receiving Operating Characteristic
ROI	Region Of Interest
SSCP	Set of Sums of Cross Product
stdev	Standard Deviation
SWAT	Subjective Workload Assessment Technique
SVM	Support Vector Machine
TAI	Turkish Aerospace Industry
TLX	Task Load Index
UAV	Unmanned Air Vehicle

CHAPTER 1

INTRODUCTION

In the aviation domain, the ability of pilots and operators to vigilantly perform their tasks is critically important for flight safety. Due to its influence on pilot's vigilance and situational awareness during both routine and critical episodes of flight, the mental workload levels of pilots have a direct influence on safe and successful fulfillment of flight tasks. Therefore, methods for reliable monitoring of the changes in the mental workload levels of pilots are strongly emphasized in the aviation community. Such methods not only enable the implementation of more effective precautions for improving flight safety, but also have the potential to guide the design of future cockpit layouts and additional functions for aircrafts which will cause minimum drawbacks for the pilots. However, there is no widely accepted definition for the concept of mental workload and existing measures are primarily based on subjective survey-based instruments. Therefore, developing mental workload monitoring methods is still a subject of extensive research both in academia and industry.

Despite the lack of consensus on a common definition for the term mental workload in the aviation psychology and human factors domains, in the literature several methods have been proposed to estimate mental workload of pilots in the lab setting. The current methods primarily focus on the offline analysis of collected data in controlled lab settings during psychological test batteries that do not reflect the complexities of flight scenarios. Therefore, there is a need for online algorithms that can estimate and monitor changes in operators' mental workload in more ecologically relevant settings in aviation, such as during real or simulated flight scenarios.

Another important issue in this domain is to develop measures and methods that will not disrupt the pilot's operational performance. The excessive use of wired sensors attached to the head and the body of the pilot, and the additional adjustments needed to be made to ensure data quality (e.g. injection of conductive gels to improve electrode contact for

EEG) may affect the pilot's performance. In contrast, functional near-infrared spectroscopy (fNIRS) devices offer hardware configurations that allow the design of hand-band like sensors that are less intrusive and disruptive as compared to other brain imaging modalities such as EEG, Therefore, due to their portability and ergonomic design, fNIRS sensors offer advantages for the non-invasive monitoring of neural activity in the prefrontal cortices of pilots during simulated and real flight scenarios.

In an effort to address some of the gaps mentioned above, this thesis study aims to develop an online mental workload monitoring application based on fNIRS recordings obtained from real airline pilots while they were performing flight scenarios inside a certified Airbus A320 flight simulator. The data was obtained through the FP7 framework project called ACROSS (Advanced Cockpit for the Reduction of Stress and Workload). fNIRS is chosen as the brain imaging modality due to its ergonomic, portable and reliable design with a good balance of spatial and temporal resolution. Data collected from real pilots in a simulator environment is then tagged with mental workload levels in the time domain by considering factors affecting their mental workload levels that were designed into the flight scenario. Machine learning methods are then employed and contrasted with each other to find out to what extent changes in mental workload can be detected online by processing the features derived from optical brain imaging signals.

The rest of the thesis is organized in the following way. In the literature review chapter, firstly various mental workload definitions are given from the literature. Secondly, measurement methods of mental workload are illustrated in the aviation domain. Next, cognitive processes underlying the flight performance are explained. The findings of studies carried out with neurophysiologic measurements techniques in simulator environments are summarized. Lastly, fNIR applications/studies in the aviation domain are investigated thoroughly.

In the methodology chapter, the simulation environment and the experimental protocols used in this study are explained. Scenario definitions designed to create realistic flight operations are described. Then, the fNIR device used in the thesis is introduced. In particular, the scientific principles behind the fNIR technology, working mechanism of the fNIR device and outputs of this device are clarified briefly. The fNIR Soft program which provides a scripting tool that can process the streaming output of the device online is described. After that algorithms to predict mental workload levels of the test subjects are expressed. Firstly, an exploratory model is developed only by monitoring collected signal changes in the time domain with Linear Discriminant Analysis (LDA). The model's predictive power is evaluated over the data set and the observed inadequacies of this approach are discussed. In order to address the identified limitations, a new approach is developed by considering the factors affecting mental workload of the pilots and reports prepared by the test pilots after completion of the flight scenarios. The classification methods employed in this study, including LDA, support vector machines (SVM), multilayer artificial neural networks (ANN), recurrent neural networks (RNN)

and long-short term memory (LSTM) as well as the ways in which these methods are configured and tested in the context of this study are introduced.

In the results chapter, graphs and tables derived from the analyses explained in the method chapter are reported. SPSS results of primitive method with LDA and online process graphs indicate mental workload changes considering with pilots' signals are reported. After that enhanced method results are given. Mental workload distributions on each scenario and each test pilot are shown. Furthermore general workload distributions are also given with both tables and graphs. All graphs, confusion matrix tables are illustrated based on the used algorithms separately. The effects of the algorithms' inputs can be observed on these graphs.

In the discussion and conclusion chapter, results derived from the methods chapter are discussed. Selection of used inputs (raw data types, features, and voxel numbers) is explained, and the LDA, SVM, ANN, RNN, LSTM algorithms are compared in terms of their classification accuracy. Advantages and disadvantages of each approach is evaluated. Parameter tunings (C, gamma for SVM, number of hidden nodes in ANN etc.) are handled. Feature weights for LDA are expressed. Tools, hardware and software environment for analyses and running of algorithms are detailed. Finally, in this chapter, crucial findings are emphasized. The study concludes with the limitations of the thesis and an outline of possible future works .

Supplementary materials that complement the analyses and the data collection process are presented in the appendices. In the appendix part, test pilots' self-evaluation plots of their mental workload levels during each mission are provided. Moreover, parameters that are found to significantly affect the mental workload level during the flight are listed. The combinations of these parameters which are derived from performed tests vs. manually assigned mental workload levels are given. Furthermore, model input combinations vs. accuracy scores for each algorithms used in all analyses are listed. Graphs presented in the results chapter are derived from these tables.

CHAPTER 2

2. LITERATURE REVIEW

In this chapter, major concepts and phenomena used in the thesis will be explained in reference to the related literature. Firstly a summary of the mental workload literature is given. Then, brain-computer interface (BCI) studies related to mental workload monitoring are reviewed. Moreover, background information on flight procedures and pilot tasks which contribute to pilots' mental workload are provided. Next, the importance of workload monitoring of pilots during flight is illustrated. Finally, the working principles of the fNIRS portable optical imaging technology employed in this study for mental workload monitoring are described.

2.1. Mental Workload

Although the use of the term "mental workload", which is also called as cognitive workload, has become widespread since 1970s, it has no commonly held definition in the literature [1]. Since direct observation of this abstract concept is not possible[1], multiple mental workload definitions have been proposed. One of the proposals define mental workload as the working ratio of the brain to overcome the given tasks, which can be independent of successful completion of those tasks[2]. Thus, performance measurements of operators are not enough to identify the level of their mental workload. For instance, during an experiment two participants may complete the same task with similar performance scores, but one of them may have used less mental resources and had more free cognitive reserves to be allocated on different parallel tasks. On the other hand, the second subject may have dedicated all of his mental capacity for the single task. Therefore, the mental workload level of the second participant can be higher than the first one, even though their behavioral performances appear to be similar[3].

Hancock and Chignell give two different statements for mental workload;

- Mental workload shows a process whose inputs determined by specific requirements and aim is to meet these requirements with mental effort by independent of operators (experimenters)[4].
- Mental workload indicates relationship of task difficulties and mental sources which are allocated to handle these difficulties. Mental workload depends on

specific operators (experimenters). Even past performance of an individual operator affects evaluation of over all workload detection[4].

Cain provided the following list of mental workload definitions obtained from related literature[1]:

1) "Mental workload refers to the portion of operator information processing capacity or resources that is actually required to meet system demands."[5]

2) "... mental workload may be viewed as the difference between the capacities of the information processing system that are required for task performance to satisfy performance expectations and the capacity available at any given time."[6]

3) "… the mental effort that the human operator devotes to control or supervision relative to his capacity to expend mental effort … workload is never greater than unity."[7]

4) "... the cost of performing a task in terms of a reduction in the capacity to perform additional tasks that use the same processing resource."[8]

5) "... the relative capacity to respond, the emphasis is on predicting what the operator will be able to accomplish in the future."[9]

All these definitions prove that, people do not agree with each other to get universal mental workload definition.

It is also important to state that there is a very strict relationship between emotional strains and mental workload. While Gaillard explains that both workload and stress are arisen depending on peripheral factors, implying two different theories lie behind to these concepts. He notes that workload can be represented better with a two dimensional model consisting mental – emotional strains[10].

One of the most interesting points of view was developed by Colle and Reid. They imply that, mental workload should be evaluated by considering the related task and performance which are extended over a period of time. According to them, mental work average (not instant measures) provides more accurate mental workload detection[11]. Although they tried to specified a specific time interval to find best mental workload estimation with three experiments, they could not exactly achieve this aim[1]. Time interval for mental workload evaluation issue is also studied in this thesis.

2.2. Measurement Methods of Mental Workload

It has not found that a general measurement method of mental workload which indicates a scalar quantity and applicable for all samples yet. Therefore in the literature, there are several disparate methods. On the other hand Jex states that mental workload is released based upon cognitive activities such as focusing on interacting task accomplishment, deciding on strategy, difficulty level and making effort. Starting from this point of view Cain implies that it is possible to develop a generic cognitive measurement strategy such that workload can be defined as a function with single variable and estimate mental workload with any character[1], [12].

Roscoe, Ellis, and Chiles, first time (1979) studied on mental workload measurement methods. They tried to understand state of the art by reviewing the literature starting date is 1950s. At the end, they concluded that mission requirements, experimenter capabilities affect mental workload[13]. In 1987, same team made another studies and achieved to categorize mental workload measurement techniques as "Objective Techniques" (has two subcategories: Performance Measures, Analytic Techniques), "Subjective Techniques", "Physiological Techniques", "Combined Techniques"[14].

In one of the articles, Ayaz clearly summarized that there are four major methods to evaluate mental workload[3].

The first one is personal scoring. In this method, experimenters are asked to evaluate performance of themselves and difficulties of task levels. Test subjects report how they have difficulty in the task. This method is very practical and commonly used. However it has an important disadvantage. If they are required to evaluate task and their mental effort during task execution, they can give unhealthy report due to intrusive situations. Else if they are asked after the task, they can make subjective evaluation. Therefore, result can be distorted[3]. SWAT (Subjective Workload Assessment Technique) is widely used rating scale measurement method example[1]. It uses predefined, useful criteria. At the first phase of SWAT, scales of predefined properties are determined by training of the experimenters. At the second phase, the experimenters are asked to evaluate task difficulty and their performance[15]. NASA Task Load Index which was designed by Hart and Staveland is another example of self-scoring method[16].

The second method is workload evaluation by observing behavior of the test subject during task execution. Speed of response, correct task performance and score are used criteria to measure experimenter mental workload[3]. For instance, Dick de Waard used this method by measuring drivers' mental workload [17]. He records standard deviations of lateral positions of drivers and steering wheel movements. After that, he associates the results with mental workload levels of drivers.

Usage of secondary task loading while the participant performs primary task is another workload measurement method[3]. For instance consider the task which we used in this thesis. While the pilot performs flight procedure in the cockpit simulator environment, experiment instructor interrupt the task and asks the pilot a question irrelevant with the task. Response of the pilot gives valuable information about the mental workload to which he is subjected. For example, sequential reaction – time tasks are used as dual task which are primary and secondary in study of Schvaneveldt, Gomez and Reid[18]. However they also imply that it is not possible to be sure which task is treated as primary, which task is treated as secondary by test subjects.

Final methodology is physiological measurements. Changes in certain body functions such as iris movements, pupil dilation, eye blinks, blood pressure, heart rate, skin temperature can reflects mental workload level[3]. Measurements of these physiological factors with specific devices during task execution not only give continuous (online) information about mental workload but also provide objective results. However its drawback is that, physiological activities mentioned above can have several kinds of sources different than mental workload. For example, drinks, medicine taken before the task can change skin temperature or reflexive response which can be irrelevant with

mental workload might affect eye blinks etc. In that point data fusion should be applied carefully to get mental workload data through different measurement sources.

In the following tables, features of physiological techniques to be explained are given.

Table 1: Comparison of BCI Techniques[19].

	Spatial Resolution	*Temporal Resolution*	*Source of Signal*	*Restrictions on Subject*	*Invasive*
EEG	Approx. 1cm	ms	Post-Synaptic Potentials	Seated	No
PET	4-6mm	>10s	Tracers in blood used to measure glucose/oxygen metabolism	Injection or inhalation of radioactive tracer	Yes
fMRI	2mm	>ls	Paramagnetism of deoxy-hemoglobin	Complete rest supine	No
N1R	Approx. 1cm	>ls	Hb/HbO changes (slow optical signal) Neuronal firing (fast optical signals)	Seated/supine slight movement allowed	No

Table 2: Spatial and Temporal Sensitivity Comparison of BCI Techniques[20].

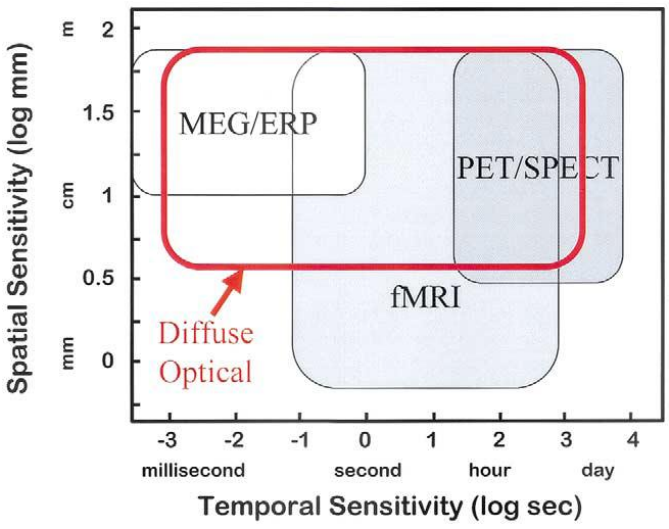

Measurement techniques on neural system such as EEG (Electroencephalography), ERPs (Event Related Brain Potentials) handle this problem with using electromagnetic signals. Information obtained from these technologies includes purer mental workload data with high temporal resolution (refresh frequency of a single scanned object). However they have restricted spatial resolution (region to be scanned in a unit)[21]. Moreover they are very sensitive to electromagnetic fields artifacts. To isolate electromagnetic interference, special test equipment should be used[22]. It places a burden to set test environment, test execution.

Unlikely EEG and ERPs, PET (Positron Emission Tomography) and fMRI (Functional Magnetic Resonance Imaging) consider hemodynamic response instead of electromagnetic signals. Besides, they avoid from effects of electromagnetic fields artifacts. Another advantages of PET and fMRI with respect to EEG and ERPs, they provides high spatial resolution. Since PET and fMRI deal with hemodynamic activities, their working mechanisms are slower than electrical signals handling on neurons mechanism which is principle of EEG and ERPs. Hence, PET and fMRI have lower temporal resolution[20]. Furthermore, usage of radioactive isotope in PET method causes unrepeatable experiment. It also limits usage of PET for children[3]. In contrast, fMRI is safer and more noninvasive neuroimaging than PET. Measurements of fMRI are very accurate with high resolution. Due to these advantages, fMRI is accepted as "gold standard" among mental activation monitoring techniques[3]. Handicap of fMRI is needed costly and cumbersome equipment. In aviation sector, it can be used in ground control station but in the cockpit environment current fMRI technology is impossible to use due to both uncapacious and uncomfortable structure. Moreover it requires a large well qualified staffs. Therefore, in the literature there are fewer mental workload measurement studies using fMRI than studies using EEG or fNIR. Similar to fMRI, fNIR works based hemodynamic measurement. However fNIR has more portable system to fMRI. It makes sensitive measurement. Although fMIR measurements are more accurate and called as "golden standard", size of fNIR equipment and practical usage make it as an optimum method for many platforms.

2.3. Brain Computer Interface Without fNIRS

Brain Computer Interface is a system that collects neurophysiological signals from human brain and gives them as input to special devices which processes to control external environment [23]. BCI is applied also for measurement of brain activities to use them for several studies [24]. Mechanism of BCI system can be figured as shown in Figure1.

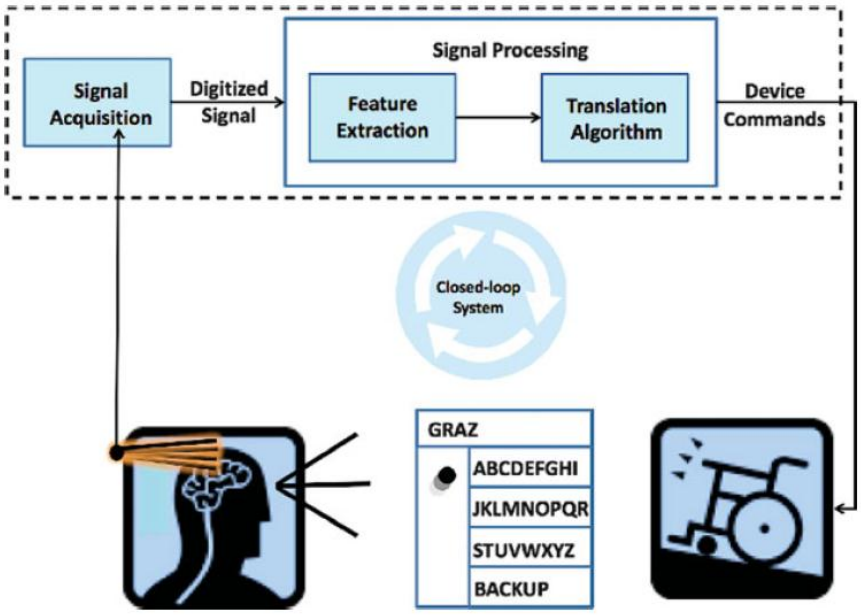

Figure 1: Subsystems of a BCI System[25].

Formerly BCIs are generally designed for dealing with health problems of human. People who cannot move their muscles due to disease such as Lou Gehrig's disease are supplied to communicate with the medium by interpreting thoughts in their minds or by controlling their arms, foots thanks to BCIs. Later, with improvement of software applications and hardware devices, usage of BCIs became widespread in different areas such as entertainment sector. Controlling of keyboards, monitors without touching them can be possible. Therefore healthy people started to be familiar with BCIs for fun[25]. Moreover BCIs are used for reducing workload of people who are very busy with several different tasks which should be done in a specific time. Measurement of human brain signals for different recoveries is another area of BCI which we studied on in this thesis. Meanwhile Allison mentions an issue on BCI concept. He notes that, getting usage areas and number of people gaining insight about BCI larger and larger brings same negative feedback. End users get unrealistic wrong expectations and have wrong idea without doing sufficient research. In the media, unsafety and unethical reports are released, even in scientific literature. Therefore he believe that an infrastructure containing terms, definitions, methods, ethical issues etc. should be developed[25]. Whereas, Allison thinks that BCI lives its "Golden Age" thanks to new applications, and devices support flexible and reliable measurements[25].

Sourina, Wang, Liu and Nguyen developed a concentration and stress management training system by using EEG signals[25]. Collected EEG signals from the brains are processed by fractal based algorithms and obtained values are used as inputs to the virtual reality games which test subjects play during the experiments. Experimenters are tested and trained with two applications; "Shooting" game is designed for measuring of stress. The mission of this game is to shoot flying objects. "Breaking Wall" is second application; the wall is broken according to concentration level of the experiment. With the feedback mechanisms between the applications and measured brain signals, 2D/3D games are changed dynamically and experimenter response is updated. Usage of fractal

algorithms in this experiment provides more accurate and efficient results with respect to other traditional neurofeedback algorithms. Being real time experiment is another advantage of the experiment. However the limitations come from nature of EEG mentioned in section 2.2 (Measurement Methods of Mental Workload) are drawbacks of this experiment.

Chaouachi, Jraidi and Frasson created mental workload model with EEG signals for intelligent systems[26]. They purpose to detect cognitive workload of the learners and improve communication and interaction methods. By this way Chaouachi, Jraidi and Frasson believe that an intelligence tutoring system could be developed. The experiment is performed in non-laboratory environment with two phases. At the first phase, brain signals are collected from test subjects via 6-channel EEG headset, two video feeds and devices. Beginning of the phase, all the subjects (17 participants) close their eyes during 5 second and keep eyes open in following 5 second to take baseline used determination of neural reference. Then, three tasks are given successively to derive workload indexes. At the second phase, obtained indexes are analyzed and validated to train mental workload model using Gaussian Process Regression which is a machine learning technique. Developed workload model is also supported by NASA_TXL subjective workload technique to compare results and examine their correlations. At the end of the study authors observed that model results are correlated with NASA_TXL result. Moreover they conclude that performance scores and mental workload level are not linearly related with each other opposed to laboratory condition. Having offline analysis approach and not considering experimenter profiles to detect threshold signals, tasks are accepted as vulnerabilities of this study by authors. For future work, they plan to study on these issues.

Moreover in the article of this experiment, authors mentioned that developing EEG index for workload assessment was studied before with different machine learning technique. Wilson achieved 90% of classification accuracy of workload level using Neural Network Artifact on pilots during flights[26], [27]. Kohlmorgen performed similar study on drivers with Linear Discriminant Analysis[26], [28]. Besides, Support Vector Machine technique is used in different study but same aim by Heger. Results are satisfied with 92% of classification accuracy[26], [29]. However they are only two classes which are low and high mental workload state. Three level classifications (low, medium, high) as we tried to determine causes more complex result to handle.

There are few studies on cognitive workload detection with fMRI due to the reasons explained in the previous section (2.2 Measurement Methods of Mental Workload). Korsnes and his colleagues made an experiment to monitor mental workload in occipitotemporal, lateral precuneus and medial precuneus regions[30]. In this study authors asks 16 participants to detect real and unreal objects visually. Two presentations are performed. Behavioral procedures, fMRI measurements and ROI (region of interest) analyzing are performed. For fMRI measurement top-hat elliptical quadrature birdcage head-coils are placed on experimenters' heads. Then bite-bars, formed with each participant's dental impression are used to eliminate noisy signals due to head movement. For data processing, SPM2 statistical analysis tool (*www.fil.ion.ucl.ac.uk SPM*) is used. After analyzing of the result, authors conclude that, occipitotemporal, lateral precuneus regions are related with object priming. Whereas medial precuneus is more related with mental workload activations. Moreover they realized that repetitive events reduce brain

activities including mental workload. In fact this reduction is observed more on unfamiliar objects than familiar objects. Although mental workload is measured in this study, it is not a main mission. Moreover investigated brain regions are different than prefrontal cortex which we in interested in this thesis. In the literature, there is no any kind of study to focus on prefrontal cortex to detect mental workload by using fMRI. However many labors focusing brain activations except for workload are placed in the literature. For instance, in 2008, Rota studied on brain activations driven by language processes with fMRI. He evaluates data in real time[31], [32]. Real time processing is an important development. Indeed, until 2004 there were no any online BCI with fMRI due to time consuming data analysis[33]. In 2004, Yoo implement one of the first real time BCI applications with fMRI. He also mentioned in the article about his study that fMRI is economically unfavorable[34]. Sitaram worked on emotional behaviors of criminal psychopaths with fMRI and gave therapeutic support for patients[35].

2.4. Measurement Method Based on fNIRS

Near Infrared Spectroscopy is an optical measurement method to capture brain activations by monitoring cerebral oxygenation changes. It was firstly introduced to the literature by Jobsis in 1977[36]. In 1990s, functional near infrared (fNIR) technology became a viable alternative to existing brain imaging modalities due to the fact that it provides safe, non-invasive and low cost imaging of the brain. [37][21][38][39]. With the improvement of hardware and software usage of fNIR including on adults and children was spread dramatically in 2000s[40][41].

Working principle of fNIR is based on absorption of infrared waves through tissue. Light with 700-900 nm wavelengths are absorbed mostly through hemoglobin molecules in erythrocytes (Figure 2). Other molecules such as water in the blood tissue cause minimum absorption. Also skull and other tissues have semi translucent features for 700-900 nm near infrared. By considering of these facts, characters of reflected lights emitted with an infrared light source placed on skin, give valuable information about hemodynamic changes in blood. Photons from light sources to skin influence tissues. Light intensity decreases while passing through tissues due to refraction and absorption. With infrared detectors which are also placed on skin strategically with respect to light source reflected photons are captured. Monitoring of light intensity changes by this method provides calculation of optical specifications of the region between light detectors and tissues where light passing through. Since blood flow and blood absorptions are the most influencing factors of light intensity changes, it is possible to monitor hemoglobin intensity changes via fNIR technology.

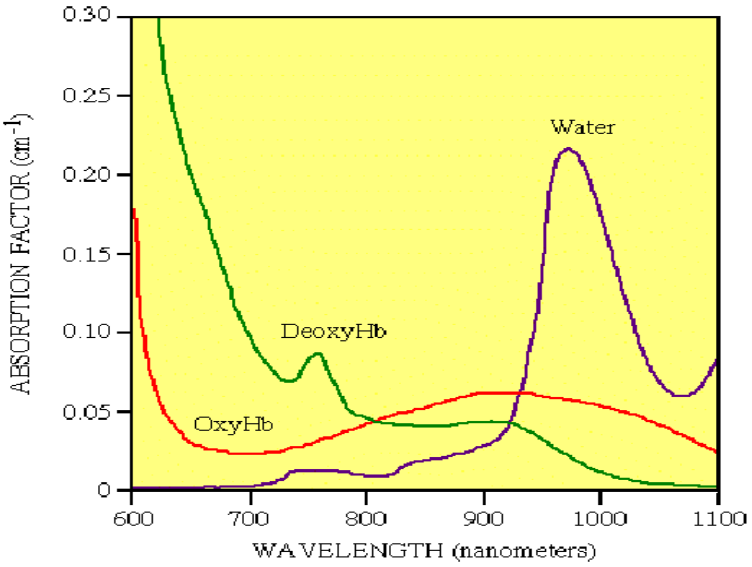

Figure 2: Absorption Spectrum in Near Infrared[42]

Most effectively, photons are refracted and absorbed partially during interferences of the lights and hemoglobin. Absorption intensity of the light is directly proportionate to amount of methemoglobin (oxy hemoglobin). As is known, oxygen which is needed for working of neurons is transferred with hemoglobin. With working of brain, oxygen demand consequently arterial blood supply is increases. Increasing of arterial blood flow and volume mean increasing of oxy hemoglobin number. This reactions cause infrared light to be absorbed much more. fNIR principled to this physical mechanism enables to trace changing of cognitive functions which are related with working of nerve cells.

2.5. Aviation World and fNIR Based BCI Applications

Flight simulators have critical roles in contemporary flight training since they not only provide pilots to use realistic flight instruments but also allow make mistake. Simulators help pilot candidates prepare actual flights by specializing on flight controllers. They enable experienced pilots to keep their knowledge and skills on flight procedures fresh. Moreover simulators provide training of the cases which cannot be tested on real platform due to containing life critical dangers but having occurrence probabilities. These cases can be performed safely and with low cost via simulators. Another advantage is that new developed avionic design alternatives can be tested by pilots with usability perspective on simulator platforms more easily before serial production.

Although improvements on aviation technology support pilots with high-tech equipment and decrease workload on pilots, it is expected from pilots that they should maintain their situational awareness, detect possible problems/failures on time and make whatever it takes, and perform related procedures. According to statistics of accident investigation reports of International Civil Aviation Organization (ICAO), 26% of all aviation accidents have been occurred because of the factors affecting cognitive states of pilots[43]. When considering accidents involving death, this ratio increases much more. Also The British Civil Aviation Authority reported than only in 2009, 32 recorded events

occurred when pilots were incapacitated during flights[44]. For these reasons improvement of the systems which are able to monitor cognitive workload of pilots safely are very important to prevent potential accidents.

2.5.1. Cognitive Processes on Flight Performance

In the literature of human factors in aviation, basic cognitive components on pilot performance are expressed with cognitive concepts such as cognitive workload, situational awareness, divided attention, mental fatigue/incapacitation and drowsiness. In the simulator environments these kind of cognitive processes are evaluated mainly with behavioral information. Behavioral information is analyzed via:

- measuring of correct answers to the questions which are asked to check awareness of pilots about current situation by flight trainers stopping flight scenario,
- success level of the tasks and
- submitting of surveys to take idea of pilots how much having difficulty during the tasks subjectively such as NASA-TLX.

While studies on simulator trainings show that experiences on those platforms make a great contribution on real pilotage experiences, in the literature it is stated that comprehensive and innovative approaches are needed to increase effectiveness of simulator trainings[45][46][47]. Draw backs of behavioral information is one of the major reason to be in searching of new approaches. For instance, performance of some pilots could decrease sharply in flight scenarios including secondary task such as mental arithmetic with routine flight task (primary task), while performance of same pilots are very similar with others during normal flight missions. This shows that pilots can become different with each other based on mental workload capacity with same performance[48]. In 2011, Borghini observed that same flight missions could be caused different mental workload on different pilots, so pilots using more mental workload capacity responded to events during the task with delay. However more training provides increasing of overall mental workload capacity and decreasing of the capacity using in the same task. By this way, pilots could manage to events more successfully[49]. This kind of results impossible to derive from behavioral information promotes to find different methods to make more healthy deductions. Therefore in the literature, interest in mental measurement techniques, especially evaluation of pilot cognitive workload objectively is increased every passing year[50].

2.5.2. Enrichment of Simulators with Neurophysiologic Measurements

Processing and usage of neurophysiological data obtained from pilots and making it a part of trainings on new generation flight simulators is objective of major part of R&D researches which are conducted to meet needed explained above (2.6.1 Cognitive Processes on Flight Performance). Pioneer studies on this area investigate relationship between neurophysiological parameters such as brain waves oscillation, heart rate rhythm, frequency of eye blinking, eye focusing, muscle activity, skin conductivity with cognitive states of pilots by using electroencephalography (EEG), electrocardiography (ECG), electro oculogram (EOG), electromyogram (EMG) and electro dermal (GSR/EDA)[51][52][53][27][54]. Obtained results refer that changes of pilot' cognitive

states could be monitored by pattern recognition algorithms and statistical models developed based on the neurophysiological data[55].

Neurophysiological projections of cognitive processes having critical importance from the point of aviation are studied with EEG, ECG, EMG, EOG and GSR data. They are classified as direct methods focusing brain activities (EEG) and indirect methods monitoring physiologic effects of neural systems on body (ECG, EMG, EOG, GSR). In the studies using indirect methods, when workload of pilots increases, changes such as increasing of heart rate and eye focusing, decreasing of eye blinking frequency are observed[50]. However existence of other no cognitive factors having similar effects create difficulty on measuring of cognitive workload with a single type detector. For example, light intensity change in the cockpit and light emitted from flight instruments can affect blinking frequency similarly with cognitive factors[51]. Likewise breathing rate, anxiety, and muscle weakness cause changing of heart rate similarly with cognitive factors. For this reason, usages of indirect methods together with direct methods come to the forefront in the literature recently.

Studies with EEG most usage method among direct methods show that when attention deficit exists, power distribution on theta band decreases and changes happened on alpha band. When attention level increases because of mission level, power increases on theta band where monitoring on electrodes in pre-medium lateral and top-medium lateral[56][49][50].

Although important results and approaches are developed with pioneer studies, needs for realistic applications which would use the available data by combining it meaningfully and integrate neurophysiologic data with simulators have not been met yet[50]. One of the problems of current available methods is practical difficulties to collect data due to complex technical designs of aviation nature and simulators. Moreover data analyzing and evaluation are performed with offline methods after experiments. Still, online cognitive data processing simulators are not available in the market. It is expected that online data processing methods will be developed better by integrating in continuing R&D projects such as Advanced Cockpit for Reduction of Stress and Workload (ACROSS) project[57]. ACROSS offers an insight into designing of new generation cockpits for the future. Project partners create a civil aircraft simulator and integrate/demonstrate their studies on this cockpit.

ACROSS project aims to:

- improve situational awareness of crew,
- increase automation in cockpit,
- improve human machine interaction in cockpit,
- improve support in the case of abnormal conditions during flight[57].

In this project we study on collection of pilot's brain waves by using optical monitoring technique with fNIR, processing collected data and calculate a mental workload level continuously. Performing all processes with online and fNIR method create a great advantage to use this technology in the near future practically.

2.5.3. fNIR Applications in Aviation Domain

In the scope of a research project managed in Drexel University fNIR application was developed to train unmanned air vehicle (UAV) operators and monitor cognitive workload of them. It is observed that measures derived from prefrontal cortexes varied statically across test subject group according to their experience levels[41][58][59]. For inexperienced participants, approach and landing test scenarios are performed repeatedly in the simulator environment (Figure 3) during three weeks. These exercises include 9 seasons and each season takes an hour. Used scenarios are designed to reveal neurophysiologic effects of beginner pilots' behavioral development over time. It is achieved by preparing realistic and having great importance tasks. In the first scenario, test subjects are asked to aviate the UAV based on directives indication on the screens and return the UAV runway again. In the second scenario, successful landing of UAV approaching to the runway is the mission. In both scenarios, experimenters are subjected to bad air conditions and they are expected to follow some speed and roll angle constraints.

Figure 3: Designed Simulator Environment[59]

It is checked that whether there are meaningful changes on total hemoglobin density (hbT) of participants collected from prefrontal cortex by monitoring via fNIR according to experience levels (beginner, intermediate, advanced) which improving day by day with ANOVA for single factor. Since findings deduced from previous studies[41] illustrate that inferior frontal gyrus of left prefrontal cortex region (AF7 region according to universal 10-20 system) measured from second channel gives stable respond, AF7 is focused area for this research. Statistical results prove that hbT quantities measured from second channel decrease with respect to increasing of experience levels ($F(2,24) = 1.26$, $p<0.01$). These results shows that improvement of experiences and skills gained in simulator environment and in time are possible to monitor from prefrontal cortex with fNIR. Also changes on fNIR signals with level variety are observed; at the beginner level fNIR signal trends increase (so neural activities increase) in time, but fNIR signal trends decrease (so neural activities decrease) when experience level upper and upper (Figure 4). Since real pilots do not participate in this study, it can be only said that effects of repetitive performances on mental workload capacity usage are shown. On the other hand, Figure 4 (on left side) presents distribution of fNIR signal trends on experience levels. At

the same time, it implies quantitative expression of cognitive reserve. In other words, getting more experience results with less mental capacity usage. Hence, pilots can respond to unexpected events faster with remaining mental capacity and this change can be displayed on prefrontal cortex with fNIR.

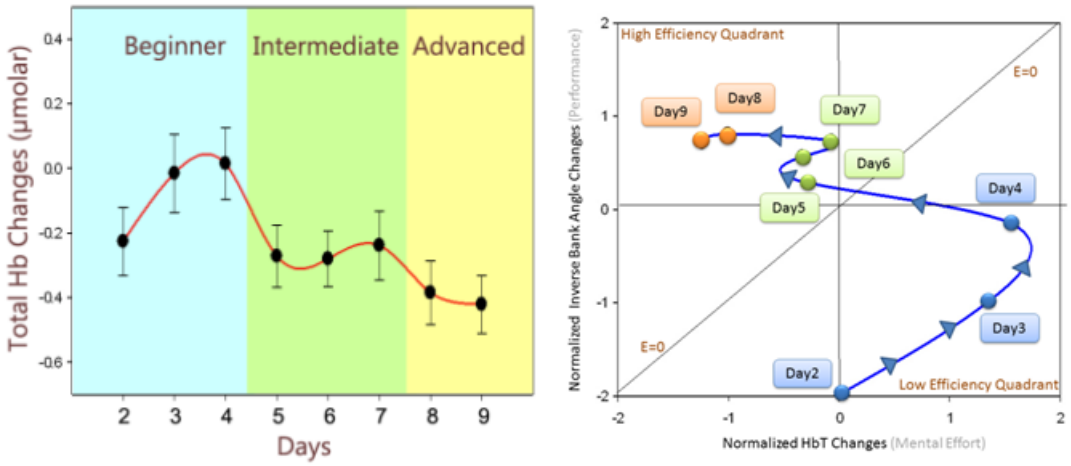

Figure 4: Left: Changes on fNIR Measurement in Time, Right: Performance vs. Mental Effort in Time[41]

In another study, changes on cognitive workload while performing given tasks in ecological valid environments are monitored with fNIR. One group air traffic controllers are submitted n-back tests and perform air traffic control missions with two different user interfaces[2]. In n-back test parts, air traffic controllers are asked to press a button according to repetition frequency of characters which are displayed on the screen and test subjects watch. During test, participants press button when same characters displays successively in 0-back case, press button when displayed character is same as previous step in 1-back case, press button when displayed character is same as two steps before in 2-back case and so on. Since number of characters should be keep in mind increase with increasing of n-back level, this test is used often in neuropsychology and human factors literatures[60]. In air traffic controlling test parts, operators use two types of interfaces between pilots and controllers. In the first missions, controllers contact with pilots via voice based interface. In the second missions, controllers contact with pilots via text based interface. Mission difficulties are increased by increasing number of aircrafts to be followed as 6, 12, and 18 systematically[61][62]. Results generated from measurements of fNIR signals on prefrontal cortexes are shown in figure 5. When related graphs are analyzed, it shown that activation levels on prefrontal cortexes increase parallel with task difficulties. Besides, results show us voice based user interface causes more activations on prefrontal cortexes than text based user interface. Therefore this study also explained that fNIR methods can be used for designing of new interfaces to consider mental workload of pilots.

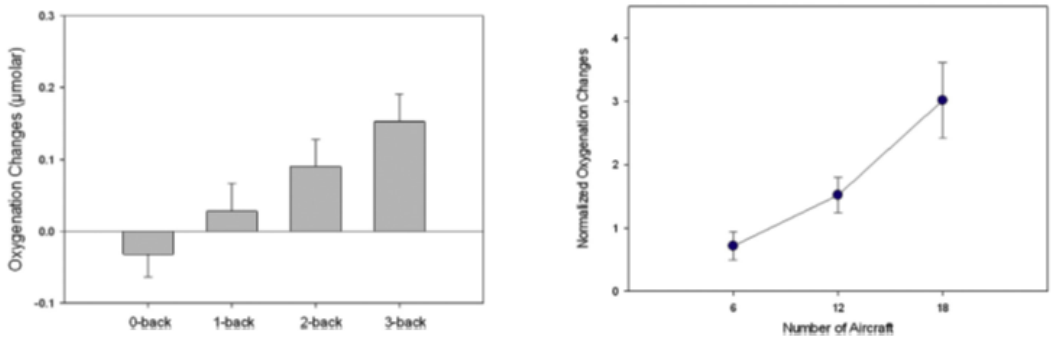

Figure 5: Left: Average Oxygenation Changes on hbo vs. n-back Test Level, Right: Average Oxygenation Changes on hbo vs Number of Aircrafts[2]

Gateau and colleagues completed a study in 2015[63]. Their objective is to development of an online fNIR based interference system to asses working memory. For those purpose, nineteen pilots are joined to experiments. Test scenarios involve listening ATC messages and dialing corresponding flight parameters in the autopilot systems by using four knobs of Flight Control Unit (FCU) which are speed, heading, altitude and vertical speed controllers in a flight simulator. For fNIR monitoring, fNIR100 with 16 channels device is selected and its software interface COBI Studio is used. This device and tool are same as what we selected for our thesis. fNIR100 collects fNIR data from prefrontal cortex and COBI processes and monitors signals for each channels. It is also mentioned that channels 8 and 10 are removed because of saturation. Moving Average Convergence Divergence (MACD) filter is applied in processing of first part to distinguish task states of pilots (on task – not on task). Moreover MACD eliminates trending, low frequency drifts, high frequency physiological and measurement noise of raw signals. With the help of literature, as features: 1-means of hemoglobin with oxygen (hbo) and hemoglobin without oxygen (hbr) changes, 2- mean amplitudes of hbo & hbr, 3- kurtosis (peakedness of probability distribution) of hbo & hbr, 4- skewness (asymmetry of probability distribution) of hbo & hbr are selected[64][65][66][67]. In the second part of processing phase, assessing of working memory levels (low - high) is trying to achieve. For this aim Support Vector Machine (SVM) machine learning algorithm is used. Low working memory tasks are defined by asking participants to set one major digit of flight parameter values such as 15 for speed 150, heading for 150 and altitude for 1500. In high working memory tasks, successive flight parameters are different with each other. For example ATC asks pilots to set speed 164, heading 235, altitude 8700 and vertical speed -1600.

For real time process Gateau and colleagues used sliding window. First 20 trial data in this window is used to train pilots and determine decision boundary of SVM. Next second 20 data placed also in the window determines working memory level of the pilot. MACD based state estimation results with 61.74% time, 58.24% mean specificity and 71.88% mean sensitivity accuracy. Latency is negligible because of speed of MACD processing (< 0.4 ms). SVM based MW load estimation results give 89.5% mean specificity and 72.1% mean sensitivity accuracy. Due to 16 second maximum sliding window offset, 15 second maximum sliding window length and 2 second total process time, working

memory load estimation is updated nearly each 32 second. Classification response is available in the worst case less than 3.3 second after pilot's response window[63].

Moreover, based on obtained result authors state that MW decreases when instructions are remembered. They also extract a topology maps to see neural activity of prefrontal cortex. From the map, it is observed that task difficulty changes modularity of oxygenation level in especially left and right dorsolateral of prefrontal cortex. They conclude that fNIRS is an appropriate methods for monitoring of MW load level.

At the end of the study authors explain some limitations. They illustrate that working environment is not realistic cockpit. It is simplified PC-based simulations and ATC communications were tried to be realistic. They also assert that delay time could be decrease with deeply study. Furthermore, accuracy of estimations could be increase by trying different model such as Hidden Markov Model. In fact using of more than one model at same time could be give more consistent results[63][68][69]. Another constraint is period of training part. Gateau and colleagues think that duration of training process should be decrease to use in real operations. Some real operational factors will affect working mechanism of designed system. For instance G-Force will affect blood flow or pilot's head movement will created motion artifact. Although last limitation is also valid for our study, it is out of scope since real aircrafts and movable simulators are not considered as our working environment.

In 2013, another offline experiment was designed to investigate mental workload during a simulated piloting task by using fNIR[70]. Durantin and his friends set a PC based simulation environment. During the tests, participants are expected to track target aircrafts labelled with color names. When any of the color name is indicated at right edge of the screen, test subject should approach the correct labelled target aircraft which placed at left edge of the screen by moving controllable own aircraft via joystick (Figure 6). 20% of indicated words are not color names such as read, grin to create possibility of making mistakes. Two different classifications are designed for the experiment; difficulty of control (easy, hard) and processing load (low, high). Difficulty of control is specified by varying the strength of the crosswind (no crosswind in the easy condition, strong crosswind in the hard condition) and the inertia of the plane (low vs. high). Processing load is specified with N-back-like sub task. For low processing load (in terms of working memory), tester should follow the aircraft labelled with color indicated at right (similar with 0-back). For high processing load, the aircraft labelled with color indicated at right but one cycle before (similar with 1-back). HbO_2 (hbo) concentrations from prefrontal cortex are measured with fNIR monitoring method and fnirSoft software tools. Hbo mean values are calculated via Matlab and these values are used to determine mental work level. Moreover heat rates of test subjects are measured parallel with fNIR measurement. After the tasks, NASA-TLX subjective evaluations are also performed.

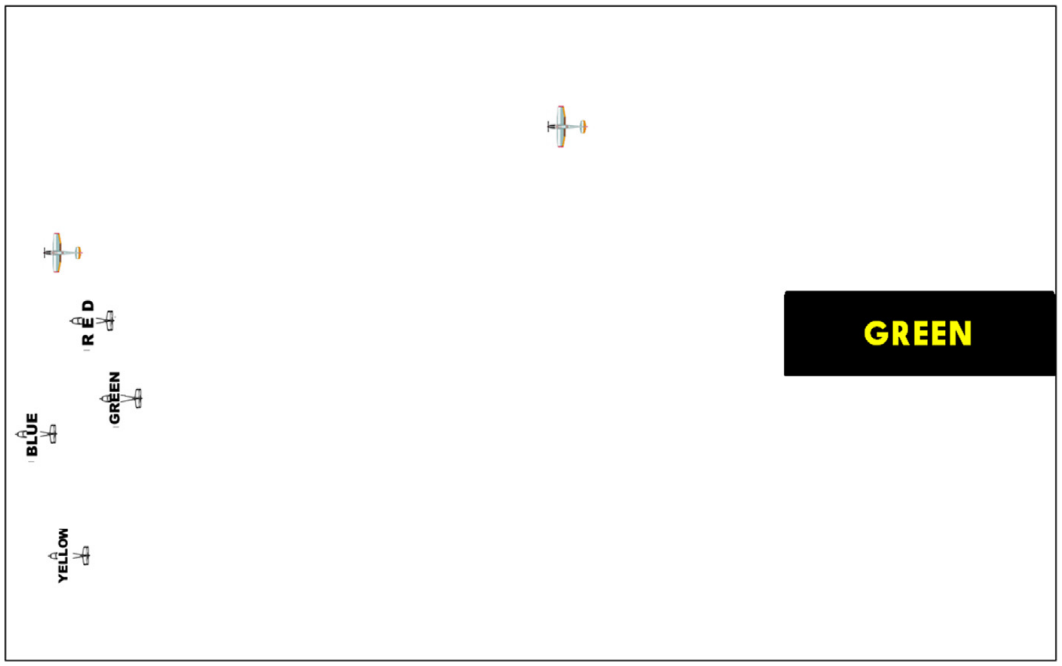

Figure 6: Screenshot of the Durantin's Experiment Setup[70]

Major effect of control difficulty is observed on optode 6 with ANNOVA results: F (1, 11) = 5.82 and $p<0.05$ showing an increase in hbo with an increase in control difficulty. Moreover it is observed that hbo concentration increases when high processing load in easy control condition is performed while hbo concentration decreases with high processing with hard control. (optode 3: ANNOVA results: F (1, 11) = 5.11 and $p<0.05$). This cause - effect is detected most clearly in optode 3 which placed in the left dorsolateral prefrontal cortex (Figure 7 left side). In fact same observation is made in all optodes with smooth changes. Important information gained from optode3 results is computing of correlation between measured data and performance scores. When highest level of hbo changes are measured, best scores are recorded shown in figure 7 (right side).

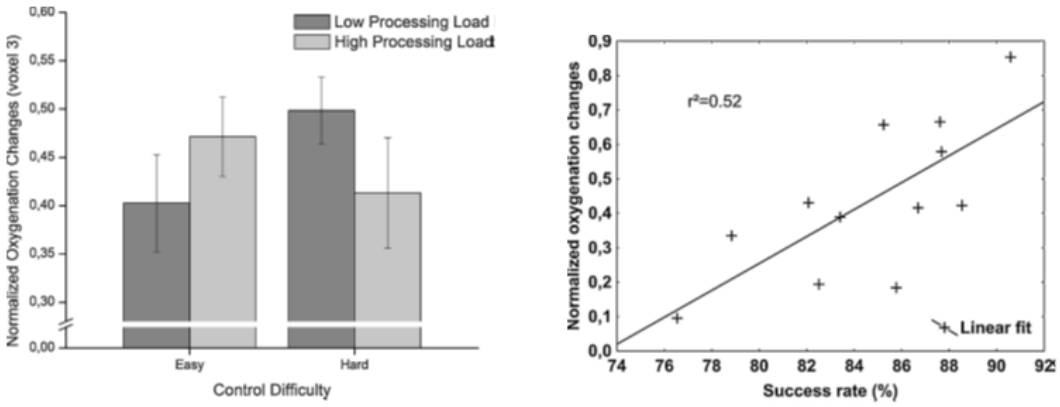

Figure 7: Results of optode3[70]

Authors also point that, hbo concentration vs task difficulty level graph has a U-shape. It means normalized hbo change increases correlated with task difficult level for a while, but then inverse proportion is seemed between hbo and task level. Durantin bases this

result on frustration on the participants in the very difficult tasks. Lastly they conclude that task performances are not enough to evaluate mental workload solely. fNIR measurement technique is suitable to monitor cognitive signals and gives important clues to detect mental work levels. In the future work, suggestion is using fNIR and another measurement technique such as eye movement, operator's response time.

In Karlsruhe Institute of Technology (Germany) a mental workload monitoring study is completed in 2014[71]. This study has provided continuously workload monitoring with fNIR and classification of workload with three different levels. Herff and other authors have also proposed to develop dynamically adaptable with behavior of the interface. Although experiments are designed based on n-back tests only (no another flight simulator etc.), three classes for mental workload levels and continuous measurement approach which are major objectives of this study are also our thesis goals. Used headband has 4 light sources, 8 receivers (2 sources& 4 receivers are left eye above, 2 sources& 4 receivers are right eye above) different than which we use. N-back tests are applied 10 test subjects whom did not experience before with n-back. In order to avoid from trend effect which is observed especially long term tasks, moving average filter is used by subtracting mean of 120 second before and after every sample from every Hbo (hemoglobin with oxygen) and Hbr (hemoglobin without oxygen) data point. Moreover, wavelet artifact removal method is used to compensate head movement effects. Although in the article of the study, it is stated that mean value of the signal in a specific window or mean changes between windows is simple and effective feature[71][72], Herff and colleague prefers slope of straight line fitted in a window as feature to able to use linear regression with a least square approach. Furthermore they reduce 16 features (8 channel * 2 data type – hbo/r) by using Mutual Information[73] and Linear Discriminant Analysis to classify data. In order to specify classes, optode signals are monitored and following graphs are obtained.

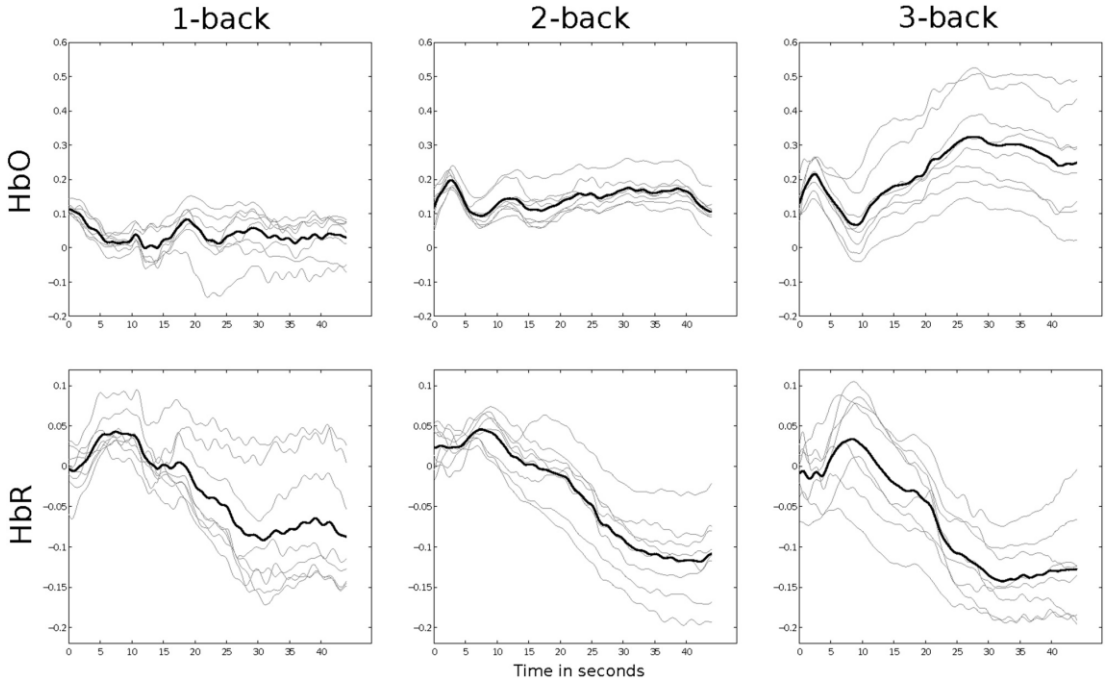

Figure 8: fNIR Signals from Optodes (Gray lines: each optode values, Black lines: mean of all optodes) [71]

As seen figure 8, positive slopes increase from easiest task (1-back) to most difficult task (3-back) for hbo and vice versa for hbr. Therefore slope feature is seen as a good choice to classify mental work level. Another important result is observation of offset between tasks. For 44 second tasks 10 second relaxes time give best classification accuracies. If relax time is not given between tasks, classification accuracies decrease since without offsets (relax time) test subjects are just beginning to memorize stimuli and work load is not experiencing yet. As expected classifications in 3-back vs relax phase has maximum accuracy value with 81%. Windows size using to process data and output a mental workload level is also affect accuracy level. As shown in figure 9, with 25 second – window length maximum accuracy score obtained. Decreasing of classification accuracy after 25 second is related with decreasing of instance number according to authors. Again in figure 9, it is shown that classification success between 1-back and 3- back is highest since difficulty difference between 1 – 3 back tests is highest.

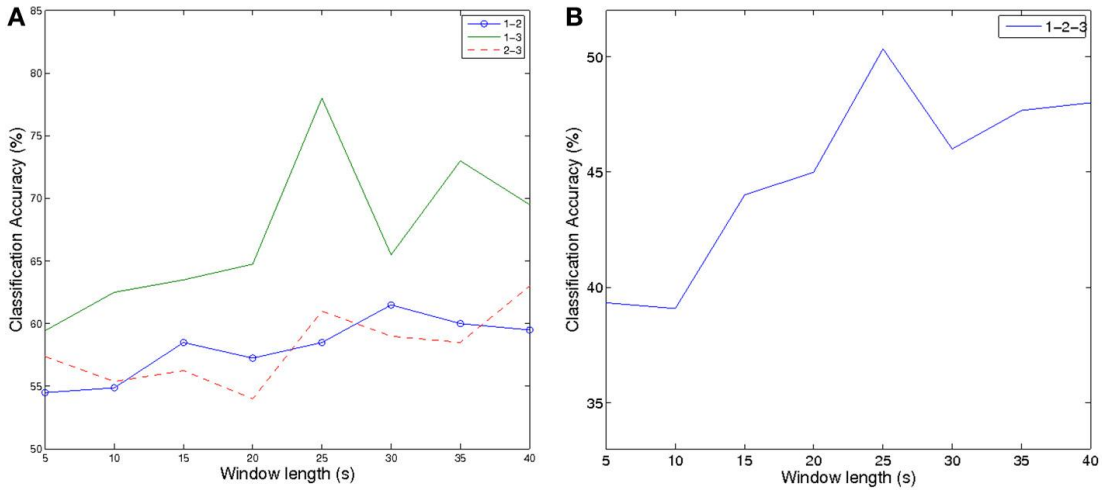

Figure 9: Classification Acc. vs. Window Length for Couple of Difficulty Levels (Left side) Classification Acc. vs. Window Length for All Difficulty Levels (Right side)[71]

It is conclude that even though further investigation is need to distinguish workload levels between each other more clearly, continuous monitoring and three level classification (this case is founded rarely in the fNIR literature) have been achieved. Authors point that fNIR has great potential to supply mental workload evaluation in daily life. In my thesis similar classifications are performed in aviation domain with real pilot fNIR data and in a realistic cockpit environment.

CHAPTER 3

3. METHOD

In this chapter the experiment environment and all system components are explained. Figure 10 shows the general structure of the system starting from data acquisition and ending with mental workload level estimation. After description of the experiment environment, details of each subsystem and used algorithms which are supervised learning algorithms are explained separately in next sections.

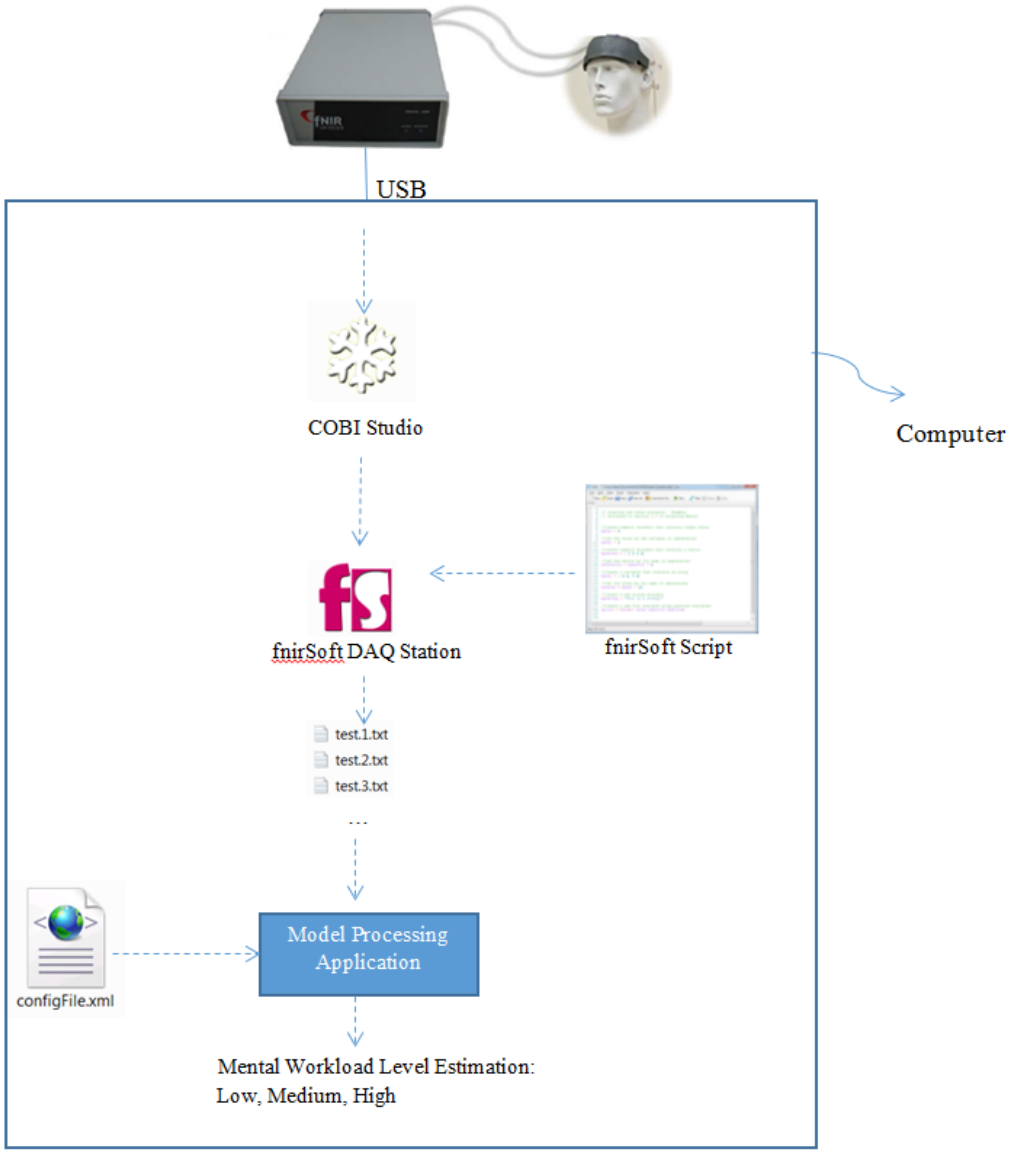

Figure 10: Structure of the System

3.1. Experiment Environment and Protocol

All data for this thesis is collected by using the infrastructure of the ACROSS (Advanced Cockpit for Reduction of Stress and Workload) project. The ACROSS project was carried out within the scope of European Union Seventh Framework Program. At the end of the project the following capabilities were aimed to be achieved:

- Reduction of workload of flight crew in critical parts of flights,

- Reduction of communication problems among human pilots and air traffic controllers by automatization of intercommunication between aircrafts and air traffic controllers,

- Removal of cross-check activities,

- Monitoring of mental workload and situational awareness of pilots during flight and suggesting interventions during emergency cases,

- Increasing of flying safety by using innovative feedbacks, controlling with voice, recognition of pilots' voice and faces[57].

With the goals listed above, a single-pilot cockpit concept is aimed to be developed for civilian aviation. Turkish Airspace Industry (TAI) joined the ACROSS project to lead the work package on pilots' online mental workload estimation by using fNIRS. Due to the information sharing restrictions of TAI and the overall project, not all details of the project and the conducted studies could be given.

Technologies for the project were developed by a consortium including tens of companies and universities. They are verified through acceptance tests designed by the project lead and the project is officially concluded in 2017.

From measuring of pilot mental workload to recognition of pilot face, several studies were conducted on the subjects. A certified Airbus A320 aircraft simulator is used for this purpose. The following figure illustrates the test environment and the employed operator monitoring technologies.

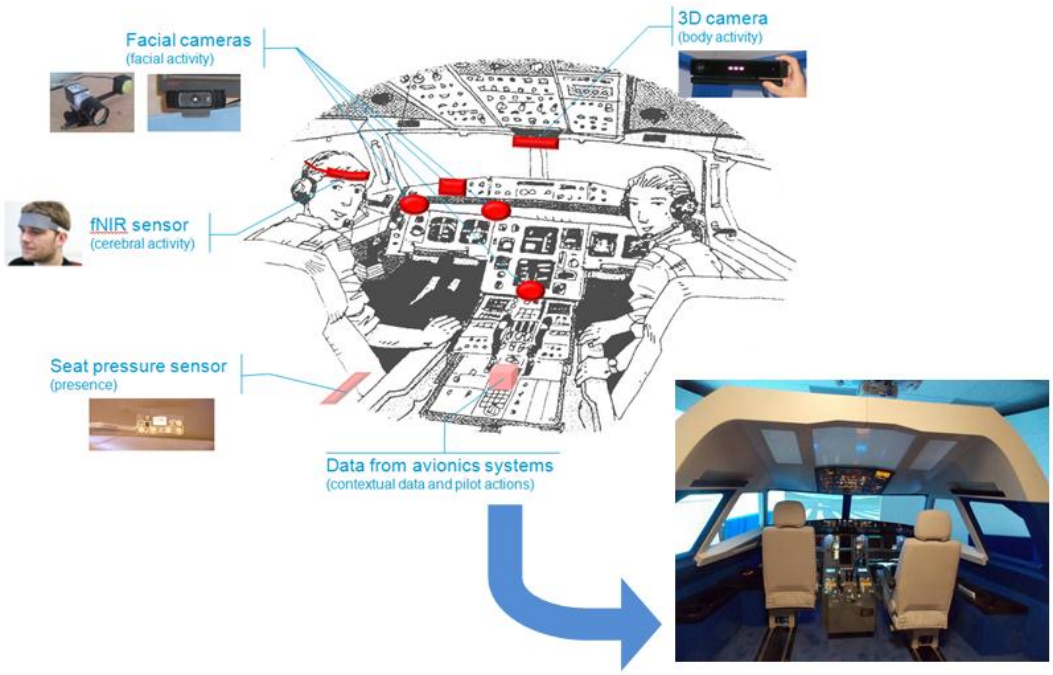

Figure 11: Test Environment[74]

8 test subjects were separately involved in the identical flight scenarios which we use to collect data. Test subjects were experienced pilots having 10712 of flight hours on average (minimum value of flight hours is 3500, maximum value of flight hours is 17000. Standard deviation is 5057). All of them are male. Test subject 5 is left handed and the others are right handed. They were asked to aviate the aircraft simulator based on the test procedure.

Each test consists of four scenarios. They are designed to be realistic by taking of aviation specialists and pilots.

Scenario0 - Free Play: It is designed to help test subjects to get used to the test environment. They familiarized themselves with the equipment and experienced the simulator instruments. They performed a simple flight that took about half an hour. Two test pilots did not participate in the free play scenario since they had already been familiar with the test environment during development of the simulator.

Scenario1 - Normal Workload Flight: This scenario included the execution of a normal landing on a runway after the cruise phase. It did not include a significant emergency event to create out of ordinary action. It includes all phases of a standard flight from takeoff to landing. It takes about an hour.

Scenario2 - Landing with Workload: The scenario started from cruise phase and included non-routine ATC directives in approach and landing phases (e.g. passing the airstrip and executing a fly-around) which are expected to increase the mental workload level of the pilot. The scenario took nearly half an hour.

Scenario3 - Landing with High Workload: Similar to scenario2 it started in cruise phase, but was carried out in bad weather conditions such as poor visibility. Moreover in approach and landing phases, the scenario included equipment fails and abnormal ATC directives. It takes about half an hour.

ACROSS Project members detail all scenarios as following below[74]:

Scenario0:

- "Start the simulation with aircraft on ground, at Airport 1
- Crew performs take-off from Airport 1
- Free flight from Airport 1 (for at least 15 min)
- At the end of the session, crew performs the descent, approach and uneventful landing at Airport 1. Good visibility and weather."

Scenario1:

- "Start the simulation in cruise, on normal long haul flight to Airport 1 (e.g. trans-oceanic cruise)
- No unexpected event during cruise (for at least 30min), pilot's solicitation (and workload) shall be minimal. No weather threat.
- 5 minutes before Top of Descent, crew performs the Descent briefing.
- Crew performs the descent, approach and uneventful landing at airport 1. Good visibility and weather."

Scenario2:

- "Start the simulation in cruise, in cruise to Airport 1, 15 min before the Top of Descent (same flight plan than in scenario 1, as a resuming of the previous mission - TBC).
- 5 minutes before Top of Descent, crew performs the Descent briefing.

- Crew performs the descent, and begins approach to Airport 1. Good visibility and weather.
- When A/C is at about FL100, ATC requests the flight to divert to Airport 2 (never flown by the crew).
- Crew re-route the aircraft, performs the briefing, descent, approach and landing to Airport 2. During this operation, PNF is expected to be less skillful than usual (then, perform his duty slower than usual, to increase PF's workload). Good visibility and weather."

Scenario3:

- "Start the simulation in cruise, in cruise to Airport 1, 15 min before the Top of Descent (same flight plan than in scenario 1, as a resuming of the previous mission - TBC).
- 5 minutes before Top of Descent, crew performs the Descent briefing.
- Crew performs the descent, and begins approach to Airport 1. Very low visibility, foggy weather. During the descent, attempt to distract the pilot with questions not directly related to the mission duty.
- When A/C is below Decision Height, late aircraft incursion on runway (just ahead of the aircraft) that triggers a sudden Go-Around.
- Crew flies the Missed Approach procedure.
- During the climb, during flaps retraction operation, an unexpected system failure occurs (flaps remain blocked in extended position).
- Crew performs a new landing attempt at Airport 1 (same or other runway)."

Each scenario is executed in given order above.

3.2. fNIR Device and COBI Studio

fNIR Model 1100 manufactured by fNIR Devices Company is used to image non-invasive oxygenation and blood volume trends in the prefrontal cortex. This product consists of a control box, a silicon headband housing the fNIR sensors with 16 channels, power cable/adapter and USB cable as seen in figure 12. COBI Studio software that is provided by the manufacturer was used for the visualization and initial processing of the data.

Figure 12: fNIR Model 1100 system

3.2.1.fNIR Sensors

The optical sensor pad contains 10 photo detectors and 4 IR light sources (LEDs) which are integrated into an elastic band as shown in figure 13. Each number represents channels. They are also called optodes or voxels. Therefore with fNIR sensor pad, 16 different regions in the prefrontal cortex of the human brain can be monitored.

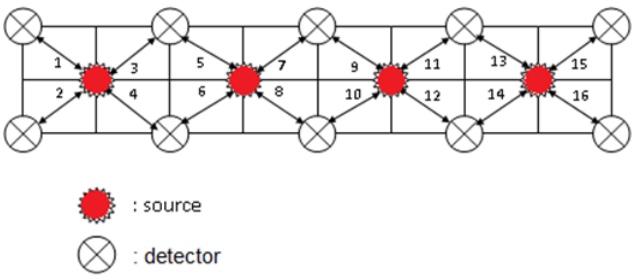

Figure 13: fNIR Sensor Pad[59]

For optical brain imaging 730 nm and 850 nm wavelength infrared rays are used. These wavelengths are selected by considering optical window of near-infrared range where most biological tissues absorb except for hemoglobin molecules. In order to check and measure the undesired ambient noise another wavelength 805 nm near infrared ray is used as third spectrum. When photons are emitted towards human head by the sources, some of them are scattered through the skin, skull, water and other tissues, but also most of them

are absorbed by hemoglobin with oxygen and without oxygen. Detectors placed at a certain distance away from the sources receives reflected lights whose characters are changed because of scattering and absorbing. During this activity, photons follow a kind of a banana path from the light source to the detector as shown in figure 14.

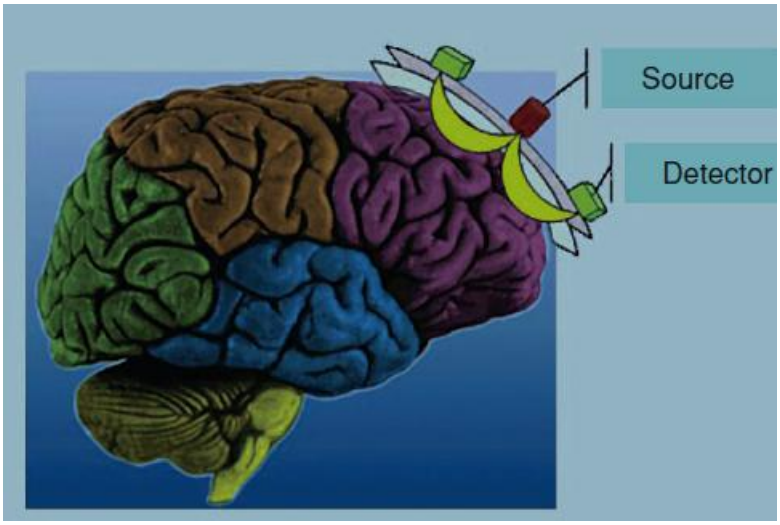

Figure 14: Photon Path[75]

3.2.2. fNIR Control Box and COBI

The sensor pad is connected to the fNIR control box via 2 proprietary signal interface cables. Through these cables signals are received from sensor. In control box, they are digitized and transmitted to computer where COBI Studio runs via USB cable.

Cognitive Optical Brain Imaging (COBI) Studio provides the user an interface to manage control box functions. With this tool many settings such as light source density, detector gains and frame rate of light are tuned. In our experiments:

- frequency of light: 2 Hz. Therefore data samples from 16 optodes are obtained every 500ms.
- LED current: Adjusts the amount of current running through the LED lamps, which in turn adjusts the brightness of the light source. Typical values range from 10-25 mA which is selected based on the skin color of the participant.
- Detector gain: Adjusts the sensitivity of the photo detectors.
- Get ambient light is ticked. It allows the experimenter to see ambient light levels in order to check for environmental noise due to poor contact between the sensor and the skin.
- Quarter1, 2, 3, 4 are ticked to obtain data collection from all 16 optodes. Optodes are organized into groups of 4, and depending on the experiment some of these groups can be turned off if they are not the focal regions. Figure 15 displays setting window of COBI.
- Port number: 6343. Since COBI is used as server to transfers all data to fNIRSoft tool, their networking is provided on a port which 6343 as default.

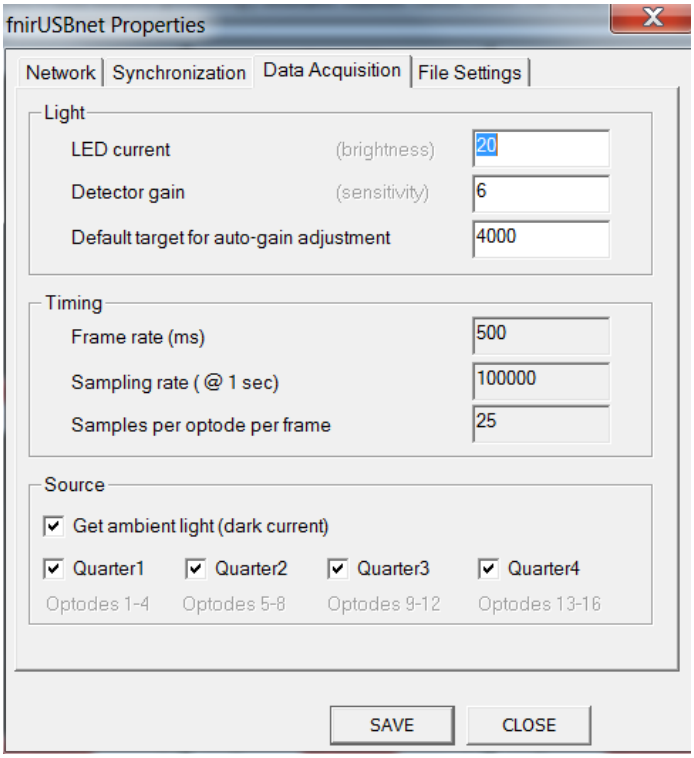

Figure 15: COBI Setting Window

After that, it starts running of control box. Continuous signals are monitored optode by optode at COBI screen as in figure 16. These signals are still raw data. It means processing for fnir imaging is not applied yet. Therefore they are in terms of millivolts.

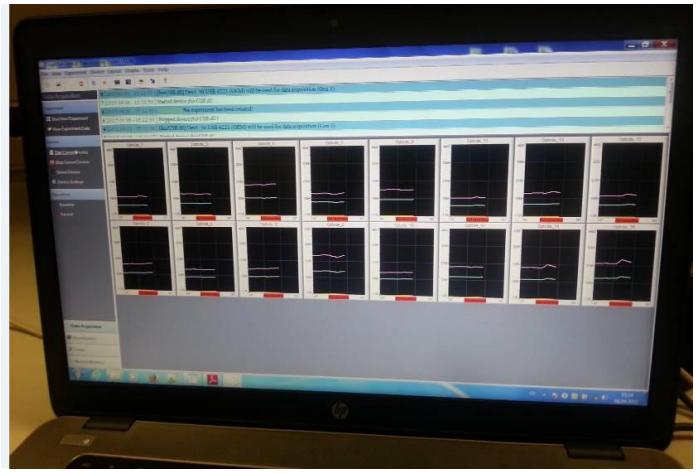

Figure 16: COBI Signal Monitoring

It is important that signals should not be saturated (exceeding of 4000 mV) and should not be very low (lower than 700 mV) to carry useful information about brain hemodynamics. Therefore, before starting the experiment, it is ensured that all optodes are placed well. If there is a weak sensor-skin contact, the signals obtained from the corresponding optode will be saturated or if there is not enough

IR isolation from the environment, signals will be too noisy. Figure 17 shows parts of the preparation of an experiment including inspecting the signal levels at each optode and the placement of the sensor pad.

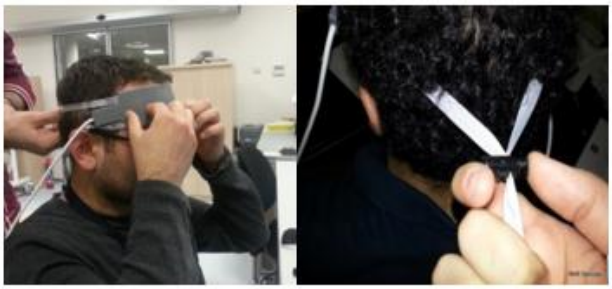

Figure 17: Placement of the Sensor

Once the setup is ready with acceptable signal strengths at each optode, a new experiment is started to record the collected data. The COBI takes baseline measurements for a duration of 10 seconds before it starts data recording. Recorded signals values are stored in a file whose extension is "*.nir*". When this file is opened with Notepad/++ or Excel, following form in figure 18 is seen. At each 500ms one line of data is generated. The meaning of all data columns are explained briefly in figure 18. When the experiment is finished, data acquisition process should be stopped with COBI to finalize the data file.

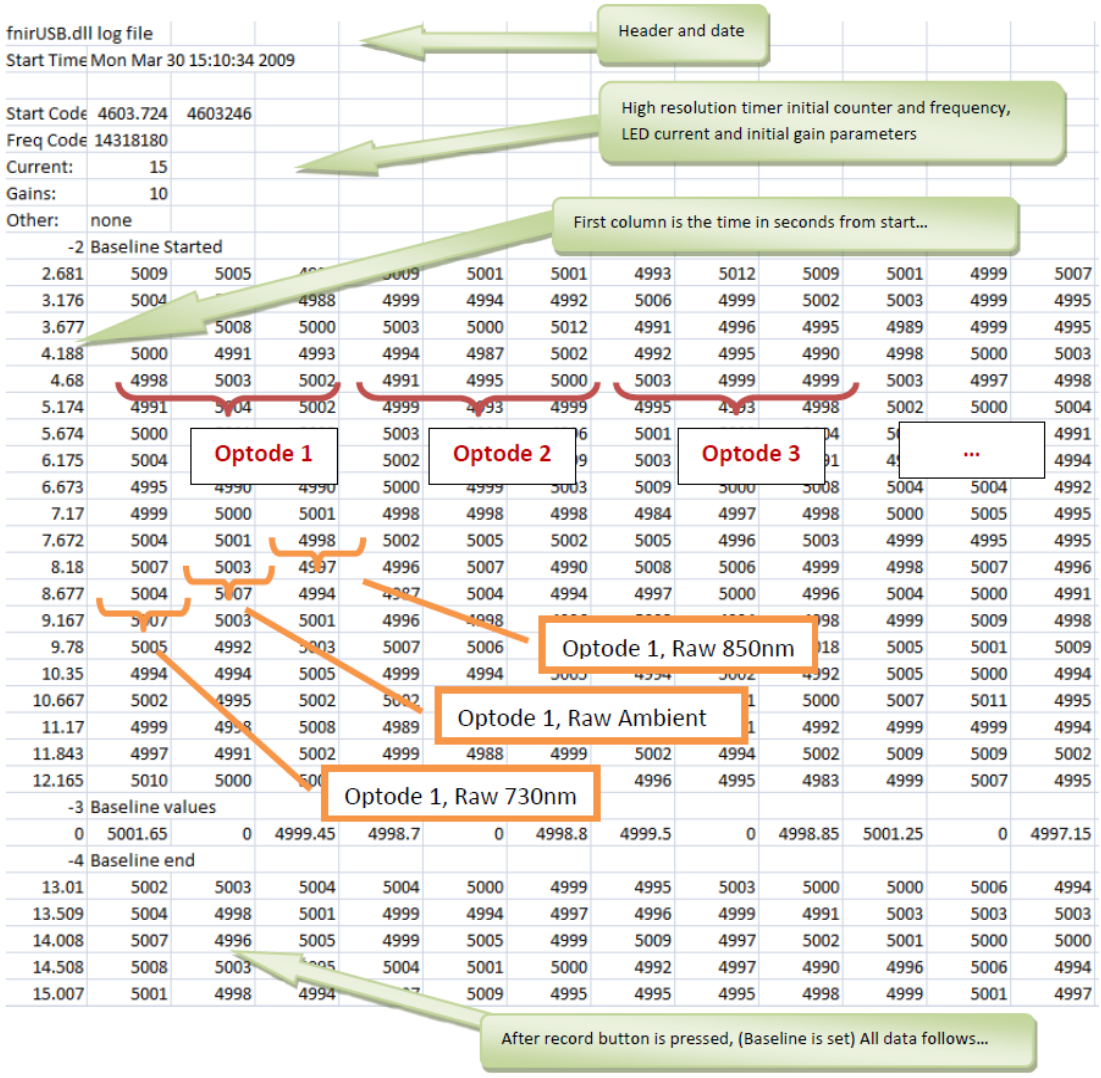

Figure 18: .nir File Format[76]

As mentioned before .nir file contains raw signals. In order to convert raw optical signals to cortical oxygenation measures, the modified Beert – Lambert Law (mbll) is used.

According to mbll, received light intensity is expressed as:

$$I = GE_o e^{-(\alpha_{HB} C_{HB} + \alpha_{HBO_2} C_{HBO_2})L}$$

where G is constant for measurement geometry. L is photon path composing of absorption μ_a and scattering μ_s constants. C_{HB} and C_{HBO2} are deoxy – hemoglobin and oxy – hemoglobin concentration in the blood. α_{HB} and α_{HBO2} are molar extinction coefficients for the oxy- and deoxy-hemoglobin molecules[77].

Optical density is expressed as:

$$\Delta OD = \log\left(\frac{I_b}{I}\right) = \alpha_{HB}\Delta C_{HB} + \alpha_{HBO_2}\Delta C_{HBO_2}$$

where I_b is light intensity measured at initial time (baseline) and I is light density at time=t. Since two wavelengths are used, the two unknowns ΔC_{HB} and ΔC_{HBO2} can be calculated. Moreover oxygenation is computed as subtracting deox-hemoglobin concentration changes from oxy-hemoglobin concentration changes. Total blood volume is summation of these two variables.

$$Oxygenation = \Delta C_{HBO_2} - \Delta C_{HB}$$
$$BloodVolume = \Delta C_{HBO_2} + \Delta C_{HB}$$

COBI Studio provides another log file which is obtained by applying mbll to raw signals with respect to the default baseline measures whose extension is .oxy. This file includes two values for each optode; the first one is related to oxy-hemoglobin concentrations whereas the second is related to deoxygenated hemoglobin concntration . Generally it has similar format with .nir file as shown in figure 19.

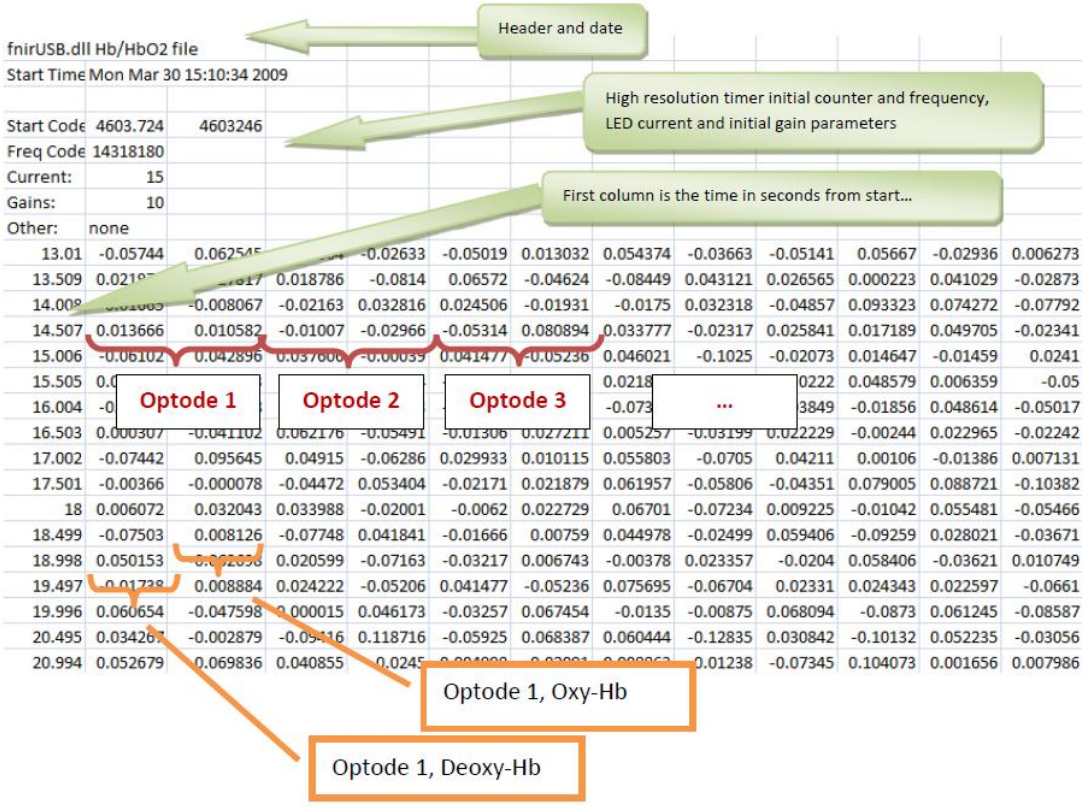

fnirUSB.dll Hb/HbO2 file
Start Time Mon Mar 30 15:10:34 2009

Start Code	4603.724	4603246
Freq Code	14318180	
Current:	15	
Gains:	10	
Other:	none	

13.01	-0.05744	0.062545	-0.02633	-0.05019	0.013032	0.054374	-0.03663	-0.05141	0.05667	-0.02936	0.006273	
13.509	0.021	0.018786	-0.0814	0.06572	-0.04624	-0.08449	0.043121	0.026565	0.000223	0.041029	-0.02873	
14.008		-0.008067	-0.02163	0.032816	0.024506	-0.01931	-0.0175	0.032318	-0.04857	0.093323	0.074272	-0.07792
14.507	0.013666	0.010582	-0.01007	-0.02966	-0.05314	0.080894	0.033777	-0.02317	0.025841	0.017189	0.049705	-0.02341
15.006	-0.06102	0.042896	0.037606	-0.00035	0.041477	-0.05236	0.046021	-0.1025	-0.02073	0.014647	-0.01459	0.0241
15.505	-0.						0.0218		0222	0.048579	0.006359	-0.05
16.004	-0						-0.073		3849	-0.01856	0.048614	-0.05017
16.503	0.000307	-0.041102	0.062176	-0.05491	-0.01306	0.027211	0.005257	-0.03199	0.022229	-0.00244	0.022965	-0.02242
17.002	-0.07442	0.095645	0.04915	-0.06286	0.029933	0.010115	0.055803	-0.0705	0.04211	0.00106	-0.01386	0.007131
17.501	-0.00366	-0.000078	-0.04472	0.053404	-0.02171	0.021879	0.061957	-0.05806	-0.04351	0.079005	0.088721	-0.10382
18	0.006072	0.032043	0.033988	-0.02001	-0.0062	0.022729	0.06701	-0.07234	0.009225	-0.01042	0.055481	-0.05466
18.499	-0.07503	0.008126	-0.07748	0.041841	-0.01666	0.00759	0.044978	-0.02499	0.059406	-0.09259	0.028021	-0.03671
18.998	0.050153		0.020599	-0.07163	-0.03217	0.006743	-0.00378	0.023357	-0.0204	0.058406	-0.03621	0.010749
19.497	-0.01738	0.008884	0.024222	-0.05206	0.041477	-0.05236	0.075695	-0.06704	0.02331	0.024343	0.022597	-0.0661
19.996	0.060654	-0.047598	0.000015	0.046173	-0.03257	0.067454	-0.0135	-0.00875	0.068094	-0.0873	0.061245	-0.08587
20.495	0.034267	-0.002879	-0.09416	0.118716	-0.05925	0.068387	0.060444	-0.12835	0.030842	-0.10132	0.052235	-0.03056
20.994	0.052679	0.069836	0.040855	0.0245				-0.01238	-0.07345	0.104073	0.001656	0.007986

Figure 19: .oxy File Format[76]

While the data is recorded and streamed by COBI, other components of the systems run in parallel. The next sections explain the fNIRSoft and application elements that process the incoming stream from COBI.

3.3. fNIRSoft

fnirSoft is a stand-alone software package designed to process, analyze and visualize functional near infrared (fNIR) spectroscopy signals through a graphical user interface and/or scripting (for automation). Below is the main window of fnirSoft with common user elements and tools identified (figure 20).

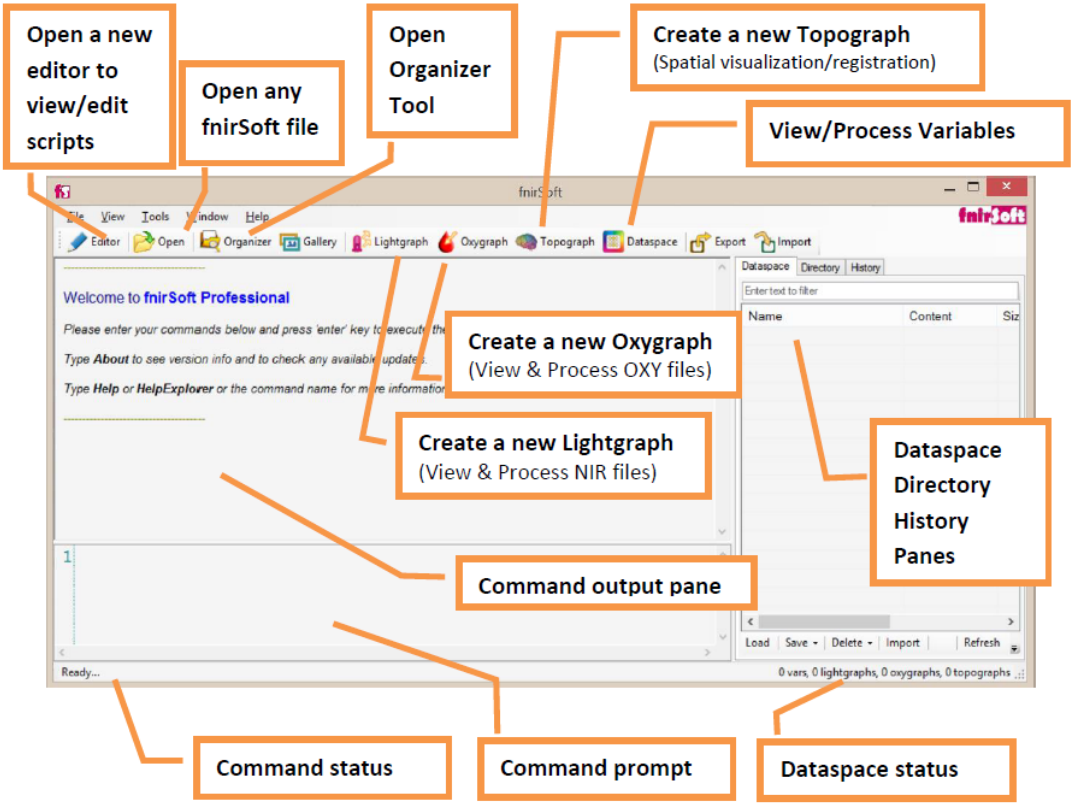

Figure 20: fnirSoft Main Interface[78]

By clicking Lightgraph -> Load File, .nir files recorded by COBI can be visualized in two different formats for offline analysis:

1- Raw light intensity measures obtained from all 16 optodes at 3 different wavelengths can be displayed altogether in a single graph as shown in figure 21. Signals colored in pink and purple represent raw measurements obtained at wavelengths 750nm and 830nm respectively. Moreover the blue colored signals correspond to ambient light measurements recorded at 805nm. Yellow and green markers tagged with numbers are used to mark key events during the experiment, such as the beginning and end of a mission, or the onset of engine failure. Markers can be triggered through the keyboard or can be automatically set through the stimulus presentation system.These keys are defined before the experiment based on a dictionary of significant events in the experiment. For instance, the marker for the event engine failure can be visualized in this way to observe its hemodynamic effects on the pilot.

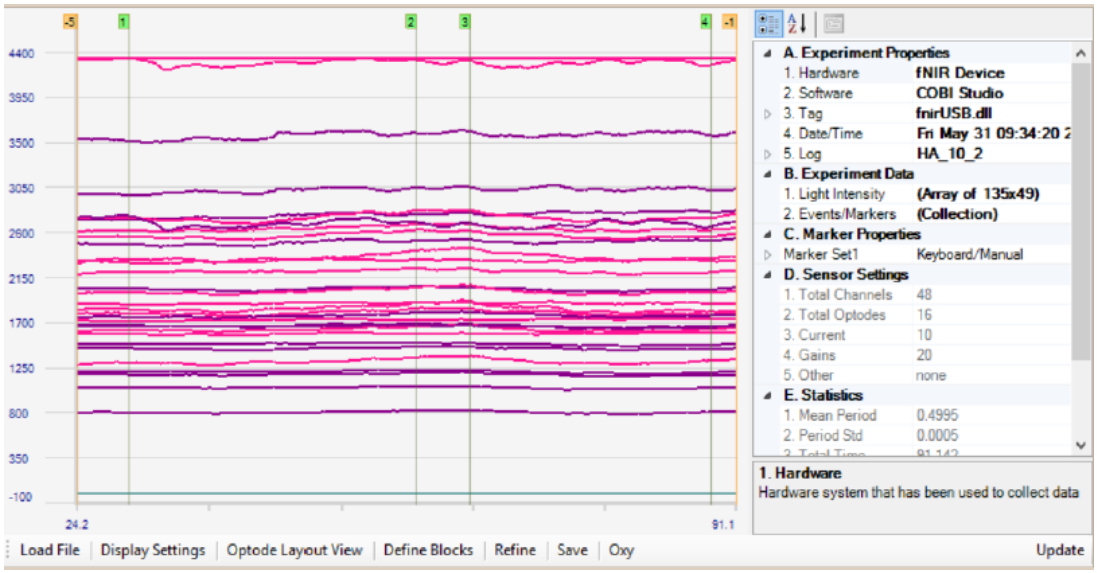

Figure 21: fnirSoft Signal Demonstration Together with All Optode

2- Each optode can be visualized separately. Thereby, problematic optodes such as saturated channels can be distinguished and eliminated. For instance optode 8 and 10 are saturated and eliminated in figure 22.

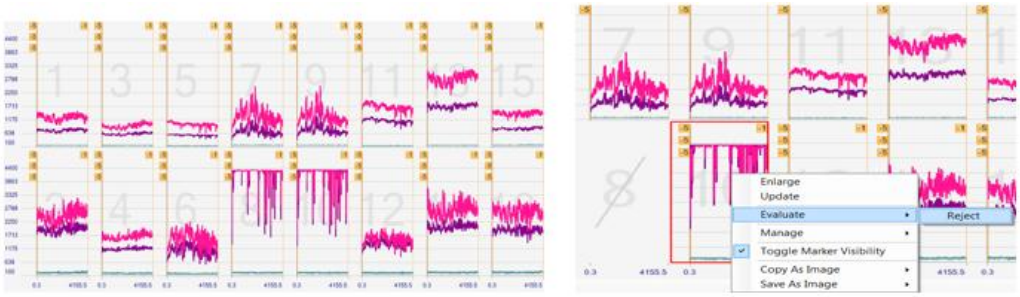

Figure 22: fnirSoft Signal Demonstration Optode by Optode

fnirSoft global memory is called Dataspace. All data variables (numeric, string, lists) and all objects (Lightgraph, Oxygraph) are created and stored in the Dataspace (figure 23). Processing Tool allows applying various functions/processing methods through user interface. All these functions are also available as commands through fnirSoft scripting.

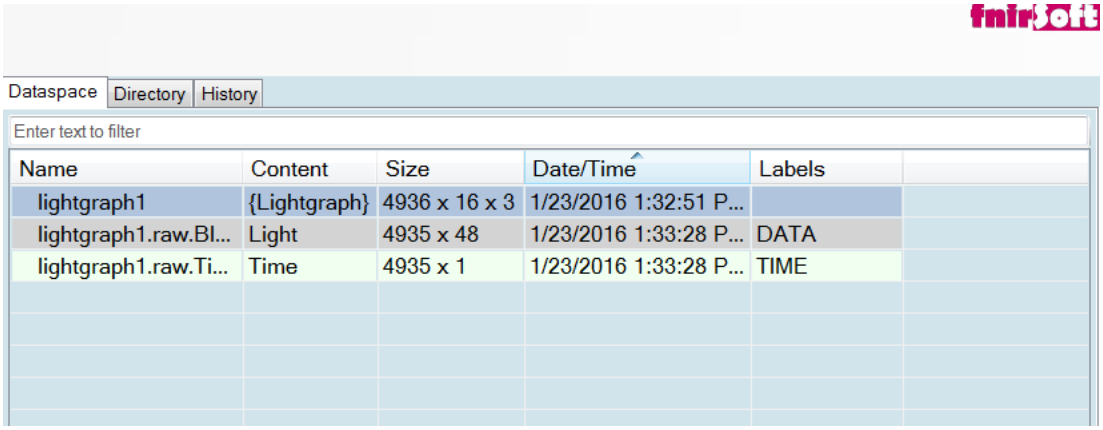

Figure 23: fnirSoft Dataspace

fnirSoft presents many functions to process on signals. Applying mbll, filters such as low pass filter, creating of data block to study specific parts of the signals, exporting generated variables and signals in txt or Matlab formats are a few of them. Moreover the scripting support allows the use of all these functions automatically. fnirSoft scripting functions also support the calculation of signal features such as mean, slope, standard deviation etc.

As explained in literature review chapter, the motivation for this thesis is to develop an online algorithm for monitoring the changes in mental workload of operators . It means that workload is estimated and updated continuously during the experiment. fnirSoft provides its features not only for offline analysis but also for online analysis thanks to scripting and DAQ Base Station plugins.

For online measurement, we need to collect brain signals through the control box and COBI continuously. Hemodynamic changes take time due to the fact that when neural activity increases in a brain region, an increased supply of oxygenated hemoglobin is supplied to that region by the vascular system. Since this occurs in the order of seconds, fNIRS can monitor slowly materializing hemodynamic changes due to neural activity. Although this is a limitation for tracing neural events that occur at higher temporal resolution, relatively slowly accumulating effects such as mental workload changes can be effectively traced by fNIRS.

Another important aspect of online analysis is to select an appropriate data buffer size, which is also referred as window size selection [63][71]. In order to detect meaningful changes in the streaming signals, they should be processed in reference to an extended period of past data point [63][71]. In the current literature online estimations of cognitive workload typically rely on window size of 30-60 seconds, where the duration is based on the task and the features considered for classification[63][71]. If the window size is too small, then the mental workload measure will be oversensitive and affected by instant unavoidable noise, head motions etc. If the window size is too large, the old data in the buffer will be too dominant and render the current hemodynamic response undetectable.

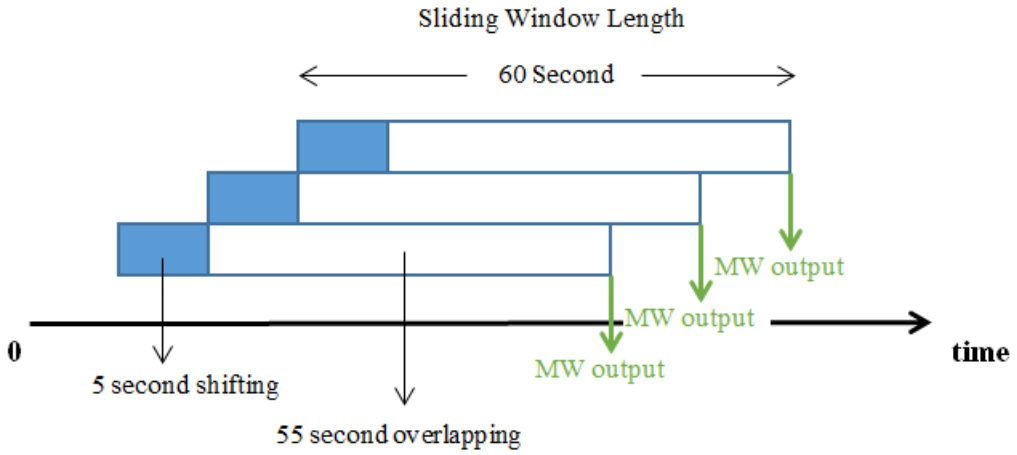

Figure 24: Online Data Processing Approach

By considering the literature and these facts, we selected a window size of 60 seconds. At every 5 second:

- new raw signals are received from the control box,
- they are processed by fnirSoft and exported in a text file,
- oldest 5 seconds of data placed at the begginning of the window is removed
- new 5 seconds of data is placed at the end of the window
- the updated text file is fed into the model processing algorithm
- a new workload estimation is generated

Therefore every 5 seconds, the sliding window is shifted and mental workload estimation is updated (figure 24).

In order to collect raw signals from the control box continuously, fnirSoft DAQ Base Station is used. fnirSoft DAQ tool is launched by clicking on Tools -> DAQ Base Station Tool on the main window of fnirSoft. Base Station window is shown below (figure 25), which has two main sections: Sources (Input) are on the left hand side where as Actions (Outputs) are on the right hand side of the window.

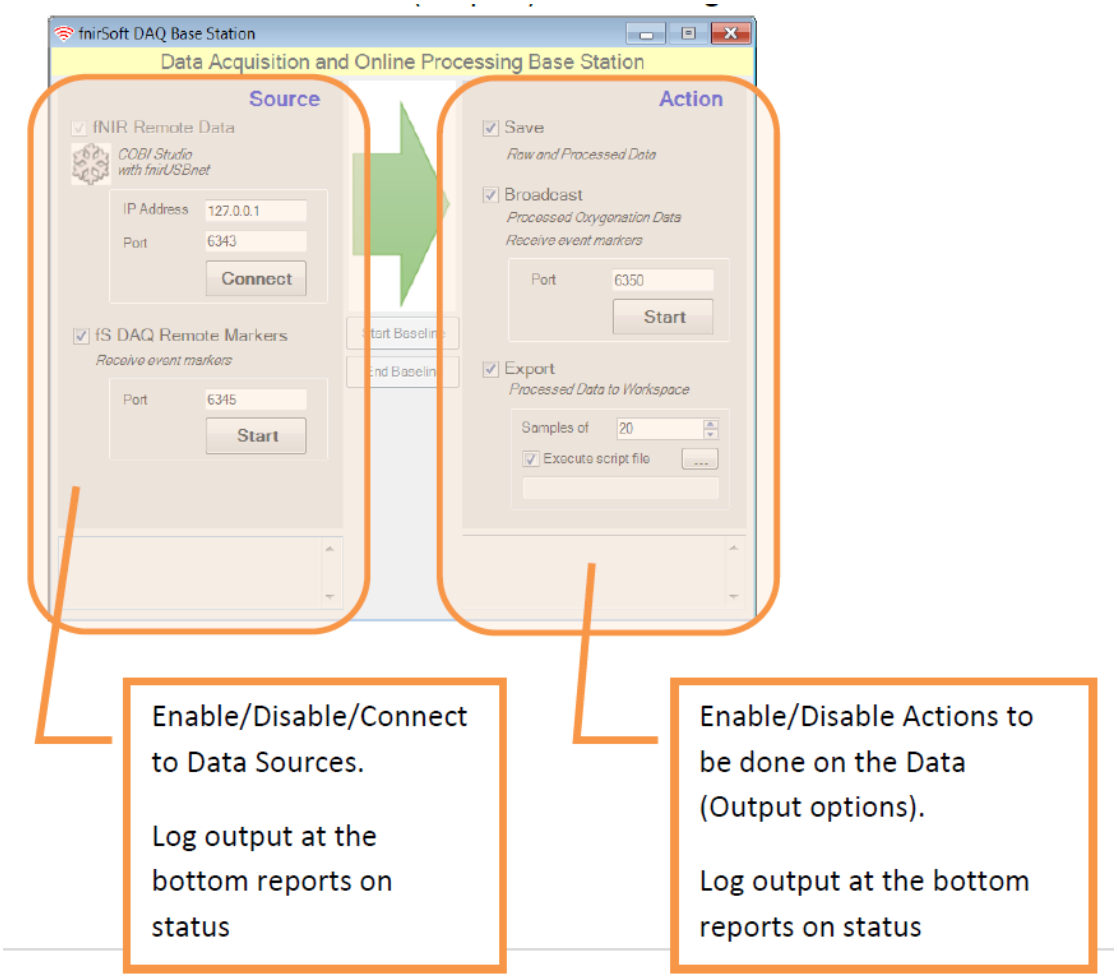

Figure 25: fnirSoft DAQ Station Window[79]

Available data sources and actions in the Base Station Tool are illustrated in figure 26. Clicking on checkbox enables and disables individual components when Base Station is idle.

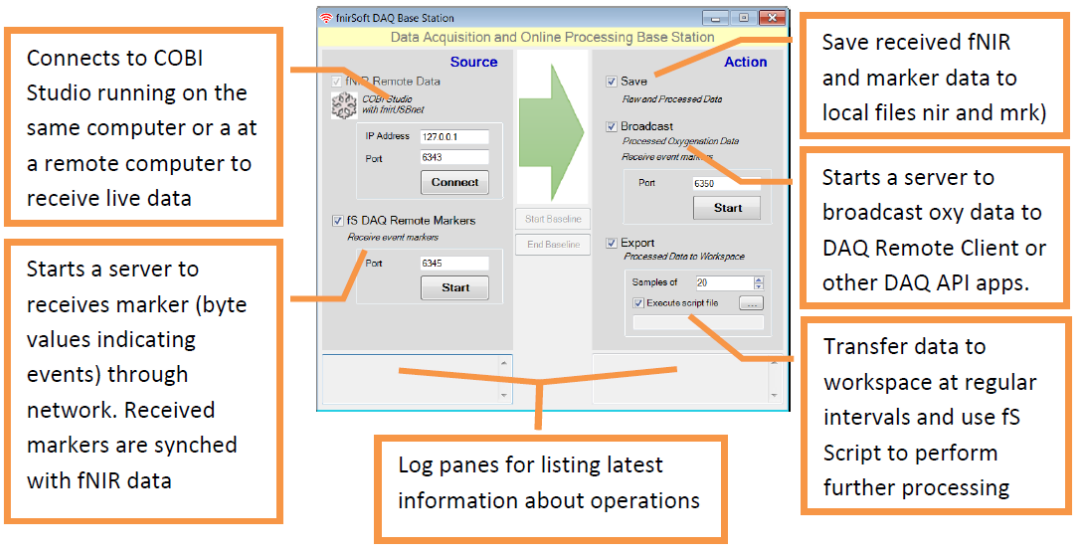

Figure 26: fnirSoft DAQ Station Component[79]

With fnirSoft DAQ, raw signals which are being sent by COBI Studio received by fnirSoft and are kept in Dataspace. Since both COBI Studio and fnirSoft typically run on the same PC, IP Address is set to default value 127.0.0.1. If they run on a different computer, the IP address would be set to IP belonging to COBI PC. The port should be set as the same as the COBI port value, which can be customizd via COBI settings. By ticking the "*enable*" and the "*sample of*" boxes, we can select the frequency of transferred raw data. Since we want to transfer new data at every 5 seconds, 10 is entered as the parameter value here. COBI Studio digitizes raw data at a frequency of 2 Hz. Therefore "10" represents 10-lines of raw data, which implies 5-seconds of new data. Clicking on the execute script file prompts the user to select the script to be used, which is executed for each new chuck of raw data sampled from the incoming stream.

Since we need to process (applying mbll etc.) raw signals to convert them into oxygenation measures to be fed into our mental workload estimation algorithm, we used a custom fnir script, which is illustrated in figure 27.

```
// delete Time.hbo, Time.hbr from fnirSoft Dataspace since they are not used
Delete (Find (name "Time"));

// define a variable to control Block(1,2,...).hbo and Block(1,2,...).hbr
j = @j + 1;

// to avoid deleting of block11,12... with block1
if (j==1)
{
    Block01 = Find(name "Block1");
    Delete(Find name "Block1");
}

// wait until first 12 data blocks(each of them is 5 second data) are obtained
if(j >= 12)
{
    // get data name of data block
    //DAQ server should be sending raw nir files every 5 seconds
    //these values are read into the 12 variables below

    // to avoid deleting of block11,12... with block1
    if (j == 12)
        myString1 = "Block01_1";
    else
        myString1 = "Block"+(j-11);

    myString2 = "Block"+(j-10);
    myString3 = "Block"+(j-9);
    myString4 = "Block"+(j-8);
    myString5 = "Block"+(j-7);
    myString6 = "Block"+(j-6);
    myString7 = "Block"+(j-5);
    myString8 = "Block"+(j-4);
    myString9 = "Block"+(j-3);
    myString10 = "Block"+(j-2);
    myString11 = "Block"+(j-1);
    myString12 = "Block"+(j);

    //concatenate nir files to get 60sec long raw data block
    appendNir = Append(Find (content "light"));

    //apply modified beer lambert law on combined raw infrared file
    //the first 20 rows of the block is considered as the baseline
    //we dont need baseline correction anymore, since we compute mbll from scratch
    mbll_out_ = Mbll(appendNir settings [20]);

    // find mean of hbo & hbr
    hboMeanVar1 = MeanWithin(Find(name "mbll.out" label "hbo"));
    hbrMeanVar1 = MeanWithin(Find(name "mbll.out" label "hbr"))
```

```
50
51      // find slopes of hbo & hbr
52      hboSlopeVar1 = SlopeWithin(Find(name "mbll.out" label "hbo"));
53      hbrSlopeVar1 = SlopeWithin(Find(name "mbll.out" label "hbr"));
54
55      // find standart deviations of hbo & hbr
56      hboStdevVar1 = StdWithin(Find(name "mbll.out" label "hbo"));
57      hbrStdevVar1 = StdWithin(Find(name "mbll.out" label "hbr"));
58
59      // find min & max values of hbo & hbr
60      hboMinVar1 = MinWithin(Find(name "mbll.out" label "hbo"));
61      hboMaxVar1 = MaxWithin(Find(name "mbll.out" label "hbo"));
62      hbrMinVar1 = MinWithin(Find(name "mbll.out" label "hbr"));
63      hbrMaxVar1 = MaxWithin(Find(name "mbll.out" label "hbr"));
64
65      // find ranges of hbo & hbr
66      hboRangeVar1 = hboMaxVar1 - hboMinVar1;
67      hbrRangeVar1 = hbrMaxVar1 - hbrMinVar1;
68
69      // append the 60 second hbo and hbr data block features which were calibrated with new baseline.
70      outputVar1 = Append(hboMeanVar1 hboSlopeVar1 hboStdevVar1 hboRangeVar1 hbrMeanVar1 hbrSlopeVar1 hl
71      // apend the 60 second hbo and hbr data block values which were calibrated with New baseline.
72      outputVar2 = Append (Find(name "mbll.out" label "hbo"));
73      outputVar3 = Append (Find(name "mbll.out" label "hbr"));
74      // apend all values to export txt file
75      outputVar4 = Append (outputVar1 outputVar2 outputVar3);
76
77      // export the calibrated hbo and hbr data to the path above by test.(1,2,3,...).txt name. TAI app
78      Export2txt("C:\Users\Administrator\Desktop\ACROSS_SW\trunk\ACROSS_TestBed\ACROSS\TAIApplication\a
79
80      // delete first 5 second data block
81
82      // to avoid deleting of block11,12... with block1
83      if (j == 12)
84      {
85          Delete (Find (name "Block01"));
86      }
87      else
88      {
89          Delete ( Find(name myString1));
90      }
91      Delete ( appendNir);
92      Clear;
93  }
```

Figure 27: fnirSoft Script used for processing the incoming raw optical signals

The script coded and shown above firstly waits 60 seconds to fill the buffer (sliding window). After that it performs the following operations:

- It converts raw signals into hbo and hbr measures by using mbll by considering the first 10 seconds as baseline. In fact, COBI can also apply mbll on raw signals and record hbo/r measures in .oxy signal as explained before. Since we perform online processing, pure raw signals are received and processed with this script. Baseline is taken to find reference values of hbo and hbr measures. Furthermore, 10 second baseline at every 60 second not only protects trending of data but also provides eliminating of instantaneous ambient impulse.
- It computes the means, slopes, standard deviations and ranges of hbo and hbr data. They are used as features in our machine learning model.
- All found features (mean, slope etc.) and hbo / hbr data are exported in a text file at every 5 seconds. These text files are named as "*test.1.txt, test.2.txt, test.3.txt,..., test.n.txt"*. An example of text file content is shown in figure 28.

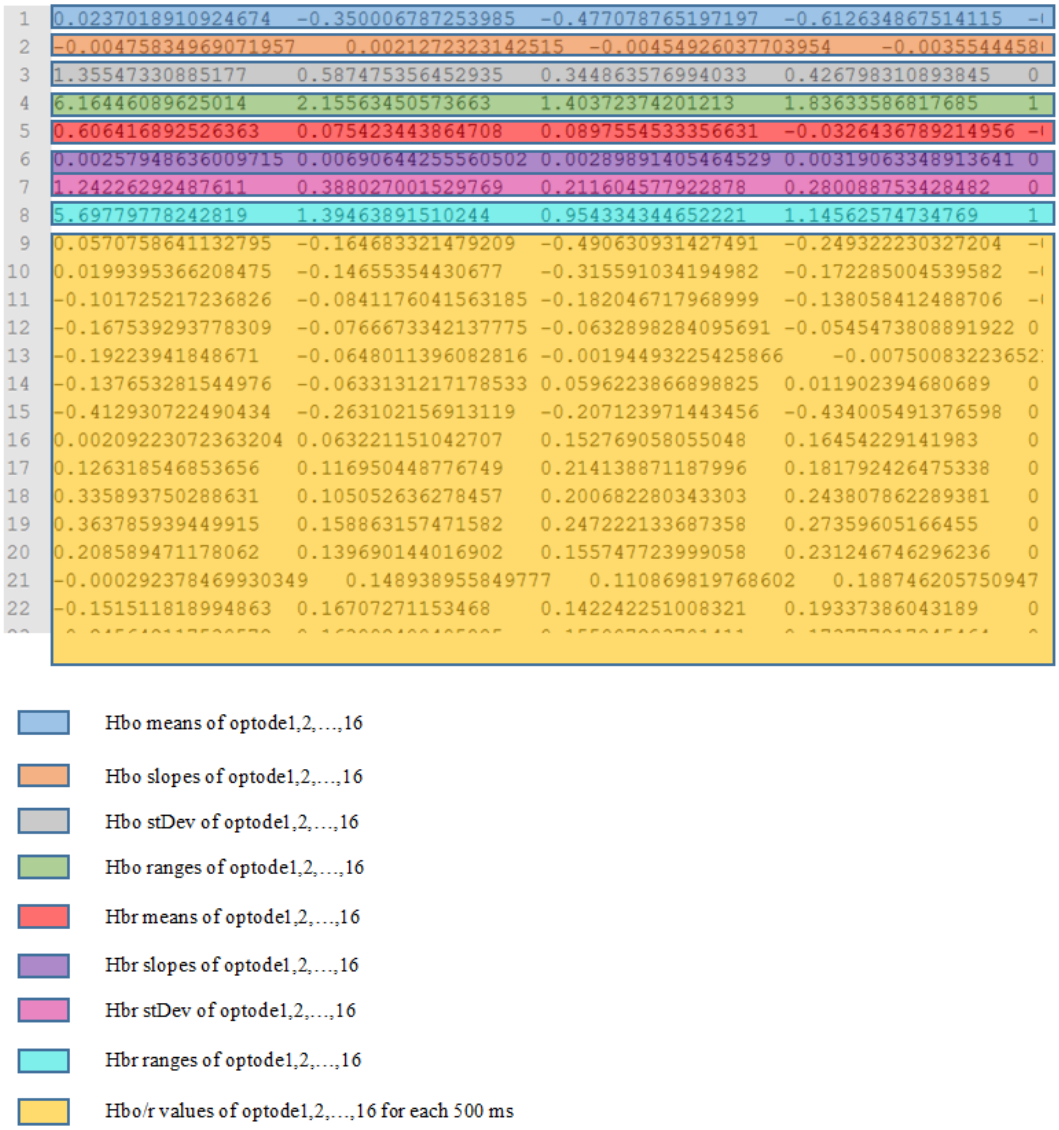

Figure 28: test.txt File Content

3.4. Model Processing Application

Model processing application is designed to feed the data generated by fnirSoft script into a Discriminant Analysis model and return the calculated mental workload estimation as an output in terms of three ordinal categories, namely low (0), medium (1), and high (2).

3.4.1. Discrimant Analysis

Discriminant Analysis (DA) is a statistical technique and used in machine learning to find features to separate data into classes. DA falls into supervised learning model and uses training data to find linear functions (canonical functions) that determine data sample that belongs to which group. Since we want to separate the data into three classes, two canonical functions are used (number of classes - 1). Canonical function is expressed as follows:

$$f = u_0 + u_1x_1 + u_2x_2 + u_2x_3 + \ldots + u_jx_j$$

where $x_{1,2,\ldots,j}$ are data and $u_{0,1,2,\ldots j}$ are coefficients of the features belonging to $x_{1,2,\ldots,j}$.

$x_{1,2,\ldots,j}$ are generated from fnirSoft and model processing application received them as text file format. $u_{0,1,2,\ldots j}$ are found by using training data. Mathematical formulas lying behind of coefficient calculation are expressed below[77].

$$t_{ij} = \sum_{k=1}^{g} \sum_{m=1}^{n_k} (X_{ikm} - X_{i..})(X_{jkm} - X_{j..})$$

where

- t_{ij} total covariance matrix of SSCP (Set of Sums of Cross Product) matrix,
- g is number of group,
- n is total number of training data in group k,
- X_{ikm} is the value of variable(feature) for m_{th} data in group k,
- $X_{i..}$ mean value of variable i.

$$w_{ij} = \sum_{k=1}^{g} \sum_{m=1}^{n_k} (X_{ikm} - X_{ik\cdot})(X_{jkm} - X_{jk\cdot})$$

where

- w_{ij} within group covariance matrix of SSCP (Set of Sums of Cross Product) matrix,
- g is number of group,
- n_k is total number of training data in group k,
- X_{ikm} is the value of variable(feature) for m_{th} data in group k,
- $X_{ik.}$ mean value of variable i for all training data in group k.

B = T – W

where

- B is between group covariance matrix,
- T is total covariance matrix,
- W is with group matrix.

Once B and T are calculated, find the solutions (v_i) to the following equations:

$$\sum b_{1i}v_i = \lambda \sum w_{1i}v_i$$
$$\sum b_{2i}v_i = \lambda \sum w_{2i}v_i$$
$$\vdots$$
$$\sum b_{pi}v_i = \lambda \sum w_{pi}v_i$$

Finally, coefficients (weights of features) are found with following formula:

$$u_i = v_i \sqrt{n. - g}$$

IBM SPSS (Statistical Package for the Social Sciences) tool is used to carry out discriminant analysis. SPSS is feed with training data, number of target classes, feature types and model type. It uses inputs and calculates coefficients of features and class centroids.

Training data is prepared based on one of the test subject signals. After the experiment (offline analysis), collected data and experiment video are synchronized with ELAN which is a professional tool for the creation of complex annotations on video and audio resources. After the sync process, voiced video is played parallel with signals monitoring. A screenshot of training data preparation is displayed in figure 29. Moreover the experiment logs some important event and we focus on them. By watching video to see behavior of the test subject and by investigating test logs and sync signals, mental workload level is assigned for every 500 millisecond manually. By this way, output of each training data is prepared.

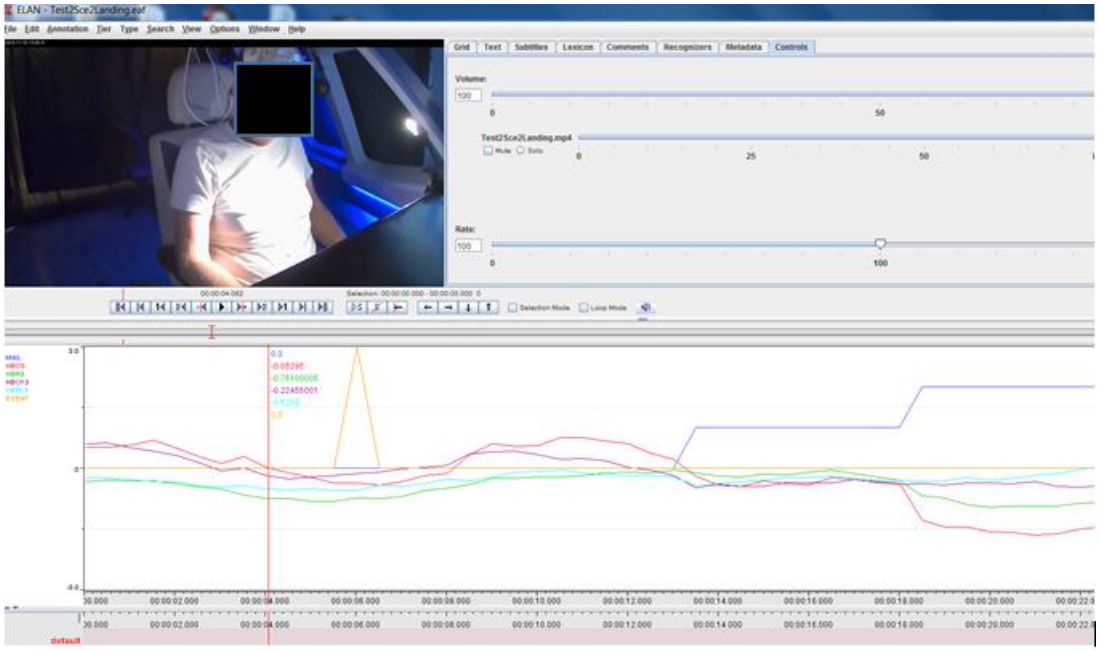

Figure 29: Training Data Preparation with ELAN

After preparing of training data, it inputs to SPSS with other parameter stated above. SPSS analyzes the given data and outputs success rate of classification, feature coefficients and class centroids of mental workload (centroid of low workload, centroid of medium workload and centroid of high workload).

Selected features as follows:

```
                    {mean_hbo
                     mean_HbR
                     std_dev_ hbo
                     std_dev_ hbo
Feature Vector =     slope_ hbo
                     slope_ hbo
                     range_ hbo
                     range_ hbo}
```

The selection of the features is guided by our literature review. Since we have 16 optodes, a total number of 128 (16x8) features are used. However optode8 and oprode10 which are located over lower fronto-polar regions of the prefrontal cortex are removed and feature weights (coefficients) belonging to these optodes are taken as 0. This was because optode8 and optode10 were saturated due to the way the sensor pad is placed on the forehead of the participant where we obtained the training data. Since the related literature states that the optodes at the left and right edges corresponding to inferior frontal gyri carry information for mental workload information more than the central optodes, information loss for the decision is negligible.

Output of the LDA model computed in SPSS is given in section *4.1.1* of the Results chapter. Obtained feature coefficients and centroids' coordinates are recorded in a configuration file in xml format. This configuration file is input together with text files generated by fnirSoft to model the mental workload processing application. The purpose was to design a generic application valid for all test subjects.

3.4.2.Processing Application

Model processing application is developed on Visual Studio 2010 by using C++ programming language and running on Windows 7. It

- waits until the first text file generation,
- reads configuration file in a specific path and takes centroids' coordinates, feature coefficients at the beginning of execution,
- Periodically at every 5 second,
    - receives text file whose format is in figure 28 and parse containing data. Each features value is kept for calculation and each hbo-hbr values are kept for analysis.
    - calculates canonical functions (f1 and f2) by using feature values parsed from text file and feature coefficients taken from configuration file,
    - considers f1 and f2 results as x-y coordinate and find Euclidean distances from each centroid coordinates,
    - selects the centroid whose distance from the calculated coordinate is the smallest one and outputs label of the centroid (0, 1 or 2).
    - waits until next text file generation.

All these actions are demonstrated in figure 30.

After application is completed, it is run and target mental workload values which are assigned before by using ELAN and predicted mental workload values which are calculated by the application is compared by selecting random 69 test instances. Perfect matches and mismatches are compared by considering conditions of the test instances. Results are given *4.1.2* of the result chapter.

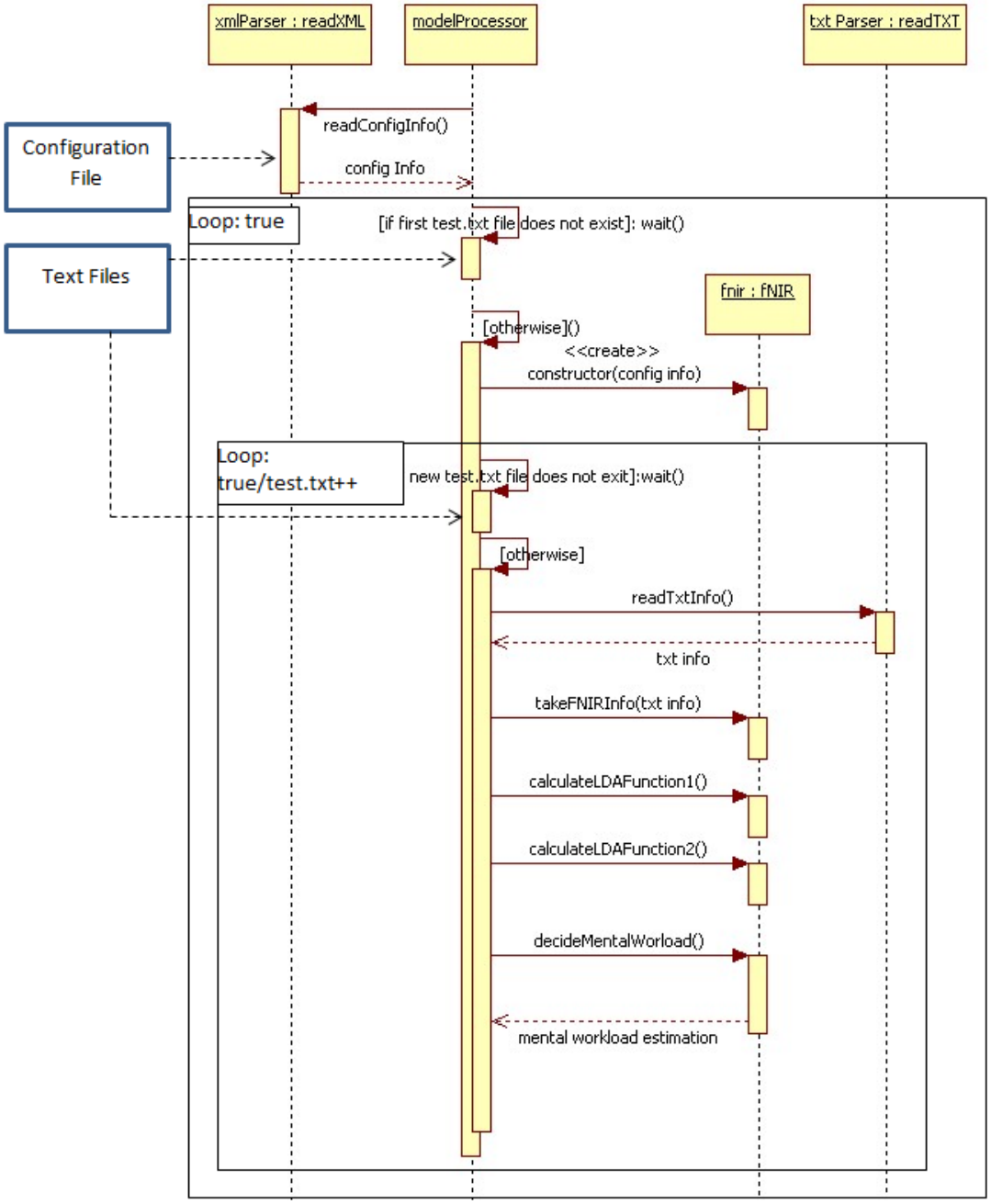

Figure 30: Sequential Diagram of Model Processing Application

3.4.3. Inadequacies of Processing Application based on Discrimant Analysis

The methodology explained in *3.4.1* and *3.4.2* has two inadequacies to achieve a de facto conclusion. One of them is that, while methodology is being developed, all of the test sessions were not analyzed. There are eight test subjects and each of them performed four test scenarios. Since scenario 0 is designed to make test subjects to be familiar with the test environment, excluding these initial sessions leaves 24 (8 test subject x 3 test scenario) test sessions, which are convenient to collect data to develop a good analytic design. However, in the methodology whose phases are detailed above, a few test sessions could be analyzed and classifications were designed based on their data. The reason is that cognitive analysis on the test sessions is tedious. Each test video should be watched second by second. Pilot situations should be observed and their conversations should be listened very carefully. Moreover test observations, test logs which were recorded during tests and pilot evaluations which were reported by the test subjects after each test session should be matched and analyzed. Pilot evaluation reports include feedbacks of the test subjects about the realism of the test scenarios, perceived difficulty levels, comfort of fNIR sensor pad etc. Graphs drawn by the pilot to evaluate his own mental workload are placed in *Appendix A - SUBJECTIVE WORKLOAD GRAPHS OF TEST PILOTS.*

Second inadequacy of the methodology was the absence of generic flight parameters to determine the mental workload levels of the pilot. When mental workload level is assigned for a test moment, the pilot's situation as captured in the video recording was considered. However, conditions causing this situation could not be studied systematically from the simulator logs, since the complete data set including simulator log files were not shared with the project partners only after the completion of the project. The workplan required us to train a model based on a single subject and test the algorithm on the remaining experiments. Therefore, the first algorithm trained on a single pilot turned out to be inadequate for training a mental workload monitoring tool applicable to multiple pilots.

3.4.3.1 Parameters Influencing Mental Workload

In order to address the limitations of the previous methodology, each test sessions is analyzed second by second. Since saturated signal levels were observed across many optodes during the entire sessions of the first test subject and the first scenario data of the second test subject, these instances were removed from the dataset. Therefore a total of 20 test sessions conducted with 7 pilots are investigated in the second stage of our analysis: (pilot2: sce2,3) + (pilot3,4,5,6,7,8: sce1,2,3). During test session analysis, each video is watched and each sound (talking, simulator environment warnings etc.) is analyzed. By considering pilot situations and their reports, mental workload values are assigned for each half second. While mental workload is tagged, pilot, flight and environment conditions are also noted, to form annotations in the format <MW: 1, flight phase: cruise, ATC (air traffic controller) talks with the pilot>. These parameters are determined based

on the related literature in aviation human factors. According to Committee on Human Factors (Panel on Workload Transmission), unexpected events, equipment failures, response demand on short time (Go Around phase for instance in our scenario), deviation in flight plan such as route recalculation, warning tones, voice message such as ATC communication, dual task (take notes, controlling checklist etc.), control with eye (flight instrument control) can be considered among the most important factors contributing to an increase in the mental workload of the pilots[80]. They also give specific results for some of these conditions. For instance, system failures can increase mental workload of the pilots by 30%, which also causes an increase in error rate by 16%. Moreover, despite their short duration, during approach and take off/landing phases pilots' mental workload level tend to increase due to the stress of low altitude flight [80]. A study of Iijima, Funabiki and Nojima corroborated with the report of Committee on Human Factors, where they detected the cases causing high mental workload as descent, approach flight phase and pilot interaction with MFDs and CPDLCs[81]. Skybrary which is an electronic repository of safety knowledge related to flight operations, air traffic management (ATM) and aviation safety in general lists periods of high mental workload as descent, approach, landing (especially during any go around), unexpected situations such as equipment failure[82]. On the other hand, Committee on Human Factors' study also pointed that during prolonged and monotonous tasks pilots typically experience low mental workload[80]. In addition, designers of the ACRROSS Project prepared all scenarios (so test scenarios of this thesis study also) concordantly with these results. Besides they consulted with many airliner pilots to improve the validity of the experimental design[74].

After analysis of all test sessions are completed, 16 generic conditions (flight phase, drowsiness, unexpected failure etc.) are defined for annotating the flight videos. These 16 behavioral dimensions aimed to characterize the mental workload level of the pilots in our test environment based on the recommendations of related work reviewed above. Moreover, cross checks between each test session of each pilot is also performed to ensure reliability. For example, if a combination of 16 conditions "1110010101100000" specifies a mental workload level of 1, it is ensured that this mental workload output of this combination is consistent in among all test sessions. If the same combination of binary features are mapped to a different mental workload level in a different test session, they are analyzed again to remove the inconsistency. If there is a difference due to a newly discovered factor between the two cases, a new dimension that affect the mental workload outcome is added to the annotation scheme. If there is no difference, most suitable mental workload assignment are done in both test instances. By that way back propagation correction is performed and a generic (valid for all test session) answer key is prepared for mental workload assessment. Through iterative analysis we observed that 16 binary dimensions were sufficienct to capture the relevant factors identified in the literature. Moreover fourth mental workload class is specified as "-1" to represent extraordinary situations such as too much head motion, weak skin contact etc. These

phases are tagged with a special marker since signal changes belonging to these parts are unreliable, so the relation between these signals and mental workload output is not clear. All these parameters and their relationship to mental workload levels are summarized in detail in *Appendix B - PARAMETERS AFFECTING MENTAL WORKLOAD.*

3.4.3.2 LDA Result with Total Data Based on Answer Key Parameters Conditions

After all tests are tagged based on the prepared answer key (16 conditions determining the mental workload), all 20 tests sessions are given input to LDA analysis on SPSS. Test subject 2,3,4,5 are used as training data, test subject 6,7,8 are used as test data. SPSS input is prepared as an excel format in figure 31. However opcodes 1,3,5,11,13,15 are considered during LDA analysis since the fNIRS signals obtained from these optodes were the least affected ones by the other infra-red sources in the cockpit (e.g. the eye tracking cameras and the Kinect body trakcer). Standard deviations, ranges, means, slopes of hbo and hbr in these optodes are used as features. Calculations of these parameters are explained in **3.3** of this chapter. Since all algorithms in this thesis use the same parameter set and their combinations such as hbt(hbo-hbr), oxy(hbo-hbr), the inputs will not be stated again in the remaining algorithms such as artificial, neural network, svm to avoid duplicate explanation.

When the LDA algorithm is run on SPSS, it is dramatically observed that training success decreases to 47.2%. Moreover it is also thought that pilot specific model might be more successful. Therefore two test subjects are selected (pilot 5 for right handed test subject and pilot 6 for right handed test subject). Their data is trained separately and derived two results. Although results increase comparing to the model derived from data of more pilots, they are still not satisfactory (training rate: 65.6% of pilot 5 - cross validation 72.23% with kfold 3 and training rate: 62.1% of pilot 6 - cross validation 68.37% with kfold 3). Results of these analyses can be seen in part *4.3* of Result chapter and *Appendix B - ACCURACY SCORES OF LDA.* Therefore alternative machine learning algorithms are investigated.

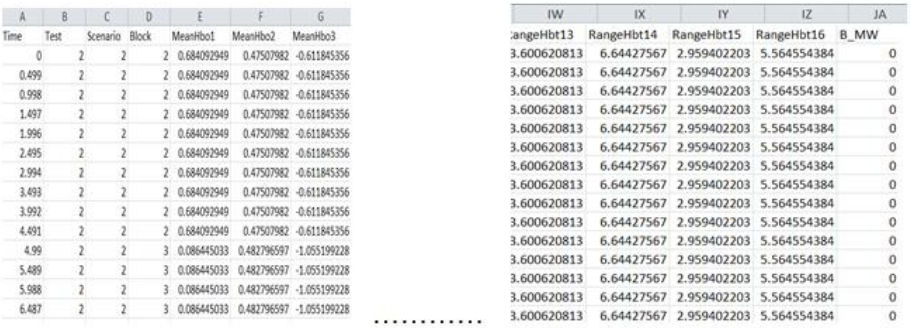

A	B	C	D	E	F	G	IW	IX	IY	IZ	JA
Time	Test	Scenario	Block	MeanHbo1	MeanHbo2	MeanHbo3	angeHbt13	RangeHbt14	RangeHbt15	RangeHbt16	B_MW
0	2	2	2	0.684092949	0.47507982	-0.611845356	3.600620813	6.64427567	2.959402203	5.564554384	0
0.499	2	2	2	0.684092949	0.47507982	-0.611845356	3.600620813	6.64427567	2.959402203	5.564554384	0
0.998	2	2	2	0.684092949	0.47507982	-0.611845356	3.600620813	6.64427567	2.959402203	5.564554384	0
1.497	2	2	2	0.684092949	0.47507982	-0.611845356	3.600620813	6.64427567	2.959402203	5.564554384	0
1.996	2	2	2	0.684092949	0.47507982	-0.611845356	3.600620813	6.64427567	2.959402203	5.564554384	0
2.495	2	2	2	0.684092949	0.47507982	-0.611845356	3.600620813	6.64427567	2.959402203	5.564554384	0
2.994	2	2	2	0.684092949	0.47507982	-0.611845356	3.600620813	6.64427567	2.959402203	5.564554384	0
3.493	2	2	2	0.684092949	0.47507982	-0.611845356	3.600620813	6.64427567	2.959402203	5.564554384	0
3.992	2	2	2	0.684092949	0.47507982	-0.611845356	3.600620813	6.64427567	2.959402203	5.564554384	0
4.491	2	2	2	0.684092949	0.47507982	-0.611845356	3.600620813	6.64427567	2.959402203	5.564554384	0
4.99	2	2	3	0.086445033	0.482796597	-1.055199228	3.600620813	6.64427567	2.959402203	5.564554384	0
5.489	2	2	3	0.086445033	0.482796597	-1.055199228	3.600620813	6.64427567	2.959402203	5.564554384	0
5.988	2	2	3	0.086445033	0.482796597	-1.055199228	3.600620813	6.64427567	2.959402203	5.564554384	0
6.487	2	2	3	0.086445033	0.482796597	-1.055199228	3.600620813	6.64427567	2.959402203	5.564554384	0

Figure 31: Input Format for Algorithms

3.4.4.SVM Analysis

Support Vector Machine (SVM) is a commonly used machine learning algorithm for classification problems. SVM is also used in the mental workload measurement literature[63]. SVM is a supervised learning algorithm. In the training phase SVM tries to find a decision boundary to separate predefined classes as seen in figure 32.

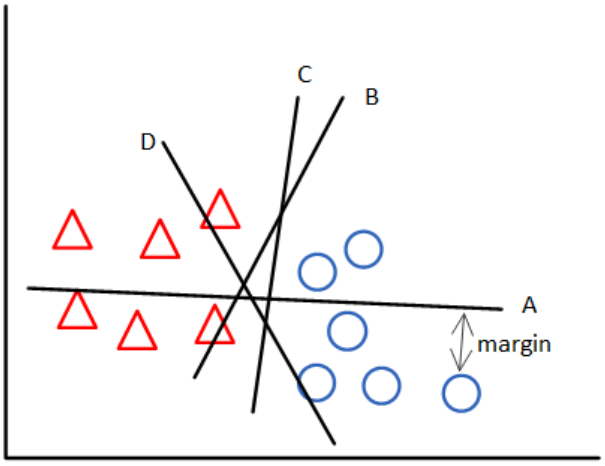

Figure 32: SVM Classification Visualization

In figure 32, red triangles represent class 1 and blue circles represent class 2. SVM aims to separate these classes with optimum decision boundary like A,B,C,D by considering margin value of nearest support vector (a red triangle or a blue circle). It calculates margin (maximum is the best to reserve space for new test supports) and error tolerance (red triangle area with minimum blue circles and blue circle area with minimum red triangles). However there is a trade off between margin and error tolerance. If SVM keeps the margin too much, error tolerance increases and vice versa. Therefore with tuning of C and gamma parameters, optimum decision boundaries should be found. Moreover, by selecting the kernel function, decision boundary can be shaped. For example polynomial kernel function defines a boundary polynomial as seen in figure 33. For polynomial kernel function the degree parameter sets the degree of the decision boundary. Another kernel function example is rbf (radial bases function). With this function, the classification area could be radial based as seen in figure 34.

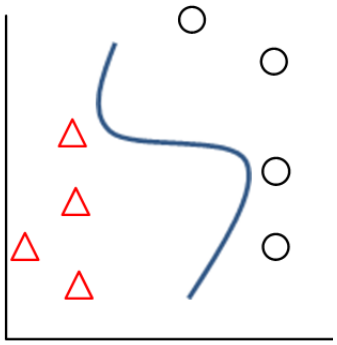

Figure 33: SVM Kernel: Polynomial

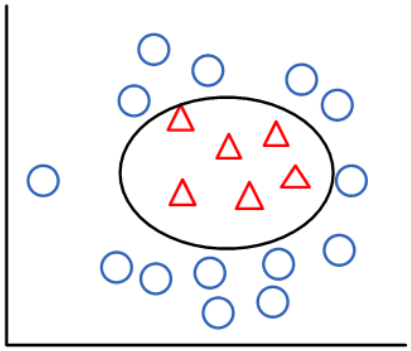

Figure 34: SVM Kernel: RBF

By adjusting kernel function types, gamma, C, and the degree value more powerful models can be developed. After a model is designed with training data and the given parameters, the test data is given as input to observe prediction score. In this thesis, for the SVM model, Keras library SVM functions are used in Python programming language. In addition, Keras svm functions have the capability to analyze not only two classes but also multiple classes. Therefore four mental workload classes (-1,0,1,2) could be modeled in this framework.

Overall, the SVM algorithm provided higher classification accuracy than the LDA model. The most optimal configuration produced 64.24% accuracy. However, the confusion matrix shows that this model is not strong enough to separate data in four classes given their non-uniform distribution in the dataset. Since there are lots of mental workload 0 cases in the dataset, a default algorithm predicting only 0 as the outcome would obtain nearly the same accuracy score. Again similar approach with LDA, pilot specific model is studied. Pilot 5 and 6 models give good training results (Cross Validation: 88.29% with kfold 3 for pilot 5 and Cross Validation: 86.27 with kfold 3 for pilot 6). However results of test processes are not good (60.39% for pilot 5 and 60.43% for pilot6). Therefore, alternative algorithms are investigated. SVM results with different parameter combinations can be seen in *4.4* part of the Result chapter and *Appendix D - ACCURACY SCORES AND INDEXIES OF SVM*.

3.4.5.Artificial Neural Network Analysis

Artificial Neural Network is another supervised machine learning algorithm. Since it is used from medical area to e-commercial sector and applied also in human computer interface literature[27], it is also employed in this thesis study. Figure 35 illustrates a simple structure of a 3-layered feedforward ANN with 2 inputs, 3 hidden and 2 output nodes.

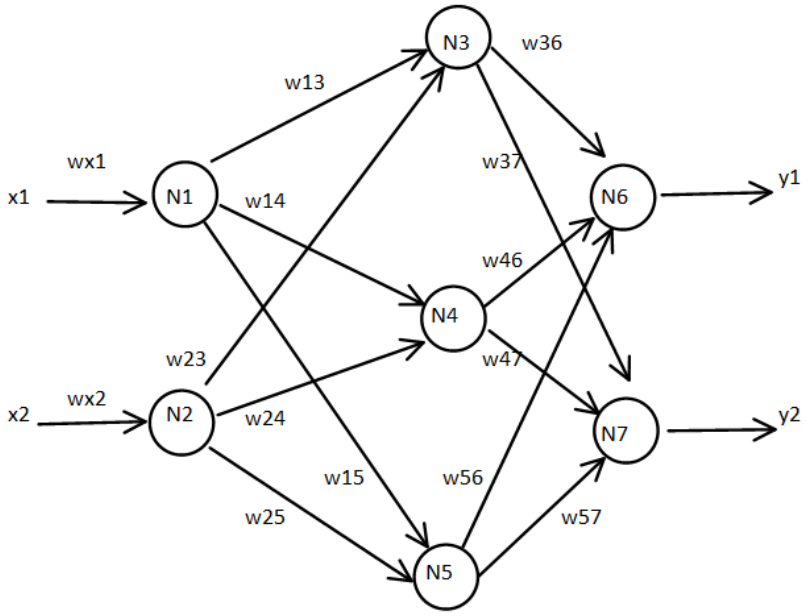

Figure 35: Artificial Neural Network Structure

In ANNs, nodes (circles in figure 35) are used to find the output. Each node value is calculated with its inputs multiplied with weights plus bias value. Bias value (b, threshold) can be changed and its effect is analyzed on the outcome value. Initially, the connection weights are assigned randomly. While the model is trained, following calculations are performed:

N1 Value =
- **0** if wx1 * x1 + b < = 0
- **1** if wx1 * x1 + b > 0

N2 Value =
- **0** if wx2 * x2 + b < = 0
- **1** if wx2 * x2 + b > 0

N3 Value =
- **0** if w13 * N1 + w23 * N2 + b < = 0
- **1** if w13 * N1 + w23 * N2 + b > 0

N4 Value =
- **0** if w14 * N1 + w24 * N2 + b < = 0
- **1** if w14 * N1 + w24 * N2 + b > 0

N5 Value =
- **0** if w15 * N1 + w25 * N2 + b < = 0
- **1** if w15 * N1 + w25 * N2 + b > 0

N6 = y1 Value =
- **0** if w36 * N3 + w46 * N4 + w56 * N5 + b < = 0
- **1** if w36 * N3 + w46 * N4 + w56 * N5 + b > 0

N7 = y2 Value =
- **0** if w37 * N3 + w47 * N4 + w57 * N5 + b < = 0
- **1** if w37 * N3 + w47 * N7 + w57 * N5 + b > 0

Outputs y1 and y2 is calculated as 0 or 1. If y1 and/or y2 mismatches with the target value, the backpropagation learning method is applied to update the weights. During the computations of the formulas above, generally node values and weight multiplications are given as input to a sigmoid function or tanh function together with a threshold so that the output of each node is kept in between 0 and 1, which simulates the behavior of biological neurons.

Let N1 error is called as Error_y1 and updated w36 is w36'. The **basic** calculation is

w36' = w36 + Error_y1 * N3

This formula is applied for all weights and N1, N2, N3, N4, N5, N6, N7 are calculated again. If any mismatch occurs for y1 and y2, back propagation procedure is repeated again. After an optimum iteration count is reached (shortly before saturation and overfitting by avoiding local minima), model training is completed and test phase is

started. Final updated weights obtained during the training phase are used in the test phase without back propagation.

In order to analyze test subjects data with artificial neural network, Matlab neural network toolkit is used in this study. This tool kit uses *Scaled Conjugate Gradient* method to update weight in back propagation. For each input a node is designed. For output (-1, 0, 1, 2), four node is decided. Outputs are represented as binary.

-1: 0001

0: 0010

1: 0100

2: 1000

In order to decide the optimum number of hidden layer nodes, we experimented with different number of nodes and observed the performance of the network. Moreover, different combinations are applied by changing the training data versus the test data percentages. All parameter combinations and success rates obtained during these trials can be seen in *4.5* of Result chapter and *Appendix E - ACCURACY SCORES OF ANN*.

Result of this algorithm also is not satisfactory. 70.4% success rate is derived as the highest score. Similar to SVM, the confusion matrix of artificial neural network shows that it is incapable of separating the four different classes. (Part *4.5* of result chapter)

3.4.6.LDA, SVM and ANN Analysis with Mixed Data

All three algorithms are unsatisfactory with unified data. Unified data means that for example test subject 2,3,4,5 are used for training data and test subject 6,7,8 are used for test data. Therefore it is suspected that models could not learn inputs – output correlation if training data does not contain the specific test subject. For this reason it is decided that all data is mixed. In other words, train data contains all test subjects data partially as well as test data contains all test subjects' partially. Hence all data is mixed as seen in figure 36 and figure 37.

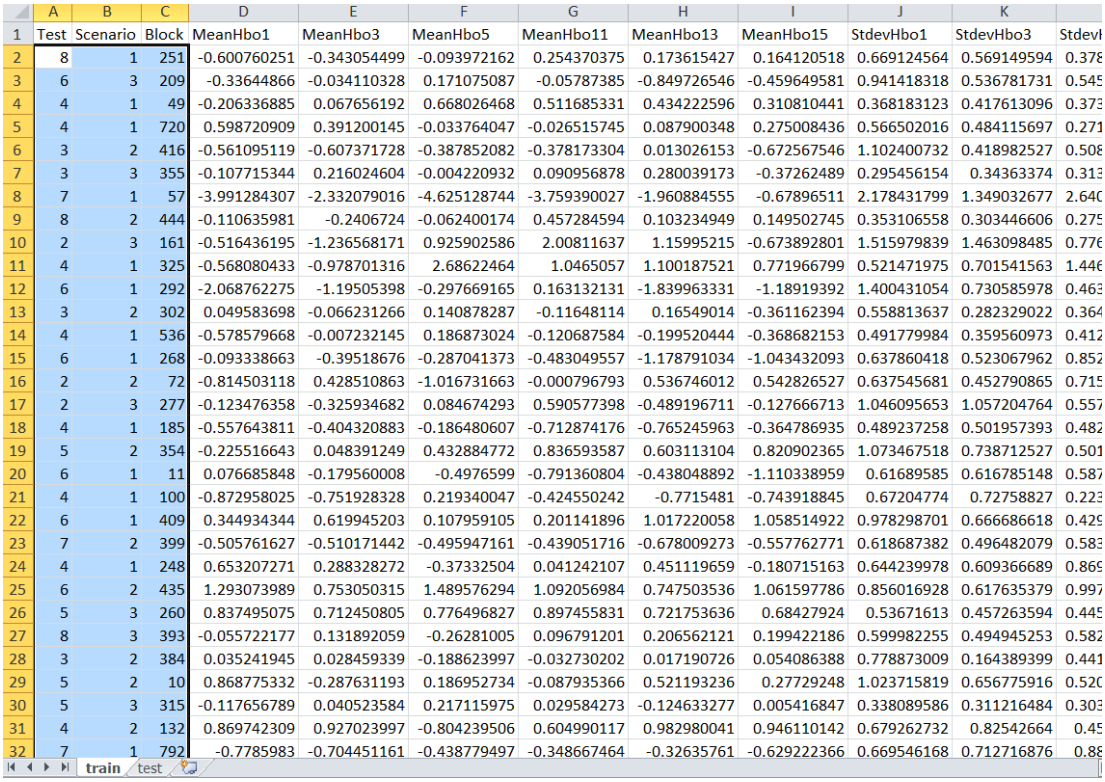

	A	B	C	D	E	F	G	H	I	J	K	
1	Test	Scenario	Block	MeanHbo1	MeanHbo3	MeanHbo5	MeanHbo11	MeanHbo13	MeanHbo15	StdevHbo1	StdevHbo3	Stdevl
2	8	1	251	-0.600760251	-0.343054499	-0.093972162	0.254370375	0.173615427	0.164120518	0.669124564	0.569149594	0.378
3	6	3	209	-0.33644866	-0.034110328	0.171075087	-0.05787385	-0.849726546	-0.459649581	0.941418318	0.536781731	0.545
4	4	1	49	-0.206336885	0.067656192	0.668026468	0.511685331	0.434222596	0.310810441	0.368183123	0.417613096	0.373
5	4	1	720	0.598720909	0.391200145	-0.033764047	-0.026515745	0.087900348	0.275008436	0.566502016	0.484115697	0.271
6	3	2	416	-0.561095119	-0.607371728	-0.387852082	-0.378173304	0.013026153	-0.672567546	1.102400732	0.418982527	0.508
7	3	3	355	-0.107715344	0.216024604	-0.004220932	0.090956878	0.280039173	-0.37262489	0.295456154	0.34363374	0.313
8	7	1	57	-3.991284307	-2.332079016	-4.625128744	-3.759390027	-1.960884555	-0.67896511	2.178431799	1.349032677	2.640
9	8	2	444	-0.110635981	-0.2406724	-0.062400174	0.457284594	0.103234949	0.149502745	0.353106558	0.303446606	0.275
10	2	3	161	-0.516436195	-1.236568171	0.925902586	2.00811637	1.15995215	-0.673892801	1.515979839	1.463098485	0.776
11	4	1	325	-0.568080433	-0.978701316	2.68622464	1.0465057	1.100187521	0.771966799	0.521471975	0.701541563	1.446
12	6	1	292	-2.068762275	-1.19505398	-0.297669165	0.163132131	-1.839963331	-1.18919392	1.400431054	0.730585978	0.463
13	3	2	302	0.049583698	-0.066231266	0.140878287	-0.11648114	0.16549014	-0.361162394	0.558813637	0.282329022	0.364
14	4	1	536	-0.578579668	-0.007232145	0.186873024	-0.120687584	-0.199520444	-0.368682153	0.491779984	0.359560973	0.412
15	6	1	268	-0.093338663	-0.39518676	-0.287041373	-0.483049557	-1.178791034	-1.043432093	0.637860418	0.523067962	0.852
16	2	2	72	-0.814503118	0.428510863	-1.016731663	-0.000796793	0.536746012	0.542826527	0.637545681	0.452790865	0.715
17	2	3	277	-0.123476358	-0.325934682	0.084674293	0.590577398	-0.489196711	-0.127666713	1.046095653	1.057204764	0.557
18	4	1	185	-0.557643811	-0.404320883	-0.186480607	-0.712874176	-0.765245963	-0.364786935	0.489237258	0.501957393	0.482
19	5	2	354	-0.225516643	0.048391249	0.432884772	0.836593587	0.603113104	0.820902365	1.073467518	0.738712527	0.501
20	6	1	11	0.076685848	-0.179560008	-0.4976599	-0.791360804	-0.438048892	-1.110338959	0.61689585	0.616785148	0.587
21	4	1	100	-0.872958025	-0.751928328	0.219340047	-0.424550242	-0.7715481	-0.743918845	0.67204774	0.72758827	0.223
22	6	1	409	0.344934344	0.619945203	0.107959105	0.201141896	1.017220058	1.058514922	0.978298701	0.666686618	0.429
23	7	2	399	-0.505761627	-0.510171442	-0.495947161	-0.439051716	-0.678009273	-0.557762771	0.618687382	0.496482079	0.583
24	4	1	248	0.653207271	0.288328272	-0.37332504	0.041242107	0.451119659	-0.180715163	0.644239978	0.609366689	0.869
25	6	2	435	1.293073989	0.753050315	1.489576294	1.092056984	0.747503536	1.061597786	0.856016928	0.617635379	0.997
26	5	3	260	0.837495075	0.712450805	0.776496827	0.897455831	0.721753636	0.68427924	0.53671613	0.457263594	0.445
27	8	3	393	-0.055722177	0.131892059	-0.26281005	0.096791201	0.206562121	0.199422186	0.599982255	0.494945253	0.582
28	3	2	384	0.035241945	0.028459339	-0.188623997	-0.032730202	0.017190726	0.054086388	0.778873009	0.164389399	0.441
29	5	2	10	0.868775332	-0.287631193	0.186952734	-0.087935366	0.521193236	0.27729248	1.023715819	0.656775916	0.520
30	5	3	315	-0.117656789	0.040523584	0.217115975	0.029584273	-0.124633277	0.005416847	0.338089586	0.311216484	0.303
31	4	2	132	0.869742309	0.927023997	-0.804239506	0.604990117	0.982980041	0.946110142	0.679262732	0.82542664	0.45
32	7	1	792	-0.7785983	-0.704451161	-0.438779497	-0.348667464	-0.32635761	-0.629222366	0.669546168	0.712716876	0.88

train test

Figure 36: Mixed Training Data

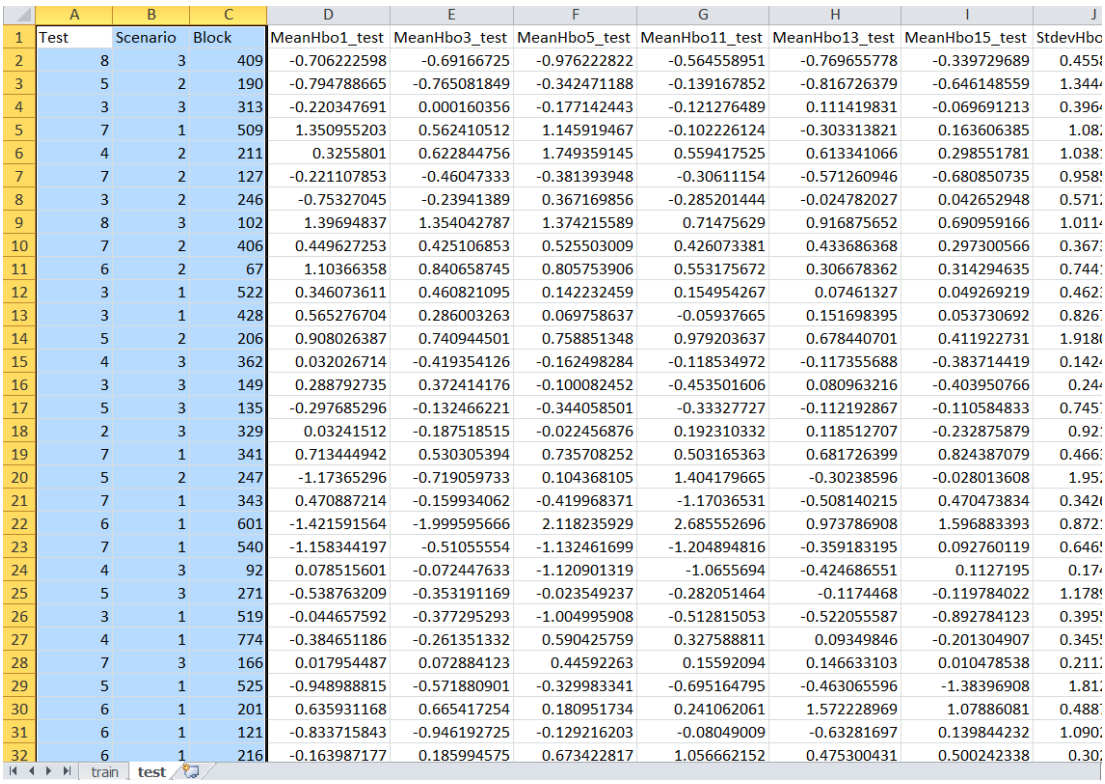

	A	B	C	D	E	F	G	H	I	J
1	Test	Scenario	Block	MeanHbo1_test	MeanHbo3_test	MeanHbo5_test	MeanHbo11_test	MeanHbo13_test	MeanHbo15_test	StdevHbo
2	8	3	409	-0.706222598	-0.69166725	-0.976222822	-0.564558951	-0.769655778	-0.339729689	0.455
3	5	2	190	-0.794788665	-0.765081849	-0.342471188	-0.139167852	-0.816726379	-0.646148559	1.344
4	3	3	313	-0.220347691	0.000160356	-0.177142443	-0.121276489	0.111419831	-0.069691213	0.396
5	7	1	509	1.350955203	0.562410512	1.145919467	-0.102226124	-0.303313821	0.163606385	1.08
6	4	2	211	0.3255801	0.622844756	1.749359145	0.559417525	0.613341066	0.298551781	1.038
7	7	2	127	-0.221107853	-0.46047333	-0.381393948	-0.30611154	-0.571260946	-0.680850735	0.958
8	3	2	246	-0.75327045	-0.23941389	0.367169856	-0.285201444	-0.024782027	0.042652948	0.571
9	8	3	102	1.39694837	1.354042787	1.374215589	0.71475629	0.916875652	0.690959166	1.011
10	7	2	406	0.449627253	0.425106853	0.525503009	0.426073381	0.433686368	0.297300566	0.367
11	6	2	67	1.10366358	0.840658745	0.805753906	0.553175672	0.306678362	0.314294635	0.744
12	3	1	522	0.346073611	0.460821095	0.142232459	0.154954267	0.07461327	0.049269219	0.462
13	3	1	428	0.565276704	0.286003263	0.069758637	-0.05937665	0.151698395	0.053730692	0.826
14	5	2	206	0.908026387	0.740944501	0.758851348	0.979203637	0.678440701	0.411922731	1.918
15	4	3	362	0.032026714	-0.419354126	-0.162498284	-0.118534972	-0.117355688	-0.383714419	0.142
16	3	3	149	0.288792735	0.372414176	-0.100082452	-0.453501606	0.080963216	-0.403950766	0.24
17	5	3	135	-0.297685296	-0.132466221	-0.344058501	-0.33327727	-0.112192867	-0.110584833	0.745
18	2	3	329	0.03241512	-0.187518515	-0.022456876	0.192310332	0.118512707	-0.232875879	0.92
19	7	1	341	0.713444942	0.530305394	0.735708252	0.503165363	0.681726399	0.824387079	0.466
20	5	2	247	-1.17365296	-0.719059733	0.104368105	1.404179665	-0.30238596	-0.028013608	1.95
21	7	1	343	0.470887214	-0.159934062	-0.419968371	-1.17036531	-0.508140215	0.470473834	0.342
22	6	1	601	-1.421591564	-1.999595666	2.118235929	2.685552696	0.973786908	1.596883393	0.872
23	7	1	540	-1.158344197	-0.51055554	-1.132461699	-1.204894816	-0.359183195	0.092760119	0.646
24	4	3	92	0.078515601	-0.072447633	-1.120901319	-1.0655694	-0.424686551	0.1127195	0.17
25	5	3	271	-0.538763209	-0.353191169	-0.023549237	-0.282051464	-0.1174468	-0.119784022	1.178
26	3	1	519	-0.044657592	-0.377295293	-1.004995908	-0.512815053	-0.522055587	-0.892784123	0.395
27	4	1	774	-0.384651186	-0.261351332	0.590425759	0.327588811	0.09349846	-0.201304907	0.345
28	7	3	166	0.017954487	0.072884123	0.44592263	0.15592094	0.146633103	0.010478538	0.211
29	5	1	525	-0.948988815	-0.571880901	-0.329983341	-0.695164795	-0.463065596	-1.38396908	1.81
30	6	1	201	0.635931168	0.665417254	0.180951734	0.241062061	1.572228969	1.07886081	0.488
31	6	1	121	-0.833715843	-0.946192725	-0.129216203	-0.08049009	-0.63281697	0.139844232	1.090
32	6	1	216	-0.163987177	0.185994575	0.673422817	1.056662152	0.475300431	0.500242338	0.30

train test

Figure 37: Mixed Test Data

After preparing of this data LDA was run on SPSS again. A slight improvement was observed due to change in the training strategy, where the highest accuracy percentage obtained was 50%. All related result table and graphs can be seen in *4.6.* part of Result chapter and *Appendix C - ACCURACY SCORES OF LDA.*

Since ANN analysis was conducted in Matlab, the test and training data had already been selected randomly. Therefore it is not repeated again.

When mixed data is given as input to SVM algorithm, the accuracy have dramatically increased from 64s% to 86%. Moreover the confusion matrix is also derived very effectively. All classes can be classified with reasonable accuracy. All related results table and the graphs can be seen in *4.6.* part of Result chapter and *Appendix D - ACCURACY SCORES AND INDEXIES OF SVM.*

Forming a training set that included samples of data from all participants was found to have a significant effect on mental workload prediction based on fNIRS measures. It is observed that for developing a model, training data should include partial data of the test subject whose mental workload would be predicted. Overall, SVM outperformed the LDA and ANN classifiers. It is thought that LDA's relatively poor performance could be due to its reliance on linear factors for classification, which apparently could not handle the nonlinear nature of the mental workload dataset.. As compared to LDA, ANNs provide more flexibility to account for the nonlinear relationships in the data. The new training strategy slightly increased the accuracy of the ANN classifier. However, a simple feedforward network cannot take into consideration the sequential dependencies within the data. Since mental workload changes have a temporal dimension, ANNs that can realize temporal dependencies such as recurrent neural nets (RNN) and their deep learning counterpart called long short term memory (LSTM) are also considered in this thesis.

Recurrent Neural Network Analysis

Recurrent Neural Network provides us to feed previous hidden layer to current hidden layer values calculation. By this way, effects of previous inputs (not only current timestamp - 1) are considered in current calculations. Although slide window design mentioned in part **3.3** of this chapter (figure 24) reflects historical data of the pilot in current data, same approach would be beneficial in the prediction of changes in mental workload levels.

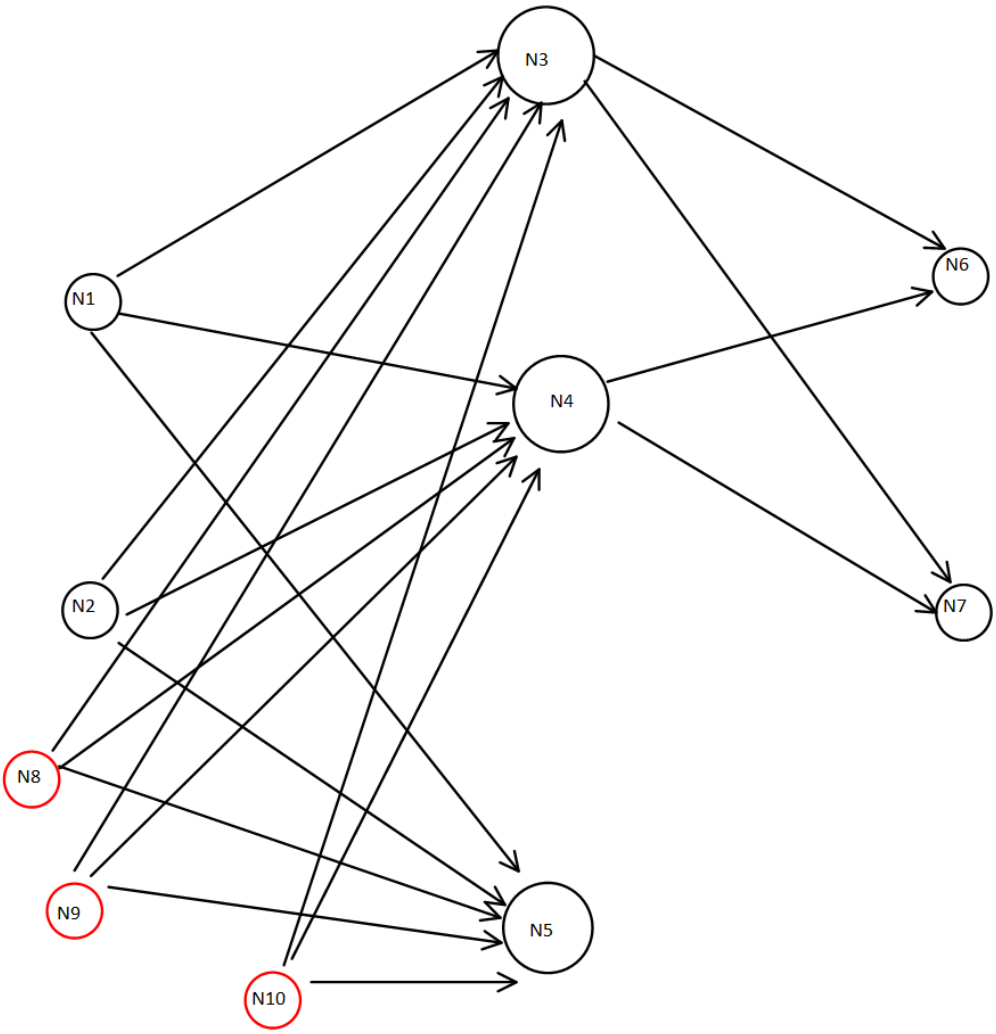

Figure 38: Recurrent Neural Network Structure

Differences of between figure 35 and figure 38 are the three extra nodes feeding hidden layer. And calculations in *3.4.5 Artificial Neural Network* part are updated as:

N1 Value = same with ANN

N2 Value = same with ANN

N3 Value =
- **0** if w13 * N1 + w23 * N2 + w83 * N8 + w93 * N9 + w103 * N10 + b < = 0
- **1** if w13 * N1 + w23 * N2 + w83 * N8 + w93 * N9 + w103 * N10 + b > 0

N4 Value =
- **0** if w14 * N1 + w24 * N2 + w84 * N8 + w94 * N9 + w104 * N10 + b < = 0
- **1** if w14 * N1 + w24 * N2 + w84 * N8 + w94 * N9 + w104 * N10 + b > 0

N5 Value =

0 if w15 * N1 + w25 * N2 + w85 * N8 + w95 * N9 + w105 * N10 + b < = 0

1 if w15 * N1 + w25 * N2 + w85 * N8 + w95 * N9 + w105 * N10 + b < = 0

N6 = y1 Value = same with ANN

N7 = y2 Value = same with ANN

N8 = N3

N9 = N4

N10 = N5

Where

w83 is weight between node 8 (N8) to node 3 (N3)

w93 is weight between node 9 (N9) to node 3 (N3)

w103 is weight between node 10 (N10) to node 3 (N3)

w84 is weight between node 8 (N8) to node 4 (N4)

w94 is weight between node 9 (N9) to node 4 (N4)

w104 is weight between node 10 (N10) to node 4 (N4)

w85 is weight between node 8 (N8) to node 5 (N5)

w95 is weight between node 9 (N9) to node 5 (N5)

w105 is weight between node 10 (N10) to node 5 (N5)

During the application of the formulas given above, the weigted sum of node values and the connection weights are given as input to a sigmoid function or tanh function so that their outputs are kept in between 0 and 1.

In order to apply recurrent neural network into this study, Keras library functions such as *model.compile(), model.fit(),model.evaluate(),model.predict_classes()* are used in python programming language. With parameter tuning (batch size, hidden layer nodes), several analyses are performed. For loss function *categorical_crossentropy,* for activation *softmax* functions are used. Even though 84% accuracy is obtained as the highest score, its hidden node number is too much(1000 hidden nodes) causing the algorithm to be slow for practical use. Therefore 78% with hidden layer node number 102 was found to be an optimal combination for the RNN model. Also its confusion matrix is satisfactory (enable

to separate all four classes). *4.7* part of Result chapter and Appendix F - ACCURACY SCORES OF RNN indicate all results of RNN analyses with different inputs.

3.4.7. LSTM Analysis

Recurrent neural network is a powerful ANN method that can take into account previous data just a few timestamps before the current time calculation into the classification results. However, when a longer data history needs to be used, exploding or vanishing gradient problems occur in standart RNNs, and therefore the model cannot learn the input – output correlations that occur for a longer period of time, leading to a low prediction accuracy [83]. In order to solve this problem LSTM (Long Short Term Memory) which is a kind of deep learning algorithm can be used. It is actually a special form of recurrent neural network and introduced to the literature by Hochreiter and Schmidhuber[84].

In the classical recurrent neural network hidden layer consists of nodes. However LSTM uses memory units instead of nodes. Each memory cell includes cells which are formed from a sigmoid/tanh function and scalar operator as seen in figure 38.

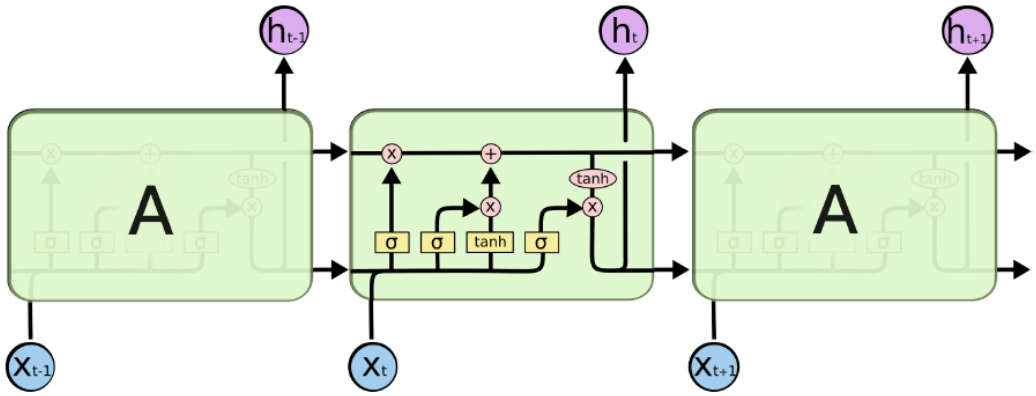

Figure 39: LSTM Structure[85]

These cells decide:

- which data is transferred to next layer,
- which data is stored into this memory,
- how weights are updated,

with following formulas in figure 40,41,42,43.

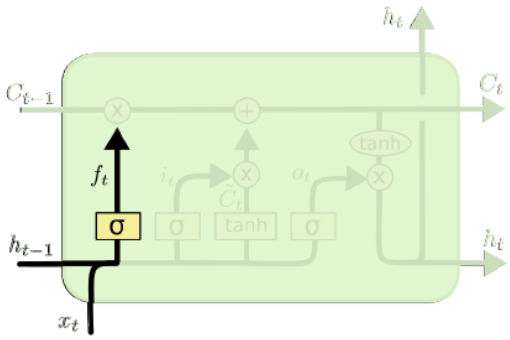

$$f_t = \sigma\left(W_f \cdot [h_{t-1}, x_t] \; + \; b_f\right)$$

Figure 40: LSTM – Data To Be Transferred Decision Structure[85]

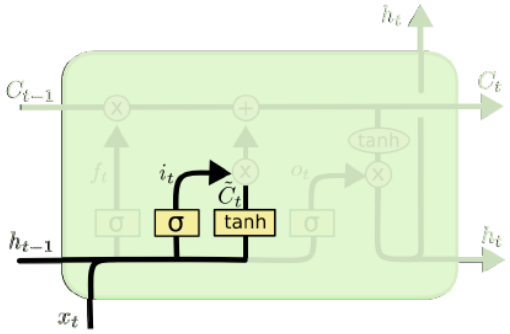

$$i_t = \sigma\left(W_i \cdot [h_{t-1}, x_t] \; + \; b_i\right)$$
$$\tilde{C}_t = \tanh(W_C \cdot [h_{t-1}, x_t] \; + \; b_C)$$

Figure 41: LSTM – Data To Be Stored Decision Structure[85]

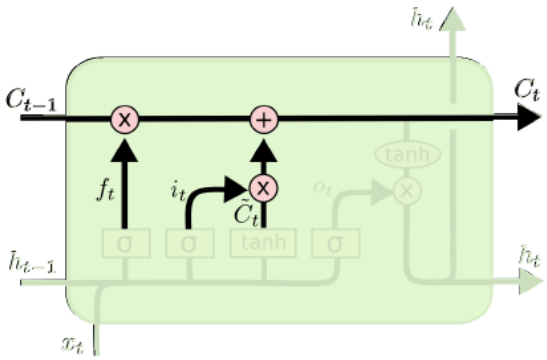

$$C_t = f_t * C_{t-1} + i_t * \tilde{C}_t$$

Figure 42: LSTM – Cell Updating Structure[85]

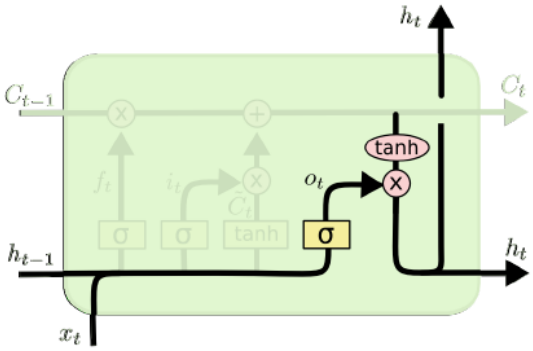

$$o_t = \sigma\left(W_o\left[h_{t-1}, x_t\right] + b_o\right)$$
$$h_t = o_t * \tanh\left(C_t\right)$$

Figure 43: LSTM – Weight Updating Structure[85]

After understating philosophy of LSTM, again Keras library functions are used in this study with Python programming language. Although several functions which are used before for RNN are same, different functions such as *LSTM()* have to be managed.

After analyzing the model with different input combinations (LSTM number, batch size) very similar results with RNNs are obtained. For instance, highest accuracy is 82% with LSTM number 100, batch size 8. All analyses results are given in *4.8* part of Result chapter and *Appendix G - ACCURACY SCORES OF LSTM.*

CHAPTER 4

4. RESULTS

In this chapter, the results obtained from each machine learning model employed are summarized and evaluated.

4.1. LDA with Primitive Methods

This part shows the results of the primitive method which is illustrated in Method chapter 3.4.1 and 3.4.2. The method employed the LDA algorithm which was trained on a single pilot and applied over the remaining test data.

4.1.1. SPSS Results

Table 3: Eigenvalues of Two Canonical Discriminant Functions

Eigenvalues

Function	Eigenvalue	& of Variance	Cumulative %	Canonical Correlation
1	1.816[a]	73.2	73.2	0.803
2	0.666[a]	26.8	100.0	0.632

a. First 2 canonical discriminant functions were used in the analysis.

Table 4: Wilk' Lambda Results Specifying Weight of the Functions

Wilks' Lambda

Test of Function(s)	Wilks' Lambda	Chi-square	df	Sig.
1 through 2	0.213	1047.319	208	0.000
2	0.600	345.810	103	0.000

Tables 3 and 4 suggest that the LDA model produced a model with 2 discriminant functions that can significantly differentiate the given workload categories. Table 5 below summarizes the classification accuracy obtained for the training sample, where the linear functions could categorize 91% of the cases correctly. In the first modeling attempt only 3 mental workload levels, namely low, medium and high, were considered. This is why the predicted group membership part is a 3 by 3 matrix. Figure 44 below shows the centroids for the 3 categories formed by the LDA algorithm.

Table 5: Success Rate of Classification

Classification Results[a]

Workload			Predicted Group Membership			Total
			0	1	2	
Original	Count	0	480	32	1	513
		1	20	152	8	180
		2	0	4	35	39
	%	0	93,6	6,2	0,2	100,0
		1	11,1	84,4	4,4	100,0
		2	0,0	10,3	89,7	100,0

a. 91.1% of original grouped cases **correctly classified**.

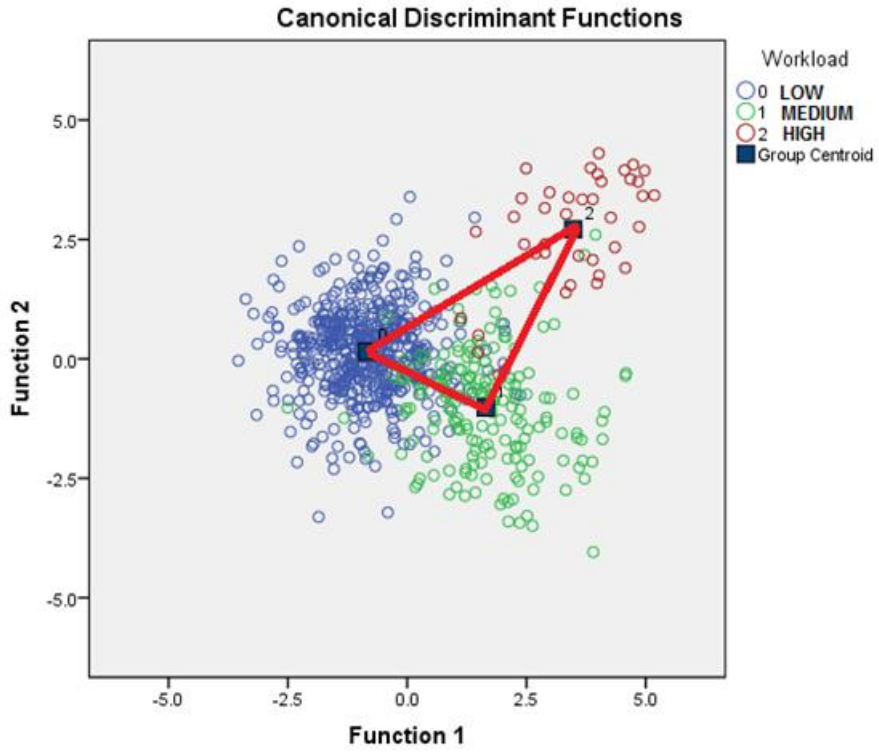

Figure 44: Distribution of the Data in 2 Dimensions

4.1.2.Experiment Results

The model processing application is executed for 8 test subjects and 30 experiments to test the LDA classifier described above as if it was running real-time during an experiment. Results are analyzed with graphs and evaluated by looking at specific events where mental workload changes are expected. Following 30 graphs shows hbo/hbr signal changes and corresponding workload level changes. Moreover specific events are put into the graphs. These events are logged during test executions and illustrate the critical events occuring at those times. However, in tests 7 and 8 no such additional information was present in the dataset, so only the videos are used to evaluate the matching of expected mental workload levels with actual mental workload levels in those cases. Furthermore, only the optodes located at the edges (i.e. close to dorsolateral prefrontal cortex) are displayed in the graphs below, since these are the optodes that most significantly contributed to the LDA model, possibly due to these regions role in working memory management [70].

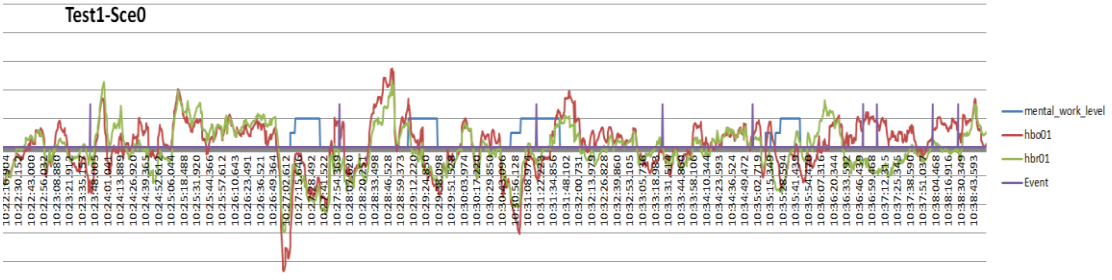

Figure 45: Test Subject1, Scenario0 Graph

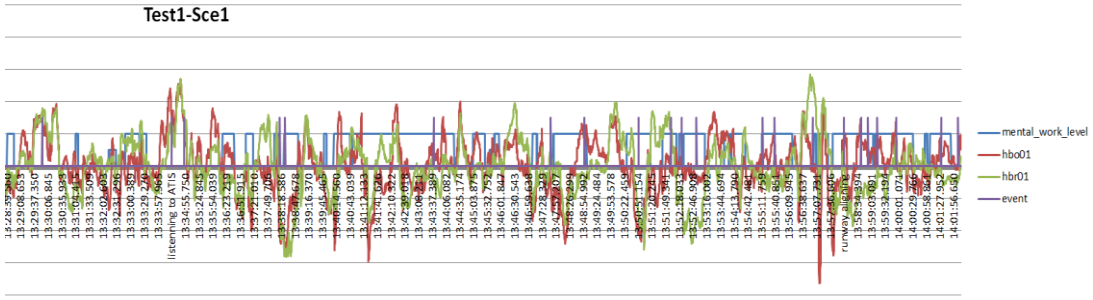

Figure 46: Test Subject1, Scenario1 Graph

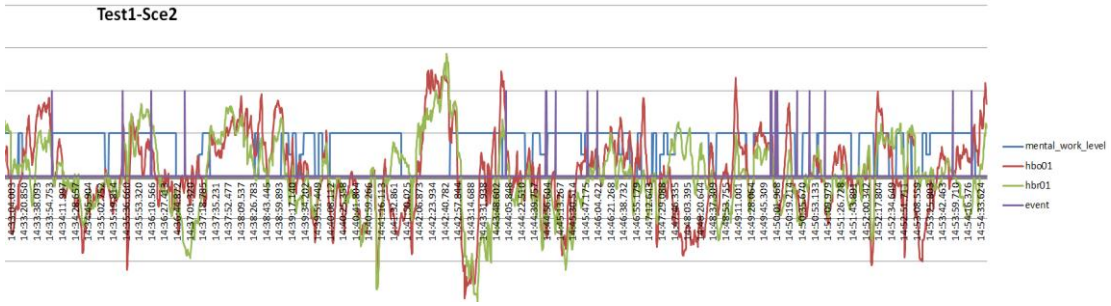

Figure 47: Test Subject1, Scenario2 Graph

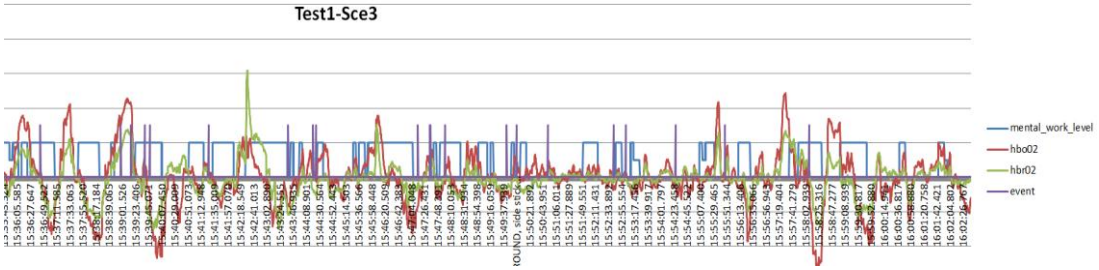

Figure 48: Test Subject1, Scenario3 Graph

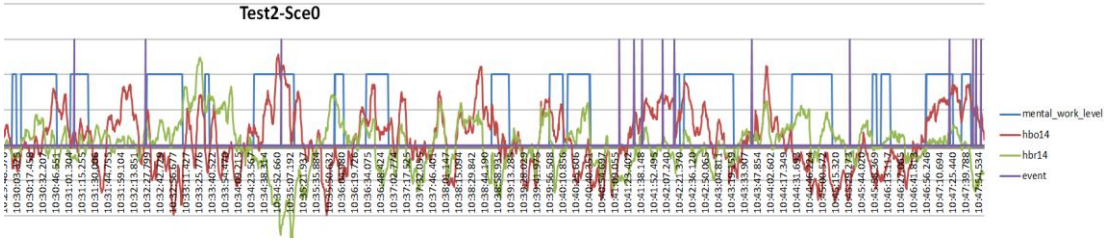

Figure 49: Test Subject2, Scenario0 Graph

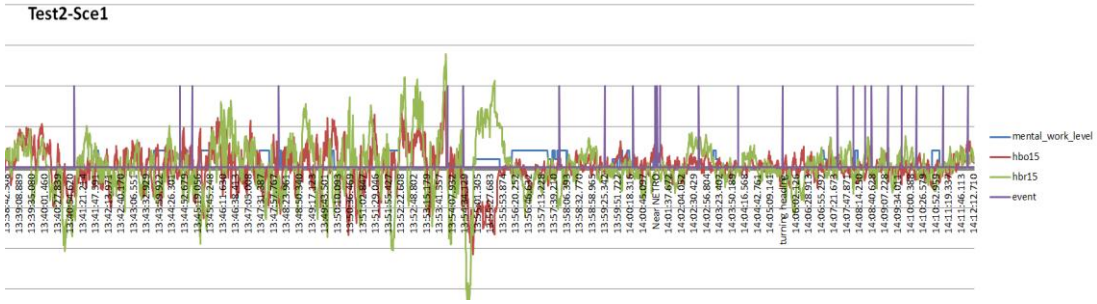

Figure 50: Test Subject2, Scenario1 Graph

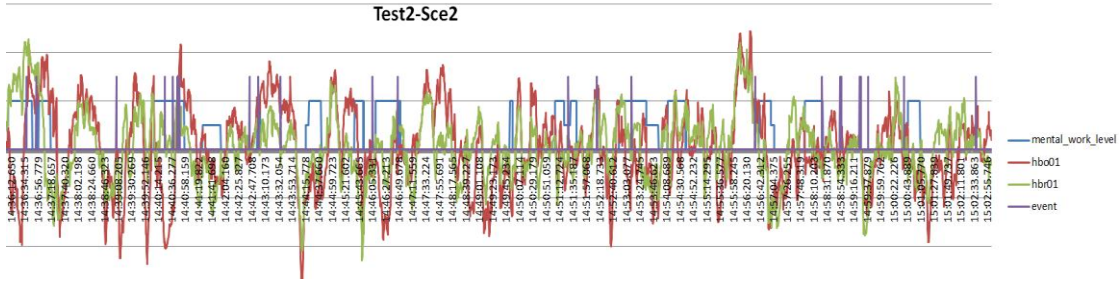

Figure 51: Test Subject2, Scenario2 Graph

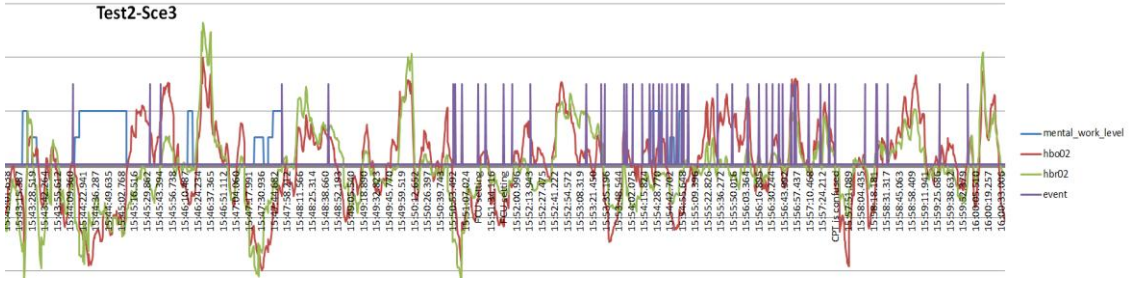

Figure 52: Test Subject2, Scenario3 Graph

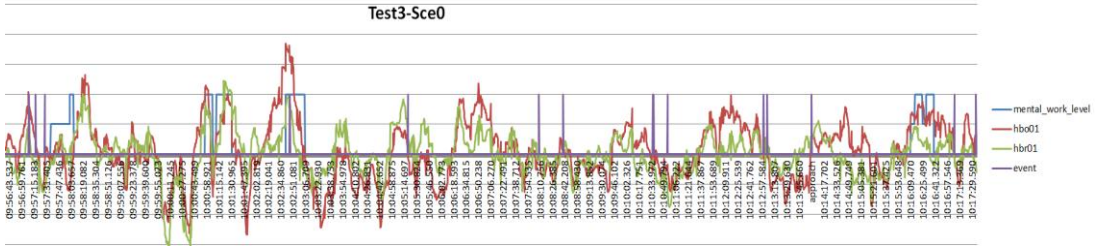

Figure 53: Test Subject3, Scenario0 Graph

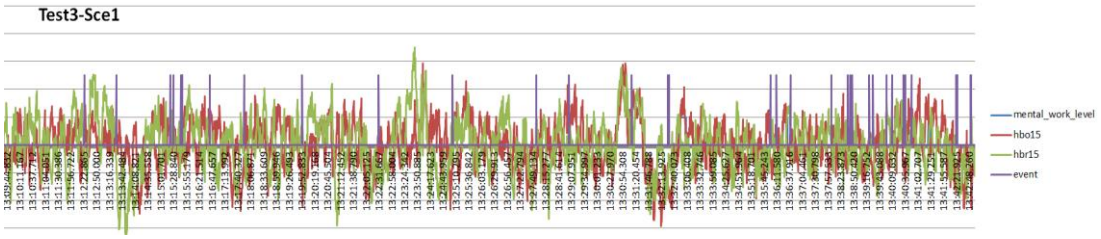

Figure 54: Test Subject3, Scenario1 Graph

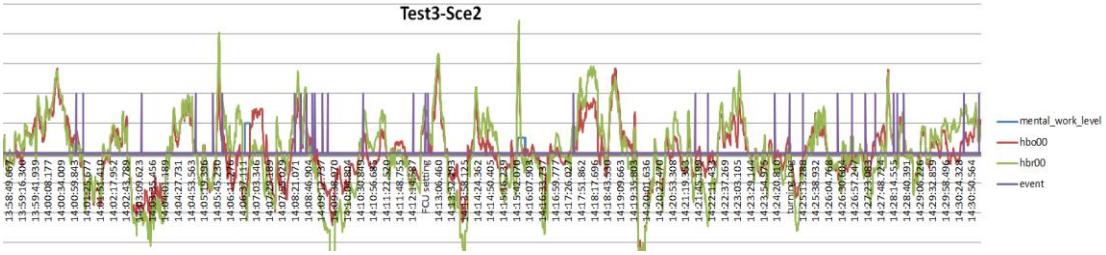

Figure 55: Test Subject3, Scenario1 Graph

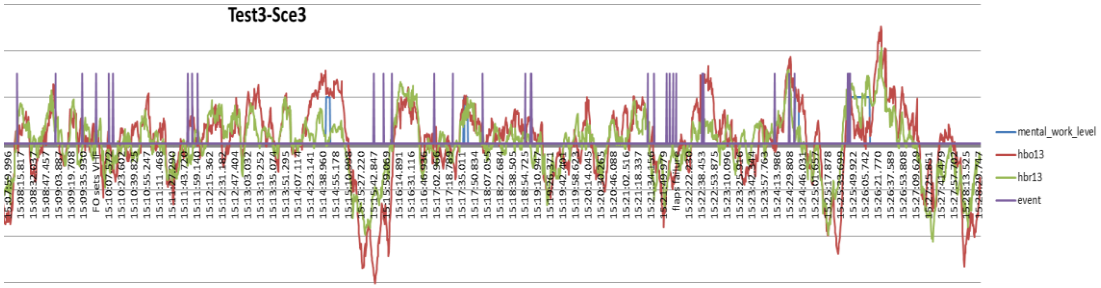

Figure 56: Test Subject3, Scenario3 Graph

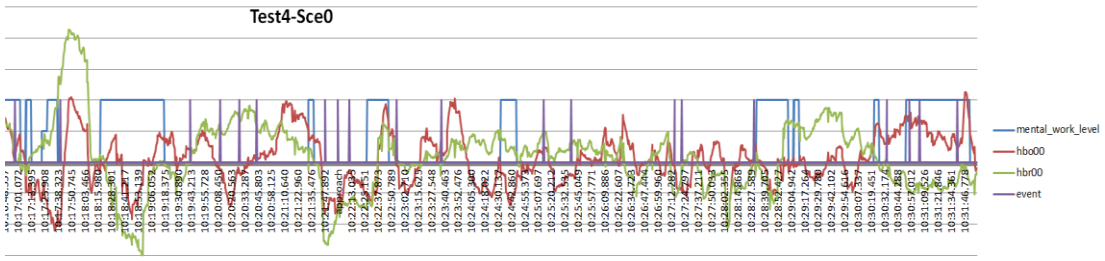

Figure 57: Test Subject4, Scenario0 Graph

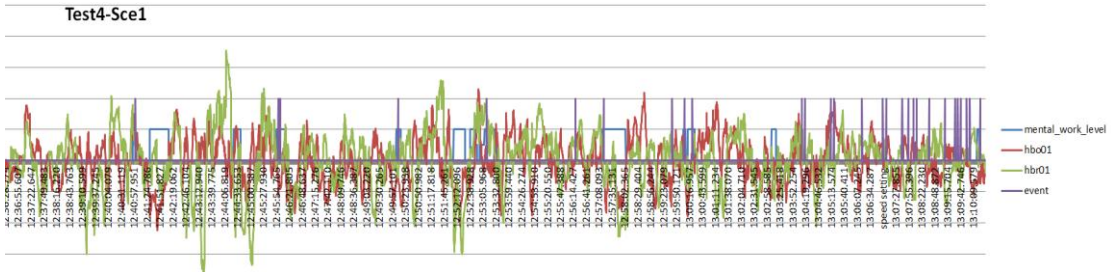

Figure 58: Test Subject4, Scenario1 Graph

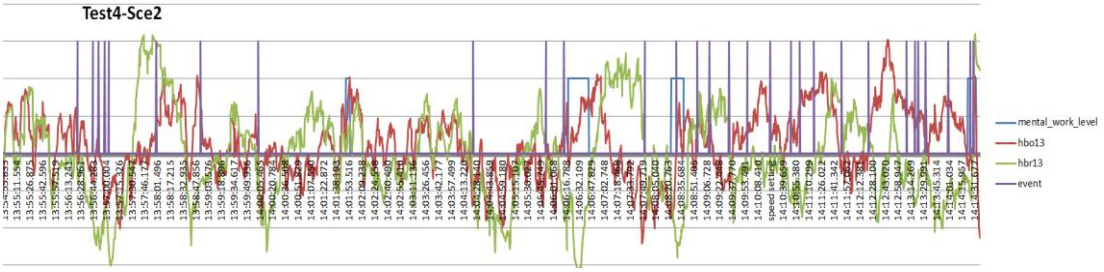

Figure 59: Test Subject4, Scenario2 Graph

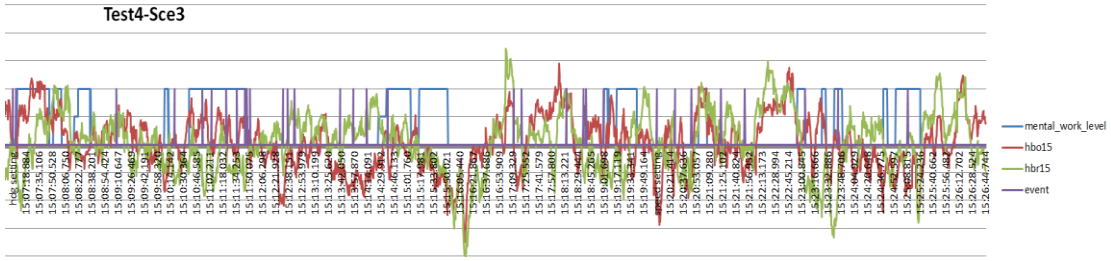

Figure 60: Test Subject4, Scenario3 Graph

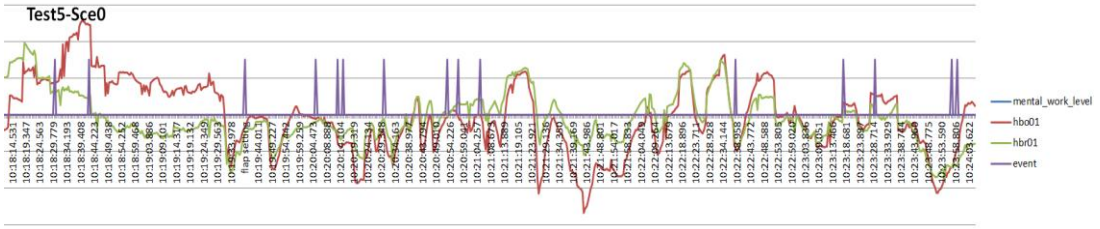

Figure 61: Test Subject5, Scenario0 Graph

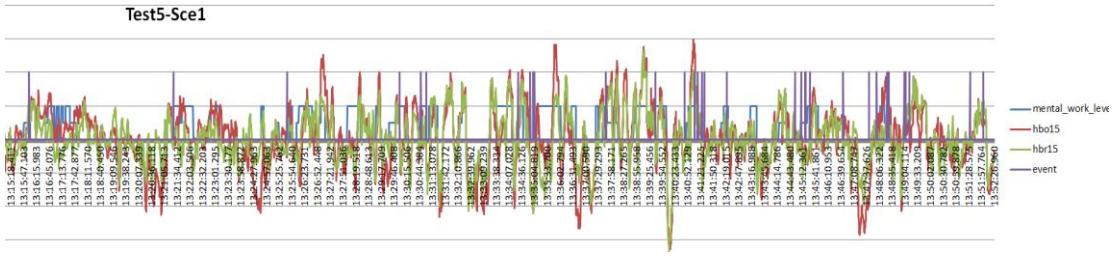

Figure 62: Test Subject5, Scenario1 Graph

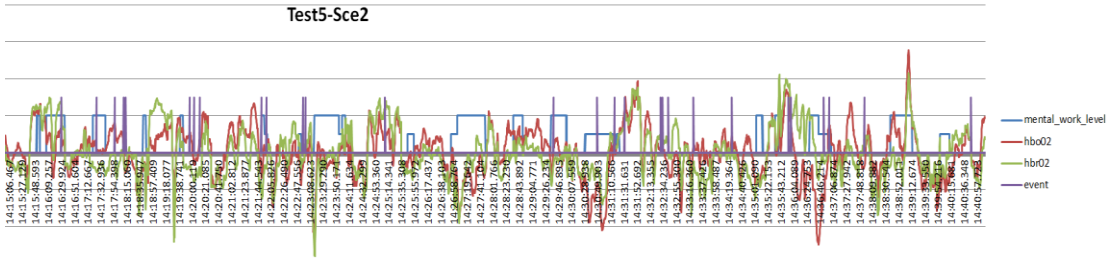

Figure 63: Test Subject5, Scenario2 Graph

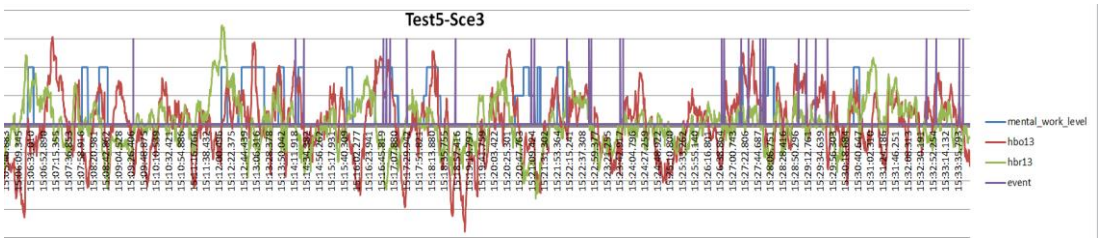

Figure 64: Test Subject5, Scenario3 Graph

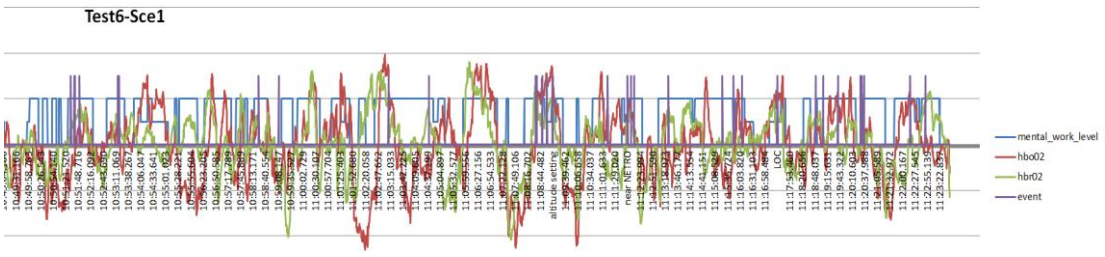

Figure 65: Test Subject6, Scenario1 Graph

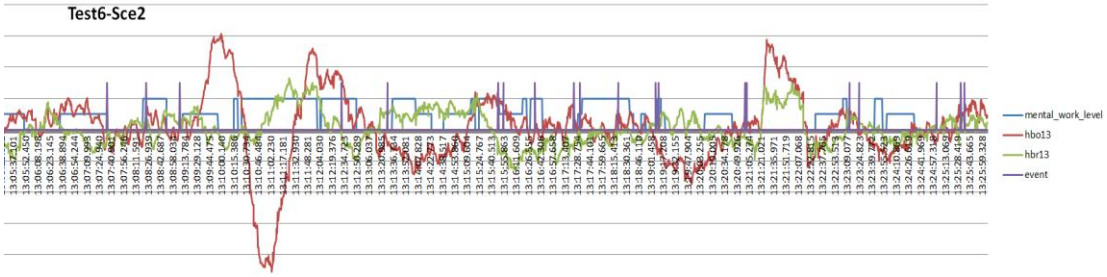

Figure 66: Test Subject6, Scenario2 Graph

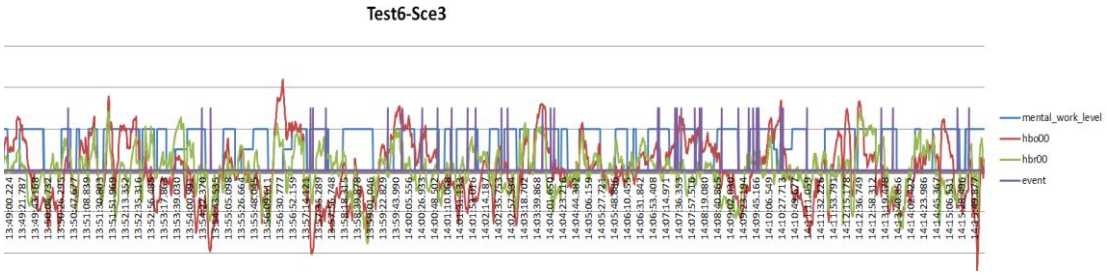

Figure 67: Test Subject6, Scenario3 Graph

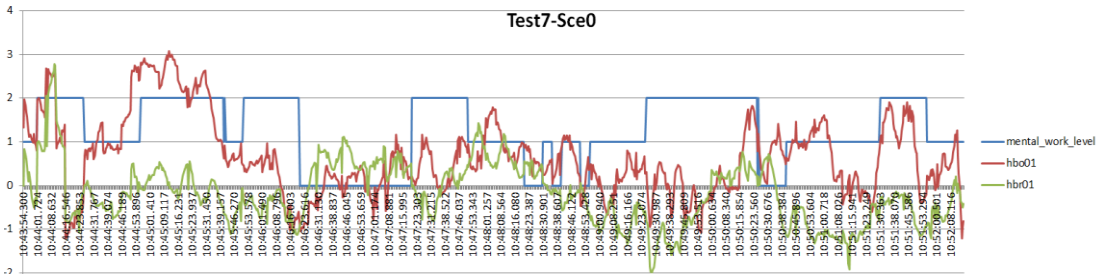

Figure 68: Test Subject7, Scenario0 Graph

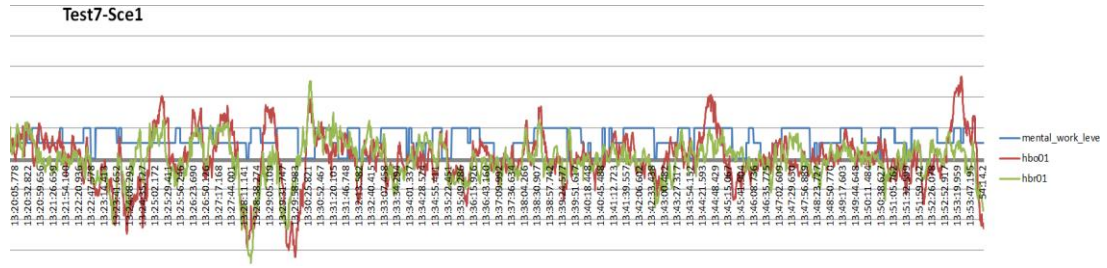

Figure 69: Test Subject7, Scenario1 Graph

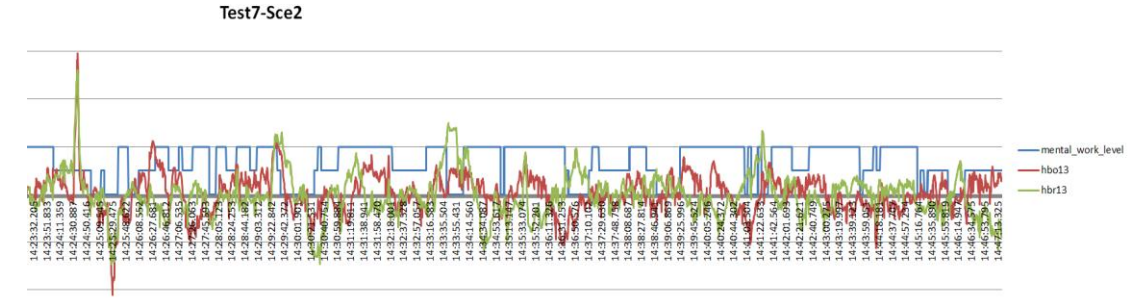

Figure 70: Test Subject7, Scenario2 Graph

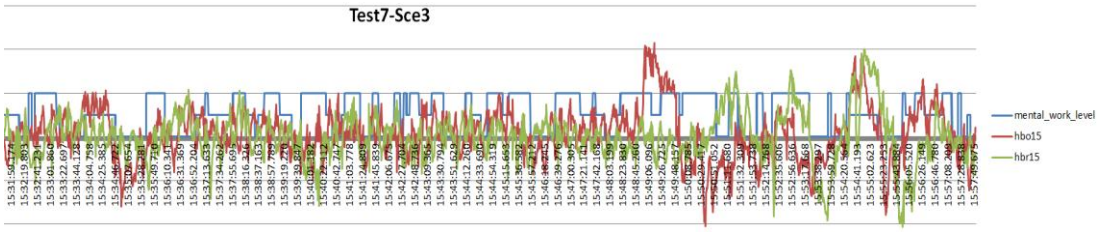

Figure 71: Test Subject7, Scenario3 Graph

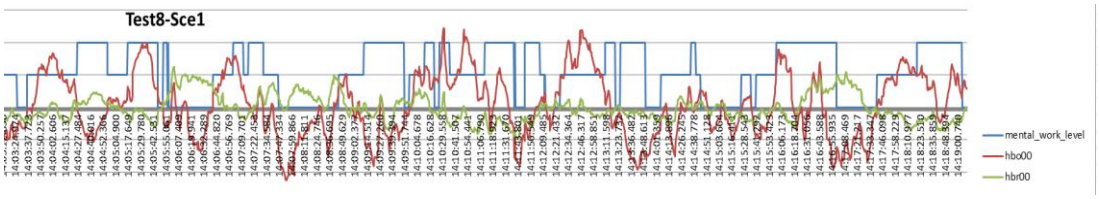

Figure 72: Test Subject8, Scenario1 Graph

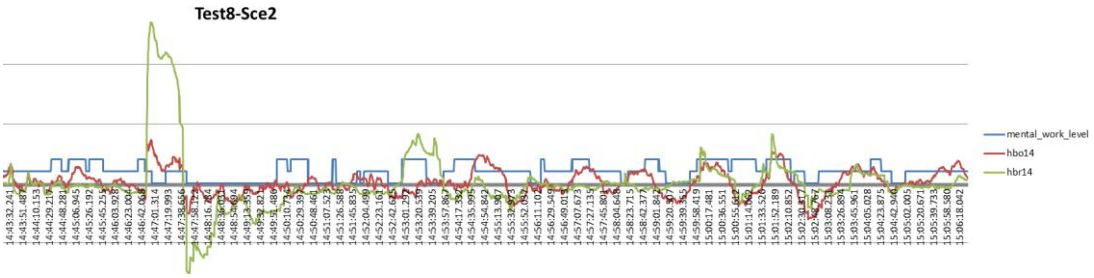

Figure 73: Test Subject8, Scenario2 Graph

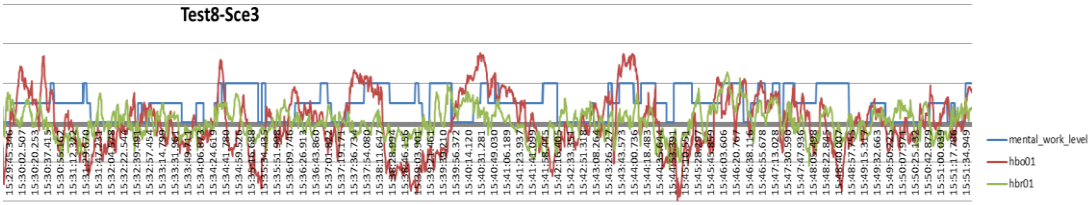

Figure 74: Test Subject8, Scenario3 Graph

The graphs displayed above capture the modulation of buffered fNIRS signals in relation to predicted mental workload levels and critical events during the entire session. In order to illustrate how the accuracy analysis was conducted, a shorther excerpt is illustrated in the examples below. Figures 62 and 63 are the sessions from which these two samples were obtained. We evaluated the test results by considering whether the actual mental workload level matches with the expected workload level for each specific event. For this analysis, test videos were played in parallel with hbo, hbr signals while deciding whether there is a robust correspondence between signal change and workload levels. Moreover, the events logged by the experimenters are also considered while counting matching and mismatching cases.

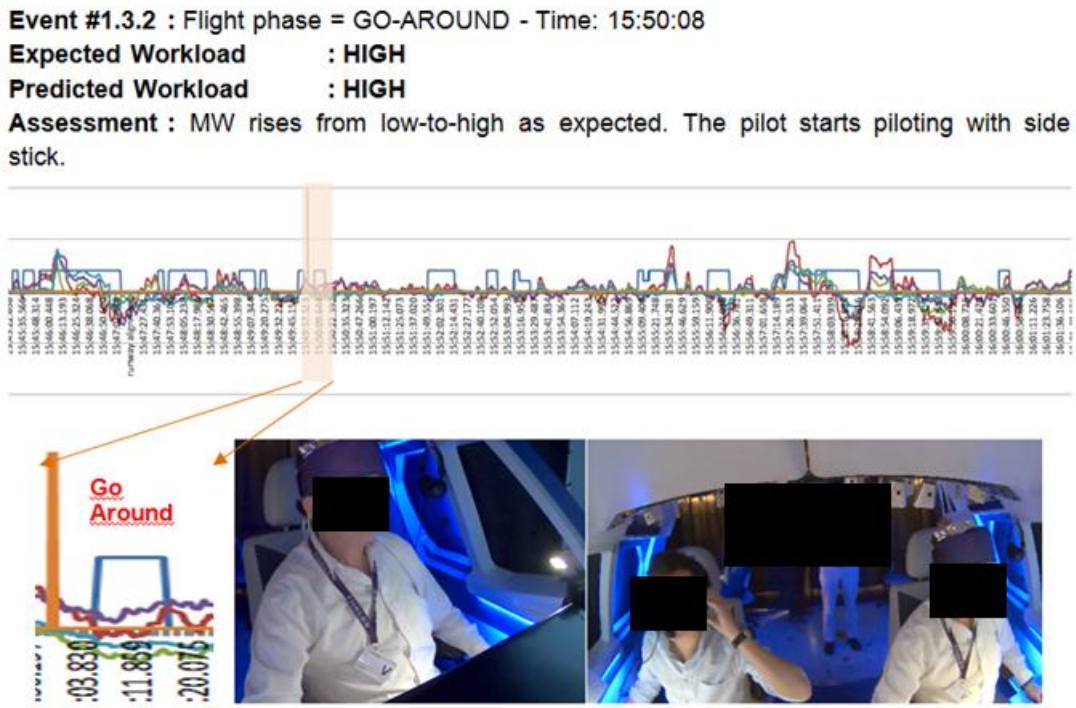

Figure 75: A sample of Test Result Evaluation

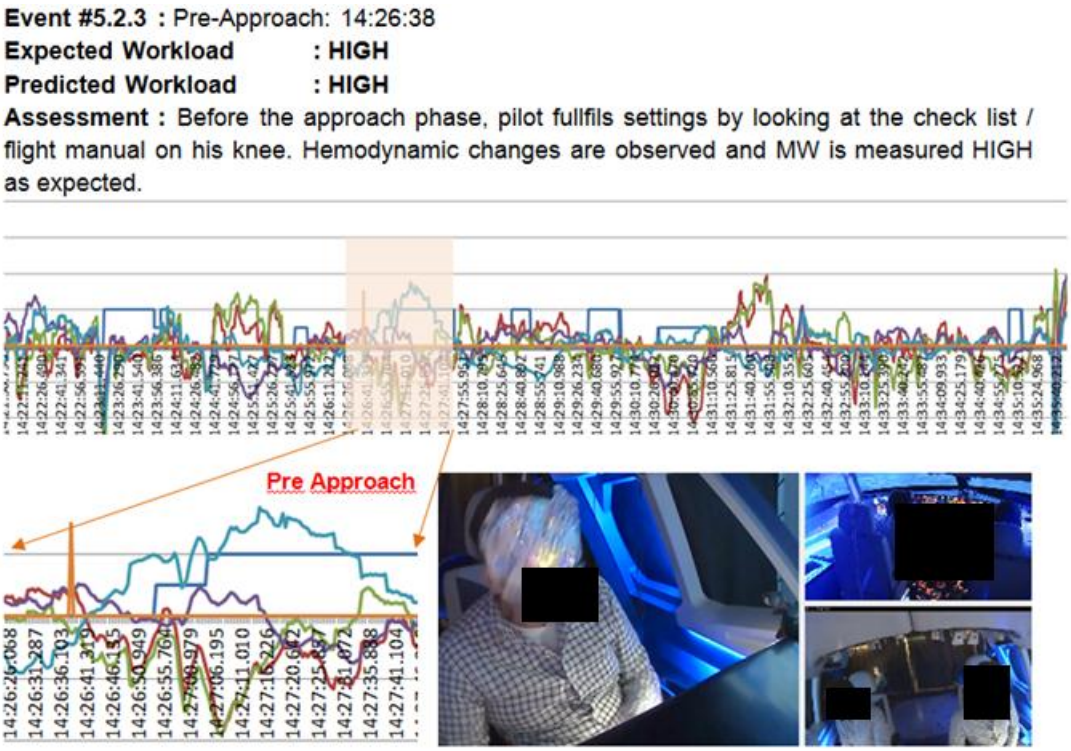

Figure 76: A sample of Test Result Evaluation

After analyzing 69 test events sampled from 18 tests with 6 test subjects, we obtained the following results.

Table 6: Success Rate on Matching of Actual vs. Expectation Mental Workload

Predicted * Expected Crosstabulation						
			Expected			Total
			0	1	2	
Predicted	0	Count	**13**	2	5	20
		% of Total	**18.8%**	2.9%	7.2%	29.0%
	1	Count	0	**5**	0	5
		% of Total	0.0%	**7.2%**	0.0%	7.2%
	2	Count	11	4	**29**	44
		% of Total	15.9%	5.8%	**42.0%**	63.8%
Total		Count	24	11	34	69
		% of Total	34.8%	15.9%	49.3%	100.0%

Of the 69 cases we analyzed, in 68.1% of the cases there was a perfect match between the predicted and expected mental workload levels. The highest number of mismatches occurred when the model predicted a high MW case, whereas the expectation was low MW. As indicated under specific instances above, such cases arose due to fluctuations in the raw oxygenation measures due to excessive head motion or noise in some of the optodes that contribute to the model.

In our first analysis the 69 test cases were handpicked from the data, especially to check for the model's performance in high workload critical situations generated in the simulator. The cases included 24 low, 11 medium and 34 high mental workload cases, and the model could accurately predict 68% of these special cases. This analysis focuses on the high predictions mainly, to understand whether the model could predict high load cases, and to what extent it generates false alarms. The results suggested that the model succeeded in capturing 29 out of 34 high MW cases, misclassified 5 medium and 11 low MW cases as high MW. Moreover, in 5 instances the model predicted low workload, where the expectation was high. Although the handpicked examples were important for proof of concept analysis, it did not reflect the actual distribution of events observed during the tests. For that reason, the analysis is expanded even further with a more sophisticated multidimensional annotation scheme and more advanced machine learning algorithms.

4.2. Mental Workload Distributions

Following two tables shows mental workload level distributions of the test subjects in all test scenarios. As you can see in the graphs, mental workload level 0 is most common mental workload level to be met. Due to test scenario design, most mental workload level 2 is observed in scenario3. Moreover mental workload level -1 is very few in all scenarios of all test subjects since the sensor was in general accurately placed over the forehaed, especially the signals obtained from odd-numbered optodes corresponding to the top row were successfully shielded from other infra-red sources, and the pilots performed minimal excessive head movements.

Table 7: Mental Workload Distributions on the Pilots

Test Subject	MW	Count	%
2	-1	24	2.973977695
2	0	500	61.95786865
2	1	207	25.65055762
2	2	76	9.417596035
	Total	**807**	**100**
3	-1	22	1.337386018

3	0	1279	77.75075988
3	1	306	18.60182371
3	2	38	2.310030395
	Total	**1645**	**100**
4	-1	28	1.677651288
4	0	1115	66.80647094
4	1	469	28.10065908
4	2	57	3.415218694
	Total	**1669**	**100**
5	-1	35	2.092050209
5	0	1139	68.08129109
5	1	465	27.79438135
5	2	34	2.032277346
	Total	**1673**	**100**
6	-1	28	1.664684899
6	0	931	55.35077289
6	1	652	38.76337693
6	2	71	4.221165279
	Total	**1682**	**100**
7	-1	40	2.37953599
7	0	1146	68.17370613
7	1	413	24.5687091
7	2	82	4.87804878
	Total	**1681**	**100**
8	-1	19	1.528559936
8	0	880	70.79646018
8	1	303	24.37650845
8	2	41	3.29847144
	Total	**1243**	**100**

Table 8: Mental Workload Distributions Based on Test Scenarios

Test Scenario	**MW**	**Count**	**%**
1	-1	107	2.494754022
1	0	3248	75.72860807
1	1	934	21.77663791
1	2	0	0
	Total	**4289**	**100**
2	-1	37	1.158422041
2	0	1983	62.08515967
2	1	1173	36.72510958
2	2	1	0.031308704

	Total	**3194**	**100**
3	-1	52	1.783264746
3	0	1759	60.3223594
3	1	707	24.24554184
3	2	398	13.64883402
	Total	**2916**	**100**

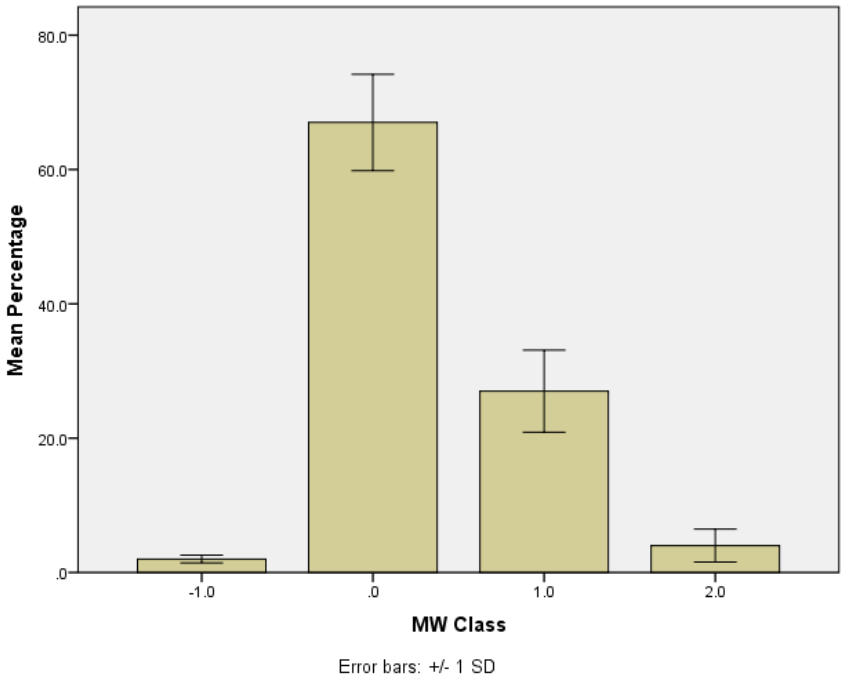

Figure 77: Mental Workload Distribution on All Tests

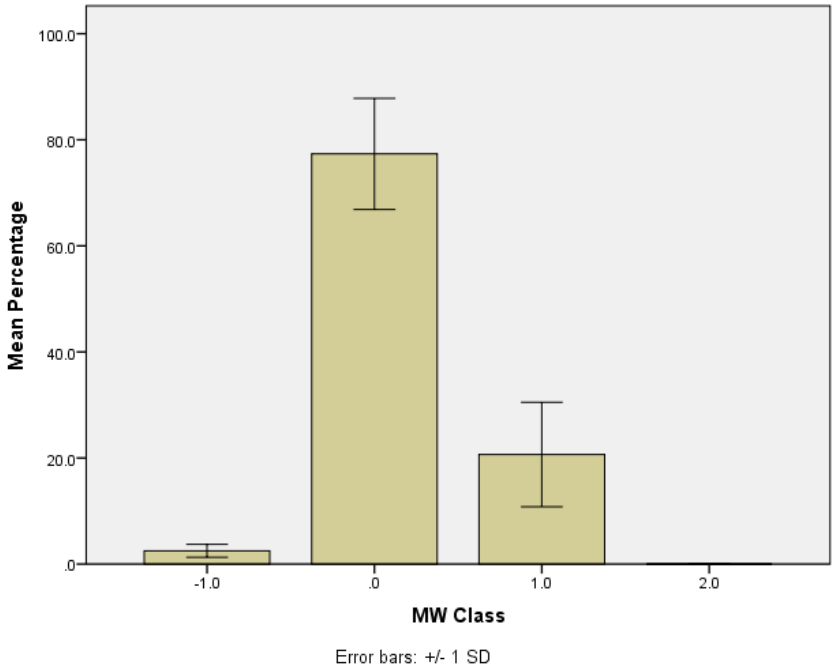

Figure 78: Mental Workload Distribution on All Scenario1s

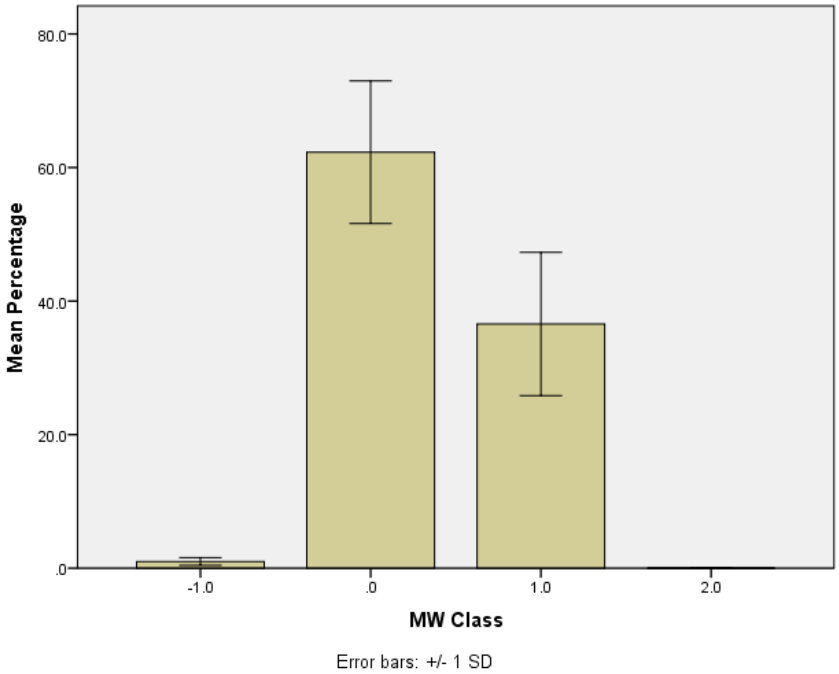

Figure 79: Mental Workload Distribution on All Scenario2s

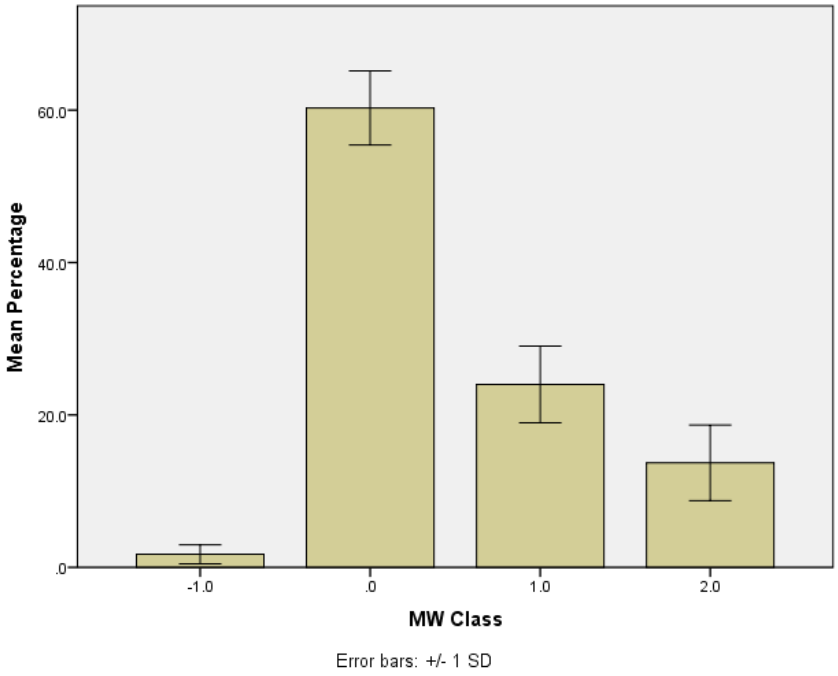

Figure 80: Mental Workload Distribution on All Scenario3s

4.3. LDA with Enhanced Methods

This part illustrates results of the LDA algorithm explained in the Method chapter 3.4.3 (Training Data does not include data samples from all pilots). As you can see in the tables and figures below, LDA results are not satisfactory when expanded over the entire dataset. Moreover different input combinations of LDA and accuracy results are given in Appendix C. Following results are sample of all analysis in Appendix C (Training Data: 2,3,4,5, Raw Data: hbo, hbr, features: mean, stdev, slope, range).

Table 9: Eigenvalues of Two Canonical Discriminant Functions

Function	Eigenvalue	% of Variance	Cumulative %	Canonical Correlation
1	.123[a]	51.0	51.0	.331
2	.079[a]	33.0	84.0	.271
3	.038[a]	16.0	100.0	.192

a. First 3 canonical discriminant functions were used in the analysis.

Table 10: Wilk' Lambda Results Specifying Weight of the Functions

Test of Function(s)	Wilks' Lambda	Chi-square	df	Sig.
1 through 3	.795	1325.678	144	.000
2 through 3	.892	657.775	94	.000
3	.963	217.234	46	.000

Table 11: Standardized Canonical Discriminant Function Coefficients

	Function		
	1	2	3
MeanHbo1	-.121	.238	.486
MeanHbo3	-.166	-.067	-.394
MeanHbo5	.093	.060	.071
MeanHbo11	-.312	.002	.050
MeanHbo13	.103	-.276	-.068
MeanHbo15	.305	.213	.117
StdevHbo1	.541	-.210	-.577
StdevHbo3	-.209	-.052	.138
StdevHbo5	.455	.243	-.188
StdevHbo11	-.591	-1.323	.676
StdevHbo13	.904	.085	-.561
StdevHbo15	-.142	-.111	-.405
SlopeHbo1	-.809	-.117	-.160
SlopeHbo3	.669	.025	.352
SlopeHbo5	-.293	-.106	-.013
SlopeHbo11	.393	.052	-.286
SlopeHbo13	-.386	.707	.192
SlopeHbo15	.121	-.232	-.418
RangeHbo1	-.586	.178	1.114
RangeHbo3	.139	.566	-.591
RangeHbo5	-.177	.228	.372
RangeHbo11	.493	.988	-.848
RangeHbo13	-.435	-.260	-.002
RangeHbo15	-.256	.117	.175
MeanHbr1	.287	-.201	-.263
MeanHbr3	-.500	-.219	.174
MeanHbr5	.171	.104	.105

MeanHbr11	.065	-.164	.090
MeanHbr13	-.146	.190	-.253
MeanHbr15	-.002	-.182	.021
StdevHbr1	-1.038	-.653	.661
StdevHbr3	-.662	.019	1.027
StdevHbr5	-.439	.520	-.373
StdevHbr11	-.417	-.966	-.438
StdevHbr13	.180	-.227	-.853
StdevHbr15	.476	.092	1.150
SlopeHbr1	.387	.009	.112
SlopeHbr3	.249	.465	-.090
SlopeHbr5	-.124	.010	.250
SlopeHbr11	-.294	.192	-.014
SlopeHbr13	.416	-.416	.023
SlopeHbr15	-.372	-.211	-.152
RangeHbr1	.787	.366	-.690
RangeHbr3	.824	.051	-.642
RangeHbr5	.570	-.731	.692
RangeHbr11	.433	1.282	.347
RangeHbr13	-.416	.168	1.123
RangeHbr15	.292	-.345	-.839

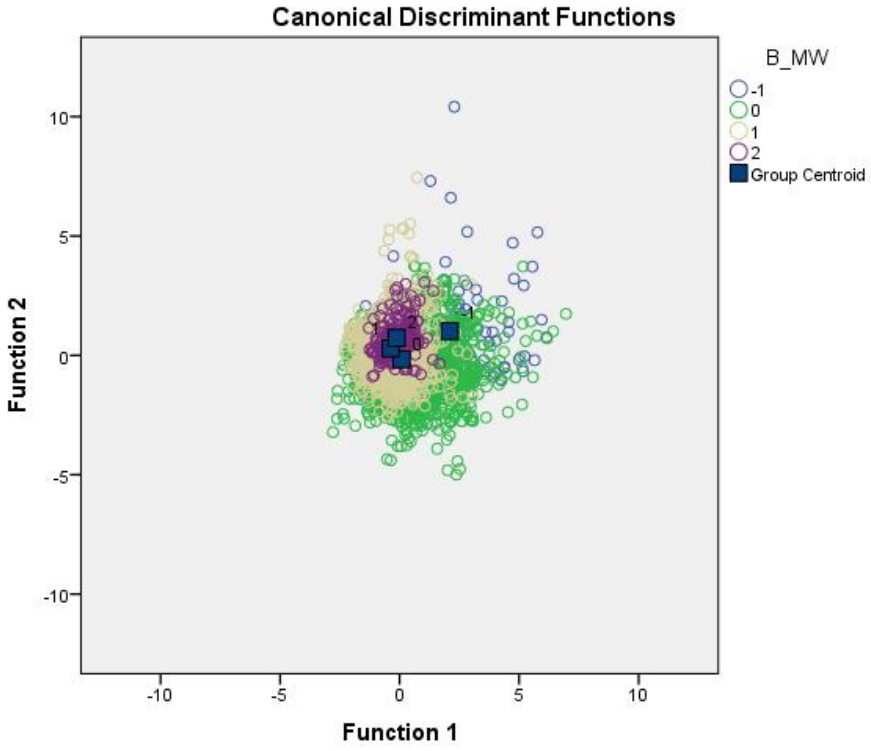

Figure 81: Distribution of the Data in 2 Dimensions

Table 12: Success Rate of Classification

Classification Results[a]

			Predicted Group Membership				
		B_MW	-1	0	1	2	Total
Original	Count	-1	71	14	11	13	109
		0	395	1807	1124	707	4033
		1	68	386	708	285	1447
		2	2	26	30	147	205
	%	-1	65.1	12.8	10.1	11.9	100.0
		0	9.8	44.8	27.9	17.5	100.0
		1	4.7	26.7	48.9	19.7	100.0
		2	1.0	12.7	14.6	71.7	100.0

a. 47.2% of original grouped cases correctly classified.

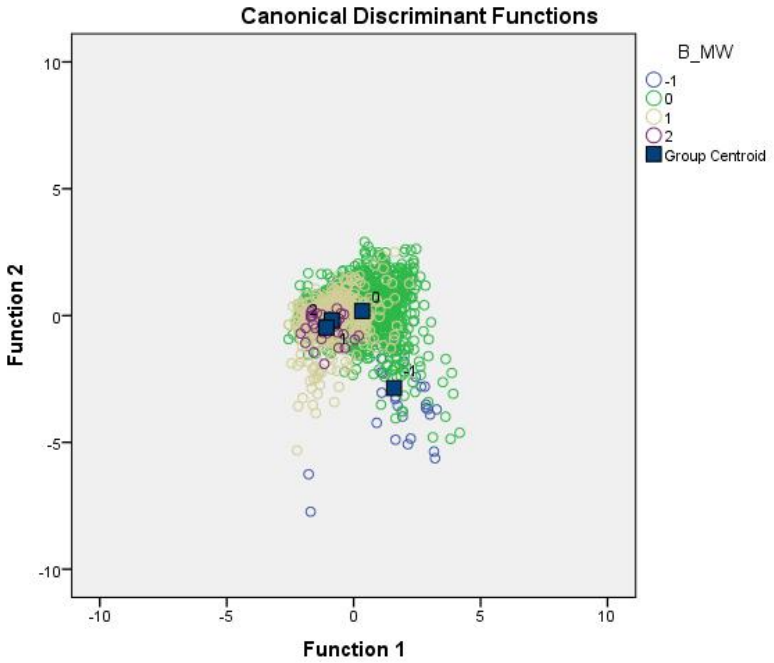

Figure 82: Distribution of the Data in 2 Dimensions for Subject 5

Table 13: Success Rate of Classification for Subject 5

Classification Results[a]

			Predicted Group Membership				
		B_MW	-1	0	1	2	Total

Original	Count	-1	26	7	1	1	35
		0	66	723	257	93	1139
		1	5	95	320	45	465
		2	0	0	5	29	34
	%	-1	74.3	20.0	2.9	2.9	100.0
		0	5.8	63.5	22.6	8.2	100.0
		1	1.1	20.4	68.8	9.7	100.0
		2	.0	.0	14.7	85.3	100.0

a. 65.6% of original grouped cases correctly classified. (kfold:3 = 72.23%)

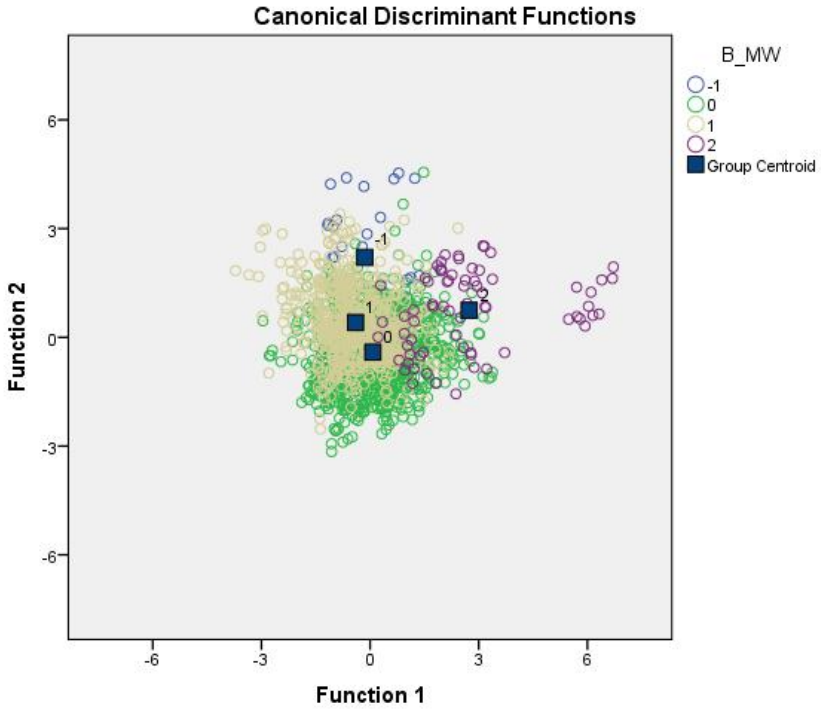

Figure 83: Distribution of the Data in 2 Dimensions for Subject 6

Table 14: Success Rate of Classification for Subject 6

Classification Results[a]

			Predicted Group Membership				
		B_MW	-1	0	1	2	Total
Original	Count	-1	19	4	5	0	28
		0	31	571	261	68	931
		1	28	207	400	17	652
		2	2	12	3	54	71
	%	-1	67.9	14.3	17.9	.0	100.0
		0	3.3	61.3	28.0	7.3	100.0
		1	4.3	31.7	61.3	2.6	100.0
		2	2.8	16.9	4.2	76.1	100.0

a. 62.1% of original grouped cases correctly classified. (kfold:3 = 68.37%)

4.4. SVM Results

This section summarizes the results of the SVM algorithm explained in Method chapter 3.4.3 (Training Data does not include data sample of all pilots). All graphs are derived from tables placed on Appendix D. Although results of analyses are seen to have high score (64%), their confusion matrixes show that separations of the classes are not good. Developed models are able to predict only class 0. A sample of the confusion matrixes can be seen first next table.

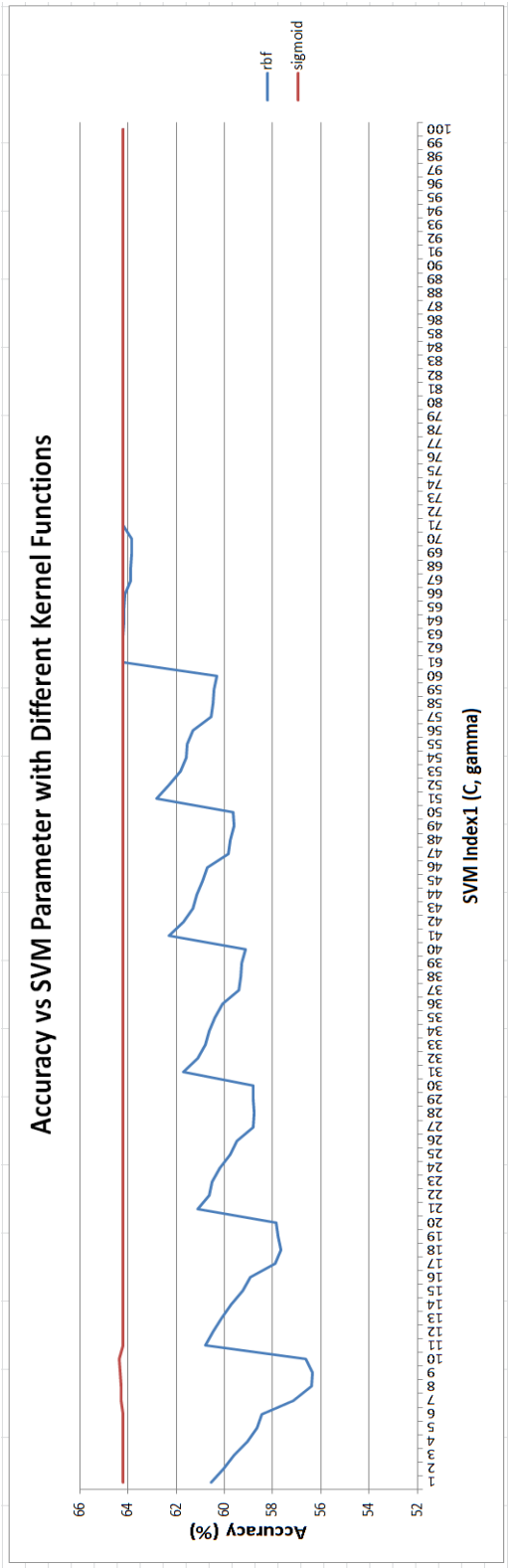

Figure 84: Accuracy vs SVM Parameter Index1 (C, gamma), Kernel Function: rbf, sigmoid, Raw Data: No Mixed hbo, hbr

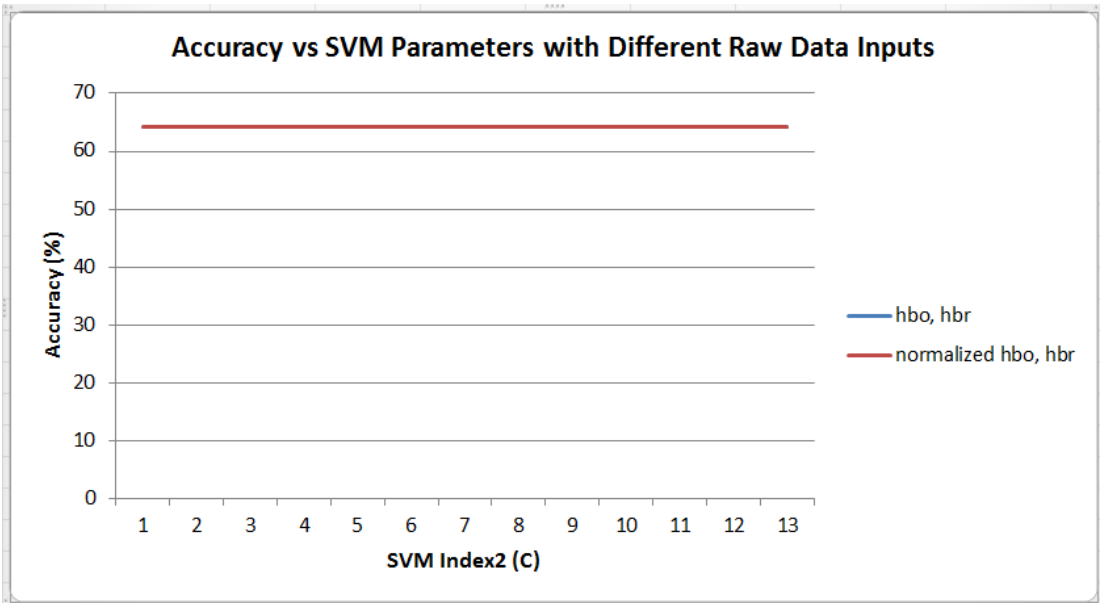

Figure 85: Accuracy vs SVM Parameter Index2 (C), Kernel Function: Linear, Raw Data: No Mixed hbo, hbr Note: Both two raw data outputs are same.

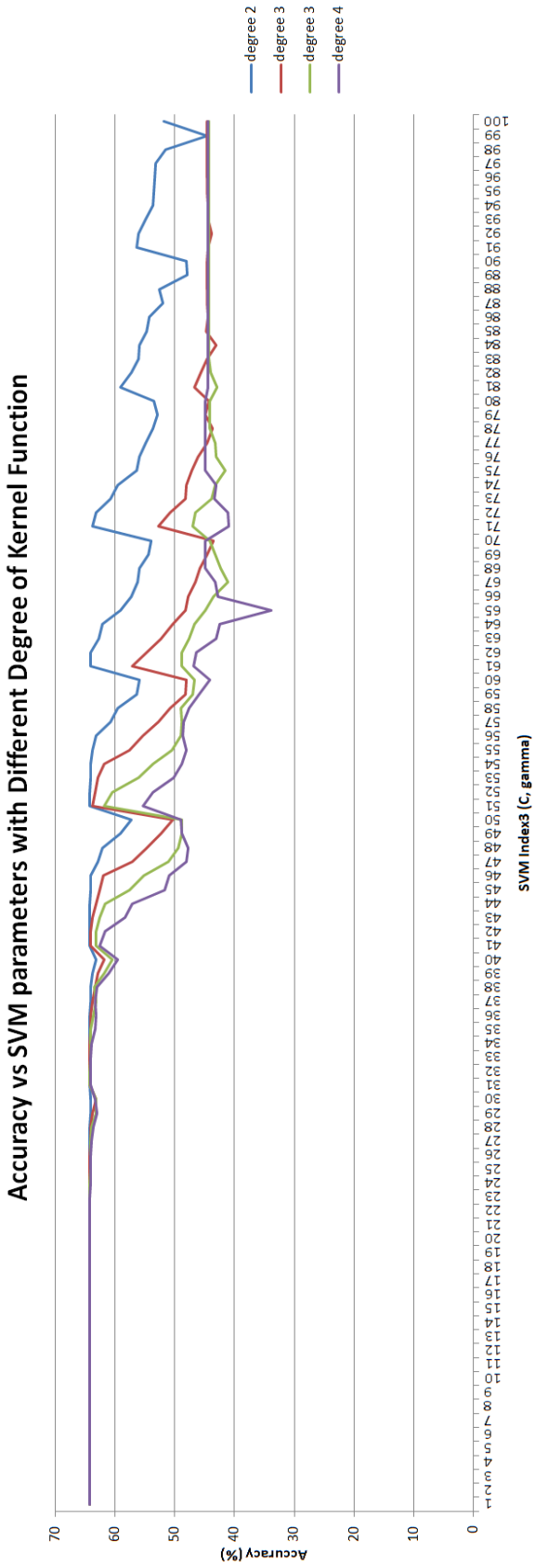

Figure 86: Accuracy vs SVM Parameter Index3 (C, gamma), Kernel Function: Polynomial, Raw Data: No Mixed hbo, hbr

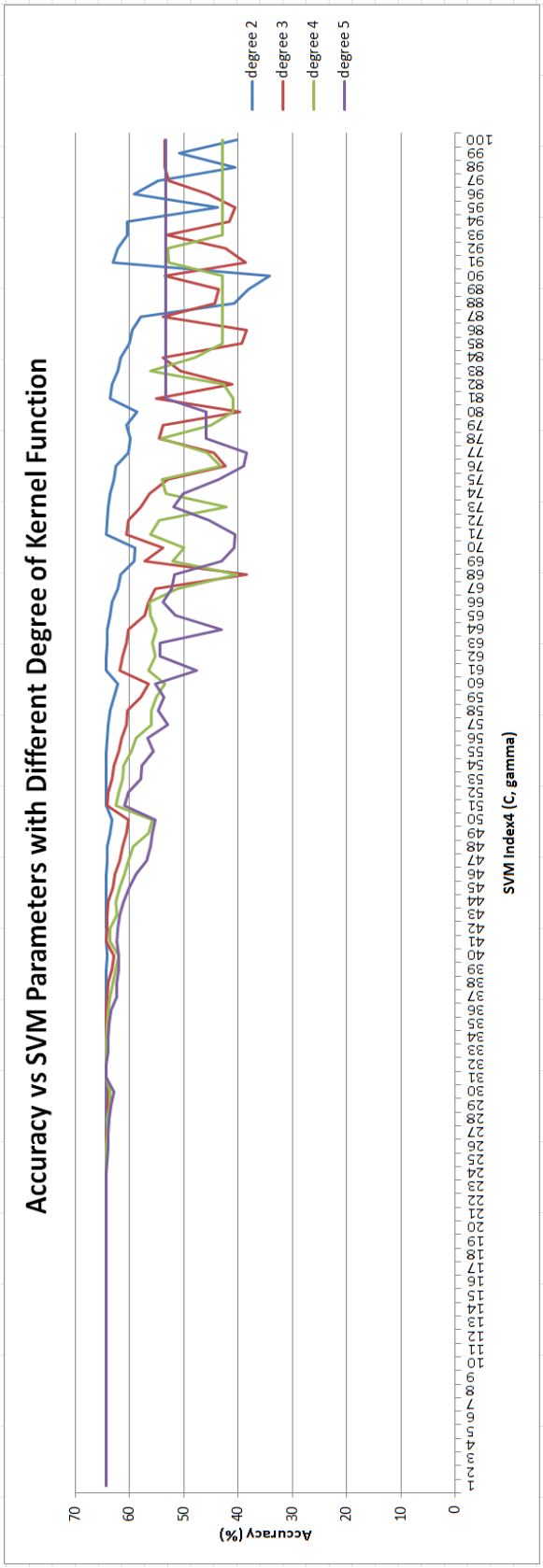

Figure 87: Accuracy vs SVM Parameter Index4 (C, gamma), Kernel Function: Polynomial, Raw Data: No Mixed hbt

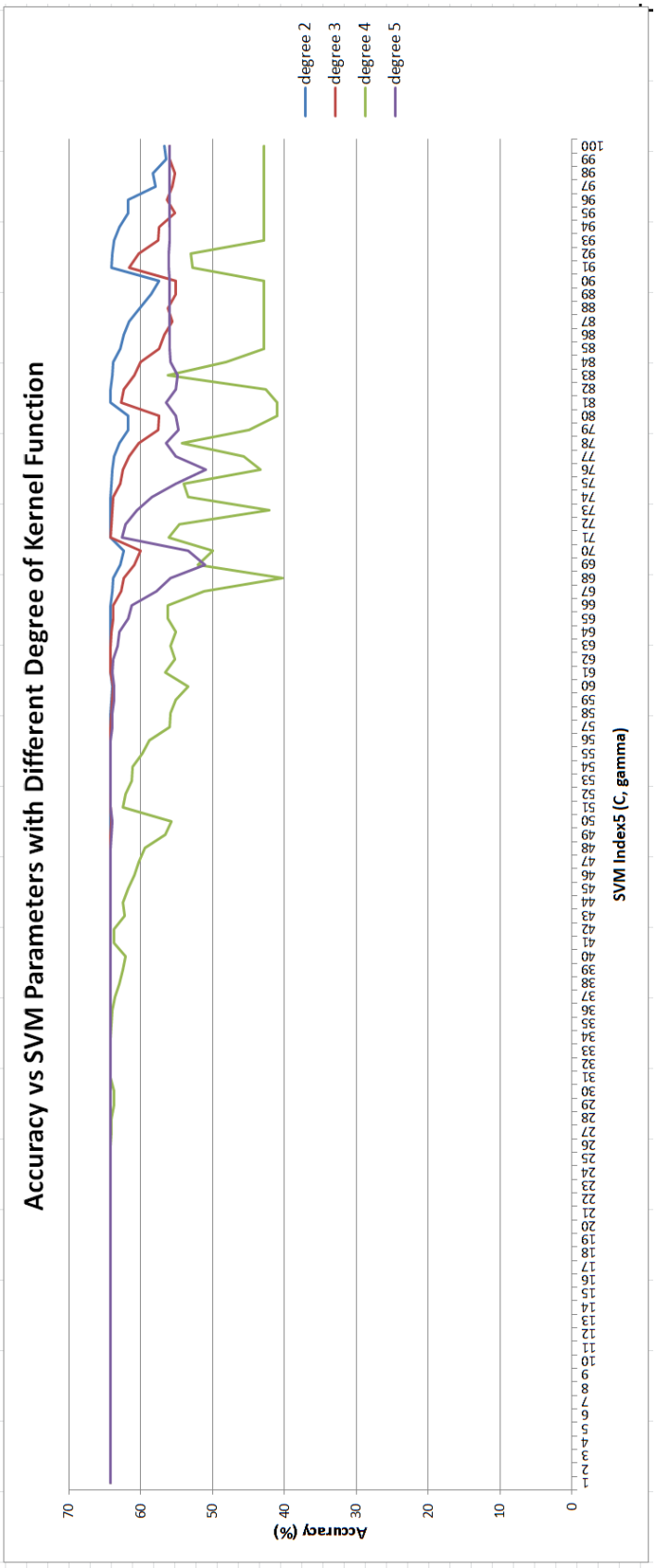

Figure 88: Accuracy vs SVM Parameter Index5 (C, gamma), Kernel Function: Polynomial, Raw Data: No Mixed Normalized hbo, hbr

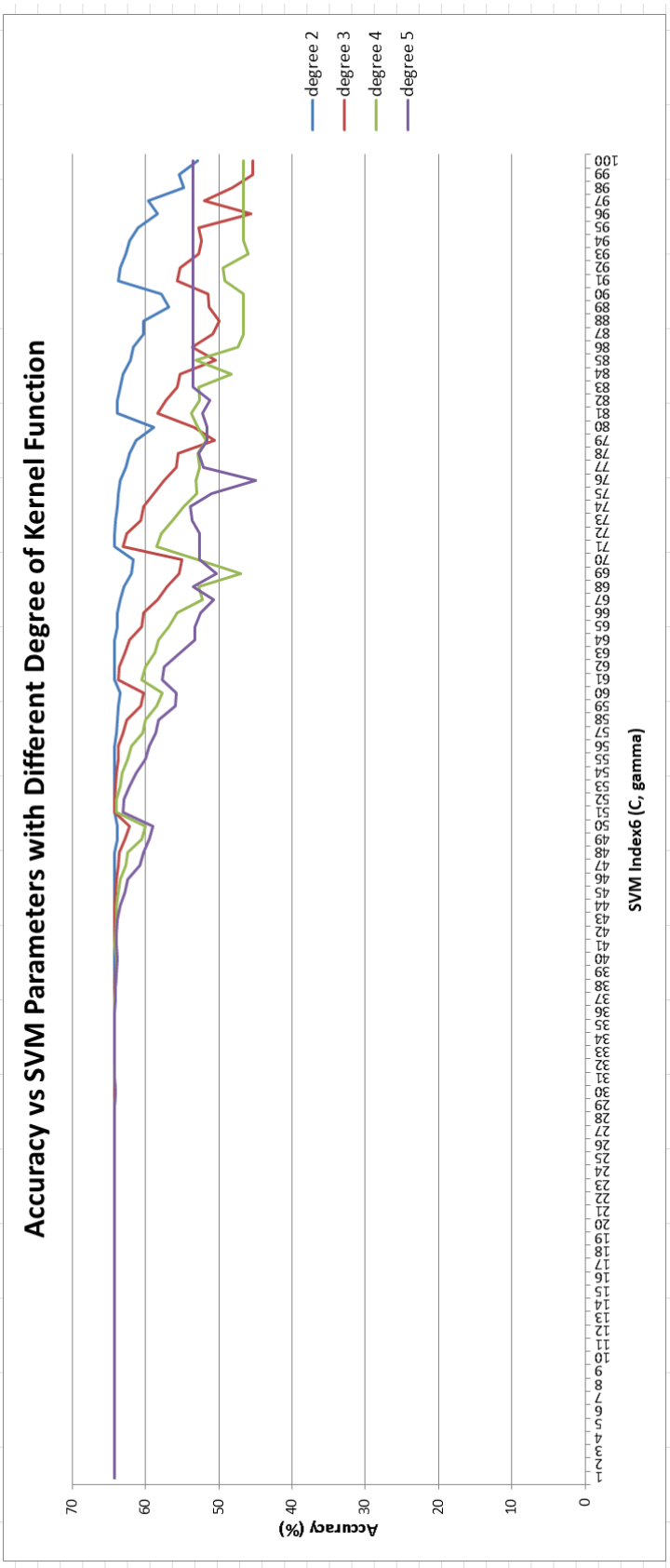

Figure 89: Accuracy vs SVM Parameter Index6 (C, gamma), Kernel Function: Polynomial, Raw Data: No Mixed oxy

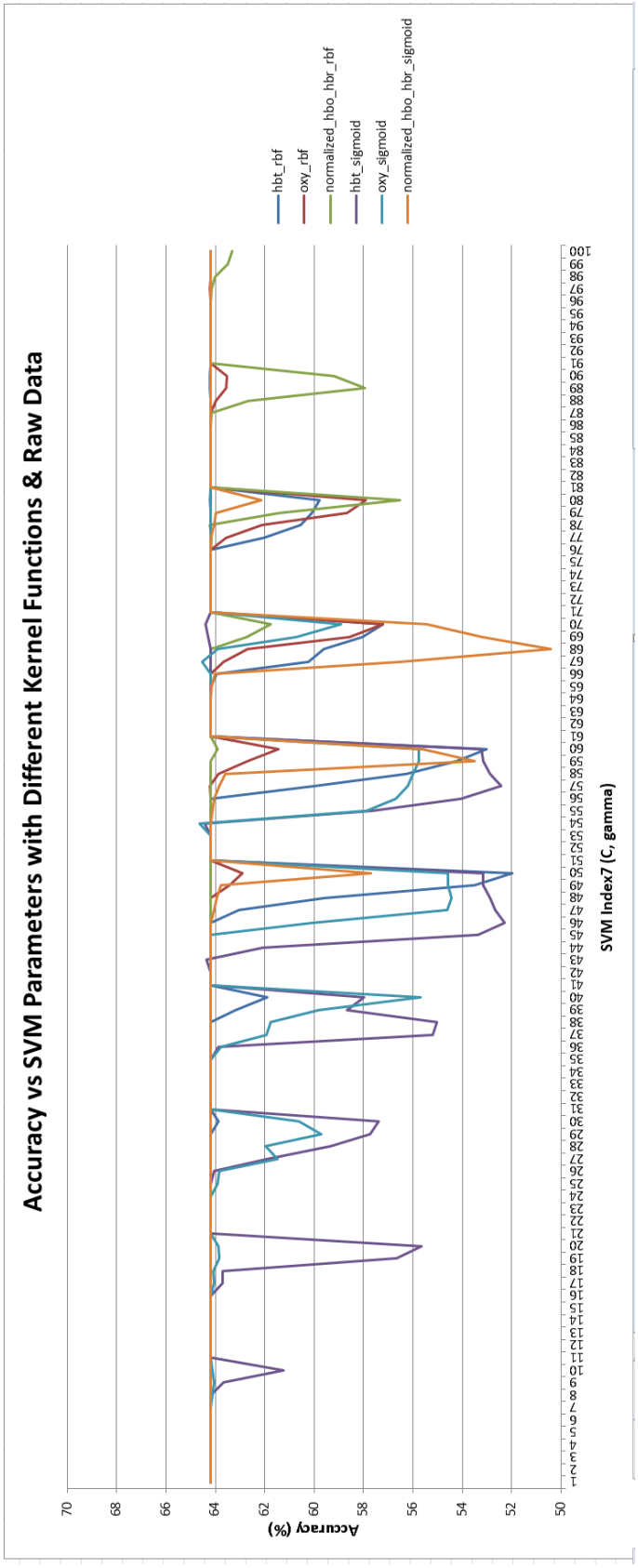

Figure 90: Accuracy vs SVM Parameter Index7 (C, gamma), Kernel Function: RBF, Sigmoid, Raw Data: No Mixed hbo-hbr, oxy, hbt, normalized hbo-hbr

Table 15: Confusion Matrix – Normalized Data, C: 1, Gamma: 0.5, function: RBF

Predict \ Target	-1	0	1	2	
-1	0 0.00%	0 0.04%	0 0.00%	0 0.00%	
0	87 1.89%	2957 64.20%	1368 29.70%	194 4.22%	
1	0 0.00%	0 0.00%	0 0.00%	0 0.00%	
2	0 0.00%	0 0.00%	0 0.00%	0 0.00%	Total
	0% 100%	100% 0%	0.00% 100%	0.00% 100%	64.20% 35.80%

4.5. ANN Results

This part illustrates the results of the ANN algorithm. The training data includes data samples obtained from all pilots. Confusion matrix, error histogram, validation performance, receiving operating characteristic are put for a sample (Training Data: 60%, Validation Data: 20%, Test Data: 20%, Raw Data: hbo, hbr, Scaled Conjugate Gradient) of all analyses. ANN result graph is derived from the table placed on Appendix E. Although results of analyses are seen to have high score (near to 70%), their confusion matrixes show that separations of the classes are not good. Developed models are able to predict only class 0 well. Other classes' predictions are wrong. A sample of the confusion matrixes can be seen first next table.

Table 16: Confusion Matrix – Training Data: 60%, Validation Data: 20%, Test Data: 20%, Raw Data: hbo, hbr, Scaled Conjugate Gradient

Figure 91: Error Histogram – Training Data: 60%, Validation Data: 20%, Test Data: 20%, Raw Data: hbo, hbr, Scaled Conjugate Gradient

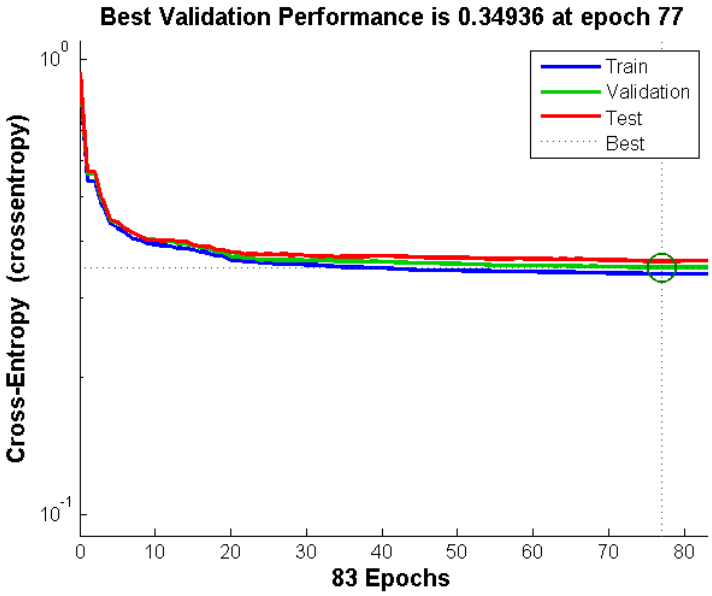

Figure 92: Validation Performance – Training Data: 60%, Validation Data: 20%, Test Data: 20%, Raw Data: hbo, hbr, Scaled Conjugate Gradient

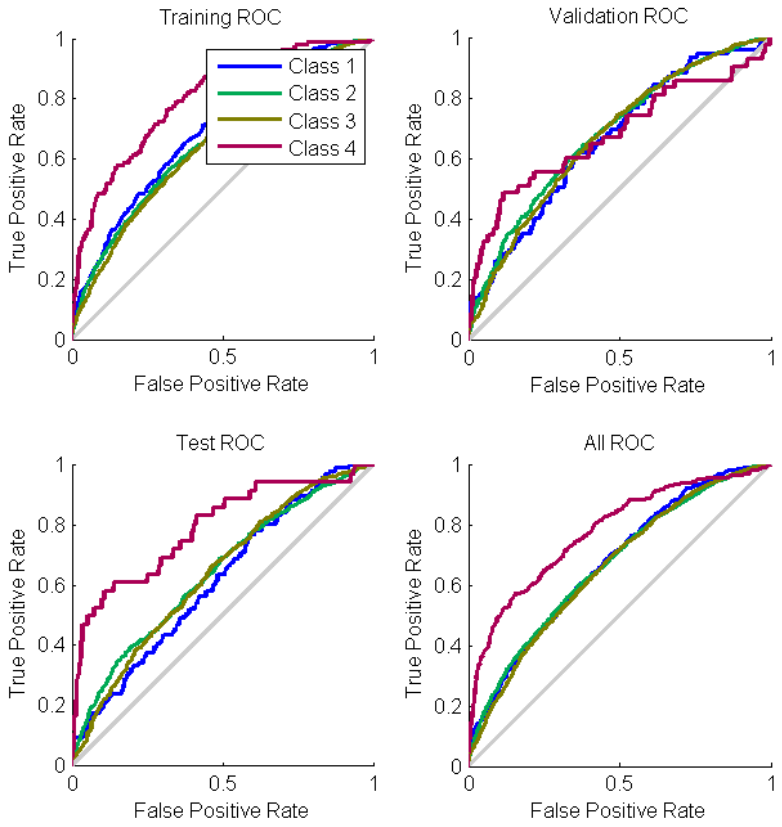

Figure 93: Receiving Operating Characteristic – Training Data: 60%, Validation Data: 20%, Test Data: 20%, Raw Data: hbo, hbr, Scaled Conjugate Gradient

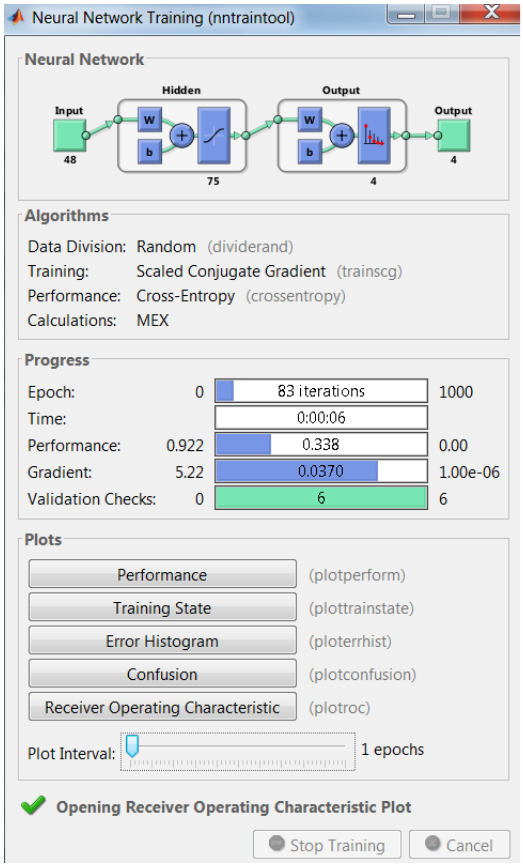

Figure 94: ANN Summary – Training Data: 60%, Validation Data: 20%, Test Data: 20%, Raw Data: hbo, hbr, Scaled Conjugate Gradient

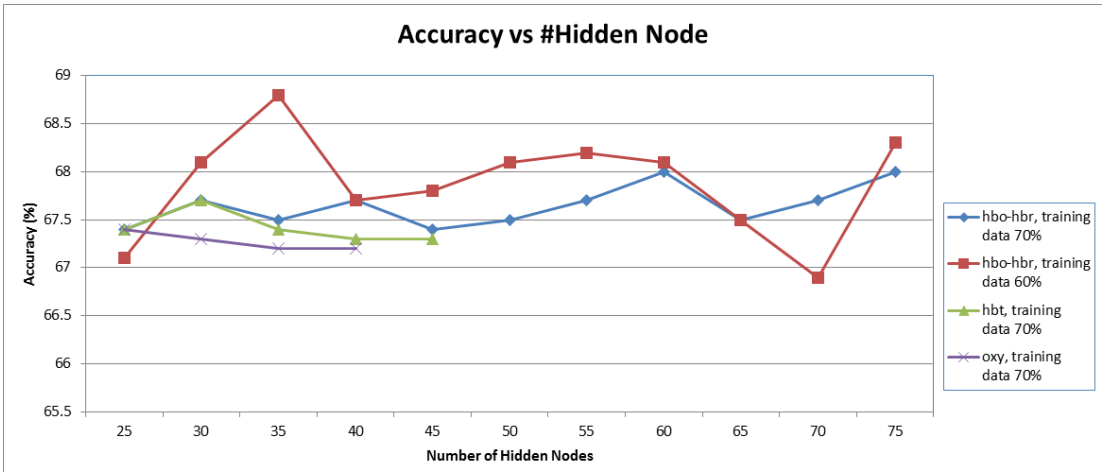

Figure 95: ANN Results for Four Classes (-1, 0, 1, 2)

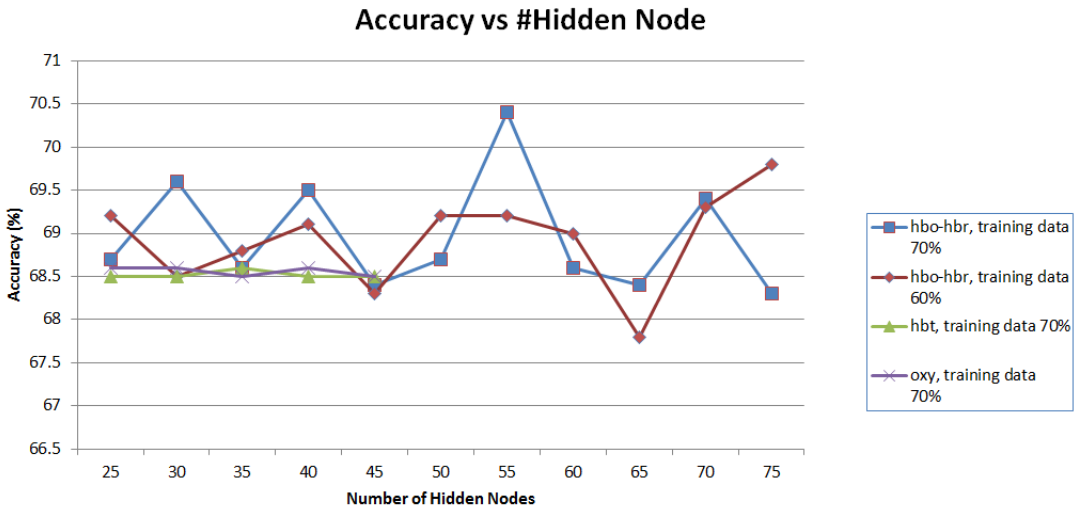

Figure 96: ANN Results for Three Classes (0, 1, 2)

4.6. LDA and SVM Analysis with Mixed Data

This part illustrates the results of the LDA and SVM algorithms explained in Method chapter 3.4.6 (Training Data includes data sample of all the all pilots). All graphs are derived from tables placed on Appendix C (last line of the table) and Appendix D – Index8, 9. Mixing of the training data does not increase success rate of prediction for LDA (success rate: 50% with kfold:3 cross validation score is 45.07%). However SVM results increase dramatically with this method. Confusion matrix of highest score (85.5%, with kfold:3 cross validation score is 81%) placed on first next table demonstrate that class separation power of this model is strong.

Table 17: Eigenvalues of Two Canonical Discriminant Functions

Function	Eigenvalue	% of Variance	Cumulative %	Canonical Correlation
1	.096[a]	38.1	38.1	.296
2	.090[a]	35.5	73.7	.287
3	.066[a]	26.3	100.0	.249

a. First 3 canonical discriminant functions were used in the analysis.

Table 18: Wilk' Lambda Results Specifying Weight of the Functions

Test of Function(s)	Wilks' Lambda	Chi-square	df	Sig.
1 through 3	.785	1390.847	216	.000
2 through 3	.861	863.272	142	.000
3	.938	369.814	70	.000

Table 19: LDA - Standardized Canonical Discriminant Function Coefficients

	Function		
	1	2	3
MeanHbo1	.053	.144	.047
MeanHbo3	-.004	.001	-.123
MeanHbo5	.031	-.010	.088
MeanHbo11	-.022	-.130	-.110
MeanHbo13	-.406	.430	.202
MeanHbo15	.314	-.333	-.140
StdevHbo1	-.119	-.625	-.982
StdevHbo3	-1.132	1.350	-1.616
StdevHbo5	.699	.504	-.445
StdevHbo11	-1.369	.447	2.358
StdevHbo13	1.925	-1.355	-.747
StdevHbo15	-.944	-.228	-.201
SlopeHbo1	-.311	.404	.235
SlopeHbo3	.199	-.088	.151
SlopeHbo5	.228	.207	.118
SlopeHbo11	-.031	-.049	-.131
SlopeHbo13	.486	-.156	-.296
SlopeHbo15	-.410	.158	-.005
RangeHbo1	.313	-.195	.176
RangeHbo3	.475	.288	.769
RangeHbo5	-.796	-.731	1.609
RangeHbo11	.967	-.511	-.001
RangeHbo13	-1.500	.398	-.024
RangeHbo15	.421	-.001	.383
MeanHbr1	-.109	-.215	-.071
MeanHbr3	-.028	.029	.117
MeanHbr5	.029	-.114	-.044
MeanHbr11	-.226	.065	.080
MeanHbr13	.103	-.239	-.116

MeanHbr15	-.129	.202	.200
StdevHbr1	-2.125	-.863	-.657
StdevHbr3	-.244	.500	-.187
StdevHbr5	.380	1.412	.403
StdevHbr11	-1.635	-.464	1.385
StdevHbr13	.401	-.640	-1.399
StdevHbr15	-.148	.005	2.362
SlopeHbr1	.229	-.208	-.054
SlopeHbr3	-.110	.065	-.081
SlopeHbr5	-.109	.323	.158
SlopeHbr11	.336	.039	-.008
SlopeHbr13	-.145	.055	.072
SlopeHbr15	.101	-.279	-.277
RangeHbr1	2.070	-.450	-.612
RangeHbr3	.217	.693	-.302
RangeHbr5	-.637	-1.492	.165
RangeHbr11	1.492	.059	.036
RangeHbr13	-.537	.834	1.313
RangeHbr15	.271	-.504	-1.471
StdevOxy1	-.072	.075	-.090
StdevOxy3	.532	-.476	.752
StdevOxy5	-.560	-.530	-.664
StdevOxy11	.379	.181	.254
StdevOxy13	-.611	.236	-.577
StdevOxy15	.374	-.224	.462
RangeOxy1	.365	-.066	.316
RangeOxy3	-.062	.097	-.355
RangeOxy5	.502	.327	.447
RangeOxy11	-.276	.293	-1.085
RangeOxy13	.209	.018	.474
RangeOxy15	-.221	.702	-.785
StdevHbt1	1.662	.855	1.398
StdevHbt3	.369	-1.748	2.277
StdevHbt5	-.066	-.866	-.250
StdevHbt11	.718	-.910	-2.985
StdevHbt13	-1.063	1.100	1.187
StdevHbt15	1.065	.931	-.761
RangeHbt1	-1.877	.952	.757
RangeHbt3	.066	-.128	-1.440
RangeHbt5	1.077	1.225	-1.075
RangeHbt11	-.493	1.218	.092

RangeHbt13	.874	-.683	-.530
RangeHbt15	-.456	-.803	-.012

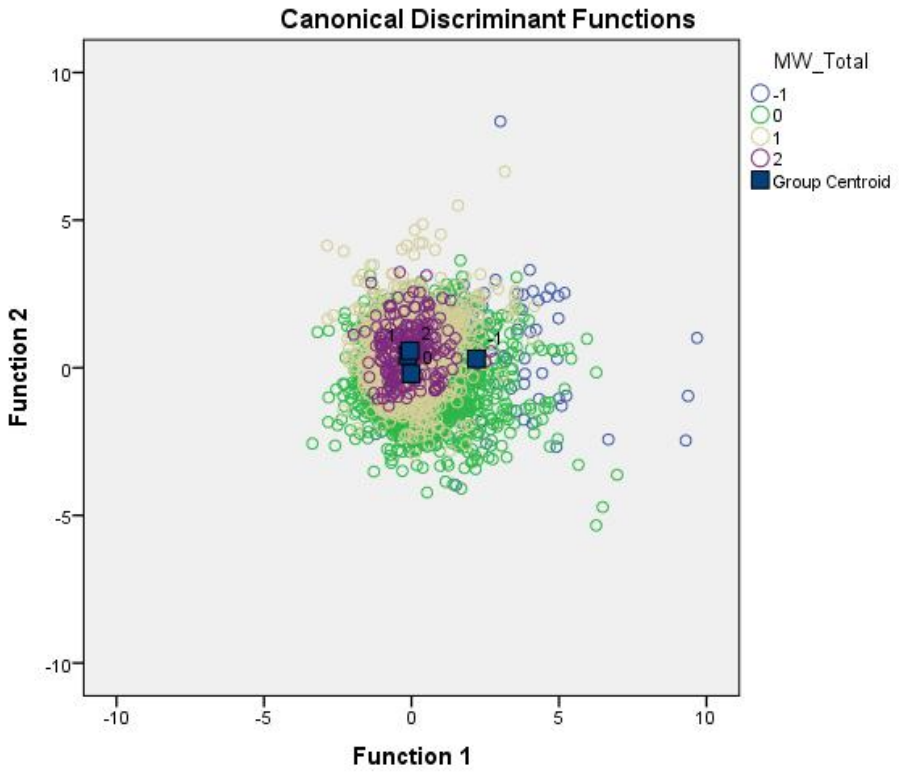

Figure 97: LDA - Distribution of the Data in 2 Dimensions

Table 20: LDA - Success Rate of Classification (with kfold:3 cross validation is 45.07%)

Classification Results[a]

			Predicted Group Membership				
		MW_Total	-1	0	1	2	Total
Original	Count	-1	68	17	15	10	110
		0	324	1989	1124	499	3936
		1	127	464	721	211	1523
		2	4	53	47	121	225
	%	-1	61.8	15.5	13.6	9.1	100.0
		0	8.2	50.5	28.6	12.7	100.0
		1	8.3	30.5	47.3	13.9	100.0
		2	1.8	23.6	20.9	53.8	100.0

a. 50.0% of original grouped cases correctly classified.

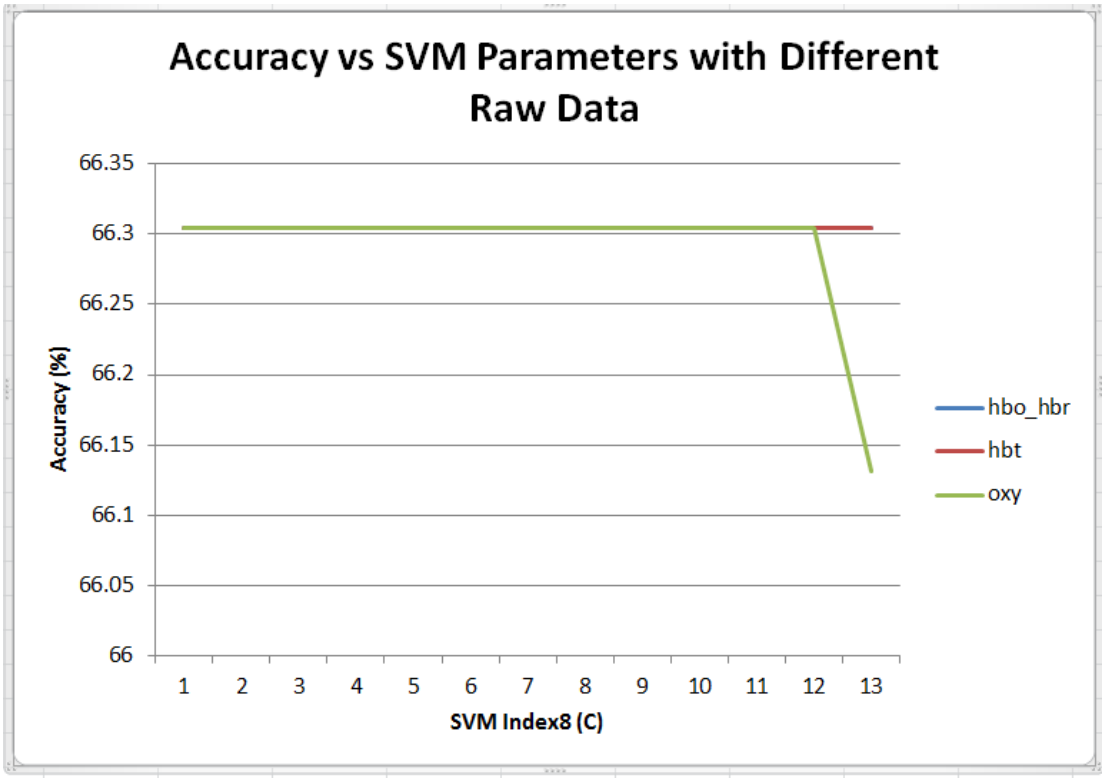

Figure 98: Accuracy vs SVM Parameter Index8 (C), Kernel Function: Linear, Raw Data: Mixed hbo-hbr, oxy, hbt, Note: All three raw data output are same until Index 12, At Index 13 oxy output decreases, others are same.

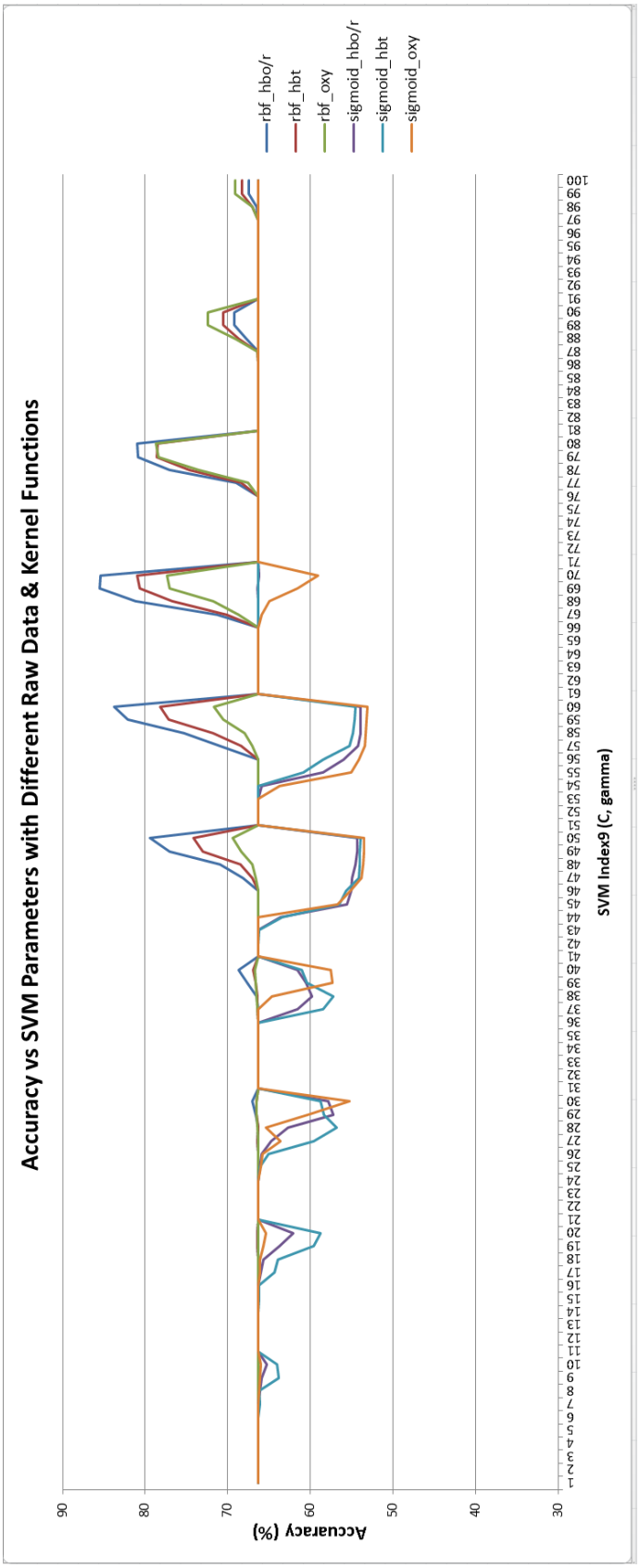

Figure 99: Accuracy vs SVM Parameter Index9 (C, gamma), Kernel Function: RBF, Linear, Raw Data: Mixed hbo-hbr, oxy, hbt,

Table 21: Confusion Matrix – Mixed Data, C: 5, Gamma: 0.5, function: RBF, Cross Validation Accuracy: 81% (kfold: 3)

Predict \ Target	-1	0	1	2	Total
-1	21 0.46%	6 0.12%	1 0.02%	0 0.00%	
0	64 1.39%	2948 64.00%	424 9.21%	51 1.11%	
1	2 0.04%	99 2.15%	861 18.69%	16 0.35%	
2	0 0.00%	1 0.02%	6 0.12%	107 2.32%	
	24% 76%	97% 3%	67% 33%	61% 39%	85.50% 14.50%

4.7. RNN Results

This part illustrates results of RNN algorithm explained in Method chapter 3.4.7 (Training Data includes data sample of all the all pilots). The graph is derived from table placed on Appendix F. As you can see in the graph and the confusion matrix which is a sample (Mixed Data, Hidden Node: 60, Epoches: 362, Batch size: 16, Raw Data: hbo, hbr, Features: mean, slope, range, standard deviations, with kfold:3 cross validation score is 71.67%) confusion matrixes obtained from the developed analyses, results can be considered acceptable for practical use.

Table 22: Confusion Matrix – Mixed Data, Hidden Node: 60, Epochs: 362, Batch size: 16, Raw Data: hbo, hbr, Features: mean, slope, range, standard deviations, Cross Validation Accuracy: 71.67% (kfold: 3)

Predict \ Target	-1	0	1	2	Total
-1	23 0.50%	18 0.39%	7 0.00%	1 0.16%	
0	48 1.04%	2719 59.03%	608 13.20%	57 1.24%	
1	11 0.24%	286 6.21%	656 14.24%	28 0.61%	
2	3 0.07%	31 0.67%	21 0.46%	87 1.89%	
	27.06% 72.94%	89.03% 10.97%	50.77% 49.23%	50.29% 49.71%	75.66% 24.34%

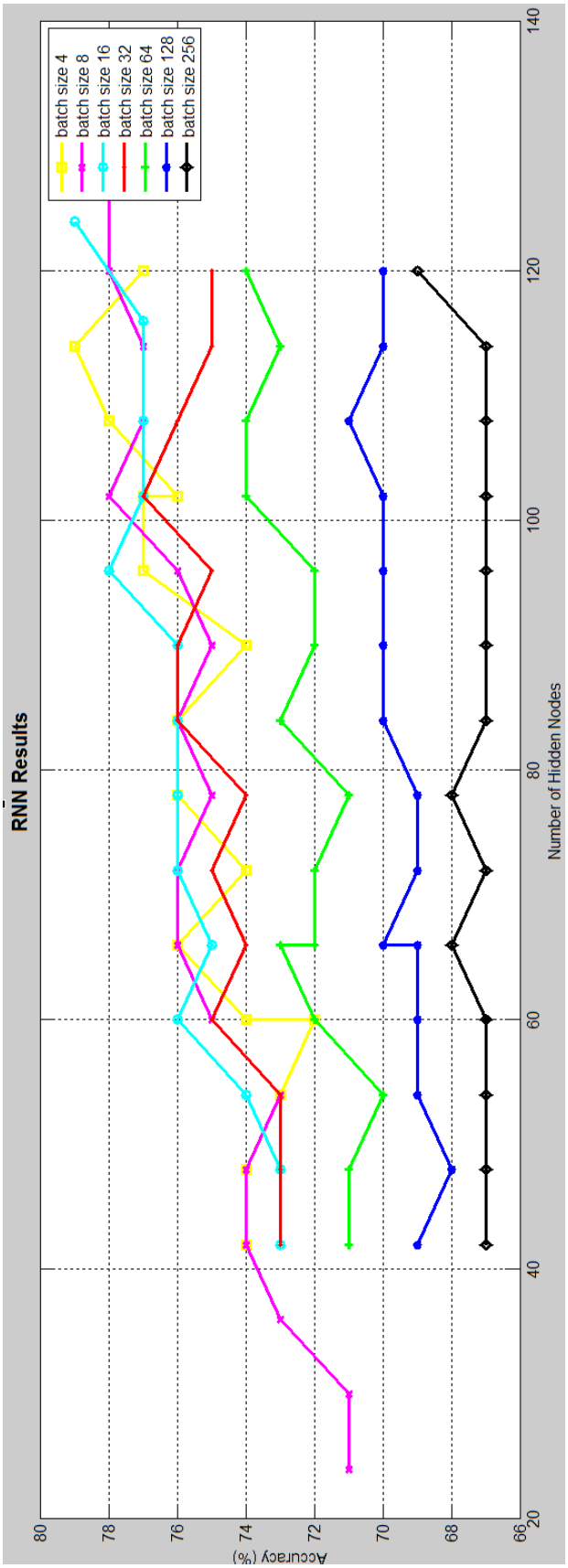

Figure 100: RNN Results

4.8. LSTM Results

This part illustrates results of the LSTM algorithm explained in Method chapter 3.4.8 (Training Data includes data sample of all pilots). The graph is derived from table placed on Appendix G. As you can see in the graph and the confusion matrix which is a sample (Mixed Data, LSTM Number: 90, Epoches: 724, Batch size: 8, Loss Function: Categorical Crossentropy, Activation: Softmax, Raw Data: hbo, hbr, Features: mean, slope, range, standard deviations with kfold:3 cross validation score is 77.03%) confusion matrixes obtained from the developed analyses, results are good.

Table 23: Confusion Matrix – Mixed Data, LSTM Number: 90, Epochs: 724, Batch size: 8, Loss Function: Categorical Crossentropy, Activation: Softmax, Raw Data: hbo, hbr, Features: mean, slope, range, standard deviations, Cross Validation Accuracy: 77.03% (kfold: 3)

		Target				
		-1	0	1	2	
Predict	-1	34 0.74%	22 0.48%	8 0.17%	0 0.00%	
	0	44 0.96%	2710 58.84%	360 7.82%	34 0.74%	
	1	8 0.17%	294 6.38%	907 19.69%	33 0.72%	
	2	0 0.00%	28 0.61%	17 0.37%	107 2.32%	Total
		27.06% 72.94%	89.03% 10.97%	50.77% 49.23%	50.29% 49.71%	81.59% 18.41%

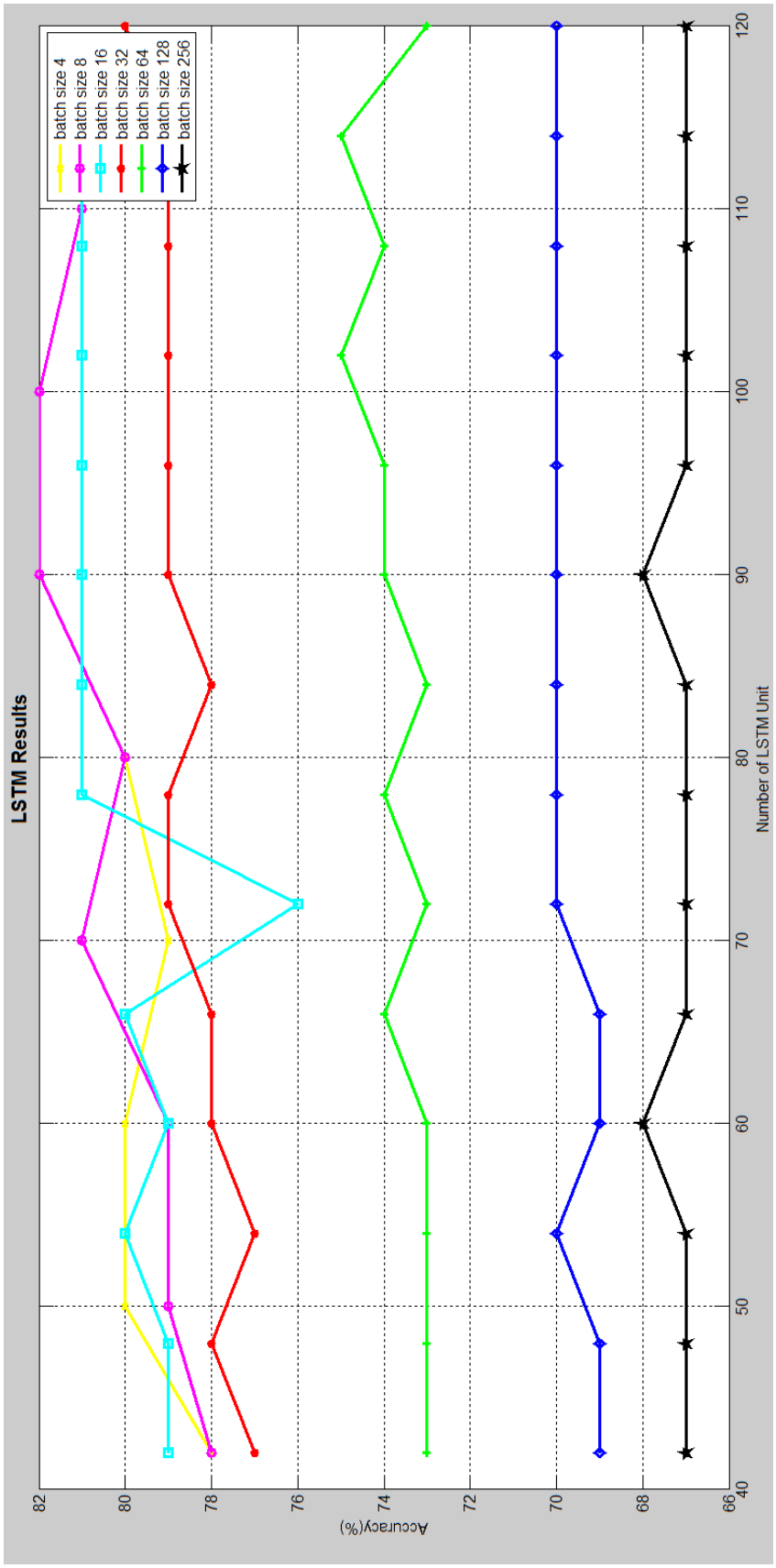

Figure 101: LSTM Results

CHAPTER 5

5. DISCUSSION AND CONCLUSION

The main goal of this thesis study is to develop online algorithms based on fNIRS measures to estimate changes in the mental workload levels of pilots while they are performing realistic flight scenarios. In other words, instead of analyzing and detecting mental workload changes after data collection is completed (i.e. offline analysis), we aimed to monitor changes in the mental workload of the pilots during flight scenarios in real time. For this purpose, realistic cockpit simulators and test scenarios were used in the context of a broader research project. By considering the related literature, feedback obtained from the pilots who participated in the ACROSS project as subjects, and the insights developed via in depth qualitative analysis of flight videos, 16 parameters that affect the mental workload of pilots were specified. The data obtained from fNIR sensor during all test procedures are integrated and tagged by the scenario id, test subject id, time info and predefined mental workload level (detected with 16 parameters). This large data set includes 4 types of fNIRS based oxygenation measures (i.e. hbo, hbr, hbt, oxy), obtained from 16 optodes over the prefrontal cortex, and 4 features (i.e. slope, mean, range, standard deviation) measured at every half second from 8 experienced pilots while they flew 4 different scenarios. This data set formed the backbone of the online estimation algorithms developed and tested as part of this thesis.

After the annotation of the data with 16 behavioral parameters, it was observed that that 67.26%, 27.06% and 3.84% of the data was assigned a mental workload level of low (i.e. 0), medium (i.e. 1) and high (i.e. 2) respectively. Only 1.89% of the data was assigned a "-1" tag, which correspond to cases where the signals were modulated due to artifacts such as excessive head movements. The distribution of mental workload levels were compatible with the test scenario design and pilots' self-evaluations after each scenario. Generally parameters that correspond to high mental workload instances covered a small proportion of the entire dataset, since such cases typically took a short period of time

during adverse events. For example, in scenario 3 the percentage of high level mental workload was observed as 13.65%, due to the fact that this scenario included mentally demanding, non-routine tasks for the pilots such as performing a go around, dealing with malfunction of instruments, engaging in new route calculations etc. On the other hand, mental workload level 0 reaches 75.73% in scenario1, which included a routine flight operation. Nearly all drowsiness cases were observed in scenario1 whose cruise phases were longer than those of other scenarios, and it was performed just after the pilots had their lunch.

Since the aim is to design a generic mental workload estimation model applicable for all test subjects, we focused on the optodes from which the best quality data was obtained during the experiments. The flight simulator included additional sensors besides fNIRS, some of which relied on infra-red sources such as eye trackers and Kinect cameras. Although the fNIRS sensor was shielded with a special cap, even numbered optodes that were closer to the eyebrows of the participants were subjected to the highest levels of interference. In contrast, the fNIRS signal quality was consistently better across all subjects at odd numbered optodes which cover areas within the frontal cortex close to the hairline. For this reason, the models developed in the thesis focused on optodes 1, 3, 5, 11, 13, 15 only for model development, which cover areas within left and right dorsolateral (1,3,13,15) and dorsomedial (5, 11) prefrontal cortex and dorsomedial prefrontal cortex. Therefore cognitive data types used for mental workload estimation for each half second was reduced to 96 dimensions (i.e. 4 biosignals (hbo, hbr, hbt, oxy), 6 optodes, 4 features (slope, mean, range, standard deviation)).

For the initial attempt based on LDA, 91.1% training accuracy and 70% test accuracy scores were obtained over a hand-picked set of cases that emphasized high workload instances. This approach was aimed at investigating how such a basic model trained over a single pilot could succeed in detecting the high workload instances for other pilots, and to what extent it would generate false alarms (i.e. mistakenly classifying low MW instances as high MW). However, this approach was not sufficient for a more general purpose model that estimates the MW changes during the entire flight in a continuous manner. Moreover, the mental workload level assignments were made without using the scheme with 16 dimensions. Therefore, the LDA approach was re-evaluated over the entire dataset that was manually annotated with the new categorization scheme. These changes led to a significant decrease in the accuracy of the LDA model, which was dropped to 51.86% on average. In these trials nearly 60% of all the data was used as training data. When training data was narrowed to a single subject's dataset (14%), the training accuracy reached around 77% on average. For some individuals, the training accuracy was as high as 90%. These results suggest that LDA's prediction power decreases dramatically when the training data size is increased. In addition to this, including training data samples from all pilots did not improve LDA model's accuracy, which was around 60%.

LDA analyses were performed by using SPSS. Since SPSS provides standardized discriminant function coefficients for each input (e.g. hbo_slope_voxel_1, hbr_mean_voxel_4 etc.), the predictive effect of each parameter on the developed model can be compared. Based on the analysis results in which high accuracy scores were obtained (e.g. when single subject data is used as training data), it was observed that slope features of hbo and hbr were the stongest predictors of mental workload. Overall, LDA models turned out to be more suitable for personalizing a mental workload prediction scheme in this domain.

The SVM algorithm with non-mixed training data had higher accuracy scores than LDA. C and gamma parameters for RBF and Sigmoid kernel functions, C, gamma, degree parameters for polynomial kernel function and C parameter for linear kernel functions were tuned in the analyses. C and gamma values from 0.00001 to 10000 and degree values from 2 to 6 were used. Since representations of all analysis results (tables, graphs) would take hundreds of pages, only the narrowed parameter range results were reported in this study (Appendix D and derived SVM graphs in the results chapter). The abovementioned ranges produced the highest accuracy scores. Although higher accuracy scores were obtained with SVM than LDA, confusion matrices showed that SVM was not good at separating the four classes (-1, 0, 1, 2). Generally all SVM models predicted 0 for most data points. Since 67.26% of all data is classified as mental workload level 0, the accuracy scores are misleading.

All results obtained by using a linear kernel function with hbo and hbr had the same accuracy percentage(67%). The average accuracy with the RBF function was 63.12% among 400 analysis results. Highest accuracy percentage obtained was 64.24% with (C: 0.6, gamma: 2, data type: hbo, hbr) and (C: 10, gamma: 5, data type: hbt), and (C: 0.5, gamma: 0.1, data type: oxy) and (C: 1, gamma: , data type: normalized hbo and hbr). Lowest score is 51.98% with (C: 10, gamma: 0.05, data type: hbt). Whereas, the average score with the sigmoid function was observed to be 63.19% among 400 analyses results. Highest score is 64.63% with (C: 0.01, gamma: 1, data type: oxy). Lowest score is 50.41% with (C: 1, gamma: 0.5, data type: normalized hbo, hbr).

Average accuracy percentage obtained with the sigmoid function was 58.95% among the 1600 data points in the dataset. The highest score was 64.22% (C: 5, gamma: 0.005, degree: 2, data type: hbt) and (C: 10, gamma: 0.005, degree: 2, data type: hbt) and (C: 0.05, gamma: 0.05, degree: 2, data type: hbt) and (C: 0.1, gamma: 0.05, degree: 2, data type: hbt) and (C: 0.0005, gamma: 0.5, degree: 2, data type: hbt) and (C: 0.001, gamma: 0.5, degree: 2, data type: hbt). The lowest score was 33.93% with (C: 0.05, gamma: 0.5, degree: 5, data type: hbo, hbr).

The previous models were constructed by splitting the pilots into training and test groups, so that after training the models would be tested on other pilots' fNIRS measurements. When the training set included samples from all pilots, not only the accuracy scores got

better but also class separation power of SVM had increased. Moreover with the previous model (with non-mixed data) pilot specific models were also developed. However an efficient model could not be obtained. Not only for this reason but also having aim to develop generic workload estimation model, mixed data approach is adopted. Since it is observed that previous approach is not appropriate for generic model development, other algorithms (ANN, RNN and LSTM) are not applied on non-mixed approach any more.

40 different analyses with linear kernel function resulted in similar accuracy scores with the score obtained by using a non-mixed data set; 66.3%. However, when RBF and Sigmoid functions were used the accuracy scores varied from 53.1% (C: 10, gamma: 0.1, data type: oxy, function: sigmoid) to 85.5% (C: 5, gamma: 0.5, data type: hbo, hbr, function: RBF) in 600 analyses. Since C is only a parameter having impact on the result for the linear kernel function, the number of analysis is smaller than RBF and Sigmoid kernel functions whose effective parameters are C and gamma.

The results suggest that linear function is not appropriate for a generic mental workload estimation algorithm suitable for multiple individuals. In fact LDA (success rate 50%, kfold:3 cross validation is 45.07%) whose rates are very low according to SVM with RBF or sigmoid is similar with SVM with linear function. In addition, the graph in figure 96 shows analyses outputs with RBF increase compared to the others with sigmoid decrease. Therefore it might be stated that SVM with RBF by using mixed training data set is favorable method for our study. Also best prediction score 85.5% is obtained with C: 5, gamma: 0.5, data type: hbo, hbr, function: RBF with kfold:3 cross validation score is 81%. Confusion matrix belonging to the best score (Table 19) indicates that the most confusion of class separation is lower than 10% (prediction 0, target 1). There is another remarkable result in Table 19 is low percentage of -1 separation: 24%. Only 21 of 87 samples assigned to -1 class are predicted correctly. Whereas, 64 sample (74%) is predicted as 0. The reason of this unsatisfactory result is guessed as cases whose outputs are targeted to -1 have different internal factors. Thus, weak skin contact cases cause to acquire too low signal from fNIR sensors and excessive head motion cases cause to acquire too high signal from fNIR sensors are considered as being member of same class: -1. This approach is bought into since, both cases are same for our aim; they are cannot be used to calculate clear mental workload level. Therefore weak skin contact and excessive head motion cases are not assigned to different classes such as class -1 for weak skin contact and class -2 for excessive head motion. Finally, as indicated by the graph presented in Figure 96, it was observed that the use of hbo, hbr as input is more successful than the use of hbt or oxy.

For ANN trials, Matlab's neural network toolkit was utilized. Scaled Conjugate Gradient was used as default. Number of hidden nodes ranged from 12 to 75, percentage of training data was 60% or 70%, and input data types were hbo-hbr, hbt, and oxy. The Matlab toolkit randomly selects the training and testing data. 31 analyses were performed and the average accuracy rate was 67.64%. The highest prediction score came from the

case “#of hiden nodes 35, training data set 60%, data type hbo-hbr” combination and worst score was derived from the case “#of hiden nodes 70, training data set 60%, data type hbo-hbr”. According to the graph in figure 93, hbo-hbr usage as input data type produced higher prediction accuracy than hbt or oxy. Moreover analyses with 60% training data generally provided better accuracy than analyses with 70% training data. Although the sharpest decline in accuracy was observed in the case of 60% training data as well (66.9% accuracy with 70 hidden nodes), the sharpest increase was also observed in a configuration using 60% training data with a different number of hidden nodes (68.8% accuracy with 35 hidden nodes). Another evaluation of the graph is that number of hidden nodes effect depends on other parameters such as percentage of training data set and input data type. However in the range of hidden node number between 45 and 75, behaviors of the analyses with 60% and 70% training data hbo-hbr are similar. Moreover 32 analyses with the same input combinations are performed for three classes (0, 1, 2) by deleting of data tagging with -1. These analyses are studied due to investigate effect of class number and effect of class -1. Neither significant effect is not observed between three classes or four classes nor investigation of analyses without class “-1” is not meaningful. Since in real time processing it is not possible to expect that “-1” class due to weak skin contact or excessive head motion is not occurred. Always incalculable data should be considered and take precaution for this case. In table 14 shows that, even though ANN has stronger power than LDA to separate classes each other, it is not enough accuracy percentage for this issue. Especially the model confuses too much to separate class 0 from class 1.

One hidden layer usage might be an important reason of unsatisfactory ANN results. Number of hidden layer selection is controversial issue. Kolmogorov’ Theorem says that one hidden layer is sufficient for universal approximation[86], and Cybenko also did research whose results promote this theorem[87]. However, according to Reed and Marks, limitations of Kolmogorov and Cybenko indicate that one hidden layer is not always enough[88]. Sontag explains that there are some functions which cannot be approximated with one hidden layer, thus two hidden layers are needed for these models[89]. Besides Lippmann show that two hidden layers capable of separate classification regions in any shape[90]. Since in this thesis Matlab 2014a ANN package containing single hidden layer design is used, advantage of two hidden layers is not observed. If multiple hidden layers were used, accuracy rate of ANN might be increased.

Another critical selection for ANN design is hidden layer nodes number which affects network architecture directly and it is a big question. Reed and Marks state that although m – 1 hidden nodes supply exact learning for m training data, inefficiency of it is obvious. Therefore new approach are sought to detect hidden node number. They list several methods for this issue[88]. However they expressed that, these methods are only guidelines, not strict rules to must be obeyed. One of these methods is calculated by Windrow and Lehr as[91]:

$$\frac{N_y N_p}{1+\log_2 N_p} \leq N_w < N_y \left(\frac{N_p}{N_x}+1\right)(N_x+N_y+1)+N_y.$$

where;

Ny: output node number (4 for our case)

Np: number of pattern (5794 for our case)

Nx: input node number (48 for hbo, hbr ,6 optodes and 4 features)

Nw: number of weights (number of hidden nodes * (48 + 4) for our case).

From this formula number of hidden nodes for our study should greater than 34 and smaller than 496.

Karsoliya gives other rule of thumbs for hidden layer nodes which matched with the studies of Panchals. They say[92],[93]:

- hidden layer nodes should be in the range of output and input layer nodes (4 < #hidden nodes < 48, for our study)
- hidden layer nodes contains 2/3 nodes of input layer + output layers (#hidden nodes = 48 * 2/3 + 4 = 36, for our case)
- hidden layer nodes should not exceed twice of input layer nodes (#hidden nodes <= 48 * 2 = 96 for our case).

As seen in the literatures, although there is no certain calculation of hidden nodes due to several dependencies such as training pattern size, character of data etc., as far as possible, hidden layer is designed by considering of these approaches in this thesis.

207 analyses with different combination of model inputs listed in Appendix F are performed for RNN algorithm. Their average score is 72.12% with kfold:3 cross validation score is 72.12%. Nearly 60% of all data is used for training which is supplied to model as batch size * epochs. These parameters and number of hidden nodes are tuned. Highest score is obtained with “batch size: 16”, “epochs: 362” and “number of hidden nodes: 1000” as 84%. However 1000 hidden nodes are not rational according to Windrow and Lehr[91]. Therefore, more realistic higher score can be acceptable as 79% whose tuned parameters are “batch size: 4”, “epochs: 1448” and “hidden nodes: 114”. Worst accuracy rate is 10% with “batch size: 5794”, “epochs: 1” and “hidden nodes: 66”. In order to understandability and readability, only batch size 4, 8, 16, 32, 64, 128, 256 – analyses are expressed on the graph in figure 98. As seen in this graph, prediction power of RNN is increased by decreasing of batch size. Moreover success rate is increased by increasing of hidden node number until 100 approximately. After this point, accuracies are seen to be saturated. Only 84% accuracy with 1000 hidden nodes which is extremely high is arisen for this reason. Another note about RNN analyses is that while decreasing

of batch size, performing of analysis takes more and more time. In fact “batch size: 1” and “batch size: 2” studies cannot be resulted due to taking hours. Our analysis PC has 8 GB RAM, Intel i7-4600U CPU, 2.10 GHz and 64 bit Windows 7 installation. For implementation, Keras libraries on Python 2.7.13 environment are used. Moreover, class separation capabilities of analyses having satisfactory prediction outputs are significant. Confusion matrix derived from analysis “batch size: 16”, “epochs: 362” and “hidden nodes: 60” is given in table 20 as an example.

LSTM results are measured as slightly better than RNN. Average accuracy score of 92 analyses which are formed with combination of LSTM number from 42 to 120 (increasing step size is 6 LSTM units) and batch size 2^n (n variants from 2 to 8) is 74.65% with kfold:3 cross validation score is 73.51%. While choosing number of LSTM units same references are consulted with ANN’s[88][91][92][93]. 82% is highest score obtained with “LSTM memory cell number: 90, batch size: 8” and “LSTM memory cell number: 100, batch size: 8”. Lowest score is 67% with “Nearly all LSTM memory cell number and batch size: 256”. Similar to RNN behavior, LSTM algorithm run time also takes longer time when batch size is getting smaller. In fact batch size 2 – analyses also cannot be completed with same analyses environment and PC with RNN’s. Again in parallel with RNN results, the graph in figure 99 shows that accuracy rates increase when batch sizes decrease. Moreover, while increasing of LSTM number, prediction power is stronger and saturation level is reached at the point of 90-100 LSTM number. Class separation is also satisfied in consideration of confusion matrixes. Table 21 illustrates an example confusion matrix derived from the analysis whose model inputs are LSTM Number: 90, epochs: 724, Batch size: 8.

Following graph illustrates a summary of the average prediction accuracies observed across all algorithms tested in this thesis.

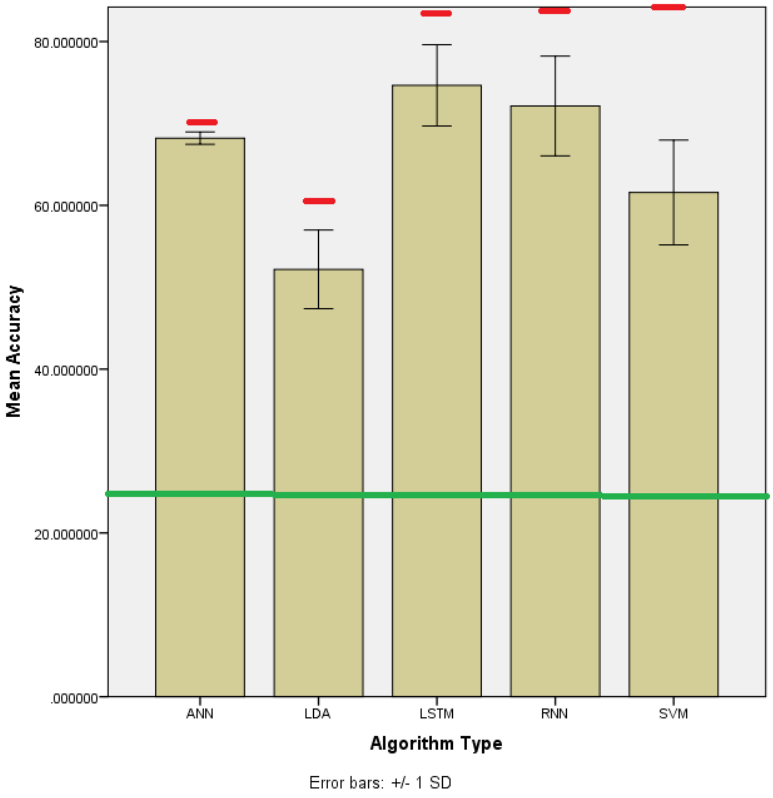

Figure 102: Algorithm Accuracy Scores

Green line pointing to 25% represents average prediction score with four optional outputs; -1, 0, 1, 2. Mean of accuracies for all algorithms are higher than this line which means that all algorithms give better results than random prediction. Red lines represent best scores for the algorithms separately. Standard deviations are marked as line segments. Large standard deviations belonging to ANN, LDA, LSTM, RNN and SVM indicate very large variations of input combinations are tried for these models. Although several analyses are performed for ANN also, narrow standard deviation of it means stacked cases occurred for ANN. Therefore different new approaches should be applied for ANN to observe effects of ANN inputs. Mean accuracy of SVM is seen smaller than LSTM, RNN and ANN due to no-mixed data. When mixed data is used and correct parameters are selected, highest accuracy score is obtained by SVM which is 85% and marked as red line.

In short, all algorithms considered in this study can be ordered in terms of their prediction accuracy as SVM > LSTM > RNN > ANN > LDA based on the highest accuracy percentage obtained in a trial. However there are small differences between SVM, LSTM and RNN. RNN and LSTM give previous data to current mental workload calculation as an input. Since the sliding window approach including a buffer of 60 seconds already makes use of historical data, the advantages of RNN and LSTM for temporal data might not be fully reflected in the study.

One of the most important findings of this thesis is that pilot specific model development for online mental workload detection gives much more effective results than generic models. If any pilot data is not used during training phase of the models, test results decreases significantly due to the fact that developed model is not learnt behavior of this specific pilot. If all pilots' data is partially fed to the training of the model, the accuracy percentage and class separation power of the model were found to increase dramatically.

Studies carried out in this thesis aimed to determine mental workload level of the pilots as online by using fNIR optical brain imaging technology. Measurement of online pilot mental workload might be a crucial input to take precautions for unexpected conditions. If out of ordinary mental workload is detected during the flight, pilots can be stimulated or autopilot can take control of the aircraft. Even warning signals can be sent to ATCs or air control towers. Moreover this technology can provide diverse capabilities like comparing different cockpit designs by sorting the workload induced on specific test pilot during the operational use.

In order to improve this work, some future studies may focus on the following aspects. For instance, in this thesis slope, mean, standard deviation and range features were selected as the main predictors based on our literature survey. These four features and their combinations are used in all analyses. For feature extraction, more research can be done and different features can be used such as kurtosis, skewness etc.

Working principle of fNIRS bases on monitoring of hemodynamic activities on the brain by transmitting and receiving infrared waves via the sensors touched on forehead. Therefore, instant changes of blood volume or untouched infrared sensors can cause misleading prediction of mental workload. -1 classification in this thesis is arisen from this phenomenon. In order to overcome this problem, different filters can be designed. By this way oxy-deoxy hemoglobin change detection originating from only mental activities, not head motion or weak skin contact can be specified and more robust design can be developed. This improvement also creates a chance for using of fNIR technology on different platforms exposing pilots to high G such as fighters.

Moreover, in this thesis, 60 second buffer is created and it is shifted at each 5 second (sliding window technique). Buffer size is detected by researching of the related literature and 5 second is identified by trying a few periods. Additional studies focusing on different buffer sizes and shifting periods could be beneficial for obtaining more acccurate mental workload estimation results.

While SPSS tool is used for LDA, Matlab is used for ANN and Python Keras libraries are used for SVM, RNN and LSTM. When using of SPSS, all feature and voxel weights on the models could be extracted so that the contribution of each feature on the models can be analyzed. However due to the constraints of Matlab ANN package and Python Keras libraries, feature and voxel weights cannot be investigated while developing and experimenting with ANN, SVM, RNN and LSTM models. Therefore, there is a need for

tools that allow researchers to better observe the internal structures of these algorithms to better grasp which features were the most effective predictors of mental workload levels.

REFERENCES

[1] B. Cain, "A Review of the Mental Workload Literature," *Def. Res. Dev. Toronto*, no. 1998, pp. 4–34, 2007.

[2] H. Ayaz, P. A. Shewokis, S. Bunce, K. Izzetoglu, B. Willems, and B. Onaral, "Optical brain monitoring for operator training and mental workload assessment," *Neuroimage*, vol. 59, no. 1, pp. 36–47, 2012.

[3] H. Ayaz *et al.*, "Estimation of cognitive workload during simulated air traffic control using optical brain imaging sensors," *Found. Augment. Cogn. Dir. Futur. Adapt. Syst.*, pp. 549–558, 2011.

[4] P. A. Hancock and M. H. Chignell, "Toward a theory of mental workload: Stress and adaptability in human-machine systems," *Proc. Int. IEEE Conf. Syst. Man Cybern.*, pp. 378–383, 1986.

[5] F. B. Bjørneseth, S. Renganayagalu, M. D. Dunlop, E. Hornecker, and S. Komandur, "Towards an Experimental Design Framework for Evaluation of Dynamic Workload and Situational Awareness in Safety Critical Maritime Settings," *Proc. 26th Annu. BCS Interact. Spec. Gr. Conf. People Comput.*, no. 2006, pp. 309–314, 2012.

[6] E. Gopher, D. and Donchin, "Handbook of Perception and Human Performance.," *Cogn. Process. Perform.*, vol. 2, no. Workload – An examination of the concept., pp. 41-1-49, 1986.

[7] H. S. R. Curry, H. Jex, W. Levison, "Mental workload.," in *Final Report of Control Engineering Group*, 1979, vol. 8, pp. 235–252.

[8] E. J. Kramer, A.F., Sirevaag, "A psychophysiological assessment of operator workload during simulated flight missions.," *Hum. Factors*, vol. 29, no. 2145–160, 1987.

[9] R. J. Lysaght *et al.*, "Operator workload: Comprehensive review and evaluation of operator workload methodologies," *United States Army Res. Inst. Behav. Sci. Tech. Rep.*, vol. 851, pp. 903–986, 1989.

[10] A. W. K. Gaillard, "Comparing the concepts of mental load and stress," *Ergonomics*, vol. 36, no. 9, pp. 991–1005, 1993.

[11] G. B. Colle, H.A. and Reid, “Double trade-off curves with different cognitive processing combinations: Testing the cancellation axiom of mental workload measurement theory.,” *Hum. Factors*, vol. 41, no. 1, pp. 35–50, 1999.

[12] H. R. Jex, “Measuring mental workload: Problems, progress, and promises. Human Mental Workload,” *Adv. Psychol.*, vol. 52, pp. 5–39, 1988.

[13] W. D. Roscoe, A.H., Ellis, G.A., and Chiles, “Assessing pilot workload,” *Appl. Ergon.*, vol. 10, no. 2, p. 115, 1979.

[14] A. ROSCOE, *The practical assessment of pilot workload*. 1987.

[15] G. B. Reid, S. S. Potter, and J. R. Bressler, “Adat 40,” *Distribution*, 1989.

[16] L. E. S. Hart, Sandra G., *Human Mental Workload*. 1988.

[17] D. De Waard, *The Measurement of Drivers ’ Mental Workload*, vol. 39, no. 4. 1996.

[18] R. W. Schvaneveldt, R. L. Gomez, G. B. Reid, A. Laboratories, and W.-P. Afb, “Modeling mental workload,” *Perception*, vol. 3, pp. 1–26, 1997.

[19] S. Coyle, “Near-infrared spectroscopy for brain computer interfacing,” *Eng. vol. PhD Thesis Kildare Maynooth*, no. May, 2005.

[20] J. P. Strangman, G., Boas, D.A., Sutton, “Non-invasive neuroimaging using near-infrared light,” *Biol. Psychiatry*, vol. 52, no. 7, pp. 679–693, 2002.

[21] G. Strangman, D. a Boas, and J. P. Sutton, “Non-invasive neuroimaging using near-infrared light.,” *Biol. Psychiatry*, vol. 52, no. 7, pp. 679–693, 2002.

[22] C. R. S. Jeffrey B. Brookingsa, Glenn F. Wilson, “Psychophysiological responses to changes in workload during simulated air traffic control,” *Biol. Psychol.*, vol. 42, no. 3, pp. 361–377, 1996.

[23] H. Ayaz, P. a. Shewokis, S. Bunce, and B. Onaral, “An optical brain computer interface for environmental control,” *Proc. Annu. Int. Conf. IEEE Eng. Med. Biol. Soc. EMBS*, pp. 6327–6330, 2011.

[24] F. Matthews, B. a. Pearlmutter, T. E. Ward, C. Soraghan, and C. Markham, “Hemodynamics for brain-computer interfaces,” *IEEE Signal Process. Mag.*, vol. 25, no. January, pp. 87–94, 2008.

[25] M. L. T. Cossio *et al.*, *No Title No Title*, vol. XXXIII, no. 2. 2012.

[26] M. Chaouachi, I. Jraidi, and C. Frasson, “Modeling mental workload using EEG features for intelligent systems,” *Lect. Notes Comput. Sci. (including Subser. Lect. Notes Artif. Intell. Lect. Notes Bioinformatics)*, vol. 6787 LNCS, pp. 50–61, 2011.

[27] G. F. Wilson, “An Analysis of Mental Workload in Pilots During Flight Using Multiple Psychophysiological Measures,” *Int. J. Aviat. Psychol.*, vol. 12, no. 1, pp. 3–18, 2002.

[28] J. Kohlmorgen *et al.*, “Improving Human Performance in a Real Operating Environment through Real-Time Mental Workload Detection,” in *Toward Brain-Computer Interfacing*, 2007, pp. 409–422.

[29] D. Heger, F. Putze, and T. Schultz, *Ki 2010: Advances in Artificial Intelligence*. 2010.

[30] M. S. Korsnes, A. a Wright, and J. D. E. Gabrieli, "An fMRI analysis of object priming and workload in the precuneus complex.," *Neuropsychologia*, vol. 46, no. 5, pp. 1454–62, 2008.

[31] G. Rota *et al.*, "Self-regulation of regional cortical activity using real-time fMRI: The right inferior frontal gyrus and linguistic processing," *Hum. Brain Mapp.*, vol. 30, no. 5, pp. 1605–1614, 2009.

[32] R. Sitaram, A. Caria, and N. Birbaumer, "Hemodynamic brain–computer interfaces for communication and rehabilitation," *Neural Networks*, vol. 22, no. 9, pp. 1320–1328, 2009.

[33] N. Weiskopf, F. Scharnowski, R. Veit, R. Goebel, N. Birbaumer, and K. Mathiak, "Self-regulation of local brain activity using real-time functional magnetic resonance imaging (fMRI)," *J. Physiol.*, vol. 98, no. 4–6, pp. 357–373, 2004.

[34] S.-S. Yoo *et al.*, "Brain–computer interface using fMRI: spatial navigation by thoughts," *Neuroreport*, vol. 15, no. 10, pp. 1591–1595, 2004.

[35] Sitaram, "fMRI brain computer interfaces," in *15th annual conference of international society for neurofeedback & research, current perspectives in neuroscience: Neuroplasticity & neurofeedback.*, 2007.

[36] F. F. Jöbsis, "Noninvasive, infrared monitoring of cerebral and myocardial oxygen sufficiency and circulatory parameters.," *Science*, vol. 198, no. 4323, pp. 1264–1267, 1977.

[37] L. Villringer, A. Planck, J. Dirnagl, U. Hock, C. Schleinkofer, "Near infrared spectroscopy (NIRS): a new tool to study hemodynamic changes during activation of brain function in human adults.," *Neurosci. Lett.*, vol. 154, no. 1, p. 101, 1993.

[38] B. Chance, Z. Zhuang, C. UnAh, C. Alter, and L. Lipton, "Cognition-activated low-frequency modulation of light absorption in human brain.," *Proc. Natl. Acad. Sci. U. S. A.*, vol. 90, no. April, pp. 3770–3774, 1993.

[39] B. Chance and A. Villringer, "Non-invasive optical spectroscopy and imaging of human brain function," *Trends Neurosci.*, vol. 20, no. 10, pp. 435–442, 1997.

[40] H. Obrig *et al.*, "Near-infrared spectroscopy: Does it function in functional activation studies of the adult brain?," *Int. J. Psychophysiol.*, vol. 35, no. 2–3, pp. 125–142, 2000.

[41] H. Ayaz *et al.*, "Monitoring expertise development during simulated UAV piloting tasks using optical brain imaging," *Aerosp. Conf. 2012 IEEE*, vol. 1, no. 215, pp. 1–11, 2012.

[42] K. Izzetoglu, "Neural correlates of cognitive workload and anesthetic depth: fNIR spectroscopy investigation in humans," *Biomed. Eng. (NY).*, vol. PhD, no. July, p. 72, 2008.

[43] Icao, "Safety Report 2014," p. 35, 2014.

[44] "Qatar Airways pilot dies in flight." [Online]. Available:

http://www.aljazeera.com/news/asia-pacific/2010/10/20101013125418819383.html. [Accessed: 03-Jan-2015].

[45] E. Hays, Robert T., Jacobs, John W., Prince, Carolyn, Salas, "Requirements for Future Research in Flight Simulation Training: Guidance Based on a Meta-Analytic Review," *The International Journal of Aviation Psychology*, vol. 2, no. 2. pp. 143–158, 1992.

[46] E. Salas, C. A. Bowers, and L. Rhodenizer, "It is not how much you have but how you use it: toward a rational use of simulation to support aviation training," *The International journal of aviation psychology*, vol. 8, no. 3. pp. 197–208, 1998.

[47] N. Dahlstrom, S. Dekker, R. van Winsen, and J. Nyce, "Fidelity and validity of simulator training," *Theor. Issues Ergon. Sci.*, vol. 10, no. 4, pp. 305–314, 2009.

[48] U. Yeh, Yei-yu, Honeywell Systems & Research Ctr, Phoenix Technology Group, AZ and C. D. Wickens, "Dissociation of performance and subjective measures of workload.," *Hum. Factors*, vol. 30, no. 1, pp. 111–120, 1988.

[49] F. Borghini, G., Isabella, R., Vecchiato, G., Toppi, J., Astolfi, L., Caltagirone, C., & Babiloni, "Brainshield: HREEG study of perceived pilot mental workload," *Ital. J. Aerosp. Med.*, vol. 5, pp. 34–47, 2011.

[50] G. Borghini, L. Astolfi, G. Vecchiato, D. Mattia, and F. Babiloni, "Measuring neurophysiological signals in aircraft pilots and car drivers for the assessment of mental workload, fatigue and drowsiness," *Neurosci. Biobehav. Rev.*, vol. 44, pp. 58–75, 2014.

[51] M. De Rivecourt, M. N. Kuperus, W. J. Post, and L. J. M. Mulder, "Cardiovascular and eye activity measures as indices for momentary changes in mental effort during simulated flight.," *Ergonomics*, vol. 51, no. 9, pp. 1295–1319, 2008.

[52] A. Haarmann, W. Boucsein, and F. Schaefer, "Combining electrodermal responses and cardiovascular measures for probing adaptive automation during simulated flight," *Appl. Ergon.*, vol. 40, no. 6, pp. 1026–1040, 2009.

[53] H. van Dijk, K. van de Merwe, and R. Zon, "A Coherent Impression of the Pilots' Situation Awareness: Studying Relevant Human Factors Tools," *Int. J. Aviat. Psychol.*, vol. 21, no. 4, pp. 343–356, 2011.

[54] G. F. Wilson, J. a. Caldwell, and C. a. Russell, "Performance and Psychophysiological Measures of Fatigue Effects on Aviation Related Tasks of Varying Difficulty," *Int. J. Aviat. Psychol.*, vol. 17, no. 906692079, pp. 219–247, 2007.

[55] G. F. Wilson and C. A. Russell, "Performance enhancement in an uninhabited air vehicle task using psychophysiologically determined adaptive aiding.," *Hum. Factors*, vol. 49, no. 6, pp. 1005–1018, 2007.

[56] Dussault, "EEG and ECG changes during simulator operation reflect mental workload and vigilance.," *Aviat. Sp. Environ. Med.*, vol. 76, no. 4, pp. 344–351, 2006.

[57] "Across | Advanced cockpit for reduction of stress and workload." [Online]. Available: http://www.across-fp7.eu/. [Accessed: 03-Jan-2016].

[58] H. Ayaz, B. Onaral, K. Izzetoglu, P. A. Shewokis, R. McKendrick, and R. Parasuraman, “Continuous monitoring of brain dynamics with functional near infrared spectroscopy as a tool for neuroergonomic research: empirical examples and a technological development.,” *Front. Hum. Neurosci.*, vol. 7, no. DEC, p. 871, 2013.

[59] K. Izzetoglu *et al.*, “Handbook of Unmanned Aerial Vehicles,” 2015.

[60] E. E. Smith and J. Jonides, “Neuroimaging analyses of human working memory,” *Proc. Natl. Acad. Sci. USA*, vol. 95, no. 20, pp. 12061–12068, 1998.

[61] U. Request *et al.*, “Sehchang Hah , Ph . D ., Ben Willems , M . A . & Randy Phillips , Supervisory Air Traffic Control Specialist * Human Factors Group- Atlantic City Federal Aviation Administration (FAA) Atlantic City International Airport , New Jersey,” *Control*, pp. 50–54, 2006.

[62] B. Willems, S. Hah, and K. Schulz, “En Route Data Communications: Experimental Human Factors Evaluation,” *Security*, no. December, 2010.

[63] T. Gateau, G. Durantin, F. Lancelot, S. Scannella, and F. Dehais, “Real-time state estimation in a flight simulator using fNIRS.,” *PLoS One*, vol. 10, no. 3, p. e0121279, 2015.

[64] G. Derosière, K. Mandrick, G. Dray, T. E. Ward, and S. Perrey, “NIRS-measured prefrontal cortex activity in neuroergonomics: strengths and weaknesses.,” *Front. Hum. Neurosci.*, vol. 7, no. September, p. 583, 2013.

[65] H. Sato *et al.*, “Intersubject variability of near-infrared spectroscopy signals during sensorimotor cortex activation.,” *J. Biomed. Opt.*, vol. 10, no. 4, p. 44001, 2005.

[66] G. Jasdzewski, G. Strangman, J. Wagner, K. K. Kwong, R. A. Poldrack, and D. A. Boas, “Differences in the hemodynamic response to event-related motor and visual paradigms as measured by near-infrared spectroscopy,” *Neuroimage*, vol. 20, no. 1, pp. 479–488, 2003.

[67] K. Tai and T. Chau, “Single-trial classification of NIRS signals during emotional induction tasks: towards a corporeal machine interface,” *J. Neuroeng. Rehabil.*, vol. 6, no. 1, p. 39, 2009.

[68] W. H. Lin and A. Hauptmann, “Meta-classification: Combining multimodal classifiers,” *Min. Multimed. Complex Data*, pp. 217–231, 2003.

[69] G. L. Tsirogiannis and D. Frossyniotis, “A Meta-classifier Approach for Medical Diagnosis . A Meta-classifier Approach for Medical Diagnosis,” no. January 2016, 2004.

[70] G. Durantin, J. F. Gagnon, S. Tremblay, and F. Dehais, “Using near infrared spectroscopy and heart rate variability to detect mental overload,” *Behav. Brain Res.*, vol. 259, pp. 16–23, 2014.

[71] C. Herff, D. Heger, O. Fortmann, J. Hennrich, F. Putze, and T. Schultz, “Mental workload during n-back task-quantified in the prefrontal cortex using fNIRS.,” *Front. Hum. Neurosci.*, vol. 7, no. January, p. 935, 2013.

[72] D. Heger, R. Mutter, C. Herff, F. Putze, and T. Schultz, “Continuous recognition of

affective states by functional near infrared spectroscopy signals," in *Humaine Association Conference on Affective Computing and Intelligent Interaction*, 2013, pp. 832–837.

[73] C. Ang, K. K., Chin, Z. Y., Zhang, H., and Guan, "Filter bank common spatial pattern (fbcsp) in brain-computer interface," in *International Joint Conference on Neural Networks*, 2008, pp. 2390–2397.

[74] P. P. (TTS) S. Boverie (CONTI), A. Giralt (CONTI), O. KOC (TAI), K. Papadopoulos (HAI), C. Vollard (A-F), M. Varkevisser (TRT), T. Bos (NLR), P. Kou (DAV), F. Salmon Legagneur (DAV), N. Durand (TTS), P. Cousin (TTS), Y. James (TTS), "ACROSS-WP9-DAV-TECH-DEL-0005-D9." p. 45, 2015.

[75] M. Izzetoglu, S. C. Bunce, K. Izzetoglu, B. Onaral, and a. K. Pourrezaei, "Functional brain imaging using near-infrared technology," *IEEE Eng. Med. Biol. Mag.*, vol. 26, no. August, pp. 38–46, 2007.

[76] C. Optical and B. Imaging, "fNIR Imager & COBI Studio Manual," 2014.

[77] C. Lecture, "Today ' s Class."

[78] D. C. Slaughter, M. G. Pelletier, and S. K. Upadhyaya, "S s m u nir s," vol. 17, no. 2, pp. 241–247, 2001.

[79] A. Q. S. Guide, "f nir S oft," 2011.

[80] P. on W. Transition and N. R. Council, "Workload Transition: Implications for Individual and Team Performance," vol. 1993, p. 273, 1993.

[81] T. Iijima, K. Funabiki, and T. Nojima, "Pilot workload assessment method in a new CNS/ATM environment," *Conf. Proc. - IEEE Int. Conf. Syst. Man Cybern.*, vol. 3, pp. 2699–2706, 2004.

[82] "Pilot Workload." [Online]. Available: https://www.skybrary.aero/index.php/Pilot_Workload. [Accessed: 19-Dec-2017].

[83] R. Pascanu, T. Mikolov, and Y. Bengio, "On the difficulty of training Recurrent Neural Networks," 2012.

[84] S. Hochreiter and J. Urgen Schmidhuber, "Long Short-Term Memory," *Neural Comput.*, vol. 9, no. 8, pp. 1735–1780, 1997.

[85] N. Sofiyanti, D. I. Fitmawati, and A. A. Roza, "Understanding LSTM Networks," *GITHUB colah blog*, vol. 22, no. 2, pp. 137–141, 2015.

[86] C. T. Kelley, "A note on the approximation of functions of several variables by sums of functions of one variable," *J. Approx. Theory*, vol. 33, no. 3, pp. 179–189, 1981.

[87] G. Cybenko, "Approximation by Superpositions of a Sigmoidal Function," pp. 303–314, 1989.

[88] R. J. M. Russell D. Read, "MLP Representational Capabilities," in *Neural Smitihing*, 1999, p. Chapter 4.

[89] E. D. Sontag, "Feedback Stabilization Using Two-Hidden-Layer Nets," *IEEE*

Trans. Neural Networks, vol. 3, no. 6, pp. 981–990, 1992.

[90] Richard, P., and Lippmann, "An Introduction' to Computing with Neural Nets," 1987.

[91] M. A. L. Bernard Widrow, "30 Years of Adaptive Neural Networks: Perceptron, Madaline, and Backpropagation," *Proceeding IEEE*, vol. 78, 1990.

[92] S. Karsoliya, "Approximating Number of Hidden layer neurons in Multiple Hidden Layer BPNN Architecture," *Int. J. Eng. Trends Technol.*, vol. 3, no. 6, pp. 714–717, 2012.

[93] F. S. Panchal and M. Panchal, "Review on Methods of Selecting Number of Hidden Nodes in Artificial Neural Network," *Int. J. Comput. Sci. Mob. Comput.*, vol. 311, no. 11, pp. 455–464, 2014.

APPENDICES

APPENDIX A

SUBJECTIVE WORKLOAD GRAPHS OF TEST PILOTS

After completion of each test scenario on simulator environment, test subject evaluates his own mental workload in time domain. It is also asked them to mark critical events on the graphs. Although these graphs represent subjective evaluation, they give input to determine the parameters affecting mental workload level.

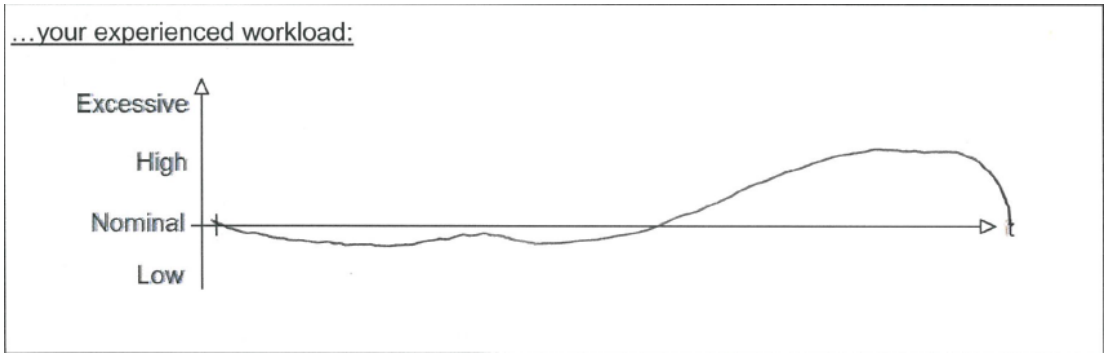

Figure 103: Subject1, Scenario1

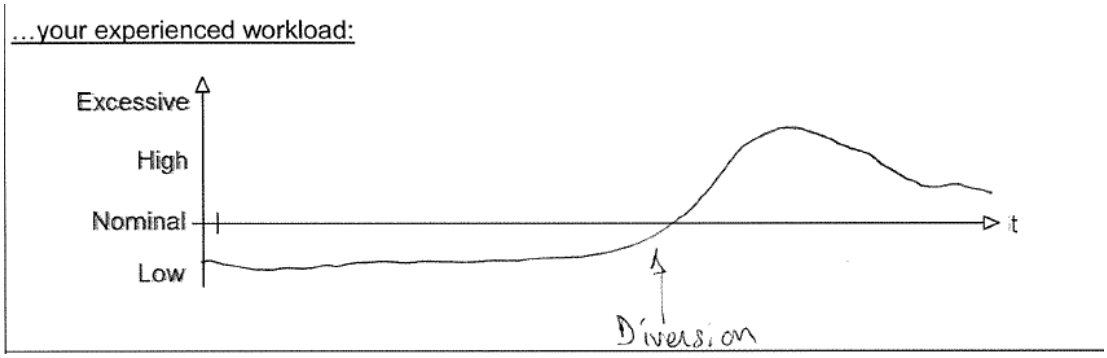

Figure 104: Subject1, Scenario2

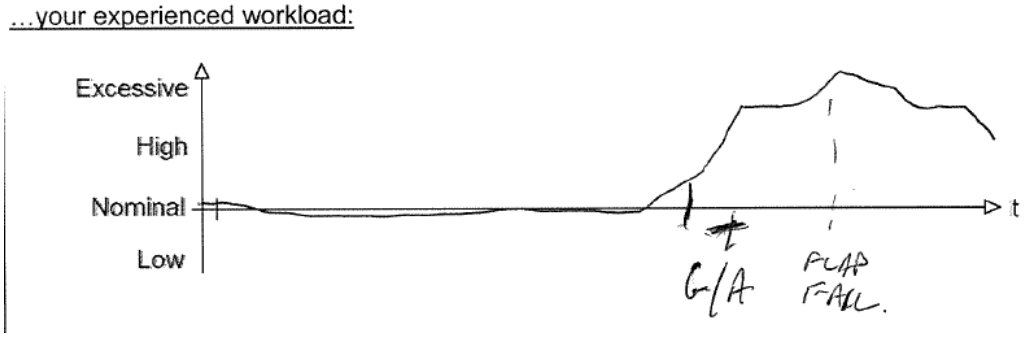

Figure 105: Subject1, Scenario3

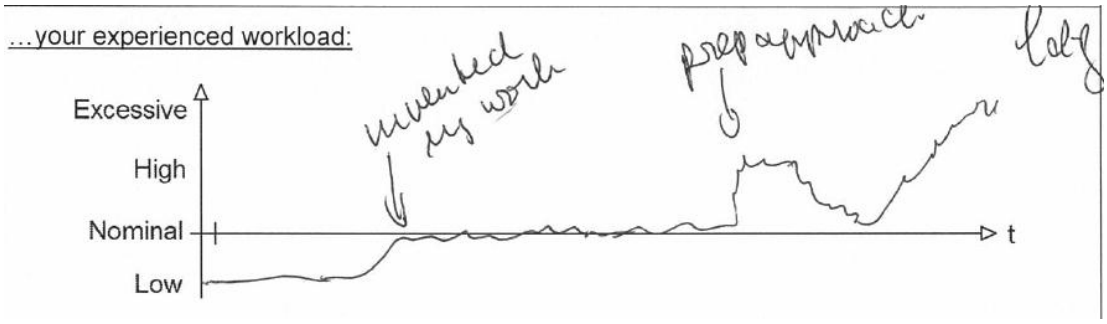

Figure 106: Subject2, Scenario1

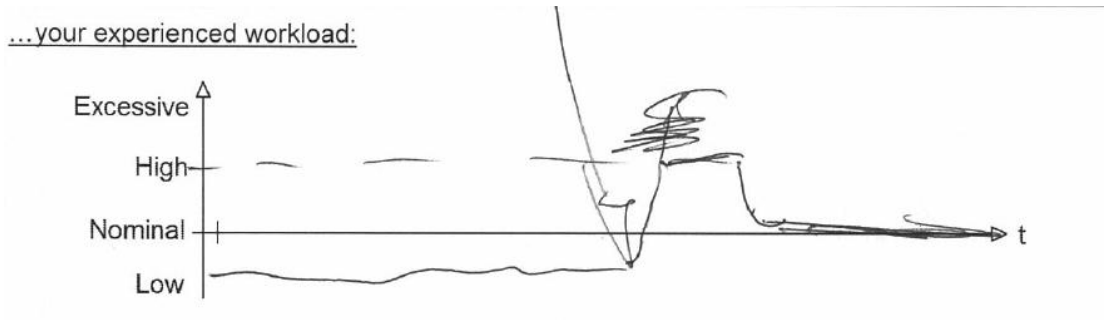

Figure 107: Subject2, Scenario2

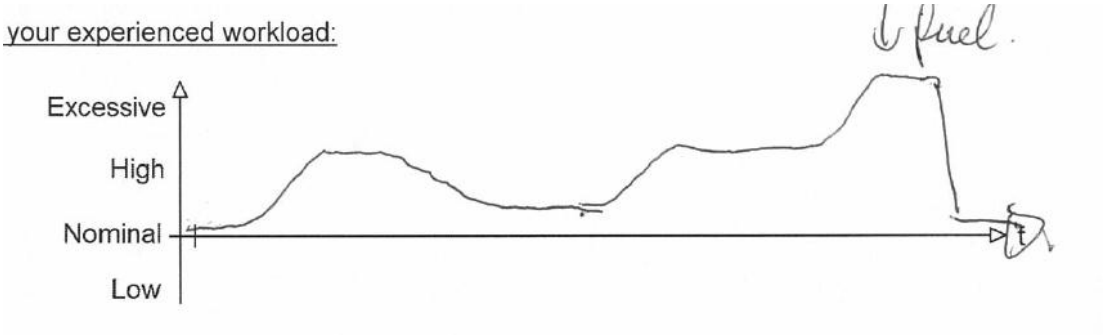

Figure 108: Subject2, Scenario3

Figure 109: Subject3, Scenario1

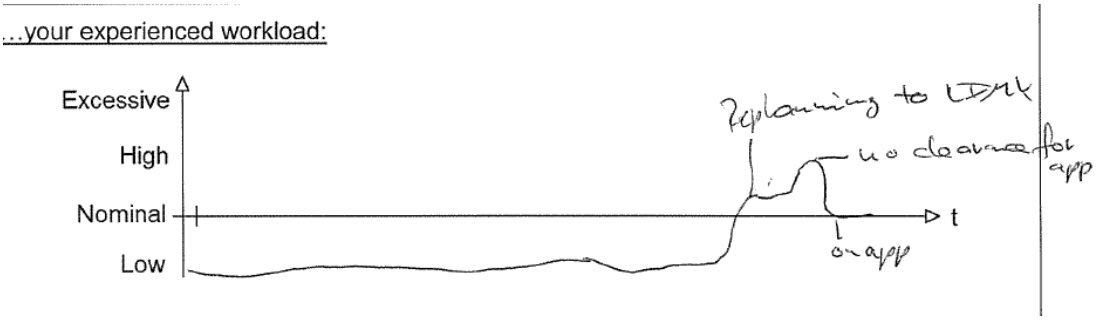

Figure 110: Subject3, Scenario2

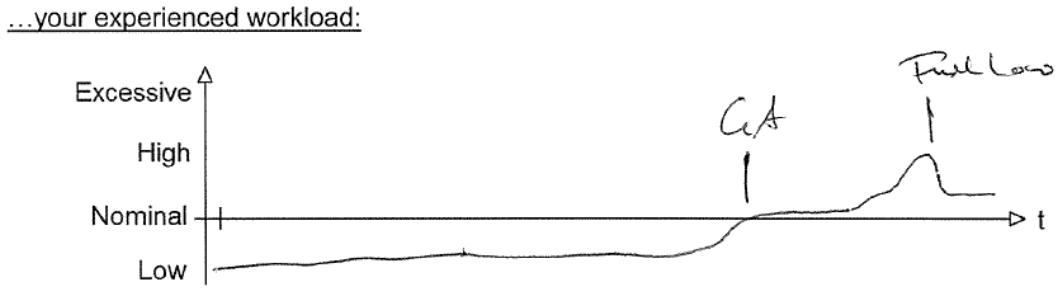

Figure 111: Subject3, Scenario3

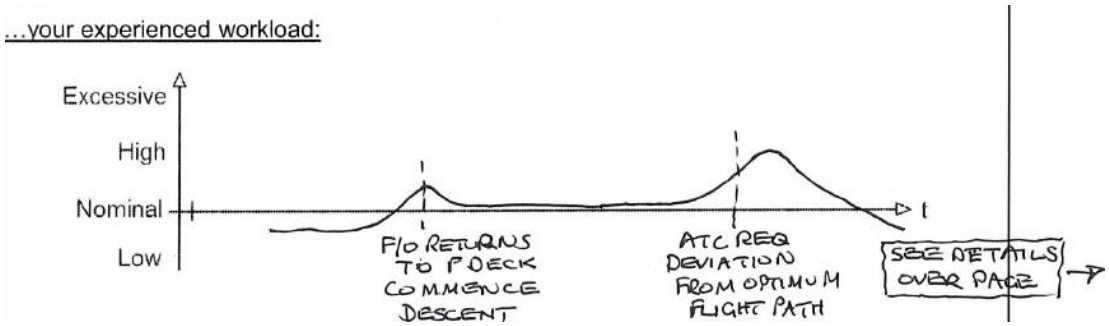

Figure 112: Subject4, Scenario1

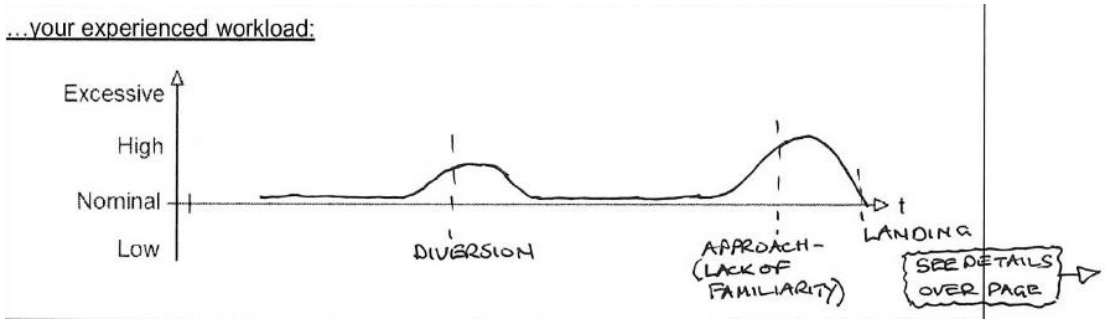

Figure 113: Subject4, Scenario2

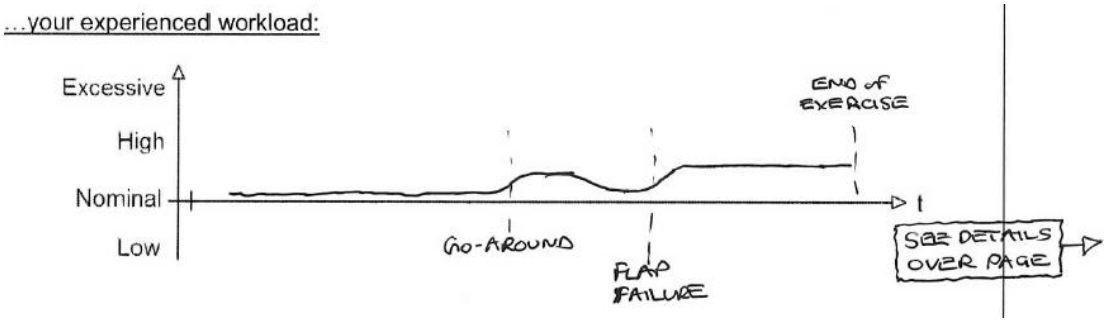

Figure 114: Subject4, Scenario3

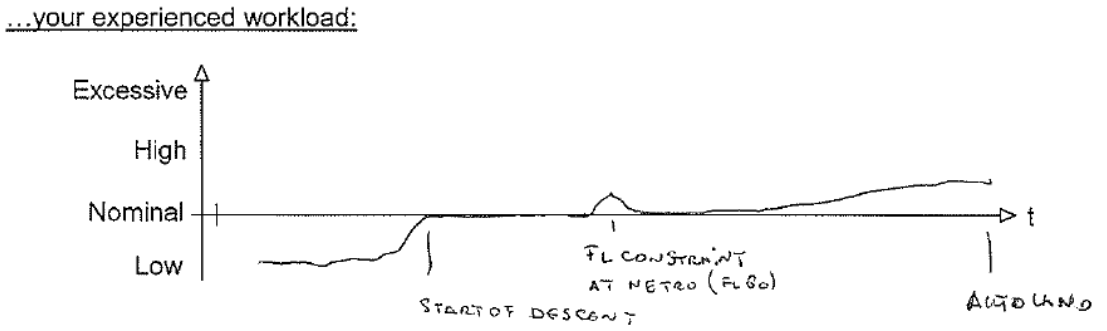

Figure 115: Subject5, Scenario1

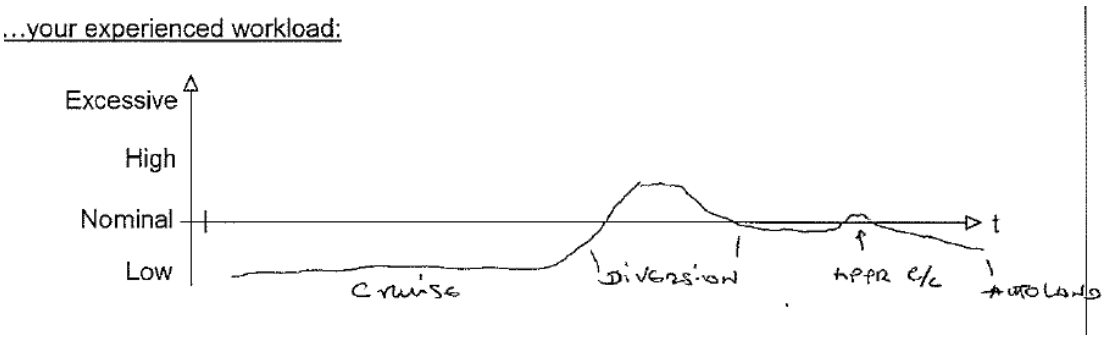

Figure 116: Subject5, Scenario2

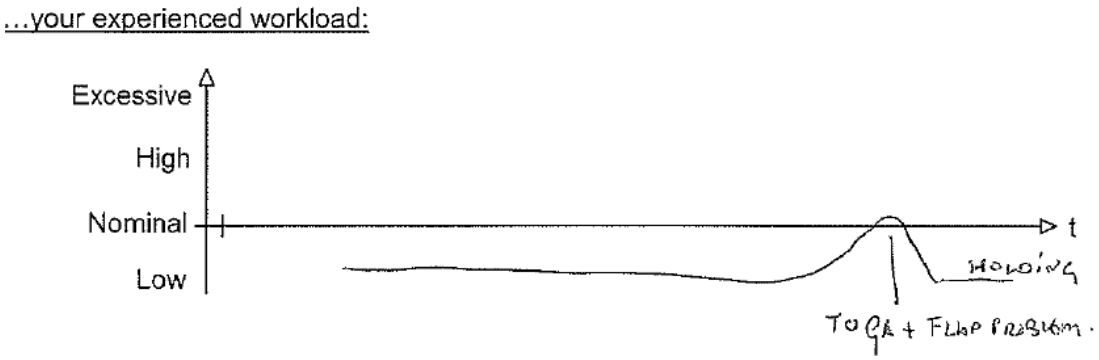

Figure 117: Subject5, Scenario3

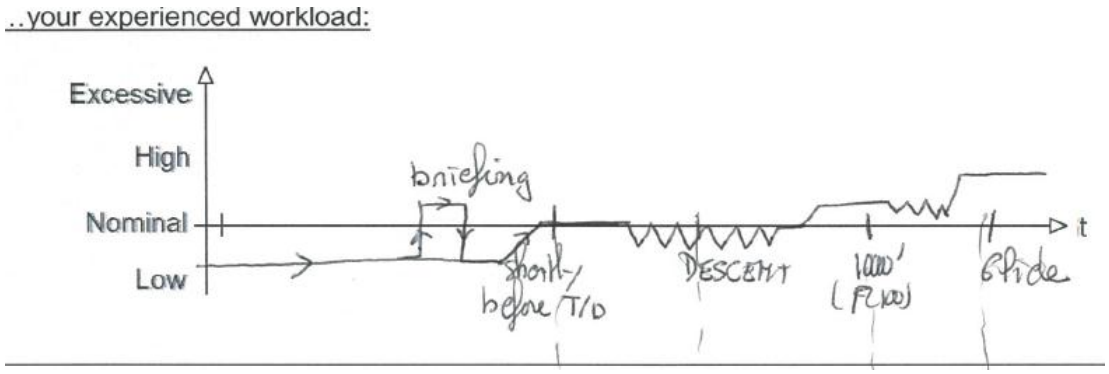

Figure 118: Subject6, Scenario1

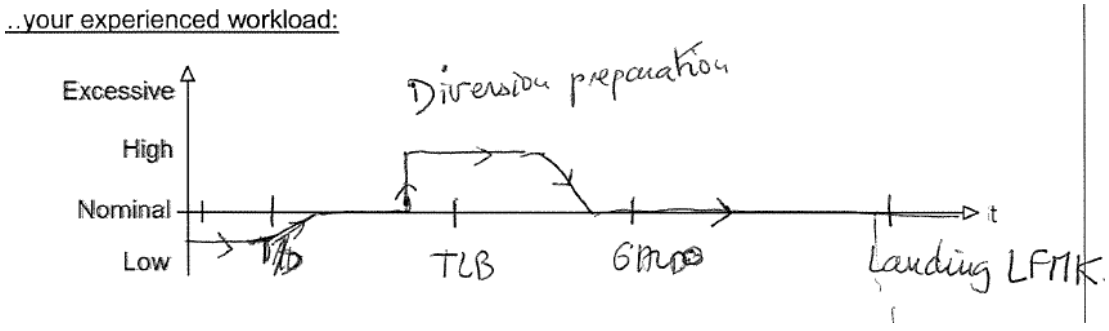

Figure 119: Subject6, Scenario2

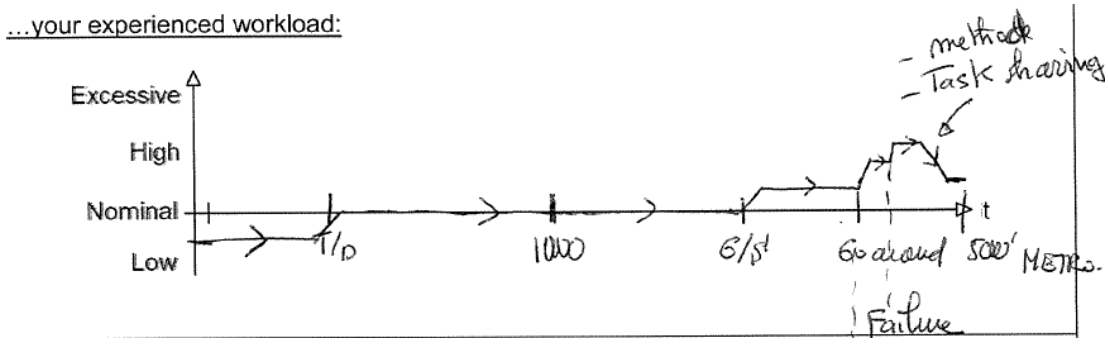

Figure 120: Subject6, Scenario3

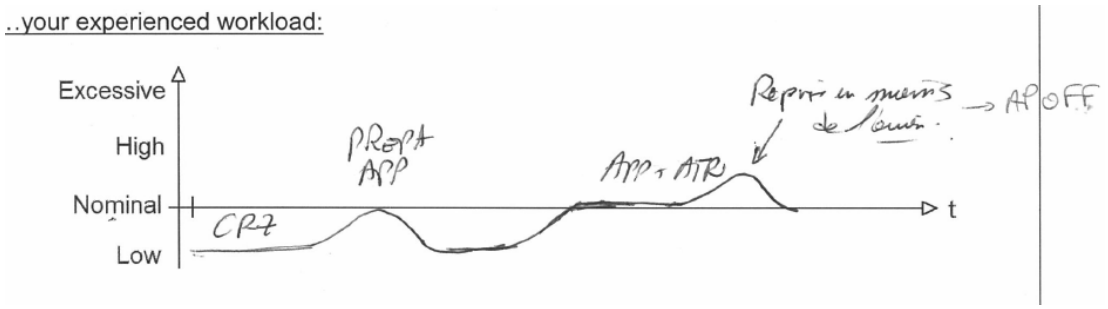

Figure 121: Subject7, Scenario1

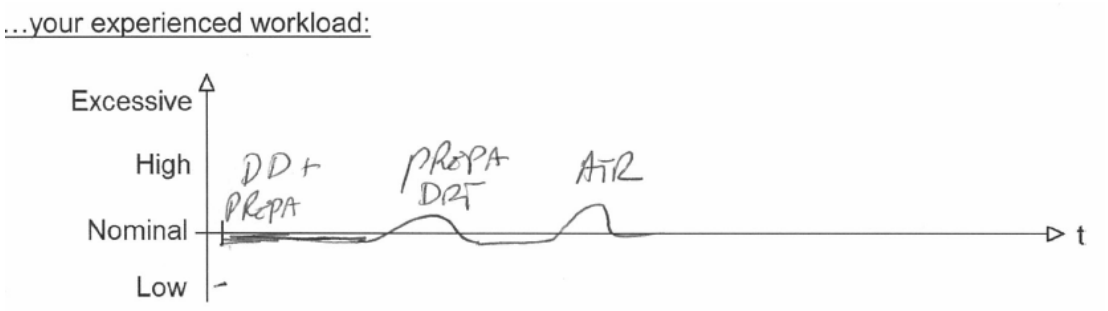

Figure 122: Subject7, Scenario2

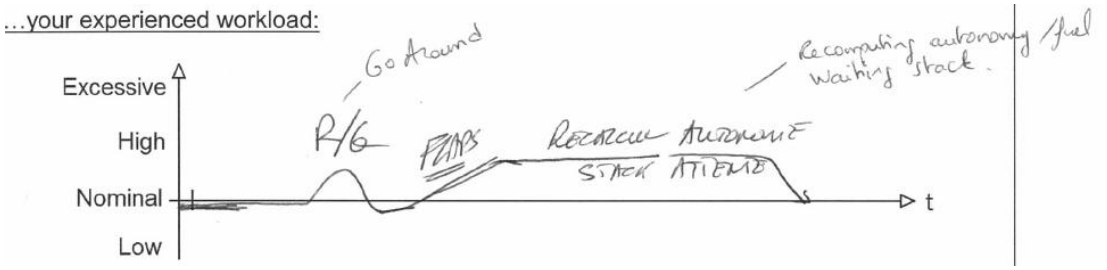

Figure 123: Subject7, Scenario3

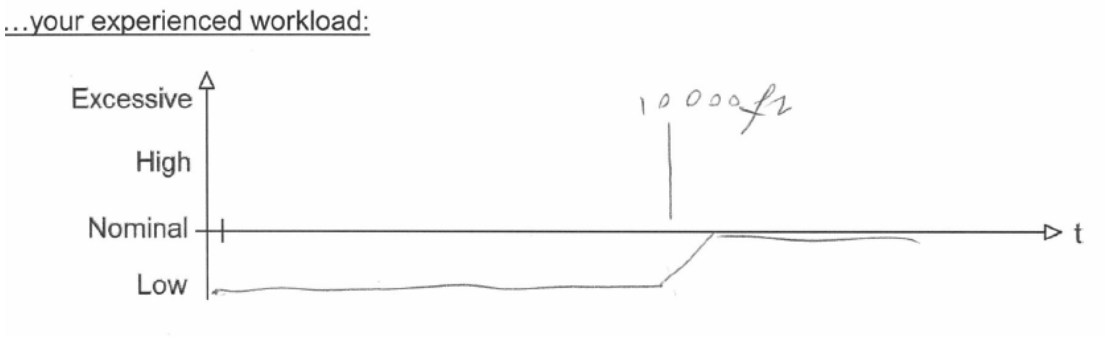

Figure 124: Subject8, Scenario1

Figure 125: Subject8, Scenario2

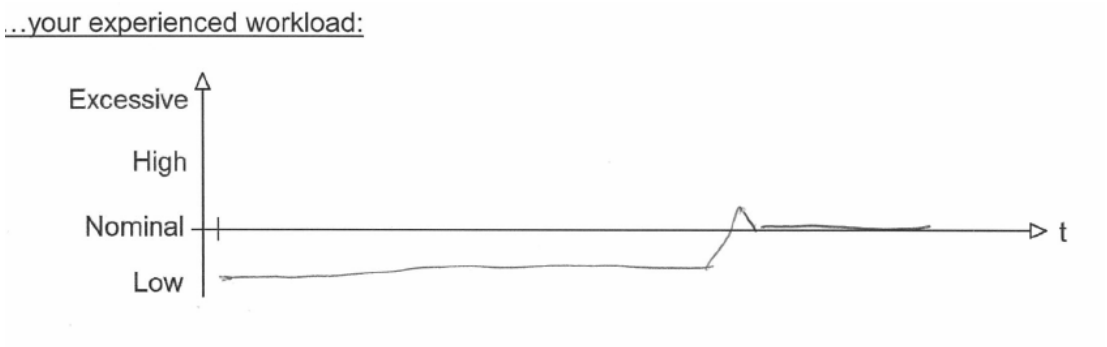

Figure 126: Subject8, Scenario3

APPENDIX B

PARAMETERS AFFECTING MENTAL WORKLOAD

Following first table lists determined parameters with their IDs which affect mental workload. Second table illustrates how their combinations affect mental workload.

Table 24: Parameter List with IDs

Parameters Description	Parameter ID
Flight phase	A
ATC talking about standard flight info	B
ATC talking about unexpected event (go around etc.)	C
CPT talks to ATC	D
CPT talks to pilot	E
Pilot talks to CPT	F
Pilot chats with CPT	G
Unexpected event (flap failure etc.)	H
Pilot sets/controls instrument (AP panel, lg, flap etc.)	I
Pilot sets/controls instrument (throttle, CDU, speed breaker, etc.)	J
Pilot reads/writes paper(checklist)	K
Pilot is confused	L
Drowsiness	M
Head movement, weak skin contact	N
Cockpit warnings (1000 feet etc.)	O
Poor visibility	P

Table 25: Effects Of Parameters on Mental Workload (0: No Exist, 1: Exist)

A	B	C	D	E	F	G	H	I	J	K	L	M	N	O	P	Mental Workload
cruise	0	0	0	1	0	0	0	1	0	0	0	0	0	0	1	0
cruise	0	0	0	0	0	0	0	0	0	0	0	0	0	0	1	0
cruise	1	0	1	0	0	0	0	1	0	0	0	0	0	0	0	0
cruise	0	0	0	0	0	0	0	0	0	0	0	0	0	0	0	0
cruise	0	0	0	0	0	0	0	0	1	0	0	0	0	0	0	0
cruise	0	0	0	0	1	0	0	0	0	0	0	0	0	0	0	0
cruise	0	0	0	0	0	0	0	1	0	0	0	0	0	0	0	0
cruise	0	0	0	0	0	1	0	0	0	0	0	0	0	0	0	0
cruise	0	0	0	1	1	0	0	0	0	0	0	0	0	0	0	0
cruise	1	0	0	1	1	0	0	0	1	0	0	0	0	0	0	0
cruise	0	0	0	1	0	0	0	0	0	0	0	0	0	0	0	0
cruise	0	0	1	0	0	0	0	0	0	0	0	0	0	0	0	0
cruise	1	0	0	1	0	0	0	0	1	0	0	0	0	0	0	0
cruise	0	0	0	1	0	0	0	0	1	0	0	0	0	0	0	0
cruise	1	0	0	0	0	0	0	0	0	0	0	0	0	0	0	0
cruise	0	0	0	1	1	0	0	1	0	0	0	0	0	0	0	0
cruise	0	0	1	0	0	0	0	1	0	0	0	0	0	0	0	0
cruise	0	0	0	0	1	0	0	1	0	0	0	0	0	0	0	0
cruise	1	0	1	0	0	0	0	0	0	0	0	0	0	0	0	0
cruise	0	0	0	0	1	0	0	0	0	1	0	0	0	0	0	0
cruise	0	0	0	0	0	0	0	0	0	1	0	0	0	0	0	0
cruise	0	0	0	1	1	0	0	0	0	0	0	0	0	0	1	0
cruise	1	0	1	0	1	0	0	1	0	0	0	0	0	0	0	0
cruise	0	0	1	1	0	0	0	1	0	0	0	0	0	0	0	0
cruise	1	0	1	0	0	0	0	1	0	0	0	0	0	0	1	0
cruise	0	0	0	0	0	0	0	0	0	0	0	1	0	0	0	0
cruise	0	0	0	1	0	0	0	0	0	1	0	0	0	0	0	0
cruise	0	0	0	0	0	0	0	1	1	0	0	0	0	0	0	0
descent	1	0	0	0	1	0	0	1	0	0	0	0	0	0	1	0
descent	0	0	0	0	0	1	0	0	0	0	0	0	0	0	1	0
descent	0	0	0	0	1	0	0	0	0	0	0	0	0	0	1	0
descent	1	0	1	0	0	0	0	0	0	0	0	0	0	0	1	0
descent	1	0	1	0	0	0	0	1	0	0	0	0	0	0	1	0
descent	0	0	0	0	0	0	0	1	0	0	0	0	0	0	1	0
descent	1	0	1	0	1	0	0	1	0	0	0	0	0	0	1	0
descent	0	0	0	0	0	0	0	0	0	0	0	0	0	0	1	0
descent	1	0	1	0	0	0	0	0	1	0	0	0	0	0	1	0
descent	0	0	1	0	0	0	0	0	0	0	0	0	0	0	1	0
descent	1	0	0	1	1	0	0	1	0	0	0	0	0	0	1	0
descent	0	0	0	1	1	0	0	0	0	0	0	0	0	0	1	0
descent	1	0	0	0	1	0	0	0	0	0	0	0	0	0	1	0

descent	0	0	1	0	1	0	0	0	1	0	0	0	0	0	1	0
descent	0	0	1	0	0	0	0	1	0	0	0	0	0	0	1	0
descent	0	0	1	0	1	0	0	0	0	0	0	0	0	0	1	0
descent	1	0	0	0	0	0	0	1	0	0	0	0	0	0	1	0
descent	0	0	0	0	0	0	0	0	1	0	0	0	0	0	0	0
descent	0	0	0	0	0	0	0	0	0	0	0	0	0	0	0	0
descent	0	0	0	0	0	0	0	1	0	0	0	0	0	0	0	0
descent	1	0	1	0	0	0	0	0	0	0	0	1	0	0	0	0
descent	1	0	1	0	0	0	0	0	0	0	0	0	0	0	0	0
descent	0	0	0	0	0	0	0	0	0	0	0	1	0	0	0	0
descent	0	0	0	1	1	0	0	0	0	0	0	0	0	0	0	0
descent	0	0	0	0	1	0	0	1	0	0	0	0	0	0	0	0
descent	1	0	1	1	1	0	0	1	0	0	0	0	0	0	0	0
descent	0	0	1	0	0	0	0	0	0	0	0	1	0	0	0	0
descent	1	0	0	0	0	0	0	0	0	0	0	1	0	0	0	0
descent	0	0	1	0	0	0	0	0	0	0	0	0	0	0	0	0
descent	1	0	1	1	1	0	0	0	0	0	0	0	0	0	0	0
descent	1	0	1	0	0	0	0	1	0	0	0	0	0	0	0	0
descent	0	0	0	0	1	0	0	0	0	0	0	0	0	0	0	0
descent	1	0	1	0	1	0	0	1	0	0	0	0	0	0	0	0
descent	0	0	0	0	0	1	0	0	0	0	0	0	0	0	0	0
descent	1	0	1	0	1	0	0	1	1	0	0	0	0	0	0	0
descent	1	0	1	0	0	0	0	1	0	1	0	0	0	0	1	0
descent	1	0	1	1	1	0	0	0	0	1	0	0	0	0	1	0
descent	0	0	0	1	1	0	0	1	0	0	0	0	0	0	1	0
descent	1	0	0	0	0	0	0	1	0	0	0	0	0	0	0	0
descent	0	0	0	1	1	0	0	1	0	0	0	0	0	0	0	0
descent	0	0	1	0	1	0	0	1	0	0	0	0	0	0	0	0
descent	0	0	1	1	1	0	0	0	0	0	0	0	0	0	0	0
descent	1	0	0	0	0	0	0	0	0	0	0	0	0	0	0	0
descent	1	0	0	1	1	0	0	1	0	0	0	0	0	0	0	0
descent	0	0	0	1	0	0	0	0	0	0	0	0	0	0	0	0
descent	0	0	1	0	1	0	0	0	0	0	0	0	0	0	0	0
descent	0	0	1	0	0	0	0	1	0	0	0	0	0	0	0	0
descent	1	0	1	0	1	0	0	0	0	0	0	0	0	0	0	0
descent	0	0	0	0	1	0	0	1	0	0	0	0	0	0	1	0
descent	0	0	0	1	0	0	0	1	0	0	0	0	0	0	0	0
approach	0	0	0	0	0	0	0	0	0	0	0	0	0	0	1	0
approach	0	0	0	0	0	1	0	0	0	0	0	0	0	0	1	0
approach	0	0	0	0	1	0	0	0	0	0	0	0	0	0	1	0
approach	0	0	0	1	1	0	0	0	0	0	0	0	0	0	1	0
approach	0	0	0	0	0	1	0	0	0	0	0	0	0	0	0	0
approach	0	0	0	0	0	0	0	0	0	0	0	0	0	0	0	0
approach	0	0	0	0	0	0	0	1	0	0	0	0	0	0	0	0

approach	0	0	0	1	1	0	0	0	0	0	0	0	0	0	0	0
approach	0	0	1	0	0	0	0	0	0	0	0	0	0	0	0	0
approach	0	0	0	0	1	0	0	1	0	0	0	0	0	0	0	0
approach	1	0	0	0	0	0	0	1	0	0	0	0	0	0	0	0
approach	0	0	0	0	1	0	0	0	0	0	0	0	0	0	0	0
approach	0	0	1	0	1	0	0	1	0	0	0	0	0	0	0	0
approach	1	0	1	0	0	0	0	0	0	0	0	0	0	0	1	0
approach	1	0	1	0	0	0	0	0	0	0	0	0	0	0	0	0
approach	1	0	0	0	0	0	0	0	0	0	0	0	0	0	1	0
approach	0	0	0	0	0	0	0	1	0	0	0	0	0	0	1	0
approach	0	0	0	0	0	0	0	0	1	0	0	0	0	0	1	0
approach	0	0	0	0	0	0	0	0	0	0	0	0	0	1	0	0
go around	0	0	0	0	0	1	0	0	0	0	0	0	0	0	0	0
end of landing	0	0	0	1	1	0	0	0	0	0	0	0	0	0	0	0
end of landing	0	0	0	0	0	1	0	0	0	0	0	0	0	0	0	0
end of landing	0	0	0	0	0	0	0	0	0	0	0	0	0	0	0	0
cruise	0	0	0	1	1	0	0	0	1	0	0	0	0	0	0	1
cruise	0	0	0	1	1	0	0	0	0	1	0	0	0	0	0	1
cruise	0	0	0	0	0	0	0	0	1	1	0	0	0	0	0	1
cruise	0	0	0	1	1	0	0	1	0	1	0	0	0	0	1	1
cruise	1	0	1	1	1	0	0	1	0	1	0	0	0	0	1	1
cruise	0	0	0	0	1	0	0	0	1	1	0	0	0	0	0	1
cruise	0	0	0	1	1	0	0	0	1	1	0	0	0	0	0	1
cruise	1	0	1	0	0	0	0	0	0	1	0	0	0	0	0	1
cruise	0	0	0	0	0	0	0	1	1	1	0	0	0	0	0	1
cruise	0	0	0	1	1	0	0	1	0	0	1	0	0	0	0	1
cruise	0	0	0	0	1	0	0	0	1	0	0	0	0	0	0	1
cruise	0	0	0	1	1	0	0	1	1	0	0	0	0	0	0	1
cruise	1	0	1	1	1	0	0	1	1	0	0	0	0	0	0	1
descent	0	0	0	1	1	0	0	0	0	0	1	0	0	0	1	1
descent	0	0	0	0	1	0	0	1	0	0	1	0	0	0	1	1
descent	0	0	0	1	1	0	0	0	1	0	0	0	0	0	1	1
descent	0	0	1	0	1	0	0	1	1	0	0	0	0	0	0	1
descent	1	0	0	0	0	0	0	0	0	1	0	0	0	0	0	1
descent	0	1	0	1	1	0	0	1	1	0	0	0	0	0	0	1
descent	0	0	0	0	1	0	0	0	1	0	0	0	0	0	0	1
descent	0	0	0	1	1	0	0	0	0	1	0	0	0	0	0	1
descent	0	0	0	1	1	0	0	0	1	0	0	0	0	0	0	1
descent	0	0	0	1	1	0	0	1	1	1	0	0	0	0	0	1
descent	1	0	1	0	0	0	0	0	0	1	0	0	0	0	1	1
descent	0	0	1	1	1	0	0	1	0	0	0	0	0	0	1	1
descent	0	0	0	1	1	0	0	1	1	0	0	0	0	0	0	1
descent	1	0	1	0	1	0	0	0	1	0	0	0	0	0	0	1
descent	1	0	1	0	0	0	0	1	1	0	0	0	0	0	0	1

descent	1	0	1	0	0	0	0	0	1	1	0	0	0	0	0	1
descent	0	0	0	0	1	0	0	0	0	1	0	0	0	0	0	1
descent	0	1	1	1	1	0	0	0	1	0	0	0	0	0	0	1
descent	1	0	1	1	1	0	0	0	0	1	0	0	0	0	0	1
descent	0	0	0	1	1	0	0	1	0	1	0	0	0	0	0	1
descent	1	0	1	0	0	0	0	1	0	1	0	0	0	0	0	1
descent	0	0	1	1	1	0	0	0	0	1	0	0	0	0	0	1
descent	0	0	0	0	0	0	0	0	0	1	0	0	0	0	0	1
descent	0	0	0	0	0	0	0	0	0	1	0	0	0	0	1	1
descent	0	0	0	1	1	0	0	0	0	1	0	0	0	0	1	1
descent	0	1	1	0	0	0	0	0	0	1	0	0	0	0	0	1
descent	1	0	1	0	0	0	0	0	0	1	0	0	0	0	0	1
descent	0	0	1	0	0	0	0	0	1	0	0	0	0	0	0	1
descent	1	0	0	0	0	0	0	0	1	1	0	0	0	0	0	1
descent	1	1	0	0	0	0	0	0	1	1	0	0	0	0	0	1
descent	0	0	0	0	0	0	0	0	1	1	1	0	0	0	0	1
descent	0	0	0	1	1	0	0	0	0	1	1	0	0	0	0	1
descent	0	0	0	0	0	0	0	1	0	1	0	0	0	0	0	1
descent	1	0	1	1	1	0	0	0	1	0	0	0	0	0	0	1
descent	0	1	1	0	1	0	0	1	1	0	0	0	0	0	0	1
descent	0	0	0	0	0	0	0	1	1	1	0	0	0	0	0	1
descent	0	0	0	0	1	0	0	1	1	0	0	0	0	0	1	1
descent	0	0	0	0	1	0	0	0	1	0	0	0	0	0	1	1
descent	0	1	0	0	0	0	0	1	0	0	0	0	0	0	0	1
descent	1	0	1	0	0	0	0	0	1	0	0	0	0	0	0	1
descent	1	0	0	0	0	0	0	0	1	0	0	0	0	0	0	1
approach	0	0	0	1	1	0	0	1	0	0	1	0	0	0	1	1
approach	1	0	1	0	0	0	0	1	0	0	0	0	0	0	1	1
approach	0	0	0	1	1	0	0	0	0	0	1	0	0	0	1	1
approach	0	0	0	1	1	0	0	1	0	0	0	0	0	0	1	1
approach	1	0	1	0	0	0	0	0	1	0	0	0	0	0	1	1
approach	1	0	0	0	1	0	0	1	0	0	0	0	0	0	1	1
approach	0	0	0	1	0	0	0	1	0	0	0	0	0	0	1	1
approach	0	0	0	0	0	0	0	1	0	0	0	0	0	1	1	1
approach	0	0	0	1	1	0	0	1	0	0	0	0	0	0	0	1
approach	1	0	1	1	1	0	0	1	0	0	0	0	0	0	0	1
approach	0	0	0	0	0	0	0	0	1	0	0	0	0	0	0	1
approach	1	0	1	0	0	0	0	1	0	0	0	0	0	0	0	1
approach	0	0	0	1	1	0	0	0	1	0	0	0	0	0	0	1
approach	0	0	0	0	0	0	0	1	0	0	0	0	0	1	0	1
approach	0	0	0	0	1	0	0	0	1	0	0	0	0	0	0	1
approach	0	0	0	0	0	0	0	0	1	0	0	0	0	1	0	1
approach	1	0	1	0	1	0	0	1	0	0	0	0	0	0	0	1
approach	1	0	0	1	1	0	0	0	1	0	0	0	0	0	0	1

approach	1	0	0	1	1	0	0	1	0	0	0	0	0	0	0	1
approach	0	0	0	1	1	0	0	1	1	0	0	0	0	0	0	1
approach	0	0	0	0	1	0	0	1	1	0	0	0	0	1	0	1
approach	1	0	0	1	1	0	0	1	0	0	0	0	0	0	1	1
approach	1	0	0	1	0	0	0	1	0	0	0	0	0	0	1	1
approach	0	0	0	0	0	0	0	0	1	0	0	0	0	1	1	1
approach	0	1	0	0	0	0	0	0	0	0	0	0	0	0	0	1
approach	1	0	1	1	1	1	0	1	1	0	0	0	0	0	0	1
approach	0	0	0	1	1	0	0	0	1	1	0	0	0	0	0	1
approach	1	0	1	1	1	0	0	1	1	1	0	0	0	0	0	1
approach	0	0	0	1	1	0	0	1	0	1	0	0	0	0	0	1
approach	1	0	1	0	0	0	0	0	1	1	0	0	0	0	0	1
approach	0	0	0	0	0	0	0	0	1	1	0	0	0	0	0	1
approach	1	0	1	1	1	0	0	0	1	1	0	0	0	0	0	1
approach	0	0	1	1	0	0	0	1	1	0	0	0	0	0	0	1
approach	0	0	0	1	1	0	0	1	1	0	0	0	0	1	0	1
approach	0	0	0	1	1	0	0	0	1	0	0	0	0	1	0	1
approach	0	0	0	1	1	0	0	0	0	1	0	0	0	0	0	1
approach	0	0	0	1	1	0	0	0	1	0	0	0	0	1	1	1
approach	0	0	0	1	1	0	0	0	1	0	0	0	0	0	1	1
approach	0	0	0	1	1	0	0	0	1	1	0	0	0	0	1	1
approach	1	0	0	0	0	0	0	1	0	0	0	0	0	0	1	1
approach	1	0	1	1	1	0	0	1	0	0	0	0	0	0	1	1
approach	0	0	0	1	1	0	0	0	0	0	1	0	0	0	0	1
approach	0	0	0	0	1	0	0	0	0	1	0	0	0	0	1	1
approach	1	0	1	0	0	0	0	1	0	1	0	0	0	0	0	1
approach	0	0	0	1	0	0	0	1	0	0	0	0	0	0	0	1
approach	0	0	1	1	1	0	0	1	0	0	0	0	0	0	0	1
approach	0	0	0	1	1	0	0	1	0	0	0	0	0	1	0	1
approach	1	0	1	1	1	1	1	1	0	0	0	0	0	0	0	1
go around	0	0	0	0	1	0	0	0	1	0	0	0	0	0	1	1
go around	0	0	0	1	1	0	0	0	0	0	0	0	0	0	1	1
go around	1	0	0	1	1	0	0	1	0	0	0	0	0	0	1	1
go around	0	0	0	1	1	0	0	1	0	0	0	0	0	0	1	1
go around	1	0	1	0	1	0	0	1	0	0	0	0	0	0	1	1
go around	1	0	0	1	1	0	0	0	0	1	0	0	0	0	1	1
go around	0	0	0	1	1	0	0	1	0	1	0	0	0	0	1	1
go around	0	0	0	1	1	0	0	0	0	0	0	0	0	0	0	1
go around	1	0	1	0	0	0	0	1	0	0	0	0	0	0	0	1
go around	1	0	0	0	0	0	0	0	0	0	0	0	0	0	0	1
landing	0	0	0	0	0	0	0	0	1	0	0	0	0	1	0	1
landing	0	0	0	0	0	0	0	0	1	0	0	0	0	0	0	1
landing	0	0	0	1	0	0	0	0	1	0	0	0	0	0	0	1
landing	0	0	0	1	1	0	0	0	1	0	0	0	0	0	0	1

end of landing	0	0	0	1	1	0	0	0	1	0	0	0	0	0	0	1
approach	0	1	0	0	1	0	1	0	0	0	0	0	0	0	1	2
approach	0	0	0	1	1	0	0	1	0	1	1	0	0	0	1	2
approach	1	0	1	1	1	0	0	0	1	0	1	0	0	0	0	2
approach	1	0	1	0	0	0	0	0	1	0	1	0	0	0	0	2
approach	0	0	0	0	0	0	1	1	0	0	0	0	0	1	1	2
approach	0	0	0	1	1	0	1	1	0	0	0	0	0	0	0	2
approach	0	0	0	1	1	0	0	1	1	0	1	0	0	0	1	2
approach	0	1	0	0	0	0	0	1	0	0	0	0	0	0	0	2
go around	1	0	1	0	1	0	0	1	0	0	1	0	0	0	1	2
go around	0	0	0	0	1	0	0	0	0	0	1	0	0	0	1	2
go around	1	0	0	1	1	0	0	1	1	0	0	0	0	0	1	2
go around	1	0	1	0	0	0	0	1	0	0	1	0	0	0	1	2
go around	0	0	0	0	0	0	1	1	0	0	1	0	0	0	1	2
go around	0	1	0	1	1	0	0	0	1	0	0	0	0	0	1	2
go around	0	0	0	1	1	0	1	1	0	0	0	0	0	0	1	2
go around	0	0	0	1	1	0	0	0	0	0	1	0	0	0	1	2
go around	0	1	1	1	1	0	0	1	1	0	1	0	0	0	0	2
go around	0	0	0	1	1	0	1	0	1	0	0	0	0	0	0	2
go around	1	0	0	1	1	0	0	0	1	0	0	0	0	0	0	2
go around	0	0	0	1	1	0	0	0	1	0	1	0	0	0	0	2
go around	0	0	0	1	1	0	0	1	1	0	0	0	0	0	0	2
go around	0	1	0	1	1	0	0	0	0	0	0	0	0	0	1	2
go around	1	0	1	1	1	0	0	1	0	0	0	0	0	0	1	2
go around	1	0	1	1	1	0	0	1	1	0	0	0	0	0	1	2
go around	0	0	0	1	1	0	0	1	1	0	0	0	0	0	1	2
go around	1	0	1	1	1	0	0	0	0	0	0	0	0	0	1	2
go around	0	0	0	1	1	0	0	0	1	1	0	0	0	0	1	2
go around	0	0	0	1	1	0	0	1	0	0	0	0	0	0	0	2
go around	1	0	1	0	1	0	0	1	0	0	1	0	0	0	0	2
go around	0	0	0	1	1	0	1	1	0	0	0	0	0	0	0	2
go around	1	0	1	0	0	0	0	1	1	0	0	0	0	0	0	2
go around	0	1	0	1	1	0	0	1	0	0	0	0	0	0	0	2
go around	1	0	1	0	0	0	1	0	1	0	1	0	0	0	0	2
go around	1	0	1	0	1	0	0	1	0	0	0	0	0	0	0	2
cruise	0	0	0	1	1	0	0	1	0	0	0	0	1	0	0	-1
cruise	0	0	0	0	0	0	0	0	0	0	0	0	1	0	0	-1
cruise	0	0	0	0	0	0	0	1	0	0	0	0	1	0	0	-1
cruise	0	0	0	0	0	0	0	0	0	0	0	0	1	0	1	-1
cruise	0	0	0	1	0	0	0	0	0	0	0	0	1	0	0	-1
cruise	0	0	0	1	1	0	0	0	0	0	0	0	1	0	0	-1
descent	0	0	0	0	0	0	0	0	0	0	0	0	1	0	1	-1
descent	0	0	0	0	1	0	0	0	0	0	0	0	1	0	1	-1
descent	0	0	0	0	0	0	0	0	0	0	0	0	1	0	0	-1

descent	0	0	0	0	0	0	0	0	0	0	0	1	1	0	0	-1
descent	0	0	0	1	1	0	0	0	0	0	0	0	1	0	0	-1
descent	0	0	0	0	1	0	0	0	0	0	0	0	1	0	0	-1
descent	0	0	0	1	1	0	0	1	0	0	0	0	1	0	0	-1
descent	0	0	1	0	0	0	0	0	0	0	0	0	1	0	0	-1
descent	0	0	0	1	1	0	0	0	0	0	0	0	1	0	1	-1
descent	0	0	0	1	0	0	0	0	0	0	0	0	1	0	1	-1
descent	0	0	0	1	1	0	0	1	0	0	0	0	1	0	1	-1
descent	0	0	0	0	0	1	0	0	0	0	0	0	1	0	0	-1
descent	0	0	0	0	0	0	0	1	0	0	0	0	1	0	0	-1
descent	0	0	1	0	0	0	0	1	0	0	0	0	1	0	0	-1
descent	1	0	1	0	0	0	0	0	0	0	0	0	1	0	0	-1
approach	0	0	0	0	0	0	0	0	0	0	0	0	1	0	1	-1
approach	0	0	0	0	0	0	0	0	0	0	0	0	1	0	0	-1
approach	1	0	0	0	0	0	0	0	0	0	0	0	1	0	0	-1
approach	0	0	0	0	0	1	0	0	0	0	0	0	1	0	1	-1
approach	1	0	1	0	0	0	0	0	0	0	0	0	1	0	0	-1
approach	0	0	0	1	1	0	0	0	0	0	0	0	1	0	0	-1
approach	0	0	0	0	0	1	0	0	0	0	0	0	1	0	0	-1
approach	0	0	0	0	0	1	0	0	1	0	0	0	1	0	0	-1
descent	0	1	1	0	1	0	0	1	0	0	0	0	1	0	0	-1
descent	0	0	0	0	0	0	1	0	0	0	0	0	1	0	0	-1
descent	0	0	0	0	0	0	0	0	0	1	0	0	1	0	0	-1
approach	0	0	0	1	1	0	0	0	0	0	0	0	1	0	1	-1
approach	0	0	0	1	1	0	0	1	0	0	0	0	1	0	0	-1
approach	0	0	0	1	1	0	0	1	0	0	0	0	1	0	1	-1
landing	0	0	0	1	1	0	0	0	0	0	0	0	1	1	0	-1
approach	0	0	0	1	1	0	0	1	1	0	1	0	1	0	1	-1

APPENDIX C

ACCURACY SCORES OF LDA

Following table lists accuracies of LDA algorithm with different combination of inputs which are training data, raw data, features, and consideration of class -1.

Table 26: LDA Success Rates with Input Combinations

Training Data (Pilot ID_Session)	Raw Data Type	Features	Evaluation of class "-1"	Discriminant Rate (%)
2345	hbo	mean_stdev_slope_range	-1 extracted	46
2345	hbr	mean_stdev_slope_range	-1 extracted	45
2345	hbt	mean_stdev_slope_range	-1 extracted	44.3
2345	oxy	mean_stdev_slope_range	-1 extracted	47.6
2345	hbo_hbr	mean_stdev_slope_range	-1 extracted	51.3
2345	hbo_hbt	mean_stdev_slope_range	-1 extracted	51.1
2345	hbo_oxy	mean_stdev_slope_range	-1 extracted	52.6
2345	hbr_hbt	mean_stdev_slope_range	-1 extracted	53
2345	hbr_oxy	mean_stdev_slope_range	-1 extracted	53
2345	oxy_hbt	mean_stdev_slope_range	-1 extracted	53.2
2345	hbo_hbr_oxy	mean_stdev_slope_range	-1 extracted	54.4
2345	hbo_hbr_hbt	mean_stdev_slope_range	-1 extracted	57.7
2345	hbr_oxy_hbt	mean_stdev_slope_range	-1 extracted	55
2345	hbo_oxy_hbt	mean_stdev_slope_range	-1 extracted	55.8
2345	hbo_hbr_oxy_hbt	mean	-1 extracted	41.4
2345	hbo_hbr_oxy_hbt	stdev	-1 extracted	52.6
2345	hbo_hbr_oxy_hbt	slope	-1 extracted	44.7

2345	hbo_hbr_oxy_hbt	range	-1 extracted	51.8
2345	hbo_hbr_oxy_hbt	mean_stdev	-1 extracted	54.1
2345	hbo_hbr_oxy_hbt	mean_slope	-1 extracted	44.2
2345	hbo_hbr_oxy_hbt	mean_range	-1 extracted	52.6
2345	hbo_hbr_oxy_hbt	stdev_slope	-1 extracted	55.8
2345	hbo_hbr_oxy_hbt	stdev_range	-1 extracted	55.9
2345	hbo_hbr_oxy_hbt	slope_range	-1 extracted	54.2
2345	hbo_hbr_oxy_hbt	mean_stdev_slope	-1 extracted	55.6
2345	hbo_hbr_oxy_hbt	mean_stdev_range	-1 extracted	57.7
2345	hbo_hbr_oxy_hbt	mean_slope_range	-1 extracted	54.2
2345	hbo_hbr_oxy_hbt	stdev_slope_range	-1 extracted	59
2345	hbo_hbr_oxy_hbt	mean_stdev_slope_range	-1 extracted	59.3
2345	hbo_hbr	mean_stdev_slope_range	-1 extracted	51.3
2345	hbo	mean_stdev_slope_range	-1 not considered	45.3
2345	hbr	mean_stdev_slope_range	-1 not considered	42.6
2345	hbt	mean_stdev_slope_range	-1 not considered	43.2
2345	oxy	mean_stdev_slope_range	-1 not considered	46.9
2345	hbo_hbr	mean_stdev_slope_range	-1 not considered	51.1
2345	hbo_hbt	mean_stdev_slope_range	-1 not considered	50.5
2345	hbo_oxy	mean_stdev_slope_range	-1 not considered	52.7
2345	hbr_hbt	mean_stdev_slope_range	-1 not considered	52.6
2345	hbr_oxy	mean_stdev_slope_range	-1 not considered	52.9
2345	oxy_hbt	mean_stdev_slope_range	-1 not considered	52.9
2345	hbo_hbr_oxy	mean_stdev_slope_range	-1 not considered	54.5
2345	hbo_hbr_hbt	mean_stdev_slope_range	-1 not considered	57.8
2345	hbr_oxy_hbt	mean_stdev_slope_range	-1 not considered	54.8
2345	hbo_oxy_hbt	mean_stdev_slope_range	-1 not considered	55.6

2345	hbo_hbr_oxy_hbt	mean	-1 not considered	41.3
2345	hbo_hbr_oxy_hbt	stdev	-1 not considered	53
2345	hbo_hbr_oxy_hbt	slope	-1 not considered	44.7
2345	hbo_hbr_oxy_hbt	range	-1 not considered	51.7
2345	hbo_hbr_oxy_hbt	mean_stdev	-1 not considered	54.1
2345	hbo_hbr_oxy_hbt	mean_slope	-1 not considered	44.3
2345	hbo_hbr_oxy_hbt	mean_range	-1 not considered	52.6
2345	hbo_hbr_oxy_hbt	stdev_slope	-1 not considered	55.5
2345	hbo_hbr_oxy_hbt	stdev_range	-1 not considered	55.7
2345	hbo_hbr_oxy_hbt	slope_range	-1 not considered	54.5
2345	hbo_hbr_oxy_hbt	mean_stdev_slope	-1 not considered	55.7
2345	hbo_hbr_oxy_hbt	mean_stdev_range	-1 not considered	57.8
2345	hbo_hbr_oxy_hbt	mean_slope_range	-1 not considered	54.8
2345	hbo_hbr_oxy_hbt	stdev_slope_range	-1 not considered	59
2345	hbo_hbr_oxy_hbt	mean_stdev_slope_range	-1 not considered	59.5
2345	hbo_hbr	mean_stdev_slope_range	-1 not considered	51.1
2345	hbo_hbr_oxy_hbt	mean_stdev_slope_range	-1 considered	54.8
2345	hbo_hbr	mean_stdev_slope_range	-1 considered	47.2
2345	oxy	mean_stdev_slope_range	-1 considered	42.4
2345	hbt	mean_stdev_slope_range	-1 considered	39.3
2678	hbo_hbr_oxy_hbt	mean_stdev_slope_range	-1 considered	53.4
2678	hbo_hbr_oxy_hbt	mean_stdev_slope_range	-1 considered	57.8
2678	hbo_hbr_oxy_hbt	mean_stdev_slope_range	-1 considered	56.9
2	hbo_hbr_oxy_hbt	mean_stdev_slope_range	-1 considered	81.5
6	hbo_hbr_oxy_hbt	mean_stdev_slope_range	-1 considered	72.6
7	hbo_hbr_oxy_hbt	mean_stdev_slope_range	-1 considered	76.5
8	hbo_hbr_oxy_hbt	mean_stdev_slope_range	-1 considered	77.2

2_2	hbo_hbr_oxy_hbt	mean_stdev_slope_range	-1 considered	89.8
2_3	hbo_hbr_oxy_hbt	mean_stdev_slope_range	-1 considered	93.4
6_1	hbo_hbr_oxy_hbt	mean_stdev_slope_range	-1 considered	80.2
6_2	hbo_hbr_oxy_hbt	mean_stdev_slope_range	-1 considered	88.7
6_3	hbo_hbr_oxy_hbt	mean_stdev_slope_range	-1 considered	86.6
7_1	hbo_hbr_oxy_hbt	mean_stdev_slope_range	-1 considered	86.1
7_2	hbo_hbr_oxy_hbt	mean_stdev_slope_range	-1 considered	89.9
7_3	hbo_hbr_oxy_hbt	mean_stdev_slope_range	-1 considered	92.1
8_1	hbo_hbr_oxy_hbt	mean_stdev_slope_range	-1 considered	97.3
8_2	hbo_hbr_oxy_hbt	mean_stdev_slope_range	-1 considered	92.4
8_3	hbo_hbr_oxy_hbt	mean_stdev_slope_range	-1 considered	89.6
5	hbo_hbr	mean_stdev_slope_range	-1 considered	65.6
6	hbo_hbr	mean_stdev_slope_range	-1 considered	62.1
6_1, 7_2, 8_3	hbo_hbr	mean_stdev_slope_range	-1 considered	61.4
Mixed	hbo_hbr	mean_stdev_slope_range	-1 considered	50.0

Table 27: Accuracy of Cross Validation vs Discriminant Rate for LDA – kfold:3

Training Data (Pilot ID_Session)	Raw Data Type	Features	Evaluation of class "-1"	Cross Validation Rate (%)	Discriminant Rate (%)
Mixed (~60% data)	hbo_hbr	mean_stdev_slope_range	-1 class is considered	45.07	50
5	hbo_hbr	mean_stdev_slope_range	-1 class is considered	72.23	65.6
6	hbo_hbr	mean_stdev_slope_range	-1 class is considered	68.37	62.1

APPENDIX D

ACCURACY SCORES AND INDEXIES OF SVM

Following tables list accuracies of SVM algorithm with different combination of inputs. Moreover they give SVM Index 1 to 9 which are used obtain mental workload vs Input graphs in Result chapter (4.4 and 4.6).

Table 28: SVM Index 1

INDEX	SVM Parameters		Accuracies % (with Raw Data Type_Kernel Function)	
	C	gamma	Hbo/hbr_RBF	hbo/hbr_SIGMOID
1	0.5	0.5	60.5732	64.1989
2	0.6	0.5	60.0521	64.1989
3	0.7	0.5	59.6179	64.1989
4	0.8	0.5	59.0317	64.1989
5	0.9	0.5	58.6626	64.1989
6	1	0.5	58.4672	64.1989
7	2	0.5	57.1429	64.264
8	3	0.5	56.4047	64.264
9	4	0.5	56.3613	64.3291
10	5	0.5	56.6435	64.3508
11	0.5	0.6	60.812	64.1989
12	0.6	0.6	60.4646	64.1989
13	0.7	0.6	60.1172	64.1989
14	0.8	0.6	59.7264	64.1989
15	0.9	0.6	59.2488	64.1989
16	1	0.6	58.9231	64.1989
17	2	0.6	57.9027	64.1989
18	3	0.6	57.6422	64.1989
19	4	0.6	57.7725	64.2206
20	5	0.6	57.8593	64.2206
21	0.5	0.7	61.1159	64.1989
22	0.6	0.7	60.6383	64.1989
23	0.7	0.7	60.5297	64.1989
24	0.8	0.7	60.1824	64.1989
25	0.9	0.7	59.7482	64.1989
26	1	0.7	59.4659	64.1989
27	2	0.7	58.8146	64.1989
28	3	0.7	58.7712	64.1989
29	4	0.7	58.7929	64.1989

30	5	0.7	58.8146	64.1989
31	0.5	0.8	61.7021	64.1989
32	0.6	0.8	61.1159	64.1989
33	0.7	0.8	60.812	64.1989
34	0.8	0.8	60.6166	64.1989
35	0.9	0.8	60.3778	64.1989
36	1	0.8	60.0955	64.1989
37	2	0.8	59.4225	64.1989
38	3	0.8	59.3356	64.1989
39	4	0.8	59.2705	64.1989
40	5	0.8	59.1403	64.1989
41	0.5	0.9	62.2883	64.1989
42	0.6	0.9	61.7021	64.1989
43	0.7	0.9	61.2896	64.1989
44	0.8	0.9	61.1594	64.1989
45	0.9	0.9	60.9205	64.1989
46	1	0.9	60.7251	64.1989
47	2	0.9	59.835	64.1989
48	3	0.9	59.7699	64.1989
49	4	0.9	59.6179	64.1989
50	5	0.9	59.6613	64.1989
51	0.5	1	62.8311	64.1989
52	0.6	1	62.2883	64.1989
53	0.7	1	61.8324	64.1989
54	0.8	1	61.5719	64.1989
55	0.9	1	61.5284	64.1989
56	1	1	61.2896	64.1989
57	2	1	60.5515	64.1989
58	3	1	60.4646	64.1989
59	4	1	60.4212	64.1989
60	5	1	60.3126	64.1989
61	0.5	2	64.1989	64.1989
62	0.6	2	64.2206	64.1989
63	0.7	2	64.1989	64.1989
64	0.8	2	64.1554	64.1989
65	0.9	2	64.1554	64.1989
66	1	2	64.1337	64.1989
67	2	2	63.8949	64.1989
68	3	2	63.8732	64.1989
69	4	2	63.8515	64.1989
70	5	2	63.8298	64.1989
71	0.5	3	64.1989	64.1989
72	0.6	3	64.1989	64.1989
73	0.7	3	64.1989	64.1989
74	0.8	3	64.1989	64.1989

75	0.9	3	64.1989	64.1989
76	1	3	64.1989	64.1989
77	2	3	64.1989	64.1989
78	3	3	64.1989	64.1989
79	4	3	64.1989	64.1989
80	5	3	64.1989	64.1989
81	0.5	4	64.1989	64.1989
82	0.6	4	64.1989	64.1989
83	0.7	4	64.1989	64.1989
84	0.8	4	64.1989	64.1989
85	0.9	4	64.1989	64.1989
86	1	4	64.1989	64.1989
87	2	4	64.1989	64.1989
88	3	4	64.1989	64.1989
89	4	4	64.1989	64.1989
90	5	4	64.1989	64.1989
91	0.5	5	64.1989	64.1989
92	0.6	5	64.1989	64.1989
93	0.7	5	64.1989	64.1989
94	0.8	5	64.1989	64.1989
95	0.9	5	64.1989	64.1989
96	1	5	64.1989	64.1989
97	2	5	64.1989	64.1989
98	3	5	64.1989	64.1989
99	4	5	64.1989	64.1989
100	5	5	64.1989	64.1989

Table 29: SVM Index 2

Index	SVM Parameters	Accuracies % (with Raw Data Type_Kernel Function)	
	C	hbo/hbr_LINEAR	Normalized_hbo/hbr_LINEAR
1	0.0001	64.19887	64.19887
2	0.0005	64.19887	64.19887
3	0.001	64.19887	64.19887
4	0.005	64.19887	64.19887
5	0.01	64.19887	64.19887
6	0.05	64.19887	64.19887
7	0.1	64.19887	64.19887
8	0.5	64.19887	64.19887
9	1	64.19887	64.19887
10	5	64.19887	64.19887
11	10	64.19887	64.19887
12	50	64.19887	64.19887
13	100	64.19887	64.19887

Table 30: SVM Index 3

Index	SVM Parameters		Accuracies % (with Raw Data Type_Kernel Function)			
	C	gamma	hbo/r_POLY (degree2)	hbo/r_POLY (degree3)	hbo/r_POLY (degree4)	hbo/r_POLY (degree5)
1	0.0005	0.0005	64.19887	64.19887	64.19887	64.19887
2	0.001	0.0005	64.19887	64.19887	64.19887	64.19887
3	0.005	0.0005	64.19887	64.19887	64.19887	64.19887
4	0.01	0.0005	64.19887	64.19887	64.19887	64.19887
5	0.05	0.0005	64.19887	64.19887	64.19887	64.19887
6	0.1	0.0005	64.19887	64.19887	64.19887	64.19887
7	0.5	0.0005	64.19887	64.19887	64.19887	64.19887
8	1	0.0005	64.19887	64.19887	64.19887	64.19887
9	5	0.0005	64.19887	64.19887	64.19887	64.19887
10	10	0.0005	64.19887	64.19887	64.19887	64.19887
11	0.0005	0.001	64.19887	64.19887	64.19887	64.19887
12	0.001	0.001	64.19887	64.19887	64.19887	64.19887
13	0.005	0.001	64.19887	64.19887	64.19887	64.19887
14	0.01	0.001	64.19887	64.19887	64.19887	64.19887
15	0.05	0.001	64.19887	64.19887	64.19887	64.19887
16	0.1	0.001	64.19887	64.19887	64.19887	64.19887
17	0.5	0.001	64.19887	64.19887	64.19887	64.19887
18	1	0.001	64.19887	64.19887	64.19887	64.19887
19	5	0.001	64.19887	64.19887	64.19887	64.19887
20	10	0.001	64.19887	64.19887	64.19887	64.19887
21	0.0005	0.005	64.19887	64.19887	64.19887	64.19887
22	0.001	0.005	64.19887	64.19887	64.19887	64.19887
23	0.005	0.005	64.19887	64.19887	64.19887	64.15545
24	0.01	0.005	64.19887	64.19887	64.19887	64.11203
25	0.05	0.005	64.19887	64.19887	64.09032	64.0469
26	0.1	0.005	64.19887	64.19887	64.0469	64.0469
27	0.5	0.005	64.19887	64.0469	64.0469	63.8515
28	1	0.005	64.19887	64.0469	63.96005	63.56926
29	5	0.005	64.0469	63.74294	63.22188	63.00478
30	10	0.005	64.02519	63.13504	63.20017	63.26531
31	0.0005	0.01	64.19887	64.19887	64.19887	64.06861
32	0.001	0.01	64.19887	64.19887	64.19887	64.0469
33	0.005	0.01	64.19887	64.19887	64.06861	64.0469
34	0.01	0.01	64.19887	64.19887	64.0469	63.96005
35	0.05	0.01	64.19887	64.06861	64.0469	63.30873
36	0.1	0.01	64.19887	64.0469	63.6561	63.11333
37	0.5	0.01	64.13374	63.80808	63.17846	63.2436
38	1	0.01	64.0469	63.2436	63.39557	62.93964
39	5	0.01	63.80808	62.78767	61.74555	61.02909

40	10	0.01	63.17846	61.8541	60.4429	59.59618
41	0.0005	0.05	64.19887	64.0469	63.22188	62.57056
42	0.001	0.05	64.19887	64.0469	63.20017	61.637
43	0.005	0.05	64.19887	63.74294	62.48372	58.35866
44	0.01	0.05	64.19887	63.13504	61.61528	57.16457
45	0.05	0.05	64.0469	62.59227	57.53365	51.71515
46	0.1	0.05	64.02519	61.94095	55.14546	50.97699
47	0.5	0.05	62.78767	57.09944	51.06383	48.11116
48	1	0.05	62.09292	54.66783	49.47894	47.80721
49	5	0.05	59.09683	52.25792	48.87104	48.84933
50	10	0.05	57.29483	50.36908	48.76248	48.95788
51	0.0005	0.1	64.19887	63.80808	61.74555	55.38428
52	0.001	0.1	64.19887	63.2436	60.4429	53.62571
53	0.005	0.1	64.13374	62.78767	56.07903	50.23882
54	0.01	0.1	64.0469	61.8541	53.66913	48.80591
55	0.05	0.1	63.80808	57.59878	50.41251	48.06774
56	0.1	0.1	63.17846	55.31915	48.91446	48.69735
57	0.5	0.1	60.79027	52.69214	48.84933	48.50195
58	1	0.1	59.50934	50.84672	49.0013	47.65523
59	5	0.1	56.31785	48.17629	46.93878	45.87495
60	10	0.1	55.97047	48.02432	46.65654	44.20321
61	0.0005	0.5	64.0469	57.12115	48.84933	46.87364
62	0.001	0.5	64.02519	54.66783	48.7842	46.33087
63	0.005	0.5	62.76596	52.25792	47.65523	43.00912
64	0.01	0.5	62.09292	50.36908	46.63482	42.48806
65	0.05	0.5	59.09683	48.26314	44.91967	33.934
66	0.1	0.5	57.29483	47.69865	43.55189	42.74859
67	0.5	0.5	56.14416	46.61311	41.18541	43.22623
68	1	0.5	55.86192	45.74468	42.29266	44.83283
69	5	0.5	54.47243	44.55059	43.20452	44.83283
70	10	0.5	53.95137	43.5736	44.09466	44.83283
71	0.0005	1	63.80808	52.71385	46.96049	40.94659
72	0.001	1	63.17846	50.82501	46.56969	41.05515
73	0.005	1	60.79027	48.17629	43.83413	43.31307
74	0.01	1	59.50934	48.02432	43.20452	43.03083
75	0.05	1	56.31785	47.17759	41.61963	44.83283
76	0.1	1	55.97047	46.04863	43.13938	44.83283
77	0.5	1	54.90664	44.59401	43.29136	44.83283
78	1	1	53.604	43.74729	44.15979	44.83283
79	5	1	52.88754	44.96309	44.15979	44.83283
80	10	1	53.49544	44.22492	44.15979	44.83283
81	0.0005	5	59.09683	46.72167	42.98741	44.48545
82	0.001	5	57.31654	45.65784	44.05124	44.48545
83	0.005	5	56.12245	44.61572	44.24664	44.48545
84	0.01	5	55.86192	43.00912	44.24664	44.48545

85	0.05	5	54.77638	44.78941	44.24664	44.48545
86	0.1	5	54.2119	44.39861	44.24664	44.48545
87	0.5	5	51.95397	44.65914	44.24664	44.48545
88	1	5	52.51845	44.65914	44.24664	44.48545
89	5	5	47.93747	44.65914	44.24664	44.48545
90	10	5	48.13287	44.65914	44.24664	44.48545
91	0.0005	10	56.31785	44.3769	44.24664	44.48545
92	0.001	10	55.99218	43.769	44.24664	44.48545
93	0.005	10	54.90664	44.42032	44.24664	44.48545
94	0.01	10	53.58228	44.44203	44.24664	44.48545
95	0.05	10	53.47373	44.65914	44.24664	44.48545
96	0.1	10	53.27833	44.65914	44.24664	44.48545
97	0.5	10	53.25662	44.65914	44.24664	44.48545
98	1	10	51.47634	44.65914	44.24664	44.48545
99	5	10	44.59401	44.65914	44.24664	44.48545
100	10	10	51.91055	44.65914	44.24664	44.48545

Table 31: SVM Index 4

Index	SVM Parameters		Accuracies % (with Raw Data Type_Kernel Function)			
	C	gamma	hbt_POLY (degree2)	hbt_POLY (degree3)	hbt_POLY (degree4)	hbt_POLY (degree5)
1	0.0005	0.0005	64.19887	64.19887	64.19887	64.19887
2	0.001	0.0005	64.19887	64.19887	64.19887	64.19887
3	0.005	0.0005	64.19887	64.19887	64.19887	64.19887
4	0.01	0.0005	64.19887	64.19887	64.19887	64.19887
5	0.05	0.0005	64.19887	64.19887	64.19887	64.19887
6	0.1	0.0005	64.19887	64.19887	64.19887	64.19887
7	0.5	0.0005	64.19887	64.19887	64.19887	64.19887
8	1	0.0005	64.19887	64.19887	64.19887	64.19887
9	5	0.0005	64.19887	64.19887	64.19887	64.19887
10	10	0.0005	64.19887	64.19887	64.19887	64.19887
11	0.0005	0.001	64.19887	64.19887	64.19887	64.19887
12	0.001	0.001	64.19887	64.19887	64.19887	64.19887
13	0.005	0.001	64.19887	64.19887	64.19887	64.19887
14	0.01	0.001	64.19887	64.19887	64.19887	64.19887
15	0.05	0.001	64.19887	64.19887	64.19887	64.19887
16	0.1	0.001	64.19887	64.19887	64.19887	64.19887
17	0.5	0.001	64.19887	64.19887	64.19887	64.19887
18	1	0.001	64.19887	64.19887	64.19887	64.19887
19	5	0.001	64.19887	64.19887	64.19887	64.19887
20	10	0.001	64.19887	64.19887	64.19887	64.19887
21	0.0005	0.005	64.19887	64.19887	64.19887	64.19887
22	0.001	0.005	64.19887	64.19887	64.19887	64.19887

23	0.005	0.005	64.19887	64.19887	64.19887	64.19887
24	0.01	0.005	64.19887	64.19887	64.19887	64.19887
25	0.05	0.005	64.19887	64.19887	64.19887	64.09032
26	0.1	0.005	64.19887	64.19887	64.19887	63.98176
27	0.5	0.005	64.19887	64.19887	64.06861	63.87321
28	1	0.005	64.19887	64.17716	64.02519	63.74294
29	5	0.005	64.22058	64.0469	63.6561	63.37386
30	10	0.005	64.22058	63.8515	63.6561	62.78767
31	0.0005	0.01	64.19887	64.19887	64.19887	64.19887
32	0.001	0.01	64.19887	64.19887	64.19887	64.19887
33	0.005	0.01	64.19887	64.19887	64.19887	63.93834
34	0.01	0.01	64.19887	64.19887	64.19887	63.93834
35	0.05	0.01	64.19887	64.19887	64.02519	63.80808
36	0.1	0.01	64.19887	64.19887	63.93834	63.48241
37	0.5	0.01	64.19887	64.06861	63.63439	62.41858
38	1	0.01	64.19887	63.91663	63.02649	62.35345
39	5	0.01	64.19887	63.17846	62.50543	61.91924
40	10	0.01	64.17716	62.8528	62.07121	61.98437
41	0.0005	0.05	64.19887	64.19887	63.6561	62.39687
42	0.001	0.05	64.19887	64.17716	63.6561	62.13634
43	0.005	0.05	64.19887	64.0469	62.26661	61.8541
44	0.01	0.05	64.19887	63.8515	62.52714	61.0508
45	0.05	0.05	64.22058	62.96136	61.74555	60.00868
46	0.1	0.05	64.22058	62.74425	60.85541	58.79288
47	0.5	0.05	64.17716	61.87581	60.26921	56.92575
48	1	0.05	64.11203	61.35476	59.40078	56.12245
49	5	0.05	63.56926	60.6383	56.57838	55.75337
50	10	0.05	63.20017	60.13895	55.73165	55.34086
51	0.0005	0.1	64.19887	64.06861	62.50543	60.98567
52	0.001	0.1	64.19887	63.91663	62.07121	60.22579
53	0.005	0.1	64.19887	63.17846	61.20278	57.96787
54	0.01	0.1	64.19887	62.8528	61.15936	57.68563
55	0.05	0.1	64.19887	62.00608	59.76987	55.66652
56	0.1	0.1	64.17716	61.37647	58.79288	56.64351
57	0.5	0.1	63.91663	60.52974	56.0139	52.97438
58	1	0.1	63.63439	60.31264	55.88363	54.68954
59	5	0.1	62.91793	57.90274	55.10204	53.71255
60	10	0.1	62.22319	56.51324	53.43031	55.2106
61	0.0005	0.5	64.22058	61.87581	56.53495	47.56839
62	0.001	0.5	64.22058	61.35476	55.29744	54.36387
63	0.005	0.5	64.17716	60.6383	55.79679	54.38558
64	0.01	0.5	64.06861	60.22579	55.16717	42.98741
65	0.05	0.5	63.56926	57.18628	56.20929	51.49805
66	0.1	0.5	63.17846	56.55667	56.25271	53.90795
67	0.5	0.5	62.17977	55.23231	51.17238	52.30135

68	1	0.5	61.57186	38.51498	40.29527	51.75858
69	5	0.5	59.11854	57.12115	52.04082	43.11767
70	10	0.5	58.96657	53.90795	49.93487	40.77291
71	0.0005	1	64.19887	60.57317	56.07903	40.64264
72	0.001	1	64.17716	60.16066	54.58098	45.31047
73	0.005	1	63.91663	57.88103	42.07555	51.88884
74	0.01	1	63.63439	56.40469	53.36518	50.17369
75	0.05	1	62.91793	52.93096	53.99479	43.61702
76	0.1	1	62.54885	42.27095	43.31307	38.9492
77	0.5	1	60.29093	44.46374	45.72297	38.47156
78	1	1	59.835	54.53756	54.2119	45.83152
79	5	1	60.48632	53.88624	44.91967	45.83152
80	10	1	58.55406	39.62223	41.01172	45.83152
81	0.0005	5	63.56926	55.0152	40.99001	53.23491
82	0.001	5	63.17846	41.14199	42.66175	53.23491
83	0.005	5	62.17977	50.73817	56.20929	53.23491
84	0.01	5	61.59357	53.77768	48.08945	53.23491
85	0.05	5	59.98697	39.27486	42.90056	53.23491
86	0.1	5	59.55276	38.42814	42.90056	53.23491
87	0.5	5	57.96787	53.79939	42.90056	53.23491
88	1	5	40.72948	44.26835	42.90056	53.23491
89	5	5	38.03734	43.53018	42.90056	53.23491
90	10	5	34.21624	53.51715	42.90056	53.23491
91	0.0005	10	62.96136	38.68867	52.77898	53.23491
92	0.001	10	62.22319	42.27095	53.03951	53.23491
93	0.005	10	60.42119	53.10465	42.90056	53.23491
94	0.01	10	60.46461	41.70647	42.90056	53.23491
95	0.05	10	43.74729	40.59922	42.90056	53.23491
96	0.1	10	59.2271	45.50586	42.90056	53.23491
97	0.5	10	54.71125	52.71385	42.90056	53.23491
98	1	10	40.59922	53.51715	42.90056	53.23491
99	5	10	50.91185	53.51715	42.90056	53.23491
100	10	10	40.29527	53.51715	42.90056	53.23491

Table 32: SVM Index 5

INDEX	SVM Parameters		Accuracies % (with Raw Data Type_Kernel Function)			
	C	gamma	Normalized_hbo/r_POLY (degree2)	Normalized_hbo/r_POLY (degree3)	Normalized_hbo/r_POLY (degree4)	Normalized_hbo/r_POLY (degree5)
1	0.0005	0.0005	64.19887	64.19887	64.19887	64.19887
2	0.001	0.0005	64.19887	64.19887	64.19887	64.19887
3	0.005	0.0005	64.19887	64.19887	64.19887	64.19887
4	0.01	0.0005	64.19887	64.19887	64.19887	64.19887
5	0.05	0.0005	64.19887	64.19887	64.19887	64.19887
6	0.1	0.0005	64.19887	64.19887	64.19887	64.19887
7	0.5	0.0005	64.19887	64.19887	64.19887	64.19887
8	1	0.0005	64.19887	64.19887	64.19887	64.19887
9	5	0.0005	64.19887	64.19887	64.19887	64.19887
10	10	0.0005	64.19887	64.19887	64.19887	64.19887
11	0.0005	0.001	64.19887	64.19887	64.19887	64.19887
12	0.001	0.001	64.19887	64.19887	64.19887	64.19887
13	0.005	0.001	64.19887	64.19887	64.19887	64.19887
14	0.01	0.001	64.19887	64.19887	64.19887	64.19887
15	0.05	0.001	64.19887	64.19887	64.19887	64.19887
16	0.1	0.001	64.19887	64.19887	64.19887	64.19887
17	0.5	0.001	64.19887	64.19887	64.19887	64.19887
18	1	0.001	64.19887	64.19887	64.19887	64.19887
19	5	0.001	64.19887	64.19887	64.19887	64.19887
20	10	0.001	64.19887	64.19887	64.19887	64.19887
21	0.0005	0.005	64.19887	64.19887	64.19887	64.19887
22	0.001	0.005	64.19887	64.19887	64.19887	64.19887
23	0.005	0.005	64.19887	64.19887	64.19887	64.19887
24	0.01	0.005	64.19887	64.19887	64.19887	64.19887
25	0.05	0.005	64.19887	64.19887	64.19887	64.19887
26	0.1	0.005	64.19887	64.19887	64.19887	64.19887
27	0.5	0.005	64.19887	64.19887	64.06861	64.19887
28	1	0.005	64.19887	64.19887	64.02519	64.19887
29	5	0.005	64.19887	64.19887	63.6561	64.19887
30	10	0.005	64.19887	64.19887	63.6561	64.19887
31	0.0005	0.01	64.19887	64.19887	64.19887	64.19887
32	0.001	0.01	64.19887	64.19887	64.19887	64.19887
33	0.005	0.01	64.19887	64.19887	64.19887	64.19887
34	0.01	0.01	64.19887	64.19887	64.19887	64.19887
35	0.05	0.01	64.19887	64.19887	64.02519	64.19887
36	0.1	0.01	64.19887	64.19887	63.93834	64.19887
37	0.5	0.01	64.19887	64.19887	63.63439	64.19887
38	1	0.01	64.19887	64.19887	63.02649	64.19887

39	5	0.01	64.19887	64.19887	62.50543	64.19887
40	10	0.01	64.19887	64.19887	62.07121	64.19887
41	0.0005	0.05	64.19887	64.19887	63.6561	64.19887
42	0.001	0.05	64.19887	64.19887	63.6561	64.19887
43	0.005	0.05	64.19887	64.19887	62.26661	64.19887
44	0.01	0.05	64.19887	64.19887	62.52714	64.19887
45	0.05	0.05	64.19887	64.19887	61.74555	64.19887
46	0.1	0.05	64.19887	64.19887	60.85541	64.19887
47	0.5	0.05	64.19887	64.19887	60.26921	64.19887
48	1	0.05	64.19887	64.19887	59.40078	64.19887
49	5	0.05	64.19887	64.17716	56.57838	64.11203
50	10	0.05	64.19887	64.11203	55.73165	64.00347
51	0.0005	0.1	64.19887	64.19887	62.50543	64.19887
52	0.001	0.1	64.19887	64.19887	62.07121	64.19887
53	0.005	0.1	64.19887	64.19887	61.20278	64.19887
54	0.01	0.1	64.19887	64.19887	61.15936	64.19887
55	0.05	0.1	64.19887	64.19887	59.76987	64.19887
56	0.1	0.1	64.19887	64.19887	58.79288	64.15545
57	0.5	0.1	64.19887	64.19887	56.0139	63.93834
58	1	0.1	64.19887	64.11203	55.88363	63.89492
59	5	0.1	64.13374	63.89492	55.10204	63.74294
60	10	0.1	64.00347	63.80808	53.43031	63.67781
61	0.0005	0.5	64.19887	64.19887	56.53495	63.89492
62	0.001	0.5	64.19887	64.19887	55.29744	63.82979
63	0.005	0.5	64.19887	64.17716	55.79679	63.22188
64	0.01	0.5	64.19887	64.11203	55.16717	63.00478
65	0.05	0.5	64.19887	63.80808	56.20929	61.70213
66	0.1	0.5	64.19887	63.78637	56.25271	61.22449
67	0.5	0.5	63.93834	62.67911	51.17238	57.85931
68	1	0.5	63.87321	62.33174	40.29527	55.8185
69	5	0.5	62.83109	60.85541	52.04082	51.12896
70	10	0.5	62.37516	60.05211	49.93487	53.4086
71	0.0005	1	64.19887	64.19887	56.07903	62.63569
72	0.001	1	64.19887	64.11203	54.58098	62.11463
73	0.005	1	64.19887	63.89492	42.07555	60.46461
74	0.01	1	64.19887	63.80808	53.36518	58.44551
75	0.05	1	64.13374	62.8528	53.99479	55.14546
76	0.1	1	64.00347	62.48372	43.31307	50.97699
77	0.5	1	63.6561	61.59357	45.72297	55.10204
78	1	1	62.93964	60.29093	54.2119	56.51324
79	5	1	61.78897	57.57707	44.91967	54.75467
80	10	1	61.72384	57.40339	41.01172	55.05862
81	0.0005	5	64.19887	62.67911	40.99001	56.4264
82	0.001	5	64.19887	62.33174	42.66175	55.12375
83	0.005	5	63.93834	60.87712	56.20929	54.92835

84	0.01	5	63.87321	60.0304	48.08945	55.84021
85	0.05	5	62.83109	57.4251	42.90056	56.03561
86	0.1	5	62.37516	56.70864	42.90056	56.0139
87	0.5	5	61.637	55.64481	42.90056	56.0139
88	1	5	60.11724	56.18758	42.90056	56.0139
89	5	5	58.51064	55.16717	42.90056	56.0139
90	10	5	57.4251	55.08033	42.90056	56.0139
91	0.0005	10	64.13374	61.59357	52.77898	56.14416
92	0.001	10	64.00347	60.29093	53.03951	56.07903
93	0.005	10	63.6561	57.57707	42.90056	56.0139
94	0.01	10	62.93964	57.40339	42.90056	56.0139
95	0.05	10	61.78897	55.18888	42.90056	56.0139
96	0.1	10	61.72384	56.31785	42.90056	56.0139
97	0.5	10	57.90274	55.55797	42.90056	56.0139
98	1	10	58.33695	55.18888	42.90056	56.0139
99	5	10	56.4264	55.92705	42.90056	56.0139
100	10	10	56.75206	56.0139	42.90056	56.0139

Table 33: SVM Index 6

Index	SVM Parameters		Accuracies % (with Raw Data Type_Kernel Function)			
	C	gamma	oxy_POLY (degree2)	oxy_POLY (degree3)	oxy_POLY (degree4)	oxy_POLY (degree5)
1	0.0005	0.0005	64.19887	64.19887	64.19887	64.19887
2	0.001	0.0005	64.19887	64.19887	64.19887	64.19887
3	0.005	0.0005	64.19887	64.19887	64.19887	64.19887
4	0.01	0.0005	64.19887	64.19887	64.19887	64.19887
5	0.05	0.0005	64.19887	64.19887	64.19887	64.19887
6	0.1	0.0005	64.19887	64.19887	64.19887	64.19887
7	0.5	0.0005	64.19887	64.19887	64.19887	64.19887
8	1	0.0005	64.19887	64.19887	64.19887	64.19887
9	5	0.0005	64.19887	64.19887	64.19887	64.19887
10	10	0.0005	64.19887	64.19887	64.19887	64.19887
11	0.0005	0.001	64.19887	64.19887	64.19887	64.19887
12	0.001	0.001	64.19887	64.19887	64.19887	64.19887
13	0.005	0.001	64.19887	64.19887	64.19887	64.19887
14	0.01	0.001	64.19887	64.19887	64.19887	64.19887
15	0.05	0.001	64.19887	64.19887	64.19887	64.19887
16	0.1	0.001	64.19887	64.19887	64.19887	64.19887
17	0.5	0.001	64.19887	64.19887	64.19887	64.19887
18	1	0.001	64.19887	64.19887	64.19887	64.19887
19	5	0.001	64.19887	64.19887	64.19887	64.19887
20	10	0.001	64.19887	64.19887	64.19887	64.19887
21	0.0005	0.005	64.19887	64.19887	64.19887	64.19887

22	0.001	0.005	64.19887	64.19887	64.19887	64.19887
23	0.005	0.005	64.19887	64.19887	64.19887	64.19887
24	0.01	0.005	64.19887	64.19887	64.19887	64.19887
25	0.05	0.005	64.19887	64.19887	64.19887	64.19887
26	0.1	0.005	64.19887	64.19887	64.19887	64.19887
27	0.5	0.005	64.19887	64.19887	64.19887	64.19887
28	1	0.005	64.19887	64.19887	64.19887	64.19887
29	5	0.005	64.19887	64.19887	64.19887	64.19887
30	10	0.005	64.19887	64.19887	64.15545	64.15545
31	0.0005	0.01	64.19887	64.19887	64.19887	64.19887
32	0.001	0.01	64.19887	64.19887	64.19887	64.19887
33	0.005	0.01	64.19887	64.19887	64.19887	64.19887
34	0.01	0.01	64.19887	64.19887	64.19887	64.19887
35	0.05	0.01	64.19887	64.19887	64.19887	64.19887
36	0.1	0.01	64.19887	64.19887	64.19887	64.19887
37	0.5	0.01	64.19887	64.19887	64.19887	64.13374
38	1	0.01	64.19887	64.19887	64.13374	64.0469
39	5	0.01	64.19887	64.13374	64.02519	63.91663
40	10	0.01	64.19887	64.00347	63.91663	63.8515
41	0.0005	0.05	64.19887	64.19887	64.19887	64.02519
42	0.001	0.05	64.19887	64.19887	64.15545	63.96005
43	0.005	0.05	64.19887	64.19887	63.98176	63.80808
44	0.01	0.05	64.19887	64.19887	63.98176	63.4607
45	0.05	0.05	64.19887	64.06861	63.6561	62.8528
46	0.1	0.05	64.19887	63.96005	63.43899	62.4403
47	0.5	0.05	64.19887	63.76466	62.74425	60.79027
48	1	0.05	64.19887	63.56926	62.39687	60.33435
49	5	0.05	63.87321	62.80938	60.52974	59.50934
50	10	0.05	63.82979	62.15806	60.07382	58.94486
51	0.0005	0.1	64.19887	64.19887	64.02519	63.09162
52	0.001	0.1	64.19887	64.19887	63.91663	62.89622
53	0.005	0.1	64.19887	64.13374	63.48241	62.17977
54	0.01	0.1	64.19887	64.00347	63.26531	61.35476
55	0.05	0.1	64.19887	63.76466	62.46201	60.0304
56	0.1	0.1	64.19887	63.72123	61.89753	59.48763
57	0.5	0.1	64.02519	63.11333	60.37777	58.61919
58	1	0.1	63.89492	62.57056	60.0304	58.2284
59	5	0.1	63.74294	60.66001	58.51064	55.94876
60	10	0.1	63.48241	60.33435	57.77247	55.86192
61	0.0005	0.5	64.19887	63.76466	60.52974	57.66392
62	0.001	0.5	64.19887	63.56926	60.07382	57.51194
63	0.005	0.5	64.19887	62.80938	58.74946	55.29744
64	0.01	0.5	64.19887	62.15806	58.25011	53.2132
65	0.05	0.5	63.87321	60.46461	56.79548	53.32175
66	0.1	0.5	63.82979	60.29093	55.68823	52.51845

67	0.5	0.5	63.43899	58.40208	52.25792	50.69475
68	1	0.5	63.00478	57.12115	52.8007	53.47373
69	5	0.5	61.87581	55.44941	47.04733	50.32566
70	10	0.5	61.68042	55.0152	52.86583	52.64872
71	0.0005	1	64.19887	63.11333	58.48893	52.64872
72	0.001	1	64.19887	62.54885	57.8376	52.58359
73	0.005	1	64.0469	60.66001	56.36127	53.58228
74	0.01	1	63.89492	60.31264	54.8198	53.86453
75	0.05	1	63.74294	58.85801	53.03951	50.95528
76	0.1	1	63.48241	57.4251	53.16978	45.02822
77	0.5	1	62.6574	55.79679	52.58359	52.10595
78	1	1	62.13634	55.49284	52.93096	52.71385
79	5	1	61.2462	50.62961	51.71515	51.62831
80	10	1	58.92314	53.34347	52.82241	51.62831
81	0.0005	5	63.87321	58.35866	53.79939	52.2145
82	0.001	5	63.82979	57.16457	52.64872	51.21581
83	0.005	5	63.43899	55.66652	52.73556	53.47373
84	0.01	5	63.02649	55.34086	48.34998	53.47373
85	0.05	5	62.09292	50.45593	53.16978	53.47373
86	0.1	5	61.637	53.66913	47.43812	53.47373
87	0.5	5	60.2475	50.8033	46.63482	53.47373
88	1	5	60.29093	49.97829	46.63482	53.47373
89	5	5	56.8172	51.30265	46.63482	53.47373
90	10	5	57.79418	51.51976	46.63482	53.47373
91	0.0005	10	63.74294	55.66652	49.15328	53.47373
92	0.001	10	63.48241	55.36257	49.3921	53.47373
93	0.005	10	62.6574	52.73556	46.04863	53.47373
94	0.01	10	62.22319	52.36648	46.63482	53.47373
95	0.05	10	61.09423	52.73556	46.63482	53.47373
96	0.1	10	58.35866	45.61442	46.63482	53.47373
97	0.5	10	59.66131	51.9974	46.63482	53.47373
98	1	10	54.77638	48.21971	46.63482	53.47373
99	5	10	55.4277	45.39731	46.63482	53.47373
100	10	10	52.90925	45.39731	46.63482	53.47373

Table 34: SVM Index 7

Index	SVM Parameters		Accuracies % (with Raw Data Type_Kernel Function)					
	C	gamma	hbt_RBF	oxy_RBF	normalized_hbo/r_RBF	hbt_SIGMOID	oxy_SIGMOID	normalized_hbo/r_SIGMOID
1	0.0005	0.0005	64.1988	64.1988	64.1988	64.1988	64.1988	64.1988
2	0.001	0.0005	64.1988	64.1988	64.1988	64.1988	64.1988	64.1988
3	0.005	0.0005	64.1988	64.1988	64.1988	64.1988	64.1988	64.1988
4	0.01	0.0005	64.1988	64.1988	64.1988	64.1988	64.1988	64.1988
5	0.05	0.0005	64.1988	64.1988	64.1988	64.1988	64.1988	64.1988
6	0.1	0.0005	64.1988	64.1988	64.1988	64.1988	64.1988	64.1988
7	0.5	0.0005	64.1988	64.1988	64.1988	64.1988	64.1988	64.1988
8	1	0.0005	64.1988	64.1988	64.1988	64.1988	64.1337	64.1988
9	5	0.0005	64.1988	64.1988	64.1988	63.6561	64.0686	64.1988
10	10	0.0005	64.1988	64.1988	64.1988	61.2244	64.1337	64.1988
11	0.0005	0.001	64.1988	64.1988	64.1988	64.1988	64.1988	64.1988
12	0.001	0.001	64.1988	64.1988	64.1988	64.1988	64.1988	64.1988
13	0.005	0.001	64.1988	64.1988	64.1988	64.1988	64.1988	64.1988
14	0.01	0.001	64.1988	64.1988	64.1988	64.1988	64.1988	64.1988
15	0.05	0.001	64.1988	64.1988	64.1988	64.1988	64.1988	64.1988
16	0.1	0.001	64.1988	64.1988	64.1988	64.1988	64.1988	64.1988
17	0.5	0.001	64.1988	64.1988	64.1988	63.6995	64.0686	64.1988
18	1	0.001	64.1988	64.1988	64.1988	63.6995	64.0903	64.1988
19	5	0.001	64.1988	64.1988	64.1988	56.6435	63.8514	64.1988
20	10	0.001	64.1988	64.1988	64.1988	55.6665	63.894	64.1988
21	0.0005	0.005	64.1988	64.1988	64.1988	64.1988	64.1988	64.1988
22	0.001	0.005	64.1988	64.1988	64.1988	64.1988	64.1988	64.1988
23	0.005	0.005	64.1988	64.1988	64.1988	64.1988	64.1988	64.1988
24	0.01	0.005	64.1988	64.1988	64.1988	64.1988	64.1988	64.1988
25	0.05	0.005	64.1988	64.1988	64.1988	64.1988	63.9166	64.1988
26	0.1	0.005	64.1988	64.1988	64.1988	64.0686	63.8297	64.1988
27	0.5	0.005	64.1988	64.1988	64.1988	61.8975	61.4850	64.1988
28	1	0.005	64.1988	64.1988	64.1988	59.3356	61.9626	64.1988
29	5	0.005	64.1771	64.1988	64.1988	57.7507	59.7047	64.1988
30	10	0.005	63.8732	64.1988	64.1988	57.3816	60.6165	64.1988
31	0.0005	0.01	64.1988	64.1988	64.1988	64.1988	64.1988	64.1988
32	0.001	0.01	64.1988	64.1988	64.1988	64.1988	64.1988	64.1988
33	0.005	0.01	64.1988	64.1988	64.1988	64.1988	64.1988	64.1988
34	0.01	0.01	64.1988	64.1988	64.1988	64.1988	64.1988	64.1988
35	0.05	0.01	64.1988	64.1988	64.1988	64.1988	64.1988	64.1988

36	0.1	0.01	64.1988	64.1988	64.1988	63.8949	63.7646	64.1988
37	0.5	0.01	64.1988	64.1988	64.1988	55.1888	61.9192	64.1988
38	1	0.01	64.1988	64.1988	64.1988	55.0369	61.7455	64.1988
39	5	0.01	63.2001	64.1988	64.1988	58.6626	59.8349	64.1988
40	10	0.01	61.8975	64.1988	64.1988	57.9895	55.6882	64.1988
41	0.0005	0.05	64.1988	64.1988	64.1988	64.1988	64.1988	64.1988
42	0.001	0.05	64.1988	64.1988	64.1988	64.1988	64.1988	64.1988
43	0.005	0.05	64.1988	64.1988	64.1988	64.3725	64.1988	64.1988
44	0.01	0.05	64.1988	64.1988	64.1988	62.0712	64.1988	64.1988
45	0.05	0.05	64.1988	64.1988	64.1988	53.3651	64.1988	64.1988
46	0.1	0.05	64.1988	64.1988	64.1988	52.3013	60.0738	64.1988
47	0.5	0.05	63.0481	64.1988	64.1988	52.6704	54.6026	64.0686
48	1	0.05	59.5744	64.1771	64.1988	52.8658	54.4290	63.9383
49	5	0.05	53.5171	63.4172	64.1988	53.1697	54.5809	63.7646
50	10	0.05	51.9756	62.8962	64.1988	53.1480	54.5592	57.7073
51	0.0005	0.1	64.1988	64.1988	64.1988	64.1988	64.1988	64.1988
52	0.001	0.1	64.1988	64.1988	64.1988	64.1988	64.1988	64.1988
53	0.005	0.1	64.1988	64.1988	64.1988	64.1988	64.1988	64.1988
54	0.01	0.1	64.1988	64.1988	64.1988	64.4376	64.6330	64.1988
55	0.05	0.1	64.1988	64.1988	64.1988	57.6204	57.8593	64.1120
56	0.1	0.1	64.1988	64.1988	64.1988	54.0382	56.7086	64.0686
57	0.5	0.1	59.9435	64.2422	64.1988	52.4316	56.2092	63.8514
58	1	0.1	56.2744	63.8949	64.1988	52.8875	55.9921	63.5909
59	5	0.1	54.2336	62.7008	64.1988	53.1480	55.7533	53.5171
60	10	0.1	53.0178	61.4633	63.9166	53.2132	55.7533	55.6231
61	0.0005	0.5	64.1988	64.1988	64.1988	64.1988	64.1988	64.1988
62	0.001	0.5	64.1988	64.1988	64.1988	64.1988	64.1988	64.1988
63	0.005	0.5	64.1988	64.1988	64.1988	64.1988	64.1988	64.1988
64	0.01	0.5	64.1988	64.1988	64.1988	64.1988	64.1988	64.1988
65	0.05	0.5	64.1988	64.1988	64.1988	64.1988	64.1988	64.1554
66	0.1	0.5	63.9383	64.1988	64.1988	64.1988	64.1988	64.0034
67	0.5	0.5	60.2475	63.6778	64.1988	64.1988	64.5245	56.5132
68	1	0.5	59.6178	62.7008	64.1988	64.1988	63.916	50.4125
69	5	0.5	58.033	58.5540	62.7442	64.3074	60.7034	53.1914
70	10	0.5	57.2297	57.2297	61.7672	64.3942	58.9014	55.4494
71	0.0005	1	64.1988	64.1988	64.1988	64.1988	64.1988	64.1988
72	0.001	1	64.1988	64.1988	64.1988	64.1988	64.1988	64.1988
73	0.005	1	64.1988	64.1988	64.1988	64.1988	64.1988	64.1988
74	0.01	1	64.1988	64.1988	64.1988	64.1988	64.1988	64.1988
75	0.05	1	64.1988	64.1988	64.1988	64.1988	64.1988	64.1988
76	0.1	1	64.1988	64.1988	64.1988	64.1988	64.1988	64.1988
77	0.5	1	62.0495	63.5692	64.1554	64.1988	64.1988	64.1771
78	1	1	60.5297	62.1146	64.2422	64.1988	64.1988	64.0468
79	5	1	60.0955	58.6626	61.4198	64.1988	64.1988	63.9817
80	10	1	59.7915	57.9244	56.5132	64.1988	64.2422	62.1363

81	0.0005	5	64.1988	64.1988	64.1988	64.1988	64.1988	64.1988
82	0.001	5	64.1988	64.1988	64.1988	64.1988	64.1988	64.1988
83	0.005	5	64.1988	64.1988	64.1988	64.1988	64.1988	64.1988
84	0.01	5	64.1988	64.1988	64.1988	64.1988	64.1988	64.1988
85	0.05	5	64.1988	64.1988	64.1988	64.1988	64.1988	64.1988
86	0.1	5	64.1988	64.1988	64.1988	64.1988	64.1988	64.1988
87	0.5	5	64.1988	64.1771	64.1554	64.1988	64.1988	64.1988
88	1	5	64.1771	63.9817	62.6791	64.1988	64.1988	64.1988
89	5	5	64.2205	63.5692	57.9461	64.1988	64.1988	64.1988
90	10	5	64.2422	63.5475	59.1836	64.1988	64.1988	64.1988
91	0.0005	10	64.1988	64.1988	64.1988	64.1988	64.1988	64.1988
92	0.001	10	64.1988	64.1988	64.1988	64.1988	64.1988	64.1988
93	0.005	10	64.1988	64.1988	64.1988	64.1988	64.1988	64.1988
94	0.01	10	64.1988	64.1988	64.1988	64.1988	64.1988	64.1988
95	0.05	10	64.1988	64.1988	64.1988	64.1988	64.1988	64.1988
96	0.1	10	64.1988	64.1988	64.1988	64.1988	64.1988	64.1988
97	0.5	10	64.1988	64.2205	64.1554	64.1988	64.1988	64.1988
98	1	10	64.1988	64.1771	64.0034	64.1988	64.1988	64.1988
99	5	10	64.1988	64.1771	63.5041	64.1988	64.1988	64.1988
100	10	10	64.1988	64.1771	63.3304	64.1988	64.1988	64.1988

10

Table 35: SVM Index 8

Index	SVM Parameters		Accuracies % (with Raw Data Type_Kernel Function)	
	C	hbo/r_LINEAR	hbt_LINEAR	oxy_LINEAR
1	0.0001	66.30482	66.30482	66.30482
2	0.0005	66.30482	66.30482	66.30482
3	0.001	66.30482	66.30482	66.30482
4	0.005	66.30482	66.30482	66.30482
5	0.01	66.30482	66.30482	66.30482
6	0.05	66.30482	66.30482	66.30482
7	0.1	66.30482	66.30482	66.30482
8	0.5	66.30482	66.30482	66.30482
9	1	66.30482	66.30482	66.30482
10	5	66.30482	66.30482	66.30482
11	10	66.30482	66.30482	66.30482
12	50	66.30482	66.30482	66.30482
13	100	66.30482	66.30482	66.131133

Table 36: SVM Index 9

Index	SVM Parameters		Accuracies % (with Raw Data Type_Kernel Function)					
	C	gamma	hbo/r_ RBF	hbt_RB F	oxy_RB F	hbo/r_ SIGMO ID	hbt_ SIGMOI D	oxy_ SIGMO ID
1	0.0005	0.0005	66.3048	66.3048	66.3048	66.3048	66.3048	66.3048
2	0.001	0.0005	66.3048	66.3048	66.3048	66.3048	66.3048	66.3048
3	0.005	0.0005	66.3048	66.3048	66.3048	66.3048	66.3048	66.3048
4	0.01	0.0005	66.3048	66.3048	66.3048	66.3048	66.3048	66.3048
5	0.05	0.0005	66.3048	66.3048	66.3048	66.3048	66.3048	66.3048
6	0.1	0.0005	66.3048	66.3048	66.3048	66.3048	66.3048	66.3048
7	0.5	0.0005	66.3048	66.3048	66.3048	66.3048	66.1528	66.3048
8	1	0.0005	66.3048	66.3048	66.3048	66.1528	66.1745	66.2396
9	5	0.0005	66.3048	66.3048	66.3048	65.9574	63.8732	66.1094
10	10	0.0005	66.3699	66.3699	66.3048	65.3278	64.0686	66.0442
11	0.0005	0.001	66.3048	66.3048	66.3048	66.3048	66.3048	66.3048
12	0.001	0.001	66.3048	66.3048	66.3048	66.3048	66.3048	66.3048
13	0.005	0.001	66.3048	66.3048	66.3048	66.3048	66.3048	66.3048
14	0.01	0.001	66.3048	66.3048	66.3048	66.3048	66.3048	66.3048
15	0.05	0.001	66.3048	66.3048	66.3048	66.3048	66.1745	66.3048
16	0.1	0.001	66.3048	66.3048	66.3048	66.3048	66.2179	66.3048
17	0.5	0.001	66.3048	66.3048	66.3048	66.0442	64.3725	66.0660
18	1	0.001	66.3048	66.3048	66.3048	65.6969	63.9166	66.0877
19	5	0.001	66.4133	66.3916	66.3048	63.7646	59.6396	65.6969
20	10	0.001	66.3916	66.3916	66.3048	62.0495	58.7928	65.3712
21	0.0005	0.005	66.3048	66.3048	66.3048	66.3048	66.3048	66.3048
22	0.001	0.005	66.3048	66.3048	66.3048	66.3048	66.3048	66.3048
23	0.005	0.005	66.3048	66.3048	66.3048	66.3048	66.3048	66.3048
24	0.01	0.005	66.3048	66.3048	66.3048	66.3048	66.3048	66.3048
25	0.05	0.005	66.3048	66.3048	66.3048	66.1528	66.0877	66.0225
26	0.1	0.005	66.3048	66.3048	66.3048	65.9574	65.0890	65.7620
27	0.5	0.005	66.4133	66.4133	66.3048	64.7633	59.5961	63.6126
28	1	0.005	66.3699	66.3699	66.3916	62.6791	56.7954	65.3929
29	5	0.005	66.6087	66.5002	66.5002	57.2297	58.4020	60.3343
30	10	0.005	66.9995	66.5436	66.5219	57.8376	58.7928	55.2540
31	0.0005	0.01	66.3048	66.3048	66.3048	66.3048	66.3048	66.3048
32	0.001	0.01	66.3048	66.3048	66.3048	66.3048	66.3048	66.3048
33	0.005	0.01	66.3048	66.3048	66.3048	66.3048	66.3048	66.3048
34	0.01	0.01	66.3048	66.3048	66.3048	66.3048	66.3048	66.3048
35	0.05	0.01	66.3048	66.3048	66.3048	66.3048	66.3048	66.3048
36	0.1	0.01	66.3048	66.3048	66.3048	66.3048	66.2831	66.3048
37	0.5	0.01	66.3699	66.4568	66.3916	61.5284	58.4672	66.3048
38	1	0.01	66.5002	66.4568	66.5002	59.7915	57.2079	64.6765
39	5	0.01	67.6943	66.6304	66.6521	60.5080	60.3994	57.3382

40	10	0.01	68.6930	66.9127	66.7390	61.5935	61.0073	57.5336
41	0.0005	0.05	66.3048	66.3048	66.3048	66.3048	66.3048	66.3048
42	0.001	0.05	66.3048	66.3048	66.3048	66.3048	66.3048	66.3048
43	0.005	0.05	66.3048	66.3048	66.3048	66.3048	66.2613	66.3048
44	0.01	0.05	66.3048	66.3048	66.3048	63.5909	63.4172	66.3048
45	0.05	0.05	66.3048	66.3048	66.3048	55.5579	56.4698	56.6869
46	0.1	0.05	66.3048	66.3048	66.3048	55.0586	55.6448	55.1888
47	0.5	0.05	68.1285	67.0429	66.6739	55.0151	54.1250	53.8645
48	1	0.05	70.9292	68.4759	67.0429	54.5375	54.0816	53.6474
49	5	0.05	77.0950	73.0568	68.4324	54.3638	53.9947	53.4954
50	10	0.05	79.4832	74.1858	69.4094	54.3204	53.9513	53.4737
51	0.0005	0.1	66.3048	66.3048	66.3048	66.3048	66.3048	66.3048
52	0.001	0.1	66.3048	66.3048	66.3048	66.3048	66.3048	66.3048
53	0.005	0.1	66.3048	66.3048	66.3048	66.3048	66.3048	66.3048
54	0.01	0.1	66.3048	66.3048	66.3048	65.9357	66.3048	63.7212
55	0.05	0.1	66.3048	66.3048	66.3048	58.4455	60.8988	55.1020
56	0.1	0.1	66.3048	66.3048	66.3048	56.0138	58.4889	54.1033
57	0.5	0.1	71.0160	68.4324	67.0864	54.2118	55.2540	53.4085
58	1	0.1	75.3148	71.8193	67.9765	53.9730	54.8415	53.3217
59	5	0.1	82.1102	77.1168	70.5818	53.9513	54.6244	53.1697
60	10	0.1	83.8037	78.2023	71.7325	53.8862	54.5592	53.1046
61	0.0005	0.5	66.3048	66.3048	66.3048	66.3048	66.3048	66.3048
62	0.001	0.5	66.3048	66.3048	66.3048	66.3048	66.3048	66.3048
63	0.005	0.5	66.3048	66.3048	66.3048	66.3048	66.3048	66.3048
64	0.01	0.5	66.3048	66.3048	66.3048	66.3048	66.3048	66.3048
65	0.05	0.5	66.3048	66.3048	66.3048	66.3048	66.3048	66.3048
66	0.1	0.5	66.3048	66.3048	66.3048	66.3048	66.3048	66.3048
67	0.5	0.5	71.2548	70.1693	68.6495	66.3048	66.3048	65.9357
68	1	0.5	81.1984	76.7694	71.8410	66.3048	66.3048	65.0021
69	5	0.5	85.4971	80.7208	77.0516	66.3916	66.3265	61.6152
70	10	0.5	85.4103	80.9813	77.3339	66.2613	66.2831	59.1185
71	0.0005	1	66.3048	66.3048	66.3048	66.3048	66.3048	66.3048
72	0.001	1	66.3048	66.3048	66.3048	66.3048	66.3048	66.3048
73	0.005	1	66.3048	66.3048	66.3048	66.3048	66.3048	66.3048
74	0.01	1	66.3048	66.3048	66.3048	66.3048	66.3048	66.3048
75	0.05	1	66.3048	66.3048	66.3048	66.3048	66.3048	66.3048
76	0.1	1	66.3048	66.3048	66.3048	66.3048	66.3048	66.3048
77	0.5	1	68.9752	68.4107	67.5206	66.3048	66.3048	66.3048
78	1	1	77.0733	74.7069	73.5345	66.3048	66.3048	66.3048
79	5	1	80.9161	78.6148	78.3977	66.3048	66.3048	66.3048
80	10	1	80.9379	78.5280	78.6582	66.3048	66.3048	66.3048
81	0.0005	5	66.3048	66.3048	66.3048	66.3048	66.3048	66.3048
82	0.001	5	66.3048	66.3048	66.3048	66.3048	66.3048	66.3048
83	0.005	5	66.3048	66.3048	66.3048	66.3048	66.3048	66.3048
84	0.01	5	66.3048	66.3048	66.3048	66.3048	66.3048	66.3048

85	0.05	5	66.3048	66.3048	66.3048	66.3048	66.3048	66.3048
86	0.1	5	66.3048	66.3048	66.3048	66.3048	66.3048	66.3048
87	0.5	5	66.3265	66.4350	66.3916	66.3048	66.3048	66.3048
88	1	5	67.7594	68.6930	69.1489	66.3048	66.3048	66.3048
89	5	5	69.2357	70.5167	72.3838	66.3048	66.3048	66.3048
90	10	5	69.2357	70.5384	72.3838	66.3048	66.3048	66.3048
91	0.0005	10	66.3048	66.3048	66.3048	66.3048	66.3048	66.3048
92	0.001	10	66.3048	66.3048	66.3048	66.3048	66.3048	66.3048
93	0.005	10	66.3048	66.3048	66.3048	66.3048	66.3048	66.3048
94	0.01	10	66.3048	66.3048	66.3048	66.3048	66.3048	66.3048
95	0.05	10	66.3048	66.3048	66.3048	66.3048	66.3048	66.3048
96	0.1	10	66.3048	66.3048	66.3048	66.3048	66.3048	66.3048
97	0.5	10	66.3048	66.3265	66.3265	66.3048	66.3048	66.3048
98	1	10	66.5219	67.0429	67.0864	66.3048	66.3048	66.3048
99	5	10	67.4337	68.3239	69.1055	66.3048	66.3048	66.3048
100	10	10	67.4337	68.3239	69.1055	66.3048	66.3048	66.3048

Table 37 Accuracies of Cross Validation vs Test for SVM – kfold:3

Index	**SVM Parameters**		**Accuracies % (with** hbo/r_RBF**)**	
	C	gamma	Cross Validation	Test
1	0.0005	0.0005	67.93234	66.30482
2	0.001	0.0005	67.93234	66.30482
3	0.005	0.0005	67.93234	66.30482
4	0.01	0.0005	67.93234	66.30482
5	0.05	0.0005	67.93234	66.30482
6	0.1	0.0005	67.93234	66.30482
7	0.5	0.0005	67.93234	66.30482
8	1	0.0005	67.93234	66.30482
9	5	0.0005	67.93234	66.30482
10	10	0.0005	67.9496	66.369952
11	0.0005	0.001	67.93234	66.30482
12	0.001	0.001	67.93234	66.30482
13	0.005	0.001	67.93234	66.30482
14	0.01	0.001	67.93234	66.30482
15	0.05	0.001	67.93234	66.30482
16	0.1	0.001	67.93234	66.30482
17	0.5	0.001	67.93234	66.30482
18	1	0.001	67.93234	66.30482
19	5	0.001	68.01864	66.413374
20	10	0.001	68.13946	66.391663
21	0.0005	0.005	67.93234	66.30482
22	0.001	0.005	67.93234	66.30482
23	0.005	0.005	67.93234	66.30482

24	0.01	0.005	67.93234	66.30482
25	0.05	0.005	67.93234	66.30482
26	0.1	0.005	67.93234	66.30482
27	0.5	0.005	68.07042	66.413374
28	1	0.005	68.13946	66.369952
29	5	0.005	68.4156	66.608771
30	10	0.005	68.72627	66.999566
31	0.0005	0.01	67.93234	66.30482
32	0.001	0.01	67.93234	66.30482
33	0.005	0.01	67.93234	66.30482
34	0.01	0.01	67.93234	66.30482
35	0.05	0.01	67.93234	66.30482
36	0.1	0.01	67.93234	66.30482
37	0.5	0.01	68.07042	66.369952
38	1	0.01	68.20849	66.500217
39	5	0.01	69.20953	67.694312
40	10	0.01	70.07249	68.693009
41	0.0005	0.05	67.93234	66.30482
42	0.001	0.05	67.93234	66.30482
43	0.005	0.05	67.93234	66.30482
44	0.01	0.05	67.93234	66.30482
45	0.05	0.05	67.93234	66.30482
46	0.1	0.05	67.93234	66.30482
47	0.5	0.05	68.84708	68.128528
48	1	0.05	70.55575	70.929223
49	5	0.05	75.76804	77.095093
50	10	0.05	77.16603	79.483283
51	0.0005	0.1	67.93234	66.30482
52	0.001	0.1	67.93234	66.30482
53	0.005	0.1	67.93234	66.30482
54	0.01	0.1	67.93234	66.30482
55	0.05	0.1	67.93234	66.30482
56	0.1	0.1	67.93234	66.30482
57	0.5	0.1	70.12427	71.016066
58	1	0.1	73.97308	75.314807
59	5	0.1	78.99551	82.110291
60	10	0.1	81.04936	83.803734
61	0.0005	0.5	67.93234	66.30482
62	0.001	0.5	67.93234	66.30482
63	0.005	0.5	67.93234	66.30482
64	0.01	0.5	67.93234	66.30482
65	0.05	0.5	67.93234	66.30482
66	0.1	0.5	67.93234	66.30482
67	0.5	0.5	70.1933	71.254885
68	1	0.5	77.11426	81.198437

69	5	0.5	80.98032	85.497178
70	10	0.5	80.94581	85.410334
71	0.0005	1	67.93234	66.30482
72	0.001	1	67.93234	66.30482
73	0.005	1	67.93234	66.30482
74	0.01	1	67.93234	66.30482
75	0.05	1	67.93234	66.30482
76	0.1	1	67.93234	66.30482
77	0.5	1	69.07145	68.97525
78	1	1	74.33552	77.073383
79	5	1	77.28685	80.916196
80	10	1	77.89092	80.937907
81	0.0005	5	67.93234	66.30482
82	0.001	5	67.93234	66.30482
83	0.005	5	67.93234	66.30482
84	0.01	5	67.93234	66.30482
85	0.05	5	67.93234	66.30482
86	0.1	5	67.93234	66.30482
87	0.5	5	67.9496	66.326531
88	1	5	68.57094	67.759444
89	5	5	69.26131	69.235779
90	10	5	69.4339	69.235779
91	0.0005	10	67.93234	66.30482
92	0.001	10	67.93234	66.30482
93	0.005	10	67.93234	66.30482
94	0.01	10	67.93234	66.30482
95	0.05	10	67.93234	66.30482
96	0.1	10	67.93234	66.30482
97	0.5	10	67.93234	66.30482
98	1	10	67.98412	66.521928
99	5	10	68.46738	67.433782
100	10	10	68.5019	67.433782

APPENDIX E

ACCURACY SCORES OF ANN

Following table lists accuracies of ANN algorithm with different combination of inputs.

Table 38: ANN Success Rates with Input Combinations

Class Types	Train (%)	Validation (%)	Test (%)	# of Hidden Nodes	Raw Data Types	Accuracy (%)
0,1,2	70	15	15	25	hbo, hbr	68.7
0,1,2	60	20	20	25	hbo, hbr	69.2
0,1,2	70	15	15	30	hbo, hbr	69.6
0,1,2	60	20	20	30	hbo, hbr	68.5
0,1,2	70	15	15	35	hbo, hbr	68.6
0,1,2	60	20	20	35	hbo, hbr	68.8
0,1,2	70	15	15	40	hbo, hbr	69.5
0,1,2	60	20	20	40	hbo, hbr	69.1
0,1,2	70	15	15	45	hbo, hbr	68.4
0,1,2	60	20	20	45	hbo, hbr	68.3
0,1,2	70	15	15	50	hbo, hbr	68.7
0,1,2	60	20	20	50	hbo, hbr	69.2
0,1,2	70	15	15	55	hbo, hbr	70.4
0,1,2	60	20	20	55	hbo, hbr	69.2
0,1,2	70	15	15	60	hbo, hbr	68.6
0,1,2	60	20	20	60	hbo, hbr	69
0,1,2	70	15	15	65	hbo, hbr	68.4

0,1,2	60	20	20	65	hbo, hbr	67.8
0,1,2	70	15	15	70	hbo, hbr	69.4
0,1,2	60	20	20	70	hbo, hbr	69.3
0,1,2	70	15	15	75	hbo, hbr	68.3
0,1,2	60	20	20	75	hbo, hbr	69.8
-1,0,1,2	70	15	15	25	hbo, hbr	67.4
-1,0,1,2	60	20	20	25	hbo, hbr	67.1
-1,0,1,2	70	15	15	30	hbo, hbr	67.7
-1,0,1,2	60	20	20	30	hbo, hbr	68.1
-1,0,1,2	70	15	15	35	hbo, hbr	67.5
-1,0,1,2	60	20	20	35	hbo, hbr	68.8
-1,0,1,2	70	15	15	40	hbo, hbr	67.7
-1,0,1,2	60	20	20	40	hbo, hbr	67.7
-1,0,1,2	70	15	15	45	hbo, hbr	67.4
-1,0,1,2	60	20	20	45	hbo, hbr	67.8
-1,0,1,2	70	15	15	50	hbo, hbr	67.5
-1,0,1,2	60	20	20	50	hbo, hbr	68.1
-1,0,1,2	70	15	15	55	hbo, hbr	67.7
-1,0,1,2	60	20	20	55	hbo, hbr	68.2
-1,0,1,2	70	15	15	60	hbo, hbr	68
-1,0,1,2	60	20	20	60	hbo, hbr	68.1
-1,0,1,2	70	15	15	65	hbo, hbr	67.5
-1,0,1,2	60	20	20	65	hbo, hbr	67.5
-1,0,1,2	70	15	15	70	hbo, hbr	67.7
-1,0,1,2	60	20	20	70	hbo, hbr	66.9

-1,0,1,2	70	15	15	75	hbo, hbr	68
-1,0,1,2	60	20	20	75	hbo, hbr	68.3
0,1,2	70	15	15	12	oxy	68.6
0,1,2	70	15	15	18	oxy	68.6
0,1,2	70	15	15	24	oxy	68.5
0,1,2	70	15	15	30	oxy	68.6
0,1,2	70	15	15	36	oxy	68.5
-1,0,1,2	70	15	15	18	oxy	67.4
-1,0,1,2	70	15	15	24	oxy	67.3
-1,0,1,2	70	15	15	30	oxy	67.2
-1,0,1,2	70	15	15	36	oxy	67.2
0,1,2	70	15	15	12	hbt	68.5
0,1,2	70	15	15	18	hbt	68.5
0,1,2	70	15	15	24	hbt	68.6
0,1,2	70	15	15	30	hbt	68.5
0,1,2	70	15	15	36	hbt	68.5
-1,0,1,2	70	15	15	12	hbt	67.4
-1,0,1,2	70	15	15	18	hbt	67.7
-1,0,1,2	70	15	15	24	hbt	67.4
-1,0,1,2	70	15	15	30	hbt	67.3
-1,0,1,2	70	15	15	36	hbt	67.3
-1,0,1,2	70	5	25	60	hbo, hbr	68
-1,0,1,2	60	5	35	60	hbo, hbr	67.9
-1,0,1,2	70	5	25	35	hbo, hbr	67.5
-1,0,1,2	60	5	35	35	hbo, hbr	67.3

APPENDIX F

ACCURACY SCORES OF RNN

Following table lists accuracies of RNN algorithm with different combination of inputs.

Table 39: RNN Success Rates with Input Combinations – Loss ons: Categorical Crossentropy, Activation: Softmax

# of Hidden Nodes	Epoches	Batch Size	Accuracy (%)
24	724	8	71
30	724	8	71
36	724	8	73
42	724	8	74
48	724	8	74
54	724	8	73
60	724	8	75
66	724	8	76
72	724	8	76
78	724	8	75
84	724	8	76
90	724	8	75
96	724	8	76
102	724	8	78
108	724	8	77
114	724	8	77
120	724	8	78
126	724	8	78

132	724	8	77
138	724	8	81
144	724	8	78
150	724	8	79
156	724	8	79
162	724	8	80
168	724	8	79
174	724	8	73
180	724	8	80
186	724	8	81
250	724	8	80
350	724	8	80
500	724	8	81
42	362	16	73
48	362	16	73
54	362	16	74
60	362	16	76
66	362	16	75
72	362	16	76
78	362	16	76
84	362	16	76
90	362	16	76
96	362	16	78
102	362	16	77
108	362	16	77

116	362	16	77
124	362	16	79
130	362	16	78
136	362	16	77
142	362	16	78
148	362	16	79
154	362	16	80
160	362	16	79
166	362	16	79
172	362	16	79
178	362	16	79
184	362	16	80
250	362	16	80
350	362	16	82
500	362	16	82
1000	362	16	84
42	181	32	73
48	181	32	73
54	181	32	73
60	181	32	75
66	181	32	74
72	181	32	75
78	181	32	74
84	181	32	76
90	181	32	76

96	181	32	75
102	181	32	77
108	181	32	76
114	181	32	75
120	181	32	75
42	90	64	71
48	90	64	71
54	90	64	70
60	90	64	72
66	90	64	73
72	90	64	72
78	90	64	71
84	90	64	73
90	90	64	72
96	90	64	72
102	90	64	74
108	90	64	74
114	90	64	73
120	90	64	74
42	72	80	70
48	72	80	69
54	72	80	71
60	72	80	70
66	72	80	71
72	72	80	72

78	72	80	72
84	72	80	72
90	72	80	72
96	72	80	72
102	72	80	72
108	72	80	71
114	72	80	72
120	72	80	73
42	60	96	70
48	60	96	70
54	60	96	70
60	60	96	69
66	60	96	70
72	60	96	70
78	60	96	71
84	60	96	71
90	60	96	71
96	60	96	71
102	60	96	72
108	60	96	70
114	60	96	72
120	60	96	71
42	45	128	69
48	45	128	68
54	45	128	69

60	45	128	69
66	45	128	69
72	45	128	69
78	45	128	69
84	45	128	70
90	45	128	70
96	45	128	70
102	45	128	70
108	45	128	71
114	45	128	70
120	45	128	70
42	30	192	67
48	30	192	67
54	30	192	68
60	30	192	67
66	30	192	68
72	30	192	68
78	30	192	68
84	30	192	69
90	30	192	68
96	30	192	68
102	30	192	68
108	30	192	68
114	30	192	68
120	30	192	69

42	25	224	67
48	25	224	67
54	25	224	68
60	25	224	67
66	25	224	68
72	25	224	67
78	25	224	68
84	25	224	68
90	25	224	68
96	25	224	68
102	25	224	69
108	25	224	68
114	25	224	68
120	25	224	68
42	24	240	67
48	24	240	67
54	24	240	67
60	24	240	67
66	24	240	67
72	24	240	67
78	24	240	67
84	24	240	67
90	24	240	68
96	24	240	67
102	24	240	68

108	24	240	68
114	24	240	68
120	24	240	68
42	22	256	67
48	22	256	67
54	22	256	67
60	22	256	67
66	22	256	68
72	22	256	67
78	22	256	68
84	22	256	67
90	22	256	67
96	22	256	67
102	22	256	67
108	22	256	67
114	22	256	67
120	22	256	69
42	1448	4	74
48	1448	4	74
54	1448	4	73
60	1448	4	74
66	1448	4	76
72	1448	4	74
78	1448	4	76
84	1448	4	76

90	1448	4	74
96	1448	4	77
102	1448	4	76
108	1448	4	78
114	1448	4	79
120	1448	4	77
66	1	5794	10
66	11	512	67

Table 40: Accuracies of Cross Validation vs Test for RNN – kfold:3

# of Hidden Nodes	Epochs	Batch Size	Cross Validation (kFold 3) (%)	Accuracy (%)
42	724	8	71.081221	74
48	724	8	71.65028433	74
54	724	8	70.80531133	73
60	724	8	71.926194	75
66	724	8	72.90912233	76
72	724	8	72.92636633	76
78	724	8	72.598724	75
84	724	8	73.219521	76
90	724	8	74.28867067	75
96	724	8	74.185204	76
102	724	8	74.46111433	78
108	724	8	74.78875667	77
114	724	8	75.35782033	77
120	724	8	74.25418167	78
42	362	16	71.78823933	73
48	362	16	71.322642	73
54	362	16	72.80565633	74
60	362	16	71.66752867	76
66	362	16	72.47801367	75
72	362	16	72.20210367	76
78	362	16	72.840145	76
84	362	16	73.06432133	76
90	362	16	73.46094167	76

96	362	16	73.823073	78
102	362	16	72.70219033	77
108	362	16	73.85756133	77
116	362	16	74.323159	77
42	181	32	70.012071	73
48	181	32	70.78806667	73
54	181	32	71.374375	73
60	181	32	70.42593533	75
66	181	32	71.11570967	74
72	181	32	72.02966	75
78	181	32	72.04690467	74
84	181	32	72.70219	76
90	181	32	72.40903633	76
96	181	32	73.61614067	75
102	181	32	72.943611	77
108	181	32	72.202104	76
114	181	32	73.564408	75
120	181	32	73.478186	75
42	90	64	69.06363167	71
48	90	64	69.44300767	71
54	90	64	69.615451	70
60	90	64	70.02931533	72
66	90	64	70.04656	73
72	90	64	70.788067	72
78	90	64	70.16727	71
84	90	64	69.960338	73
90	90	64	71.20193133	72
96	90	64	71.27090867	72
102	90	64	70.75357833	74
108	90	64	71.15019833	74
114	90	64	71.94343867	73
120	90	64	71.477841	74

APPENDIX G

ACCURACY SCORES OF LSTM

Following table lists accuracies of LSTM algorithm with different combination of inputs.

Table 41: LSTM Success Rates with Input Combinations

LSTM Number	Epoches	Batch Size	Loss Function	Activation	Accuracy (%)
24	181	32	mean_absolute_error	-	70
48	181	32	mean_absolute_error	-	71
60	181	32	mean_absolute_error	-	73
70	181	32	mean_absolute_error	-	72
65	181	32	mean_absolute_error	-	73
75	181	32	mean_absolute_error	-	74
100	181	32	mean_absolute_error	-	75
150	181	32	mean_absolute_error	-	76
100	362	16	mean_absolute_error	-	79
100	724	8	mean_absolute_error	-	80
100	1448	4	mean_absolute_error	-	Cannot complated
100	5794	1	mean_absolute_error	-	Cannot complated
100	362	18	categorical_crossentropy	softmax	softmax
100	724	8	categorical_crossentropy	softmax	softmax
42	22	256	categorical_crossentropy	softmax	67
48	22	256	categorical_crossentropy	softmax	67
54	22	256	categorical_crossentropy	softmax	67

60	22	256	categorical_crossentropy	softmax	68
66	22	256	categorical_crossentropy	softmax	67
72	22	256	categorical_crossentropy	softmax	67
78	22	256	categorical_crossentropy	softmax	67
84	22	256	categorical_crossentropy	softmax	67
90	22	256	categorical_crossentropy	softmax	68
96	22	256	categorical_crossentropy	softmax	67
102	22	256	categorical_crossentropy	softmax	67
108	22	256	categorical_crossentropy	softmax	67
114	22	256	categorical_crossentropy	softmax	67
120	22	256	categorical_crossentropy	softmax	67
42	45	128	categorical_crossentropy	softmax	69
48	45	128	categorical_crossentropy	softmax	69
54	45	128	categorical_crossentropy	softmax	70
60	45	128	categorical_crossentropy	softmax	69
66	45	128	categorical_crossentropy	softmax	69
72	45	128	categorical_crossentropy	softmax	70
78	45	128	categorical_crossentropy	softmax	70
84	45	128	categorical_crossentropy	softmax	70
90	45	128	categorical_crossentropy	softmax	70
96	45	128	categorical_crossentropy	softmax	70
102	45	128	categorical_crossentropy	softmax	70
108	45	128	categorical_crossentropy	softmax	70
114	45	128	categorical_crossentropy	softmax	70
120	45	128	categorical_crossentropy	softmax	70

42	90	64	categorical_crossentropy	softmax	73
48	90	64	categorical_crossentropy	softmax	73
54	90	64	categorical_crossentropy	softmax	73
60	90	64	categorical_crossentropy	softmax	73
66	90	64	categorical_crossentropy	softmax	74
72	90	64	categorical_crossentropy	softmax	73
78	90	64	categorical_crossentropy	softmax	74
84	90	64	categorical_crossentropy	softmax	73
90	90	64	categorical_crossentropy	softmax	74
96	90	64	categorical_crossentropy	softmax	74
102	90	64	categorical_crossentropy	softmax	75
108	90	64	categorical_crossentropy	softmax	74
114	90	64	categorical_crossentropy	softmax	75
120	90	64	categorical_crossentropy	softmax	73
42	181	32	categorical_crossentropy	softmax	77
48	181	32	categorical_crossentropy	softmax	78
54	181	32	categorical_crossentropy	softmax	77
60	181	32	categorical_crossentropy	softmax	78
66	181	32	categorical_crossentropy	softmax	78
72	181	32	categorical_crossentropy	softmax	79
78	181	32	categorical_crossentropy	softmax	79
84	181	32	categorical_crossentropy	softmax	78
90	181	32	categorical_crossentropy	softmax	79
96	181	32	categorical_crossentropy	softmax	79
102	181	32	categorical_crossentropy	softmax	79

108	181	32	categorical_crossentropy	softmax	79
114	181	32	categorical_crossentropy	softmax	79
120	181	32	categorical_crossentropy	softmax	80
42	362	16	categorical_crossentropy	softmax	79
48	362	16	categorical_crossentropy	softmax	79
54	362	16	categorical_crossentropy	softmax	80
60	362	16	categorical_crossentropy	softmax	79
66	362	16	categorical_crossentropy	softmax	80
72	362	16	categorical_crossentropy	softmax	76
78	362	16	categorical_crossentropy	softmax	81
84	362	16	categorical_crossentropy	softmax	81
90	362	16	categorical_crossentropy	softmax	81
96	362	16	categorical_crossentropy	softmax	81
102	362	16	categorical_crossentropy	softmax	81
108	362	16	categorical_crossentropy	softmax	81
114	362	16	categorical_crossentropy	softmax	81
42	724	8	categorical_crossentropy	softmax	78
50	724	8	categorical_crossentropy	softmax	79
60	724	8	categorical_crossentropy	softmax	79
70	724	8	categorical_crossentropy	softmax	81
80	724	8	categorical_crossentropy	softmax	80
90	724	8	categorical_crossentropy	softmax	82
100	724	8	categorical_crossentropy	softmax	82
110	724	8	categorical_crossentropy	softmax	81
42	1448	4	categorical_crossentropy	softmax	78

50	1448	4	categorical_crossentropy	softmax	80
60	1448	4	categorical_crossentropy	softmax	80
70	1448	4	categorical_crossentropy	softmax	79
80	1448	4	categorical_crossentropy	softmax	80
90	1448	4	categorical_crossentropy	softmax	-
40	2897	2	categorical_crossentropy	softmax	-
50	2897	2	categorical_crossentropy	softmax	-
60	2897	2	categorical_crossentropy	softmax	-
70	2897	2	categorical_crossentropy	softmax	-
80	2897	2	categorical_crossentropy	softmax	-
90	2897	2	categorical_crossentropy	softmax	-
100	2897	2	categorical_crossentropy	softmax	-
120	2897	2	categorical_crossentropy	softmax	-

Table 42: Accuracies of Cross Validation vs Test for LSTM – kfold:3 (Loss Func.: Categorical Crossentropy, Activation: Softmax)

LSTM Number	Epoches	Batch Size	Cross Validation Accuracy (%)	Test Accuracy (%)
42	8	724	73.3057	78
60	8	724	77.0822	79
90	8	724	77.0305	82
42	16	362	75.1163	79
48	16	362	74.7542	79
54	16	362	74.9612	80
60	16	362	75.5819	79
66	16	362	76.7718	80
72	16	362	72.6332	76
78	16	362	76.0475	81
84	16	362	76.5649	81
90	16	362	77.4443	81
96	16	362	76.7718	81

102	16	362	76.4097	81
42	32	181	73.0470	77
48	32	181	72.6849	78
54	32	181	72.9953	77
60	32	181	73.2022	78
66	32	181	72.5297	78
72	32	181	73.4609	79
78	32	181	73.2540	79
84	32	181	74.0817	78
90	32	181	74.4438	79
96	32	181	72.9436	79
102	32	181	75.0129	79
42	64	90	70.9777	73
48	64	90	71.3398	73
54	64	90	70.3569	73
60	64	90	70.9260	73
66	64	90	70.9777	74
72	64	90	70.6156	73
78	64	90	71.1329	74
84	64	90	66.2183	73
90	64	90	71.7537	74
96	64	90	71.5985	74
102	64	90	72.1676	75